

The Design of Shading Louvres for Solar Energy Collection



Thesis Submitted to the University of Nottingham for the degree of
Doctor of Philosophy; September 2004.

PAGES 204,206-7,211-216

NOT SCANNED AT THE

REQUEST OF THE

UNIVERSITY

SEE ORIGINAL COPY OF

THE THESIS FOR THIS

MATERIAL

Dedicated to:

Prof. K.S. Ali, for putting me in this road some three decades ago;
and to:

Ms. V.H. Brobbey for helping through the latter part of the journey.

Acknowledgements

The direct contribution of Professor S.B.Riffat in directing and paving the path for this project has been tremendous, while his other contribution, of giving me a free-rein in experimenting with various designs techniques was invaluable.

Also my thanks to Dr. Prince Doherty for help laying foundation for the early part of this work, and for overseeing the compiled (written) parts of it.

Also I extend my thanks to the project partners:

Prof. Armando Oliveira (*The University of Porto, Portugal*)

Dr. Thilo Koch (*Axima, Switzerland*)

Mr. Trevor Griffith (*Thermomax -UK Ltd.*),

for their close collaboration and help in bringing this project to a successful completion.

I, on behalf of the Institute of Building Technology, thank the *EU* for funding this project

K.W.Eissa

Nottingham, England.

September 2004.

Abstract

Shading louvres on buildings must serve to allow maximum window insolation in winter, while have the prime function of intercepting unwanted direct solar radiation in summer; which could cause excessive solar heat gain, especially in glazed offices and commercial spaces. Studies of the effect of solar protection on heating and cooling loads show that shading strategies are climate dependent. And it is accepted today that solar protection does reduce energy use for cooling, and tends to increase heating loads. The balance between the benefits in cooling and the losses in heating is only achievable by good designs.

The main focus of this research work has been in harnessing the thermal energy available within the incident solar radiation intercepted by the shading louvres; hence benefiting, from shading in terms of energy savings, as well as from the collected energy. In achieving this aim, both theoretical and experimental techniques have been utilized, as design analysis tools, in order to select a design that satisfies both the efficiency and cost criteria. A suitable collector design has, then, been identified, its thermal performance characterised, and its prototype manufactured and built. The prototype of the chosen design has been field-tested in Nottingham-England and Porto-Portugal. Finally, the characteristics of the design have been incorporated into a computer simulation scenario, in which a real office building in Winterthur-Switzerland has been analysed for its total (cooling and heating) annual energy consumption.

Findings of this research work indicate that these louvres, despite certain geometrical limitations, could act as solar collectors with good energy collection characteristics. And they could contribute with substantial reductions in the overall annual energy consumption resulting from the combined effect of shading and collecting energy. This was found particularly to be the case when the collected energy is made to part-fuel, an adsorption chiller for the purpose of air-conditioning the same building.

Nomenclature

(SI units have been used through out this work).

A_{col}	Area of the collector, based on the unobstructed absorbing plate area
A_{ch}	Cross sectional area of the channel
A_{fin}	Exposed surface area of the fins array only
A_{tot}	Total exposed surface area (including the fins and un-finned surface)
A_x	Cross sectional area of the channel/fin's pipe
A_c	Area of heat-pipe condenser
C_p	Specific heat capacity (at constant pressure)
COP	Coefficient of performance of the adsorption chiller
D, d	Diameter
D_h	Hydraulic (or effective) diameter, defined as: $\frac{4A_{ch}}{P_{ch}}$
d_{av}	Representative distance
E	Distance between parallel Louvres
$Eff-f$	Efficiency of the solar louvre collector, incorporating fin-on-tubes
$Eff-c$	Efficiency of the solar louvre collector, incorporating channels
F_R	Heat removal factor, based on the inlet temperature (T_{in})
F_{av}	Heat removal factor, based on the average temperature (T_{av})
F'	Collector efficiency factor, based on the average temperature (T_{av})
g	Force due to gravity
g'	g' -value for the window
H	Length of the major axis of the louvre
H	Collector distance above window
H_w	Window height
h_{max}	Angle of maximum solar altitude at June 21 st
h_{min}	Angle of maximum solar altitude at December 21 st
h_{co}	The convection heat transfer coefficient at the outer perimeter surface of the louvre.
h_{co}	The convection heat transfer coefficient at the outer perimeter surface of the louvre, due to wind.
h_{ro}, h_{rs}	The radiation heat transfer coefficients of the cover (i.e. the glazing's outer surface) and of the back surface receptively.
h_c, h_r	The convection and radiation heat transfer coefficients within the glazing.
h_{ci}, h_{ri}	The convection and radiation heat transfer coefficients between the aluminium louvre surface, and the back surface of the channel respectively
I	Normal radiation (mostly beam)
k	Coefficient of heat transfer for window
k_{cop}	Conductivity of the channel material (copper)
k_w	Conductivity of water
k_i	Conductivity of the inner insulation material
k_o	Conductivity of the outer insulation material
L	Total distance between the most outer louvre and the wall, or length of the louvre
L	Distance between the glazing; also thickness of the outer insulation
L_b	Cubic root of the building's volume

l	Length of fin within the channel
m_w	Mass flow rate in the collector circuit
\dot{m}	Mass flow rate, as defined in the simulation (subscripted)
P_{ch}	Wetted perimeter
q_u	Useful output (net) heat energy from the collector
q_{c-a}, q_{p-c}	Heat flow between interfaces ($c-a, p-c, \dots$ etc)
q_{loss}	Total heat loss from the louvre
q_t, q_b	The top and bottom losses respectively
T_a	Ambient temperature
T_a'	Equivalent-environment temperature.
T_{in}	Temperature of the inlet to the collector
T_{out}	Temperature of the outlet form the collector
T_{pm}	Absorbing-plate mean temperature
T_{av}	The arithmetic average of the inlet and outlet
T_c	Temperature of the cover
T_p	Temperature of the cover
T_b	Temperature of the back surface of the louvre
T_s	Temperature of the outer surface of the outer insulation
U_c	Cover-absorber heat transfer coefficient (upper loss)
\bar{U}	Overall collector heat transfer coefficient (between the fluid and the ambient air)
u	Wind speed
Q	Energy demand Heat: for heating, Cooling: For cooling demand
w	Thickness of fin with in the channel
X_m	Defined as: $X_m = (T_{av} - T_a)/I$
X^{**}	Defined as: $X^{**} = (T_m - T_a)/I$
α_p	Absorptance of the plate surface
α	Collector inclination angle
β	Angle of the upper sunbeam
β	Coefficient of thermal expansion
ε_c	The emissivity of the cover
ε_p	The emissivity of the plate
ε_s	The emissivity of the back insulation's outer surface
ε_{pi}	The emissivity of the back surface of the channel
ε_{al}	The emissivity of the aluminium louvre's inner surface
ϕ	Collector inclination angle
φ	Latitude of the collector location
γ	Solar zenith angle
η_{col}	Efficiency of the solar collector
η_{ch}	The total surface temperature effectiveness (for the fins within the channel)
σ	Stefan-Boltzman constant $[= 5.67 \times 10^{-8} W/m^2 - ^\circ K^4]$.
τ_c	Transmittance of the cover glazing

Nondimensional groups (Numbers), used in this work are:

- Nu_L, Nu_D Nusselt number based on the characteristic length L , and diameter D .
 Re_D Reynolds number based on diameter D .
Pr Prandtl number
 Ra_L Rayleigh number based on the characteristic length L .

Latitudes:

- Nottingham (England): 52°N 58
London (England): 51°N
Lisbon (Portugal): 38.7°N
Winterthur (Switzerland): 47°N 30

Contents

Page No

Title

Acknowledgement

Abstract

Nomenclature

Chapter 1 – Introduction	1
1 Introduction	2
1.1 Solar Collectors	3
1.1.1 Passive systems	3
1.1.2 Active systems	4
1.1.2.1 Flat-Plate Collectors	4
1.1.2.2 Evacuated Collectors	6
1.1.2.3 Concentrating Collectors	7
1.2 Large Applications of Solar Collectors	8
1.3 Technological Improvements of Solar collectors	10
1.3.1 Cost, Efficiency and Life span	10
1.3.2 Applications	10
1.4 Shading Louvres	11
1.4.1 Daylight	11
1.4.2 Shading	13
1.5 Shading Louvres as Thermal Solar Collectors	14
Chapter 2 – Literature Survey	16
2 Literature Survey	17
2.1 The Impact of Shading on cooling and/or heating loads	17
2.2 The Impact of Shading on Annual energy use, including electricity for lights	19
2.3 Flat-plate Solar Collectors	20
2.3.1 Evacuated flat-plate collectors	21
2.3.2 Reverse flat-plate collectors	21
2.3.3 Low-Cost Solar Water Heating	22
2.4 Solar assisted air-conditioning systems	23
2.4.1 Solar Absorption Cooling	24
2.4.2 Solar Adsorption Chillers	24
2.5 Solar Louvres	25
Chapter 3 – Aesthetic Overview	27
3 Aesthetic Overview	28
3.1 Aesthetics of conventional solar collectors	28
3.2 Shading Louvres	29

Chapter 4 – Preprototype Investigations	34
4	Preprototype Investigations 35
4.1	Solar Collectors Performance Testing 36
4.2	Apparatus and instrumentation 38
4.3	Experimental procedure 40
4.4	The Results 48
4.5	Summary 53
Chapter 5 - The Design	55
5	The Design 56
5.1	Design considerations 59
5.2	The Mathematical Models 64
5.2.1	The Direct-flow Model 65
5.2.1.1	Further Assumptions and Approximations 68
5.2.1.2	The Governing Equations 69
5.2.1.3	The Solution 77
5.2.1.4	Results of the Direct-flow Model 80
5.2.2	The Heat-pipe Model 89
5.2.2.1	Further Assumptions and Approximations 89
5.2.2.2	The Governing Equations 90
5.2.2.3	The Solution 98
5.2.2.4	The Results of the Heat-pipe Model 99
5.3	Summary 103
Chapter 6 – The Experimental Work	103
6	The Experimental Work 104
6.1	Preparations 112
6.2	Apparatus and instrumentation 118
6.3	Experimental procedure 122
6.4	The Experimental Results 125
6.5	Summary 133
Chapter 7 – Viability of The Design	135
7	Viability of The Design 136
7.1	Environmental Assessment 136
7.2	Economic Analysis 137
7.2.1	Payback period 139
7.2.2	Average Energy Cost 141
7.2.3	Life Cycle Savings 142
7.3	Field Trials 143
7.3.1	Trials in Nottingham 143

7.3.2	Trials in Porto	152
7.3.3	The Efficiency equation of the Solar Louvre Collector	156
7.4	Summary	157
Chapter 8 – Simulation Case-study		159
8	Simulation Case-study	160
8.1	The typical office building floor	160
8.2	Geometrical aspects of shading by Solar Louvre	162
8.3	The effect of shading by Solar Louvres	165
8.4	Consideration of Shading and Energy Collection	168
8.5	Shading, Energy Collection and Storage	176
8.6	Summary	181
Chapter 9 – Conclusions and Recommendations		184
9	Conclusions and Recommendations	185
9.1	Conclusion	185
9.2	Recommendations	190
Appendices		195
Appendix A	References	196
Appendix B	Properties of the material, entering the construction of the solar louvre collector	200
Appendix C	<i>AutoCAD</i> drawings of previous designs	208

Chapter One

Introduction

1. Introduction

Air-conditioning is the dominating energy consuming service in buildings in many countries. In many regions of the world the demand for cooling and dehumidification of indoor air is growing due to increasing comfort expectations and increasing internal loads (compressors, equipment, etc). Conventional cooling technologies exhibit several clear disadvantages:

- Their operation creates high-energy consumptions.
- They cause high electricity peak loads.
- In general they employ refrigerants that have several negative environmental impacts.

On recent years, the need for alternative forms of energy has never been more acute. Solar energy is one important such form of alternative energy, which could be harnessed by photovoltaic cells - to produce electricity, or by the various types of thermal collectors - to produce heat.

Also shading devices could offer protection from solar gains, which can cause thermal discomfort or unnecessary loading on air conditioning and dehumidification equipment. They are simple to manufacture and can be installed to both new and refurbished buildings.

The subject of this research work has been focused on the combined effect of shading and collecting solar energy on the overall energy consumption of buildings, without adverse effects on their aesthetics. The aim, here, has been on converting shading louvres to become active thermal energy collectors, hence fulfilling a dual task. The work therefore, has become that of solar collector design and application, followed by simulations for the overall annual energy consumption for a particular building.

In order to make choices about the design, a general review of solar collectors (and working principles), shading devices have been conducted and presented in the following sections. The scientific facts presented in these sections have been summarized from the literature, but mainly from Duffie (1991), and Morrison (2001).

1.1 Solar Collectors

There have been tremendous changes in solar energy science and technology during the last three decades. Thousands of papers have been published, many meetings have been held with proceedings published, industries have come and gone, and public interest in the field has waxed, waned and is waxing again. A

solar heat collector is a special kind of heat exchanger that transforms solar radiant energy into heat. A solar collector differs in several respects from more conventional heat exchangers. The latter usually accomplish a fluid-to-fluid exchange with high heat transfer rates and with radiation as unimportant factor. In the solar collector, energy transfer is from a distant source of radiant energy to a fluid. The flux of the incident radiation is approximately (at best) around 1000 W/m^2 , and is variable. The wavelength ranges from 0.3 to $3 \mu\text{m}$, which is considerably shorter than that of the emitted radiation from most energy absorbing surfaces. Thus, the analysis of solar collectors presents unique problems of low and variable energy fluxes and the relatively large importance of radiation. Solar thermal collectors/systems are, generally, categorized under two main distinctions: Passive collectors or Active collectors.

1.1.1 Passive systems

Passive systems can be distinguished from active systems on either of two bases. The **first** distinction lies in the degree to which the functions of collection and storage are integrated to the structure of the building; windows and the rooms behind them can serve as collectors, with storage provided as sensible heat of the building structure and contents as they change temperature.

The **second**, many passive systems require no mechanical energy for moving fluids for their operation; fluids and energy move by virtue of the temperature gradients established by absorption of radiation (and hence the term passive). By nature, passive systems are intimately concerned with architecture, as the building (and its contents) function as collector and storage unit. However, there are some types of passive systems used in water heating, which are somewhat separate from the structure of the building.

These are:

- **Batch heaters** or integral collector storage systems consist of one or more storage tanks placed in an insulated box with a glazed side facing the sun. During the winter, they must be protected from freezing or drained.
- **Thermosiphon systems** rely on natural convection within the warming water to circulate water through the collectors and to the tank, which is located above the collector. As water in the solar collector heats, it becomes lighter and rises naturally into the tank above. Meanwhile, the tank's bottom cooler water flows down pipes to the bottom of the collector, causing circulation throughout the system.

There are air collectors that could operate utilizing the phenomenon of natural convection to transfer the energy absorbed by the air; these, as well, are passive systems.

1.1.2 Active systems

Active systems use electric pumps, valves, and controllers to circulate water or other heat-transfer fluids through the collectors. There are three broad categories of active systems:

- **Direct systems;** also known as an "open-loop", use pumps to circulate water through the collectors. These systems are appropriate in areas that do not freeze for long periods and do not have hard or acidic water. Air collectors (transpired or glazed) usually operate as direct systems.
- **Indirect systems;** also known as "closed-loop", pump heat-transfer fluids such as a mixture of glycol and water antifreeze through collectors. Heat exchangers transfer the heat from the fluid to the water stored in the tanks.
- **Drain back systems** are a type of indirect system - they use pumps to circulate water through the collectors. Because the water in the collector loop drains into a reservoir tank within the building when the pumps stop, this is still a good system for colder climates.

There are several types of active solar collectors used for residences, commercial and office buildings. These are Flat-plate, Evacuated-tube, and Concentrating collectors.

1.1.2.1 Flat-Plate Collectors

Flat-plate collectors are the most common collector for residential water heating and space-heating installations. A typical flat-plate collector is an insulated metal box

with a glass or plastic cover - called the glazing - and a dark-coloured absorber plate. The glazing allows the light to strike the absorber plate but reduces the amount of heat that can escape. The sides and bottom of the collector are usually insulated, further minimizing heat loss. The absorber plate is usually black because dark colours absorb more solar energy than light colours. Sunlight passes through the glazing and strikes the absorber plate, which heats up, changing solar radiation into heat under the form of infrared thermal radiation. The heat is transferred to the air or liquid passing through the collector. Absorber plates are commonly covered with "selective coatings," which have an emissivity lower than the absorptance, and are more durable than ordinary black paints.

Absorber plates are often made of metal- usually copper or aluminium - because they are both good heat conductors. Copper is more expensive and heavier, but is a better conductor and is less prone to corrosion than aluminium.

Flat-plate collectors fall into two basic categories: liquid or air. And both types can be either glazed or unglazed.

- **Liquid Collectors**

In a liquid collector, solar energy heats a liquid as it flows through tubes in or adjacent to the absorber plate. For this type of collector, the flow tubes are attached to the absorber plate so the heat absorbed by the absorber plate is readily conducted to the liquid. The flow tubes can be routed in parallel, using inlet and outlet headers, or in a serpentine pattern. A serpentine pattern eliminates the possibility of header leaks and ensures uniform flow, but is not appropriate, however, for systems that must drain for freeze protection because the curved flow passages will not drain completely.

Glazed liquid collectors are used for heating household water and sometimes for space heating. Unglazed liquid collectors are commonly used to heat water for swimming pools. Because these collectors need not withstand high temperatures, they can use less expensive materials such as plastic or rubber. They also do not require freeze proofing because swimming pools are generally used only in warm weather.

- **Air Collectors**

Air collectors are simple flat-plate collectors used primarily for space heating. The absorber plates in air collectors can be metal sheets, layers of screen, or non-metallic

materials. The air flows past the absorber by natural convection or when forced by a fan. Because air conducts/convects heat much less readily than liquid does, less heat is transferred between the air and the absorber than in a liquid collector.

In some solar air-heating systems, fins or corrugations on the absorber are used to increase air turbulence and improve heat transfer. The disadvantage of this strategy is that it can also increase the amount of power needed for fans and, thus, increase the costs of operating the system. In colder climates, the air is routed between the absorber plate and the back insulation to reduce heat loss through the glazing. However, if the air will not be heated more than 17°C or so above the outdoor temperature, the air can flow on both sides of the absorber plate without sacrificing efficiency.

Air systems have the advantage of eliminating the freezing and boiling problems associated with liquid systems. Although leaks are harder to detect and plug in air systems, they are also less troublesome than leaks in a liquid system. Air systems can often use less-expensive materials, such as plastic glazing, because their operating temperatures are usually lower than those of liquid collectors.

1.1.2.2 Evacuated Collectors

Evacuated tubular collectors consist of an absorbing surface, mounted in a vacuum to reduce convection heat loss. Two forms of evacuated tubular absorbers are used: the single glass envelope metal-fin-in vacuum type and the all-glass Dewar-tube type.

The Metal-fin-in vacuum configuration uses a metal absorber plate in a glass vacuum tube. Heat is removed from the absorber plate by circulating liquid through a metal tube bonded to the plate. Glass to metal seals are needed to seal the heat extraction tubes as they pass through the glass envelope. The disadvantage of this configuration is the need to maintain the glass-to-metal seals. Collectors in this group differ mainly in the way that heat is transported out of the vacuum enclosure:

- U-tube heat removal design
- Straight through metal tube (needs bellows to absorb differential expansion between the tube and the glass)
- Heat pipe bonded to a metal absorber plate (does not require a bellows seal)

Dewar tube consists of two glass tubes; an inner tube is melted to an outer tube. The space between the tubes is evacuated, and therefore there are hardly any thermal losses. The heat is transferred from the absorber on the inner tube through the glass onto an aluminium sheet passing it on to a U-tube through which the water circulates. A metal-glass-seal with its typical problems caused by thermal expansion is not needed.

Evacuated-tube collectors heat water in building applications that require higher temperatures. The absorbing surface is covered with a selective coating. Evacuated collectors are modular-tubes, which could be added or removed as hot-water requirements change. These collectors are more efficient than flat-plate collectors for the fact that the vacuum minimizes heat losses to the outdoors. While evacuated-tube collectors achieve both higher temperatures and higher efficiencies than flat-plate collectors, they are also more expensive. Some flat-plate collectors have been inserted within evacuated double-glazing to further reduce heat losses; but they tend to leak and intermittent vacuum pumping is required.

1.1.2.3 Concentrating Collectors

Concentrating collectors use mirrored-surfaces (or concentrators) to concentrate the sun's energy on an absorber called a receiver. Concentrators can be reflectors or refractors, can be cylindrical or surface of revolution, and can be continuous or segmented. Receivers can be convex, flat or concave and can be covered or uncovered. Many modes of tracking are possible. Concentration ratios can vary over several orders of magnitude. Concentrating collectors also achieve high temperatures, but unlike evacuated-tube collectors, they can do so only when direct sunlight is available. The mirrored surface focuses sunlight collected over a large area onto a smaller absorber area to achieve high temperatures. Some designs concentrate solar energy onto a focal point, while others concentrate the sun's rays along a thin line called the focal line. The receiver is located at the focal point or along the focal line. A heat-transfer fluid flows through the receiver and absorbs heat. These collectors reach much higher temperatures than flat-plate collectors, or even evacuated collectors. However, concentrators can only focus direct solar radiation, with the result being that their performance is poor on hazy or cloudy days. Concentrators are most practical in areas of high insolation, such as those close to the

equator or in desert climates. They perform best when pointed directly at the sun, and to do this, these systems use tracking mechanisms to move the collectors during the day to keep them focused on the sun. Single-axis trackers move east to west; dual-axis trackers move east and west and north and south (to follow the sun throughout the year). In addition to these mechanical trackers, there are passive trackers that use a refrigerant to supply the movement. While not widely used, they do provide a low-maintenance alternative to mechanical systems.

Concentrators are used mostly in commercial applications because they are expensive and because the trackers need frequent maintenance. Some residential and office buildings use parabolic-trough concentrating systems. These installations can provide hot water, space heating, and water purification. These systems use single-axis trackers, which are less expensive and simpler than dual-axis trackers.

1.2 Large Applications of Solar Collectors

Solar heating systems are designed to meet the need for large quantities of hot water or space heating at commercial/industrial/institutional buildings. A typical system consists of several hundreds square metres of ground- or roof-mounted collectors, combined with pumps, heat exchangers, controls, and one or more large-volume storage tanks. Solar process heating systems have successfully developed niche markets where facilities such as schools, military bases, office buildings, hotels and hospitals use hot water for bathing, cooking, laundry, and space heating.

Transpired air collectors mounted as an exterior cladding on a building's sun-facing wall, are used for ventilation preheating. These collectors are unglazed. A blower or fan is used to draw air through perforations in the wall to deliver ventilation air into the building. Solar ventilation air preheating systems are generally used in commercial and industrial applications that require large quantities of ventilation air, including warehouses, large manufacturing plants, and airplane maintenance hangars.

Solar industrial process heat could provide a large amount of the required low-medium temperature energy used in diverse industrial applications such as drying of lumber or food, cleaning in food processing, extraction operations in metallurgical

or chemical processing, cooking, curing of masonry products, paint drying, and many others. Temperatures for these applications can range from near ambient to those corresponding to low-pressure steam; and energy can be provided from flat-plate collectors, or concentrating collectors of low concentration ratios.

Cooling using active solar cooling systems can provide for year-round utilization of collected solar heat, thereby significantly increasing the cost effectiveness and energy contribution of solar installations. Solar-driven absorption systems use the thermal energy from the solar collector to separate a binary mixture of an absorbent and a refrigerant fluid (e.g. Ammonia or Lithium Bromide solution). The refrigerant is condensed, throttled, and evaporated to yield a cooling effect, after which it is reabsorbed to continue the cycle. Due to the medium temperature requirements of absorption cooling systems (70-90 °C), evacuated-tube or concentrating collectors are typically used. Adsorption systems could also be used to utilize the hot water from collectors. Recently low temperature sorption chillers proved to be compatible with flat plate collectors under evacuated covers.

Electricity generation, using conventional methods (steam) requires high temperature associated only with concentrating collectors. To harness the high-temperature-energy needed for vapour/steam generation, collectors of high concentrating ratios are used with dual-axis tracking systems. Alternatively, central receiver collectors are used. This concept consists of a central receiver, also called the power tower, surrounded by a field of a large number of heliostats, each reflecting beam radiation on the central receiver. The result is a Fresnel-type concentrator, a parabolic reflector broken up into small segments.

Things have moved on for electricity generation using sustainable technology. A joint project between the university of Nottingham and the university of Porto showed that n-pentane could be used in medium temperature electricity generation – (ECOCOOL 1997).

1.3 Technological Improvements of Solar collectors

1.3.1 Cost, Efficiency and Life span

From a scientific point of view, solar collectors are quite successful as a form of renewable-energy technology. However, they are still undergoing various technological and manufacturing improvements. Concentrating collectors, for example, require frequent cleaning and maintenance, particularly to retain the quality of the optical systems for long periods of time in the presence of dirt, weather, and oxidizing or other corrosive atmospheric components. Glazing in Flat-plate and Evacuated-tube collectors is still a subject of research and development today. Efforts for finding ways of maximizing incoming solar radiation, minimizing emissivity, maintaining vacuum, using mono-atomic gases or silica aerogels, solving the UV-aging problems, etc are still ongoing. The absorbing 'black' surface in any solar collector must have high absorptivity and low emissivity. Today, quite a few selective surfaces fulfil these conditions and have long life span, but their cost could still be reduced. Better manufacturing methods and better coating-processes are also needed as a prime factor in cost reduction. The efficiencies of solar collector systems have improved from the early 1970s and costs have dropped somewhat. New materials and better engineering of systems have now led to increased and wide applications of solar collectors. The improved efficiencies can be attributed to the use of:

- Low-iron, tempered glass for glazing (low-iron glass allows the transmission of more solar energy than conventional glass),
- Low-emissivity (low- ϵ) coating for glazing
- Vacuum or, a mono-atomic gases (Argon)
- Improved insulation materials, and
- The development of durable selective coatings (Black Chrome, Titanium Oxynitride, etc).

1.3.2 Applications

The lower cost, longer life and better efficiencies have recently led to an increased and wider application of solar collectors. In cooling, for example, there are systems

operating today, which use heat from solar collectors for absorption cooling (Yazaki Chillers, Japan) or to renew the desiccant material in desiccant cooling systems. Systems utilizing this active cooling technology option currently appears to have the greatest potential.

Further, as environmental laws become stricter and the price of conventional power (e.g. natural gas) increases, it is inevitable that solar collectors will be integrated further into many applications. Increased, successful application leads to larger mass production and improved products at cheaper prices.

1.4 Shading Louvres

The right choice of a shading system must prove to be effective in reducing cooling energy in summer, maximizing solar gain in winter, while keeping the daylighting levels in the building as high as possible without glare to occupants. Such shading device would be effective in reducing annual energy cost.

1.4.1 Daylight

Energy efficient buildings should make as much beneficial use of naturally available light as is practicably possible. Daylighting is also important because of the influence it has over occupants' psychological well being. Until few decades ago, the use of windows and plan form of buildings was very much influenced by the limits of natural light admission. The developments of the fluorescent tube lamp, increased environmental noise and poorer urban air quality have all contributed to the expansion of deep-plan, artificially lit and air conditioned environments. Only relatively recently have the advantages of natural daylight been recognised once again.

Maximising the admission of solar radiation into buildings through vertical windows and horizontal rooflights increase daylighting levels and has the obvious benefit of passive solar heating. This, in turn reduces energy that otherwise would have been used in artificial lighting and heating. However, maximizing natural daylighting could increase heat losses from the building in the heating seasons, which increases the energy consumption used for heating. Glazing with low U-values decrease these losses. But in certain buildings at certain climates these same glazing could, in summer, necessitate the use of air conditioning due to a reduced heat-rejection from

the building. In summer, passive gains in non-domestic buildings would substantially increase the cooling loads of the building, impacting directly with increased air-conditioning energy consumption.

Another disadvantage of attempting to maximize daylight in buildings is glare. Glare problems arise when either very high levels of sunlight enter a space, or where there is severe contrast between areas/parts on close proximity. Glare is evidently unacceptable in office buildings where visual display units are in use.

It can be concluded from the foregoing discussion that daylighting in buildings is an important design feature. In fact various innovative daylighting devices/systems have been set forth, developed and applied in order to enhance and tune the daylight levels in non-domestic buildings. Examples of these devices/systems are: Reflective systems, Light shelves, Prismatic glazing, Light pipes, Holographic glazing and Atria. However, designing for desirable daylighting levels, brings with it the problems of excessive solar heat gains and glare; and, therefore, trade-off measures and optimisation techniques are typically needed here. Seasonal variations in radiation levels and that of the Sun's elevation further complicate the problem of the design.

The need for solar control in buildings gave rise to various recent innovations in glazing technology. Apart from the heat losses issue, for which innovative insulation solutions (vacuum, mono-atomic gases, aerogels, etc) have been applied, other more advanced control mechanisms to deal with the seasonal variations have been set forth. Some of these are still under development, like 'smart windows' for example.

Smart windows rely on coating the glass with special coatings to obtain the desired behaviour of diminish solar over-heating in summer, while allowing maximum radiation passage during dull days and winter time. These methods are:

- Diminished solar heating, with good visible clarity
- Angularly selective transmission
- Dynamic radiation control (Electrochromic and Thermo-chromic)

The sole objective of these techniques is to allow as much radiation through glazing in winter, and as little as possible in summer while keeping visibility through the window clear, and energy losses minimum throughout the year.

1.4.2 Shading

Shading requirements vary according to climate and building orientation.

Shading and daylighting are so closely linked that they are often grouped under the title *sun control*. And therefore some issues regarding shading have already been mentioned in the previous section – **Daylight**.

Shading from unwanted solar heat gains in summer could be provided for by a variety of devices/methods. Simple mechanical methods of controlling solar gain – like blinds, drapers, awnings and louvres - are well known. Also well known is the proper design of fixed overhangs above the glazing, which, by taking advantage of the seasonal variation in the Sun's elevation, can also provide suitable control when the overheating problem is purely a seasonal one.

Deciduous plants could also be used to fulfil the role of shading in some specific circumstances.

Numerous issues dictate shading schemes/strategies; each is loaded with various parameters. This makes the task, like most engineering problems, a one that is characterized by trade-offs and optimisations.

In other words, it is rather hard to maximize daylight in winter, minimize it in summer while keeping the annual total energy consumption (lighting, heating, air-conditioning and ventilation) of the building low as a result of these solar control measures. There is always a trade-off or compromising decision to be made.

For example, none of the advanced control mechanisms (coatings on glazing) for Sun light control have actually fulfilled the control task idealistically. Several are able to improve comfort levels in the living space from the point of view of illumination, but their full annual energy savings potential, however, is still to be evaluated and verified. Nevertheless, some of them have good potential in performance and price. Another example is that of the fixed shading devices. Designing them so as to make full use of winter radiation brings with it, hand-in-hand, the problem of excessive heat gains in summer, especially in relatively warm climates.

Iterating the objectives of sun control, a fenestration (with/without shading) should, through out the year, serve to:

- Maximize desirable heat gains, daylighting and visibility,
- Minimize undesirable solar heat gains, energy losses and glare

In achieving these objectives, some shading strategies have showed great potential in fulfilling the overall task. Glazing that employ the method of 'Diminished solar heating, with good visible clarity' for shading, use coating materials whose reflectance or absorptance is preferentially high for radiations at the near-infra-red band (i.e. $0.7 < \lambda < 3 \mu\text{m}$).

A glazing with this property will have reduced solar gain in the winter when such energy is normally desirable, but from a total annual energy perspective, it is still the preferred option in relatively warm climates.

Also, external adjustable- and retractable- shading devices have proved to save in annual energy consumption in certain applications at certain climates.

Apart from the need for thorough analysis of the building and its use at the design stage, the solution to ideal sun control at a fenestration lies in a combination of measures; namely: Treated glazing supported by the appropriate type of external, adjustable shading device.

1.5 Shading Louvres as Thermal Solar Collectors

External shading louvres are a group of horizontal, usually aluminium, slats designed to provide shade from sunlight whilst allowing passage of daylight and view. They can be fixed in the vertical or horizontal plane (overhangs) outside the vertical window.

The types considered in this research work are generally designed from an elliptical cross-section of an aspect ratio of about (6) six. This elliptical cross-section provides a structural advantage, which allow these louvres to have long spans without showing signs of sagging. The elliptical profile, also, provide aerodynamic advantages- no lift and negligible drag.

They are usually coated with powder coats or other protective paints. These coatings/paints also serve as reflectors to incident light.

Operable External louvres provide a good shading option as they respond to the daily and seasonal variations of solar radiation. They could be operated manually by occupants, or automatically through light sensors, motors and a controller. They are favoured by architects for their aesthetics, especially when arranged horizontally on the horizontal planes and installed as overhangs, above vertical fenestrations.

Sun-facing facades benefit from such arrangement of louvres, particularly in the case of air-conditioned office buildings.

The annual energy evaluation of such offices shows that shading has somewhat made savings in the overall annual energy consumption of certain buildings even in cold climates. These savings were clearly evident at buildings in temperate and hot climates.

Shading louvres have already been designed by, *Colt International* - see appendix (a) - to collect solar energy in the form of electricity (i.e. using PV). These are made of slats of photovoltaic cells. They are arranged to provide shading as well as electricity. They are commercially known as *Shadovoltaic*[®].

The shading louvres considered in this research work are made from aluminium elliptical cross-sections, and are thermal energy collectors as well as shading devices. They are referred to in the next chapters simply as *Solar Louvres*.

The preceding sections provide a general map for excluding unsuitable designs and help identifying the most appropriate design for the solar louvres. The problem repeatedly encountered in providing hot water for cooling/Heating a building is that there isn't enough roof area for collectors to be mounted on; hence lack of hot water for the absorption/adsorption chiller. For heating, the problem is worse because in winter there less solar radiation available. A one-storey building of a certain floor-area has better chances than a two-storey building of the same footing.

As a conclusion to this chapter, one could see the need for increasing the collected energy, which, in turn, implies an increase to the collecting surface area. This consequently would direct attention to the envelope of buildings as possible collecting surfaces.

Performance of *Solar Facade Components* is an area of research, which would help increase the solar collection surface of a building. Therefore the success of converting these shading louvres to act as solar thermal collectors, would offer the designer the extra collecting-surface, hence higher energy flow rate for building heating and cooling.

Chapter Two
Literature Survey

2. Literature survey

In this chapter a survey of shading strategies and their role in annual energy use, flat plate solar collectors, solar assisted cooling (absorption and adsorption) is presented. In the case of shading strategies, the survey covers two decades of various researchers' work conducted in different parts of the world. Research in solar assisted cooling does not go as far; this field is still relatively young.

2.1 The Impact of Shading on cooling and/or heating loads

Studies of the effect of solar protection on heating and cooling loads show that shading strategies are climate dependent. While most authors agree that solar protection does reduce energy use for cooling and tends to increase heating loads, few of them agree on how much energy can be saved and what is the best shading strategy overall.

Shading devices lower the energy use for cooling. Harkness (1988) showed that exterior precast concrete overhangs and fins reduce the cooling load by at least 50% in Brisbane, Australia. Brambley *et al.* (1981) showed that sunscreens reduce cooling loads by 23% in San Diego. Halmos (1974) demonstrated that external shading devices installed on double pane, clear glass windows reduce the cooling load by 75%.

A number of researchers showed that most shading devices contribute to increases in energy use for heating while they reduce the cooling load. Bilgen (1994) found that automated Venetian blinds between panes increase the heating load by 4-6% and reduce the cooling load by 69-89% in Montreal. Treado *et al.* (1984) showed that various types of shading devices increase the heating load while the cooling load is reduced; the net energy savings only occur if the reduction in cooling energy use exceeds the increase in heating energy use. In general, it was demonstrated that cooling loads are reduced with increasing *shading coefficient* (i.e. better shade), while the opposite was observed for the heating load. Higher *shading coefficient* (i.e. better shade) results in higher heating loads. According to Treado *et al.* (1984); as the respective shares of total energy use due to heating and cooling loads depend on the climate where the building is erected, so does the shading strategy. Emery *et al.* (1981) also found that shading strategies are strongly climate dependent.

According to them, fixed overhangs and fins yield a modest reduction in energy use; and the best shading strategies in three American cities are:

- Reflective glazing,
- Heat absorbing glazing, and
- Glazing with exterior aluminium louvres.

Hunn *et al.* (1990, 1993) tested a variety of interior and exterior shading devices in a heating dominated climate and found that a higher performance is obtained with interior shading devices (as opposed to exterior fixed) when energy cost and use and peak demand reduction are analysed. Interior devices, which shade the entire glass while providing additional insulation to the window can save as much as 30% energy for cooling, resulting in annual energy savings of the order of 10% for offices.

Hunn *et al.* (1990, 1993) also showed that external shading devices are often net energy losers because they reduce useful solar gains during the winter. Heat absorbing glass, reflective glass, annual solar screens and overhangs plus fins almost always result in increased annual energy use. These observations confirm results obtained by Pletzer *et al.* (1988).

McCluney & Chandra (in Germer, 1984) found the opposite for the climate of Florida. They concluded that exterior devices (overhangs, awnings, window screens) are the best energy savers while tinted glass is the least energy efficient solution. Few authors showed that shading devices could reduce the energy use for both heating and cooling seasons.

In cold climates, however, exterior shading-devices can provide larger annual energy savings than tinted and reflective glass since they can be used seasonally; thus allowing for a passive utilisation of solar gains during the winter- (Dubois 1998). Awnings, overhangs and similar types of shading devices are of particular interest because they have low shading coefficient since:

1. They reject solar energy before it reaches the building and
2. Most of the heat absorbed in the shade is transferred by convection to the outdoor air. They also leave large part of the window view unobstructed, which is positive both in terms of occupant satisfaction and daylighting availability.

2.2 The Impact of Shading on Annual energy use, including electricity for lights

It is a fact that using dimming systems to replace artificial light by natural light reduces the energy use for lighting. Sullivan *et al.* (1992) showed that perimeter-zone electricity use for lighting is reduced by 73% through the use of daylighting. Authors disagree, however, on the benefits of using daylighting to reduce overall energy use (i.e. lighting, cooling and heating). Andresen *et al.* (1995) showed that for south facing windows in Trondheim, the use of daylighting results in 48% reduction in lighting load, 11% increase in heating loads and 70% reduction in cooling loads. Winkelmann & Lokmanhekin (1985) demonstrated that daylighting reduces the overall energy use by 10-22% and is cost effective in Miami, Los Angeles, Washington DC, and Chicago. The lowest energy use option is obtained when daylighting is coupled with clear glazing and external sun-control blinds for all the cities studied. Rundquist (1991) showed that, in Minneapolis and New York, increasing daylighting levels (through increases in window-to-wall ratio or shading coefficient) always reduce utility costs. He showed that when daylighting is used, windows provide utility savings relative to a solid wall. When daylighting is not used, increasing the window-to-wall ratio and the shading coefficient always leads to increased cooling and heating loads. This contradicts findings by Sullivan *et al.* (1992) who demonstrated that electricity use (cooling and lighting) and peak demand are almost linearly increased with increasing window-to-wall ratio and solar aperture (product of the shading coefficient and the window-to-wall ratio) in Los Angeles, when daylighting is used.

Various regulatory bodies in various parts of the world call for the well being of occupants. Also the same bodies and others call for energy efficient buildings.

In the UK, for example, daylighting standards are called for in the Workplace (Health, Safety and Welfare) Regulations. This stipulates that 'every work place shall have suitable and sufficient lighting' and that this lighting 'shall, so far as reasonably practicable, be natural light'. Also, non-mandatory advice and guidance on interior daylight is contained in BS8206 Part 2, and in the CIBSE Applications Manual on window design – see the reference list on appendix A.



IMAGING SERVICES NORTH

Boston Spa, Wetherby
West Yorkshire, LS23 7BQ
www.bl.uk

BEST COPY AVAILABLE.

VARIABLE PRINT QUALITY

2.3 Flat-plate Solar Collectors

The study-findings of thermal solar collectors through the years have reached a stage such that any attempts to increase efficiency and/or longevity of a collector, would be accompanied by substantial cost increases. Cost has, therefore, been made a top priority in research and development of solar collectors in recent years.

In flat-plate collectors – normally used in buildings - the issue of cost and payback period is somewhat more important than the efficiency itself.

The operation of a flat-plate collector is influenced by the following factors:

- Collector construction
- Solar factors: radiation intensity, diffuse fraction, incidence angle between the sun and the collector.
- Ambient conditions: fluid inlet temperature and wind speed; sky temperature.
- Operating conditions: air temperature; fluid flow rate and thermal properties; collector slope and orientation.

The efficiency of a flat-plate collector is a function of the optical properties of the cover and the absorber plate and the heat loss from the absorber plate. Typical efficiency values for flat-plate collectors are shown in Figure 2.1.

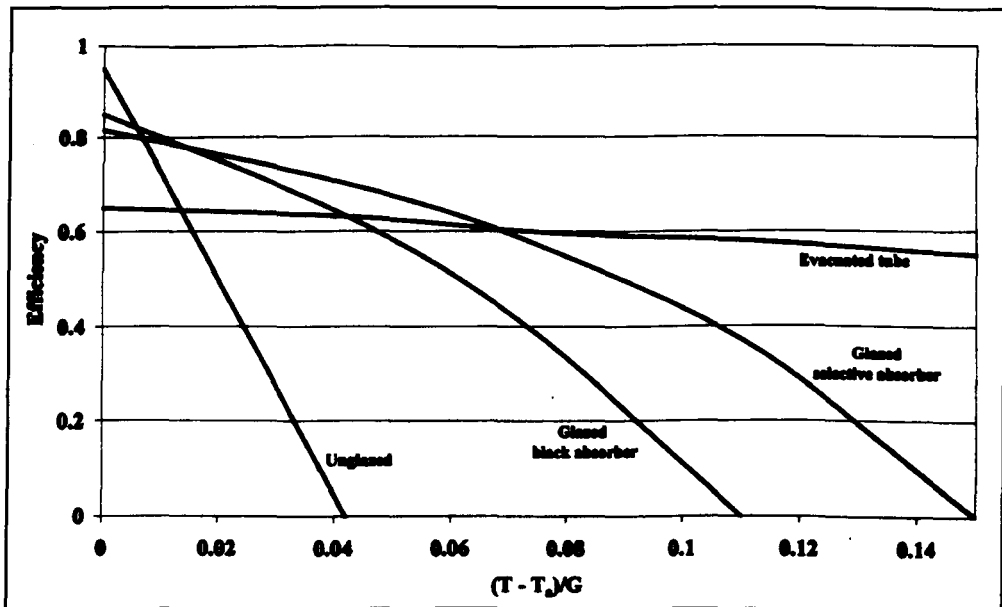


Figure 2.1 Typical efficiency of flat-plate collectors, based on the arithmetic average of inlet and outlet temperature of the collector (so $T = T_{av}$).

Taken from Morrison (2001).

Various attempts to improve the efficiency and enhance the performance of flat-plate collectors as well as lowering their cost and widening their application have been set forth. The following sections reflect these attempts.

2.3.1 Evacuated flat-plate collectors

In these, the flat-plate absorber is housed within an evacuated rectangular box. They have been developed for large collector arrays where on-site vacuum pumping can be justified. Maintenance of a vacuum in a flat-plate collector requires a structure between the back wall and the transparent cover to withstand the atmospheric pressure. The flexible edge seal around the glass cover allows slow leakage into the collector; so intermittent vacuum pumping is periodically required. If these were made to coincide with annual maintenance times, then this would be a success for evacuated flat-plate collectors, as they have better efficiency than normal flat-plate collectors.

2.3.2 Reverse flat-plate collectors

To extend the operation of flat-plate collectors to high temperatures, Kienzlen *et al.* (1998) investigated a reversed, or upside down, absorber-plate configuration. Radiation is directed onto the underside of plate by a stationary concentrator (reflector), as shown in Figures 2.2(a) and 2.2(b). Heat loss from the absorber is significantly reduced, as the upper side of the plate is insulated and there is little convective motion in the air layer below the plate.

Compared with normal flat-plate collector, the reverse plate collector has lower optical efficiency due to the scattering losses in the reflector.

An extension of this concept is the double-sided flat-plate collector investigated by Goetzberger *et al.* (1992) shown in Figure 2.3.3(a), and the systems investigated by Eames and Norton (1993,1995) shown in Figure 2.3.3(b).

It can be seen that such collectors are hard to integrate into buildings, due to their bulky geometry.

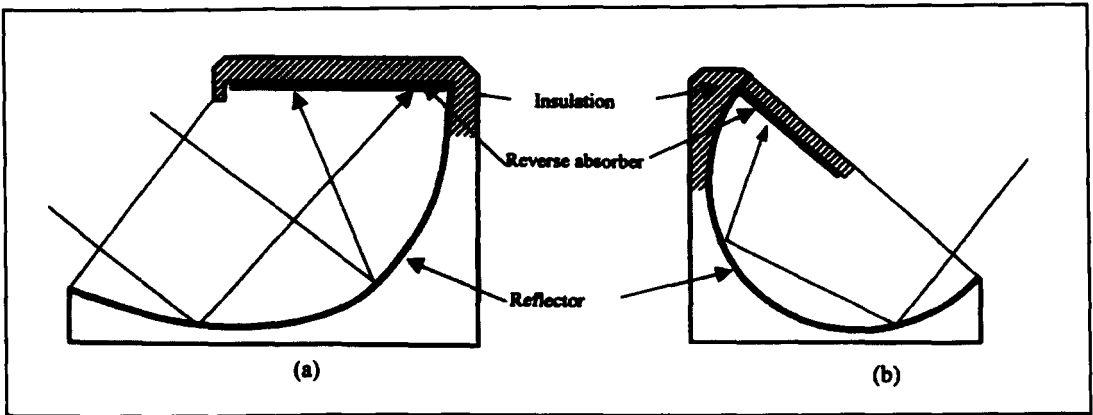


Figure 2.2 Reverse flat-plate collectors-Kienzlen *et al.* (1998)

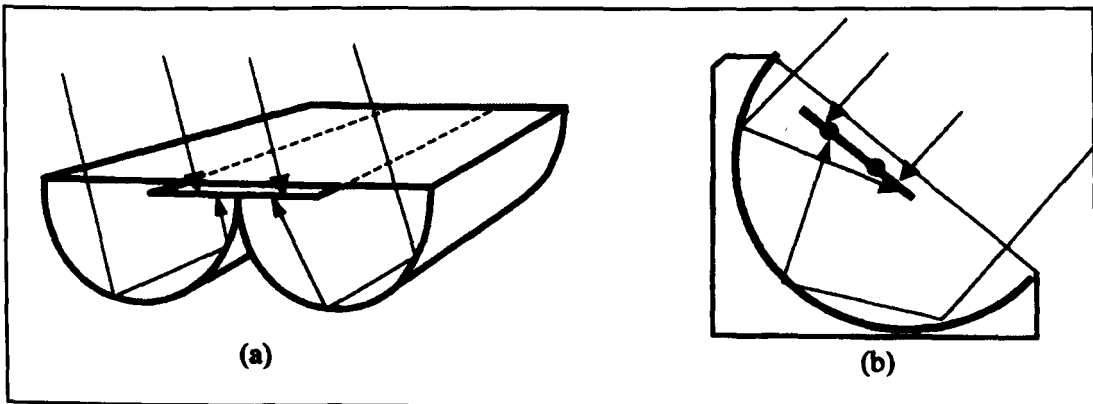


Figure 2.3 double-sided flat-plate collector- Eames and Norton (1993,1995)

2.3.3 Low-Cost Solar Water Heating

The main focus of this research has been on designing the shading louvres to act as a collector, and on the evaluation of the total effect (shading and energy collection) on the annual energy use of buildings. Nonetheless, water heating consumes some energy in office buildings.

Also if water could be heated cheaply by solar energy, then it serves as preheated water, which could be boosted by gas to fuel absorption cooling and space heating.

The low-cost water-heating concept involves replacing copper and glass in current solar domestic hot water system designs with lower-cost materials, especially

polymers and elastomers. Potential polymer solar components include un-pressurized integral collector storage and a flat-plate collector, as described in the chapter (1) – *Introduction*.

Researchers are examining the durability of thin films and other polymer components. The successful use of polymers in solar applications requires overcoming two engineering challenges:

- The thermal conductance of polymers is much lower than that of metals, which can reduce water heating performance; and
- Not all polymers weather well in the sun, due to ultraviolet solar radiation.

Lower thermal conductance can be largely accommodated with designs that place the heat transfer fluid in direct contact with the absorber – rather than indirectly, such as through the use of fins. In addition, the polymer industry is developing new polymer materials manufactured with chemical additives that result in higher thermal conductance and protection from UV radiation. The success of these attempts and efforts are to be seen. Laboratory researchers and other experts see great potential for constructing solar water heating systems with polymer materials. Polymers could replace or reduce the need for glass, copper and steel in the piping and the collector. The material and manufacturing cost per unit area is much lower for polymers, so manufacturing cost could significantly be reduced. They also weigh much less, which reduces the cost of shipping, handling, and installations.

2.4 Solar assisted air-conditioning systems

It has been pointed out, already in various literature, that the economical and energy efficiency of a solar-assisted air conditioning system does not depend on the maximum efficiency of the constituting parts only (or alone), but rather on their interaction and also the interaction of the system (i.e. the constituting parts) with the load. Furthermore, different climates will favour different choices.

The two obvious choices for solar air conditioning are absorption and adsorption systems.

2.4.1 Solar Absorption Cooling

Absorption chillers are applied in most solar-assisted air conditioning systems that are in operation today. The main challenges to achieve a further penetration of absorption chillers in solar-assisted air conditioning systems are the following:

- The machines on the market are intended for large-scale applications; but there is also a demand for smaller solar-assisted air-conditioning systems (no doubt about that)
- *LiBr* absorption chillers need a cooling tower
- Efficiency and capacities are small at low ($<70\text{ }^{\circ}\text{C}$) driving temperatures
- More expensive collector types (e.g. vacuum tubes, CPCs) are required in combination with these absorption chillers to guarantee a sufficient efficiency.

Research relevant to solar air-conditioning systems aims to address these challenges. Improving the efficiency and performance of flat-plate collectors by, for example, reducing the losses through the cover, could make them attractive for solar absorption applications. Argon filled, or even vacuum covers are a feasible option. Solar absorption cooling shows a promise for commercialisation. Various government departments, agencies and research institutions from around the world are currently working to improve the prospects of this particular renewable energy application. In the UK, for example, the department of the environment (DoE) recently issued a solicitation for proposals to significantly reduce the *life-cycle energy cost* of solar absorption cooling technology; improve the technical feasibility of advanced-cycle solar absorption cooling; and bring the technology closer to commercialisation. This would be more feasible once the cost of improved flat-plate collectors and evacuated-tube collectors drop even further.

2.4.2 Solar Adsorption Chillers

Adsorption chillers have a higher efficiency at low driving temperatures than absorption chillers. This is only so at low temperatures ($55\text{-}70\text{ }^{\circ}\text{C}$).

Adsorption technology, however, has few weaknesses:

- They are more expensive per *kW* cooling capacity than absorption chillers
- There is a limited market choice (only two manufacturers)
- The process has a cyclic nature, which requires more effort in design and control

- The machines are big and heavy.

Research in Solar adsorption chillers aims to cancel the weaknesses and improve the benefits of adsorption technology.

2.5 Solar Louvres

Shading devices could be made from either using a straight or curved surfaces. Figure 2.4 below shows cross-sections of four possible types of such shading surfaces.

East and west fenestrations could benefit from installing operable vertical strips of such surfaces, while sun-facing fenestrations (south-facing in the northern hemisphere) benefit from these surfaces arranged on the horizontal plane (overhangs) above the fenestrations.

If one seeks to convert these shading louvres to become solar collectors, then concentrating collectors (Parabolic or Fresnel type) would be excluded from early, in the selection process, based on the fact that they require a certain distance (focal length) between the concentrator/reflector and the receiver. This, consequently, would dictate the construction of the louvres in such a way that they become bulky, making them susceptible to drag force – see Figure 2.3 and Figure 2.3. Also it would impact adversely on their aesthetics. Further, concentration would need daily sun tracking, which is not possible with south-facing shading louvres; they could track seasonally, but not daily.

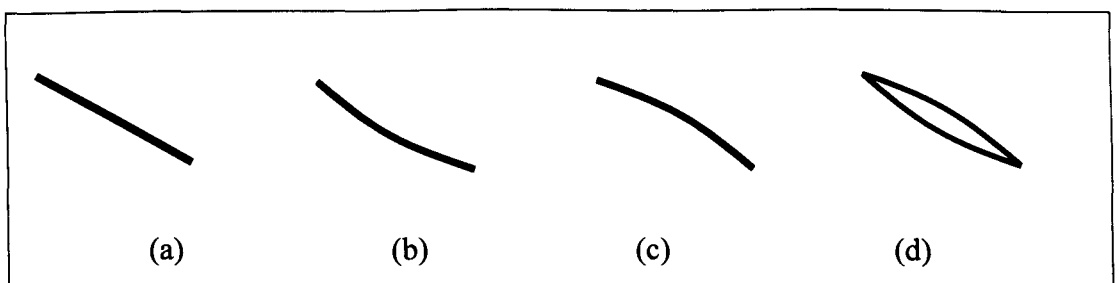


Figure 2.4 Cross sections of shading louvres.

As it has been mentioned in the previous chapter – *Introduction* – there is no evidence in the current literature to suggest that there is a shading device in the form

of louvres, which shades as well as collect thermal solar energy. Therefore there is no quantification, characterization or any attempted analysis for the louvre as a solar collector.

However, there is one that collects solar energy and converts it to electricity, via photovoltaic cells. This is commercially called “*Shadovoltaic*”. For more information on this, please refer to www.coltgroup.com

Chapter Three
Aesthetic Overview

3. Aesthetics Overview

In this chapter, the aesthetic impact of converting shading louvres into active solar collectors has been examined, and presented.

3.1 Aesthetics of conventional solar collectors

The problem facing building designers and architects today is how to integrate and blend solar collectors, (and other renewable energy systems), with the building's envelope.

Figures 3.1 and 3.2, below, show such lack of integration, and there are worse cases.

This lends support to research and development of solar façade components.

One could see that it would aesthetically be far much better if the roof tiles/slates themselves were made to act as thermal collectors. This concept has already been exploited in the case of photovoltaic.



Figure 3.1 Evacuated-tube collector



Figure 3.2 Flat-plate collector

3.2 Shading Louvres

Shading louvres offer maintenance-free aesthetically pleasing protection from solar gain. They can be fitted to both new and refurbished buildings. They are normally constructed from extruded aluminium sections, which can be supplied in an anodised, or powder coated finish to suit the building design - Figure 3.3.

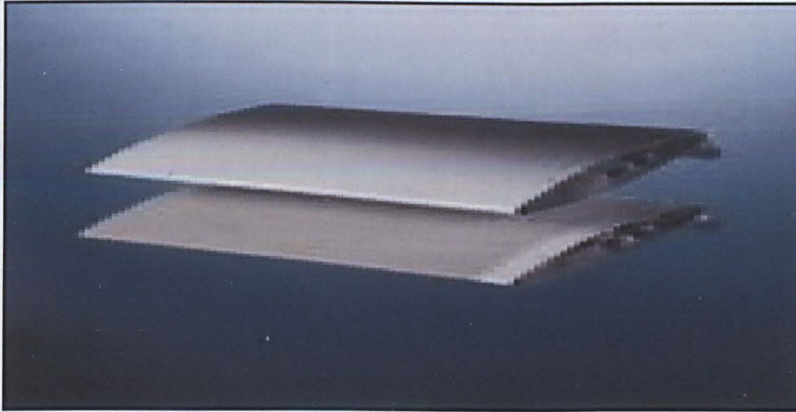


Figure 3.3 Aluminium shading louvres

Louvres fall into two main categories - *Fixed Louvres*, *Operable Louvres*.

These are available in a variety of widths, usually from 100mm to 250 mm, and can be mounted either vertically or horizontally. *Operable louvres* can either be manual or motorised. The motorised option is equipped with a low-energy synchronous motor, giving precise elevation and timed control, governed by wind and solar sensors.

With virtually no alterations, to neither the shape nor the aesthetics of these louvres, the current project is focused on harnessing energy from the solar irradiation incident on these louvres.

With modifications to the interior of these louvers, direct-flow configurations utilizing forced-convection methods, as well as heat-pipe configurations utilizing the latent heat of evaporation/condensation, have been considered, to efficiently transfer the absorbed solar energy.

The following page shows photos depicting external shading louvres in horizontal and vertical arrangements.



Figure 3.4 Shading louvres in various arrangements.

It can be seen from the above pictures that architects already use shading louvres, and as long as the shape and appearance of these louvres are kept unchanged, they could then offer energy collection opportunities without impacting adversely on the overall aesthetics of the building.

The only proposed change to the appearance of these louvres has been confined to colour.

In order to maximise heat collection rate, the outer surface facing the sun must be from the dark side of the colour spectrum. This is also dictated by economic factors such as price of the absorbing material and its application method. Titanium Oxynitride and Black Chrome have been nominated as the most plausible absorbing materials; fulfilling the thermal energy, economics and aesthetics requirements. Titanium Oxynitride has a dark-blue colour and Black chrome is simply matt-black.

Now one could draw the conclusion that no noticeable modifications should be made to the appearance/aesthetics of these louvres, except the colour. And there are few more options to colour: gunmetal green and black-grey are some examples.

The use of aluminium louvres could be extended to:

- Cladding
- Balconies
- Ventilation grills
- Roofing

This extension of application, therefore, would increase the heat-collection surface/façade of the building – see Figures 3.5, 3.6 and 3.7.

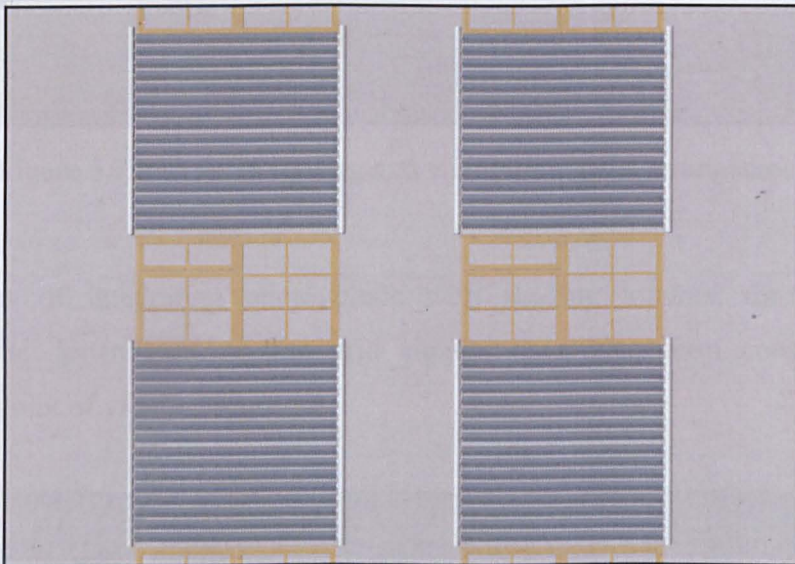


Figure 3.5 louvres in cladding arrangements.

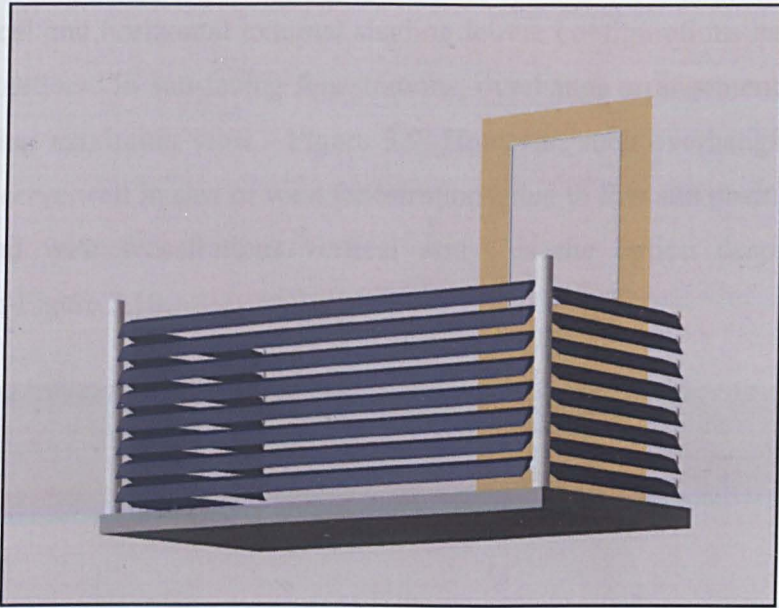


Figure 3.6 louvres in a balcony arrangement.

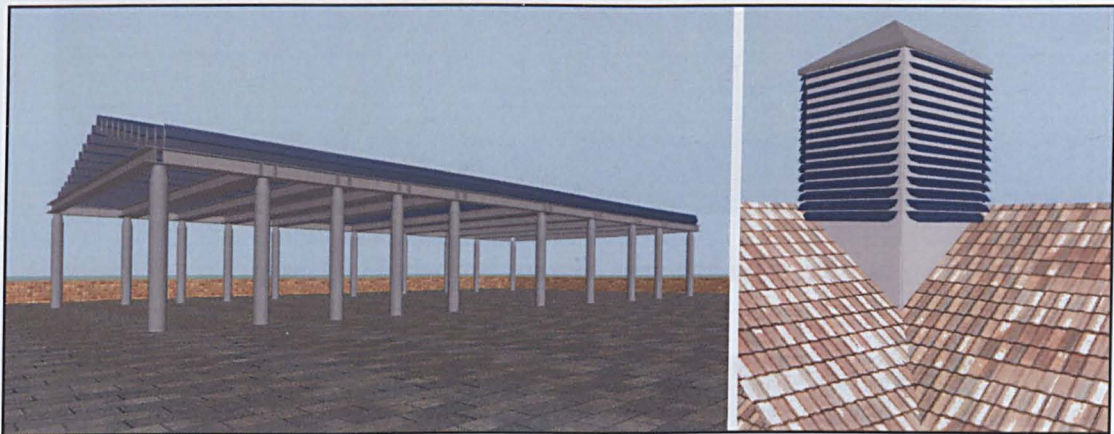


Figure 3.7 louvres in roofing and ventilation grills arrangements.

Possibilities of integrating photovoltaic with shading louvres, for pumping to decrease the dependency on the grid supply, have also been considered from aesthetics point of view – Figure 3.8.

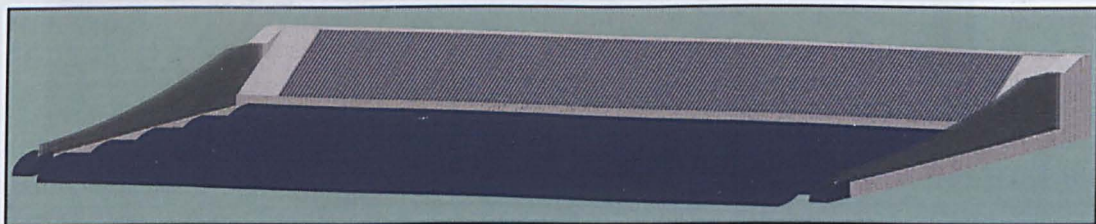


Figure 3.8 Integrated photovoltaic with louvres.

Both vertical and horizontal external shading louvre configurations have their use in various situations. In sun-facing fenestrations, overhangs arrangements are favoured for providing maximum view - Figure 3.9. However, such overhangs arrangements would not serve well in east or west fenestrations, due to low sun positions.

In east and west fenestrations vertical arrays is the option despite the vision obstruction-Figure 3.10.

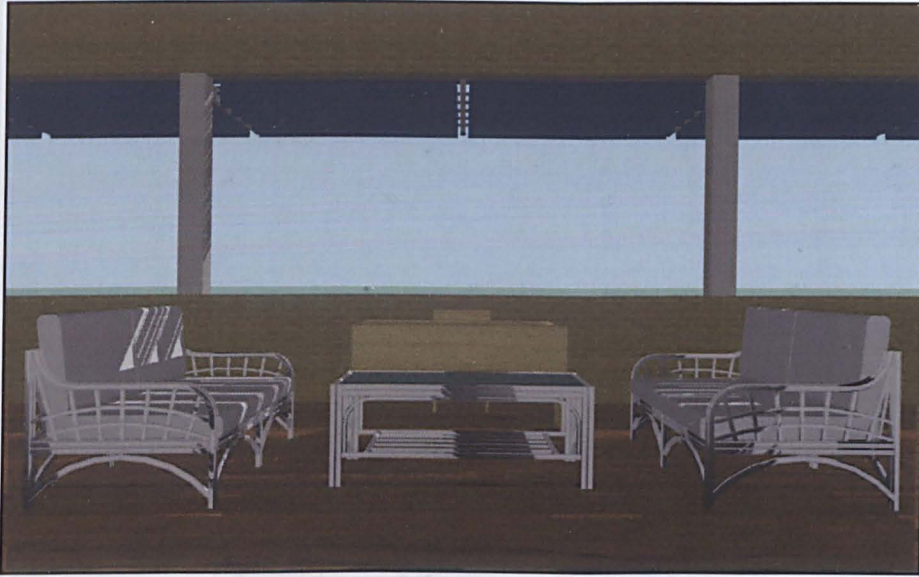


Figure 3.9 Horizontal louvres arranged as overhang.



Figure 3.10 Louvres arranged vertically.

Chapter Four

Preprototype Investigations

4. Preprototype Investigations

In order to arrive at a suitable design, the process necessitates the use of mathematical modelling, which often involves computational techniques and could entail simulation work. Modelling and simulations are powerful design-tools, today, albeit their validation and verification often obliges the user to resort back to experimental results.

Analytical techniques used as a tool in the process of the louvre design are presented in the next chapter, *chapter (5)-The Design*. Simulation scenarios, for an office building in Winterthur/Switzerland, utilizing these louvres as shading device as well as a solar collector has also been carried out, and are presented in *chapter (8) – Simulation Study*.

The work presented in this chapter, however, merely concerns the building of a reliable, indoor, solar collector testing-facility.

In order to establish confidence in the subsequent results from the test facility, the testing of a solar collector, with known performance characteristics, has been identified as the most practicable solution. This has been achieved by using two types of solar collectors, provided by *Thermomax (UK) Ltd* – see reference list on *Appendix A*. And already being commercial products, their specifications and performance characteristics are known.

These collectors are known commercially as *Mazdon*[®] and *Solamax*[®], and they utilize heat pipe and direct flow configurations, respectively - Figure 4.1.

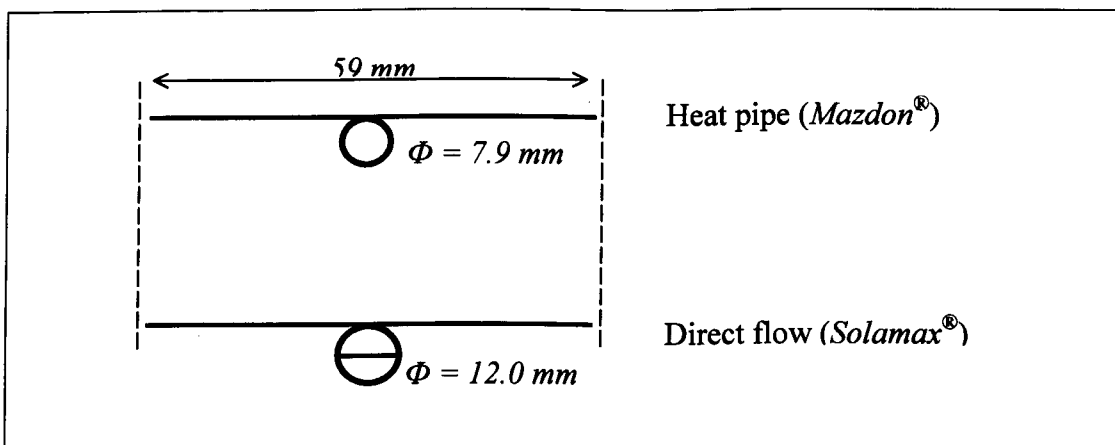


Figure 4.1 Cross sections of a heat pipe and of a direct flow solar collector

These two types of collectors have been tested completely unglazed (i.e. no cover), as well as completely glazed by factory-sealed vacuum tubes.

Both types utilize a copper strip coated with Titanium Oxynitride, having the Emissivity of 0.10 ± 0.02 , and Absorbance of 0.96 ± 0.02 .

The absorber plate/strip has dimensions as: $59 \times 1705 \times 0.127 \text{ mm}$ - Figure (4.1).

Each of the two collectors uses ten strips, giving each a total collector area, A_{col} , of approximately 1.00 m^2 – (i.e. $0.059 \text{ m} \times 1.705 \text{ m} \times 10 = 1.00595 \text{ m}^2$).

The only difference between the two types is that the direct flow pipe has a larger diameter, split into two compartments. The circulation is arranged such that the back-compartment receives the circulating fluid first – see Figure 4.1.

4.1 Solar Collectors Performance Testing

Solar collectors can be tested, in the lab, under steady state conditions or outdoor by a dynamic test procedure. Steady state testing has been widely used and the procedures are well documented for both glazed (ISO9806-1, 1994) and unglazed collectors (ISO9806-3, 1995).

The European practice is to base the collector test results on the arithmetic average of the fluid inlet and outlet temperatures, T_{av} . Other countries (USA) use others methods; they base the results on the inlet temperature, T_{in} .

According to Duffie (1991, p 305), conversion methods between test results are readily available.

The ASHRAE 93-77 recognises that test procedures differ in features, yet all can be summarized as follows:

- Means are provided to feed the collector with fluid at a controlled inlet temperature; tests are made over a range of inlet temperatures.
- Solar radiation is measured by a Pyranometer on the plane of the collector.
- Means of measuring flow rate, inlet and outlet fluid temperatures, and ambient conditions are provided.
- Mean are provided for measurements of pressure and pressure drop across the collector.

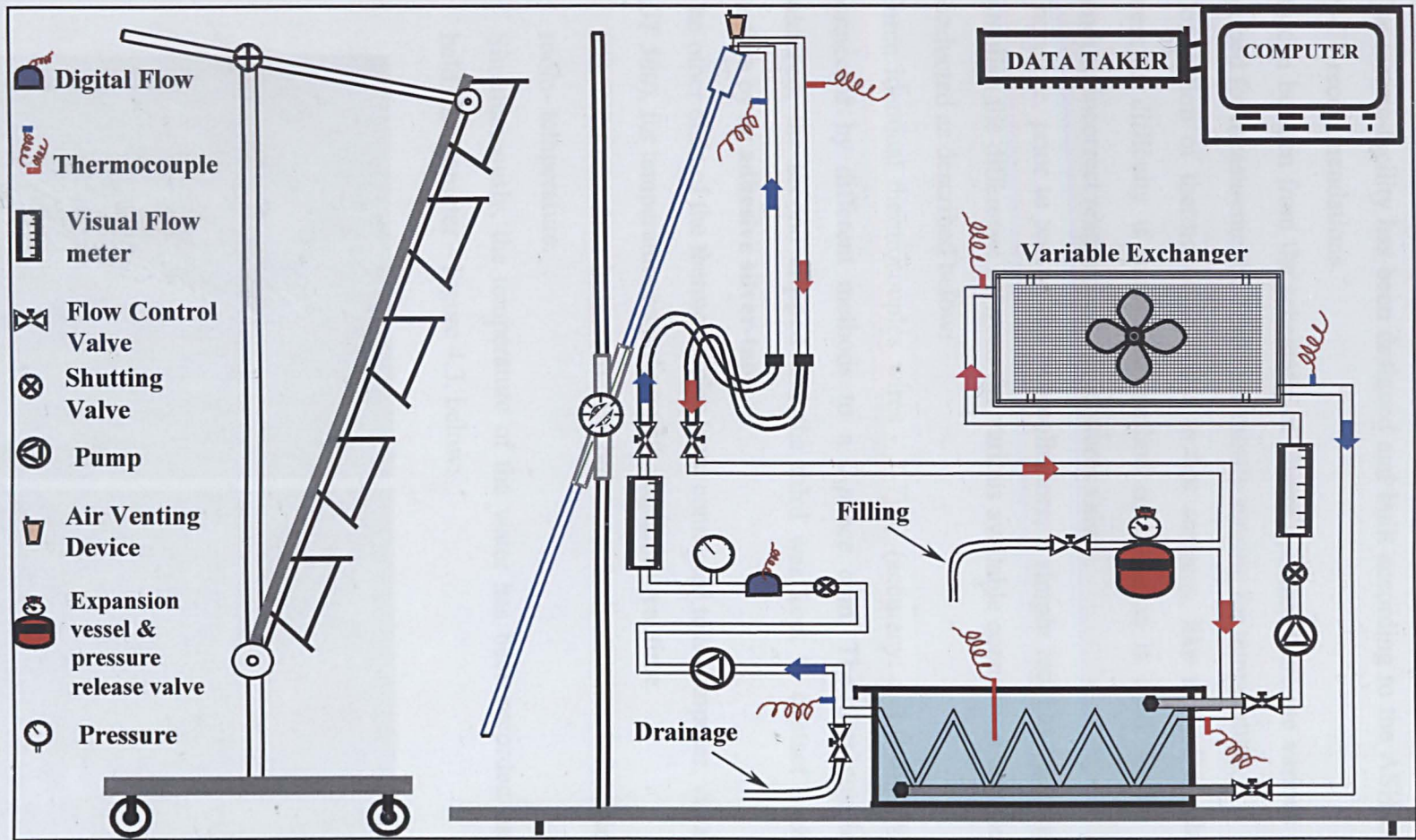


Figure 4.2 Schematic of the testing-facility for flat plate liquid solar collector

4.2 Apparatus and instrumentation

The testing-facility has been designed and built according to the ASHRAE standard 93-77 recommendations.

As can be seen from the schematic of Figure 4.2, that there are various points to be probed for measurements. These are mostly sensing for temperature.

Connection of thermocouple wires to hot surfaces, like that of a solar collector, presents difficulty if unsuitable method of adhesion is used. Loose connections produce incorrect readings of temperatures values.

Therefore, prior to testing the two collectors, a simple test has been carried out to establish the difference between the various available connection methods. This was conducted as described below:

Three identical thermocouples wires - *T-Type* (accuracy: ± 1.0 or 75%)- were all connected by different methods to a 2-pence coin. The first couple was **soft-soldered**, the second **clipped** and the third was kept in contact with the coin's surface by an **adhesive silver-tape**.

The other ends of the thermocouples were connected to a computer, via a data logger (*DT 500*), for temperature recording with respect to real time.

- The coin was then immersed in a hot water bath and was left to cool down to room- temperature.
- Simultaneously, the temperature of the water has been recorded using a hand-held thermometer – Figure 4.3, below:



Figure 4.3 Temperature of water as being measured by three couples, attached using different bonding methods.

The result of this test has been plotted as shown in Figure 4.4, below:

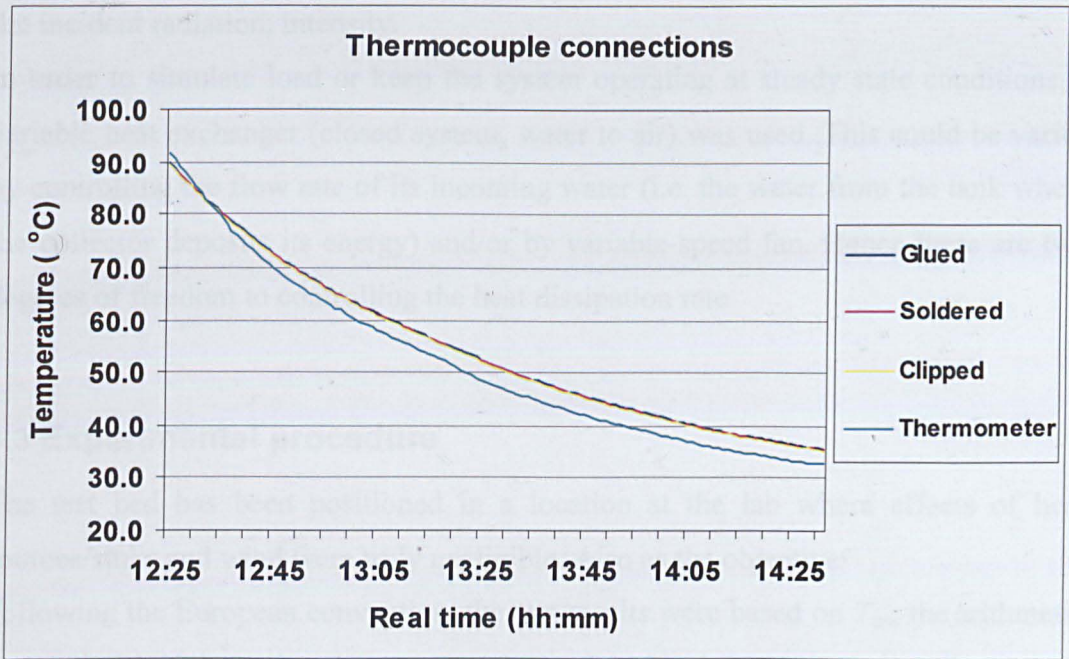


Figure 4.4 Methods of thermocouples connections.

The graph of Figure 4.4 shows negligible difference between the three methods of bonding the Thermocouples to the coin.

However, the method favoured and used throughout the tests was that of the **adhesive silver-tape**, due to its ease of application (and removal) and reliability.

The apparatus is probed for measuring temperature, pressure and flow rate at specific points as shown on Figure 4.1.

A data logger/taker (*DT 500*), in conjunction with a computer, managed these measurements in real time.

T-type thermocouples (accuracy: ± 1.0 or 75%), Turbine-type digital flow rate meter (accuracy: Linearity at FSD frequency is $\pm 1.0\%$) were utilized for the task.

Further, conventional pressure gauge (accuracy class: 1.6 per DIN 16005), a visual flow meter (accuracy: ± 2.0 , repeatability: $\pm 1.0\%$) and a hand-held thermometer (accuracy: $\pm 0.2\%$ rdg + 1°C) were all used for the validation of measurements.

A pyrometer (KIPP & ZONEN; TYPE: CM11) with sensitivity $4.56 \times 10^{-6} \text{ V/Wm}^2$) has been used in connection with a Digital Multimeter (Robin AR4003) to measure the incident radiation, intensity.

In order to simulate load or keep the system operating at steady state conditions, a variable heat exchanger (closed system, water to air) was used. This could be varied by controlling the flow rate of its incoming water (i.e. the water from the tank where the collector deposits its energy) and/or by variable-speed fan. Hence there are two degrees of freedom to controlling the heat dissipation rate.

4.3 Experimental procedure

The test bed has been positioned in a location at the lab where effects of heat sources/sinks and wind were truly negligible. Also as the objective

Following the European convention, the test results were based on T_{av} , the arithmetic average of the inlet and outlet temperatures, rather than inlet temperature, T_{in} .

Also, it must be stated that A_{col} , the area of the collector, refers to the area of the unshaded absorber-plate area – taken as (1.0 m^2) .

The closed-loop system was filled with water, as the working fluid, to a pressure of 1.0 bar and was purged completely from air. Also the heat-storage tank was filled with water (24 litres). The choice of water as the working fluid is explained in chapter (6), section 6.1, *Preparations*.

Unlike the sun a group of light sources produce nonuniform radiation distribution on the surface of the collector, creating hotspots. To avoid this, the surface of the collector was fictitiously divided into 27 small regions, on which the incident radiation intensity was allowed to be $\pm 10\%$ off the intended radiation level. Measurements at the centre of each region have been recorded, for each radiation level, as shown in Table 4.5.

The general test procedure is to operate the collector in the testing-facility under steady-state conditions, with the incident radiation normal to the collector surface.

And in order for this steady state to be achieved, the temperature of the tank, (where heat from the collector is being deposited), must be kept constant. This has been achieved during the tests via the variable-load heat exchanger.

Water was circulated at 20 g/s/m^2 (total of: 1.2 litre/min), and choices of tank-temperatures ($21, 24, 27 \dots 45 \text{ }^\circ\text{C}$) were used for each radiation level; namely, ($200, 400, 600, 800$ and 1000 W/m^2). Please note that this variation of tank temperature automatically implies a variation of the inlet temperature T_{in} .

Once Steady state conditions were achieved for the particular combination of tank temperature and radiation level (i.e. also at stable tank temperatures), measurements were recorded and averaged over 10-15 minutes.

As would be expected, this produces a vast number of readings.

Intermittent temperature checks were performed at various probed points, using the hand-held thermometer, and compared to readings from the data logger so as to establish some degree of reliability for the measurements recorded.

Values for the temperatures of the: inlet, T_{in} , the outlet, T_{out} , the mean plate T_{pm} , the ambient, T_a and the tank T_{tank} were recorded.

The mass flow rate of the water m_w , and the radiation I , were also recorded.

Further, the temperature to the inlet and outlet of the variable heat-load exchanger were also recorded (not included in the calculations).

The ambient T_a , varied between $20 - 30 \text{ }^\circ\text{C}$.

Values for the mean plate-temperature, T_{pm} , are made by taking the arithmetic average of nine thermocouples measurements attached on the back-surface of the absorbing-plates/strips, at top middle and bottom positions of the first, middle and last collector-strips. Figure 4.6 shows the positions of the top-row- top1, top2 and top3. Similar points the middle and bottom part of the collector (not Shown in Figure 4.6. For plotting purposes [graphs on Figures 4.16 and 4.17], the temperatures at the middle-row and last-row were named as: Middle1, 2 and 3 and Bottom 1,2 and 3 respectively.

200W/m² (0.91 mV)

0.8	0.8	0.8
0.9	0.8	0.8
0.9	0.9	0.8
1.0	0.9	0.8
0.9	1.0	1.0
1.0	1.0	1.0
1.0	1.0	0.9
1.0	1.0	0.9
1.0	1.0	1.0

400W/m² (1.82 mV)

1.6	1.7	1.6
1.6	1.7	1.7
1.7	1.7	1.6
1.9	1.8	1.6
2.0	1.9	1.7
2.0	2.0	1.8
2.0	2.0	1.9
2.0	2.0	1.9
1.9	2.0	1.8

600W/m² (2.74 mV)

2.5	2.5	2.4
2.6	2.5	2.5
2.8	2.8	2.5
3.0	3.0	2.8
3.0	2.9	2.9
2.9	3.0	2.8
2.9	3.0	2.9
3.0	2.9	2.8
2.7	2.8	2.7

800W/m² (3.65 mV)

3.1	3.2	3.2
3.4	3.5	3.4
3.8	3.9	3.6
4.0	4.0	3.6
3.9	4.0	3.8
4.0	4.0	3.9
3.9	4.0	3.7
4.1	4.0	3.6
3.5	3.8	3.4

1000W/m² (4.56 mV)

4.1	4.2	4.1
4.1	4.2	4.1
4.5	4.4	4.4
4.2	4.2	4.1
4.2	4.3	4.3
4.5	4.6	4.4
4.5	4.5	4.4
4.6	4.3	4.5
4.5	4.1	4.6

Table 4.5 Radiation distribution values on the collectors' surfaces, in mV.



Figure 4.6 Positions of the thermocouples (1,2 and 3) on the top-row of the unglazed collector (backside)

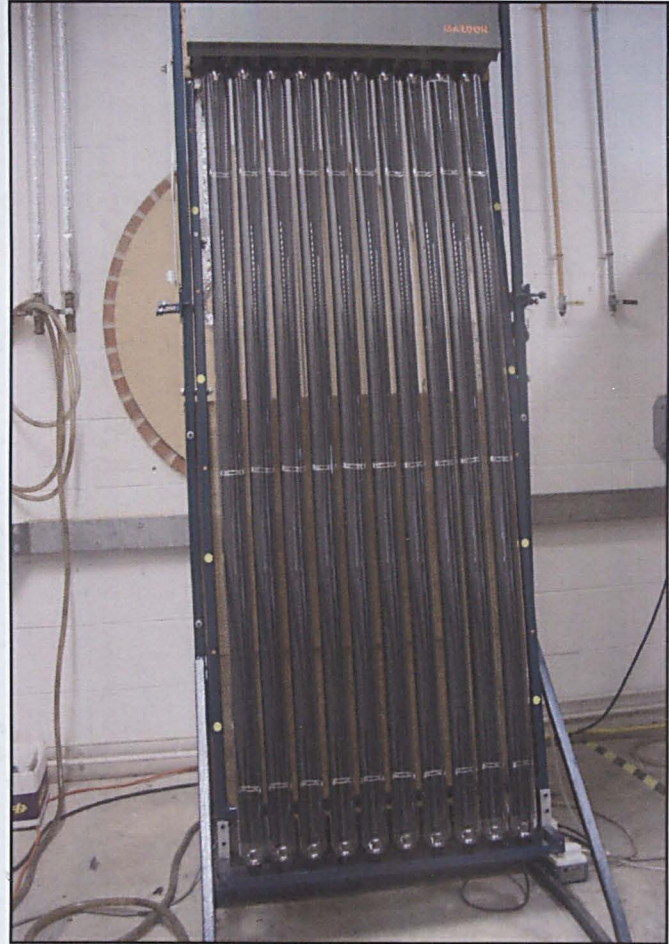


Figure 4.7 Front-side of the glazed collectors, positioned ready for testing

The analysis here is primarily based on standard procedures described in Duffie (1991, pp 301-307), and this as outlined below:

The efficiency of a flat-plate solar collector is defined as:

$$\text{Efficiency, } \eta_{col} = \frac{\text{Useful output}}{\text{Input}} \dots\dots\dots(4.1)$$

The *Input*, in the above equation, is given by

$\text{Input} = A_{col} I$; where A_{col} is the area of the unobstructed collector plate, and I is normal incident radiation, most of which is beam.

The *Useful output*, q_u is defined, in relation to its environment, as:

$$q_u = \text{Absorbed energy} - \text{Losses}$$

$$\text{i.e. } q_u = A_{col} [I(\tau_c \alpha_p) - U_c (T_{pm} - T_a)] \dots\dots\dots(4.2)$$

Where, $(\tau_c \alpha_p)$ is transmittance-absorptance product of the cover-plate for normal incident radiation; U_c is the overall loss coefficient, and T_{pm} is the mean plate-surface temperature.

T_a is the ambient temperature.

It is convenient to define a quantity that relates the actual useful energy gain of a collector, to the useful gain if the whole collector surface were at the fluid inlet temperature T_{in} .

This quantity is called the collector heat removal factor F_R , defined as “*The ratio of the actual heat transfer to the maximum possible heat transfer*”.

In equation form this is:

$$F_R = \frac{A_{col} [I(\tau_c \alpha_p) - U_c (T_{pm} - T_a)]}{A_{col} [I(\tau_c \alpha_p) - U_c (T_{in} - T_a)]} \dots\dots\dots(4.3)$$

Therefore, equation (4.1) can be rewritten as:

$$q_u = A_{col} F_R [I(\tau_c \alpha_p) - U_c (T_{in} - T_a)] \dots\dots\dots(4.4)$$

Similarly, as in equation (4.4), the *Useful output*, q_u , could be defined (European practice) in terms of the arithmetic average of the fluid inlet and outlet temperatures T_{av} , as:

$$q_u = A_{col} F_{av} [I(\tau_c \alpha_p) - U_c (T_{av} - T_a)] \dots\dots\dots (4.5)$$

Where F_{av} is the heat removal factor based on $T_{av} = (T_{in} + T_{out})/2$.

The *Useful output*, q_u can also be defined, independently of its environment, as:

$$q_u = m_w c_p (T_{out} - T_{in}) \dots\dots\dots (4.6)$$

Now the efficiency, defined as in equation (4.1), could be written in two ways:

- Using equation (4.5): $\eta_{col} = \frac{A_{col} F_{av} [I(\tau_c \alpha_p) - U_c (T_{av} - T_a)]}{A_{col} I}$; giving:

$$\eta_{col} = F_{av} (\tau_c \alpha_p) - F_{av} U_c \frac{(T_{av} - T_a)}{I} \dots\dots\dots (4.7)$$

- Using equation (4.6); giving:

$$\eta_{col} = \frac{m_w c_p (T_{out} - T_{in})}{A_{col} I} \dots\dots\dots (4.8)$$

Now Equating equations (4.7) and (4.8) gives:

$$\frac{m_w c_p (T_{out} - T_{in})}{A_{col} I} = F_{av} (\tau_c \alpha_p) - F_{av} U_c \frac{(T_{av} - T_a)}{I} \dots\dots\dots (4.9)$$

Where m_w , c_p and T_{out} are the mass flow rate, specific heat and outlet temperature of the working fluid, respectively.

Now equation (4.9), under steady-state conditions, is the key to correlating the experimental data, and plotting the efficiency curves.

In the calculation for the plotting of equation (4.9), the density (ρ) and specific heat capacity (c_p) of the water, at the different temperatures, were calculated using the equations recommended by ASME (1977).

The data points usually scatter, even for the best results, due to the fact that U_c is a function of temperature, and F_{av} (or F_R) is a weak function of temperature. However, one could assume that all U_c , F_{av} and $(\tau_c \alpha_p)$ are constants.

Once the data points of the collector have been plotted, performing linear regression on the plotted data points produces a straight line for the efficiency, as in equation (4.9). From this straight-line, it can be deduced that:

$$F_{av}(\tau_c \alpha_p) = \text{The intercept} \dots\dots\dots(4.9.a)$$

$$- F_{av} U_c = \text{The slope} \dots\dots\dots(4.9.b)$$

Parameter (4.9.a) describes how the collector absorbs energy, while parameter (4.9.b) describes how it loses it.

Further, this linearity also allows – Morrison (2001, p.197)- the following approximation:

$F' = F_{av}$, with an error of less than 0.5% if:

$$\frac{A_{col} F' U_c}{m_w c_p} \leq 0.25 \dots\dots\dots (4.10)$$

Most solar collectors satisfy the limit of equation (4.10).

The method for converting between F_{av} and F_R is given by Beckman *et al* (1977) as follows:

$$F_R(\tau_c \alpha_p) = F_{av}(\tau_c \alpha_p) \left[1 + \frac{A_{col} F_{av} U_c}{2m_w c_p} \right]^{-1} \dots\dots\dots (4.11)$$

$$F_R U_c = F_{av} U_c \left[1 + \frac{A_{col} F_{av} U_c}{2m_w c_p} \right]^{-1}$$

Equation (4.11) will be used in chapter (6) – *The Experimental Work*.



Figure 4.8 The testing facility - inset (top right) is the back part. [Collectors were tested in turn under similar/identical conditions].



Figure 4.9 Faulty vacuum picked by the colour of the oxidized chemical.

4.4 The Results

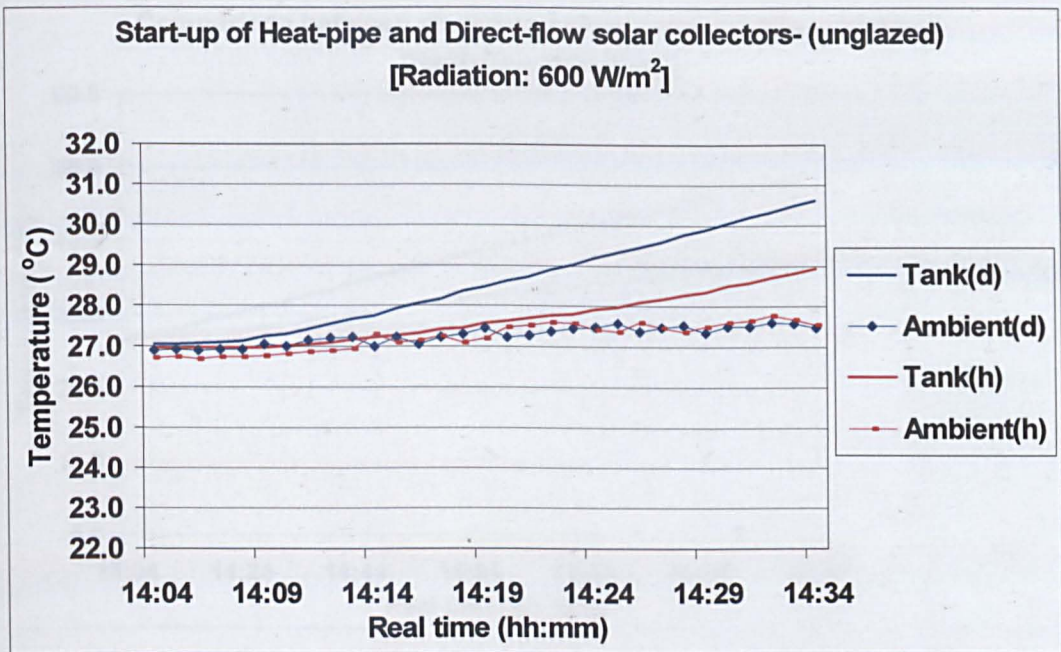


Figure 4.10 (d) indicates direct flow, while (h) indicates heat pipe collector

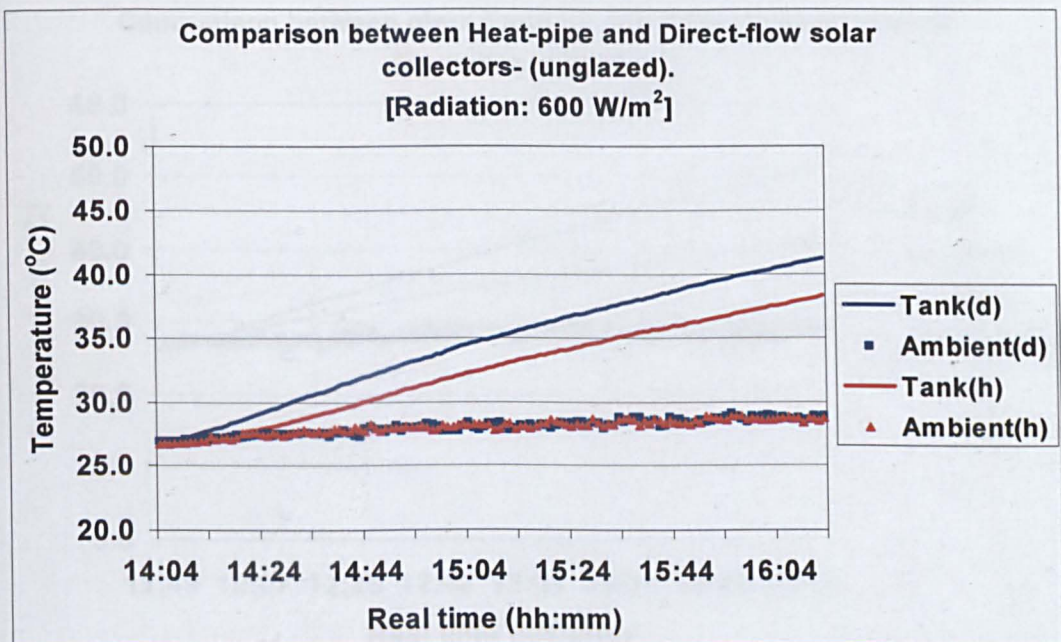


Figure (4.11) (d) indicates direct flow, while (h) indicates heat pipe collector

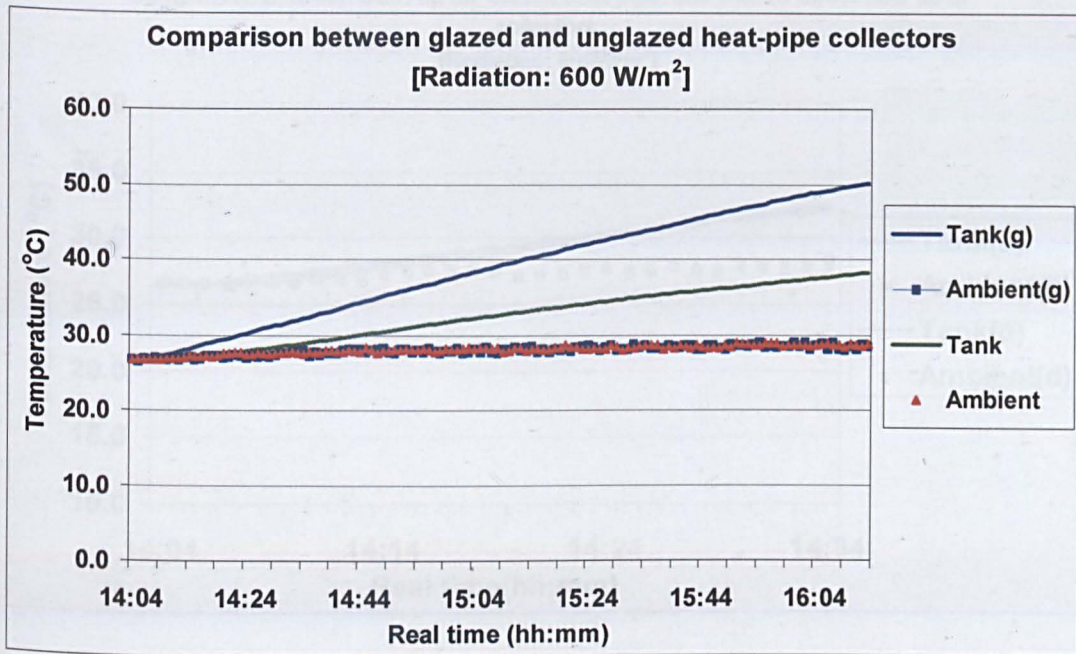


Figure 4.12 (g) indicates the glazed collector

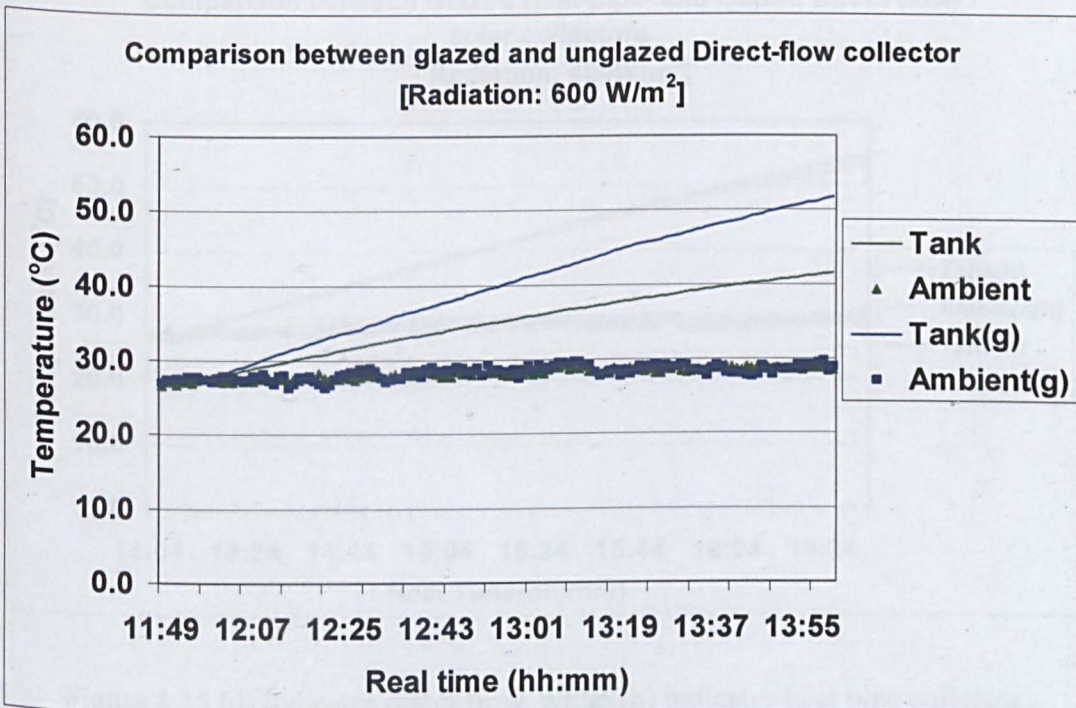


Figure 4.13 (g) indicates the glazed collector

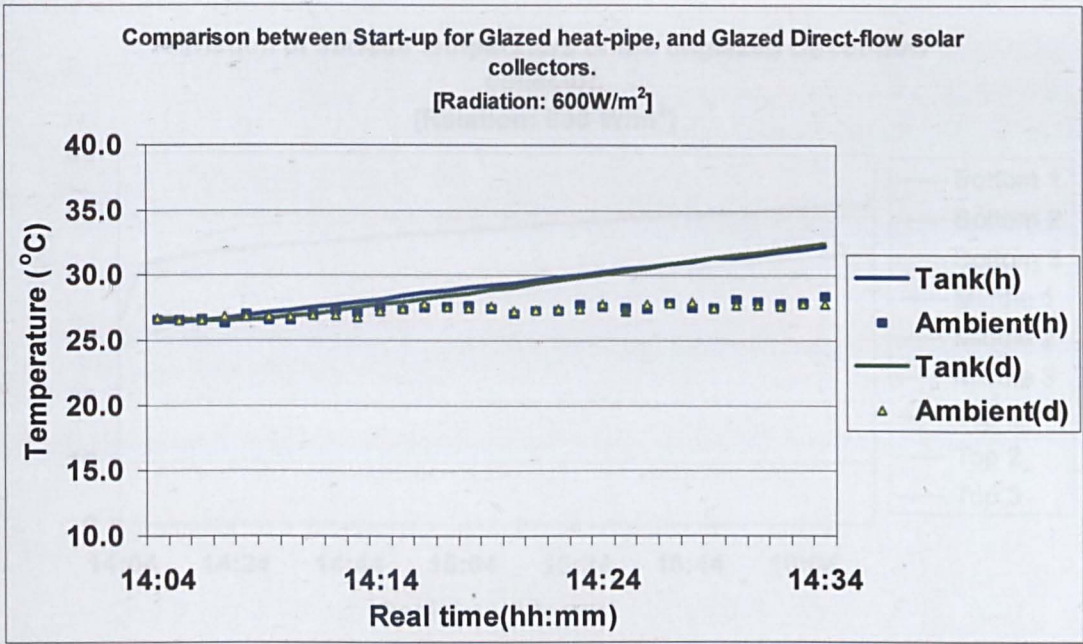


Figure 4.14 (d) indicates direct flow, while (h) indicates heat pipe collector

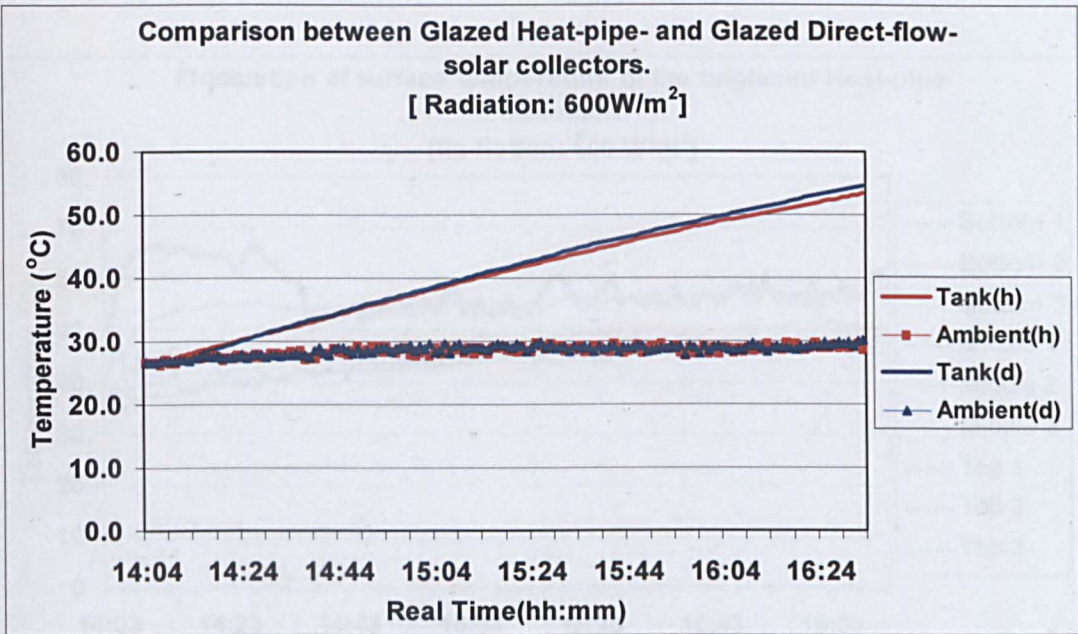


Figure 4.15 (d) indicates direct flow, while (h) indicates heat pipe collector

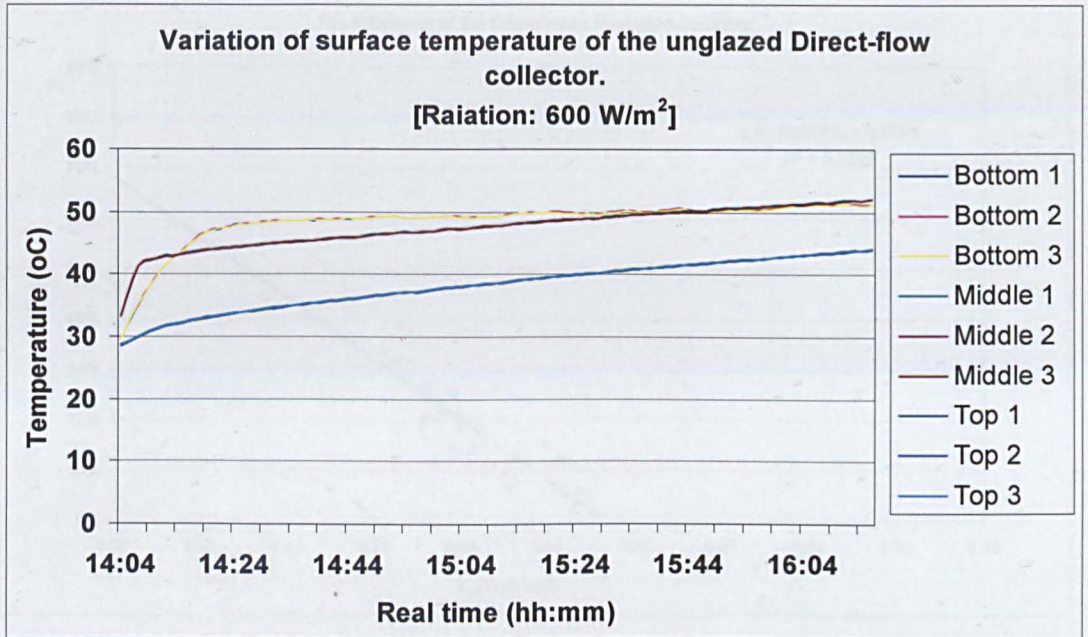


Figure 4.16 The Top, Bottom and Middle positions are as shown previously

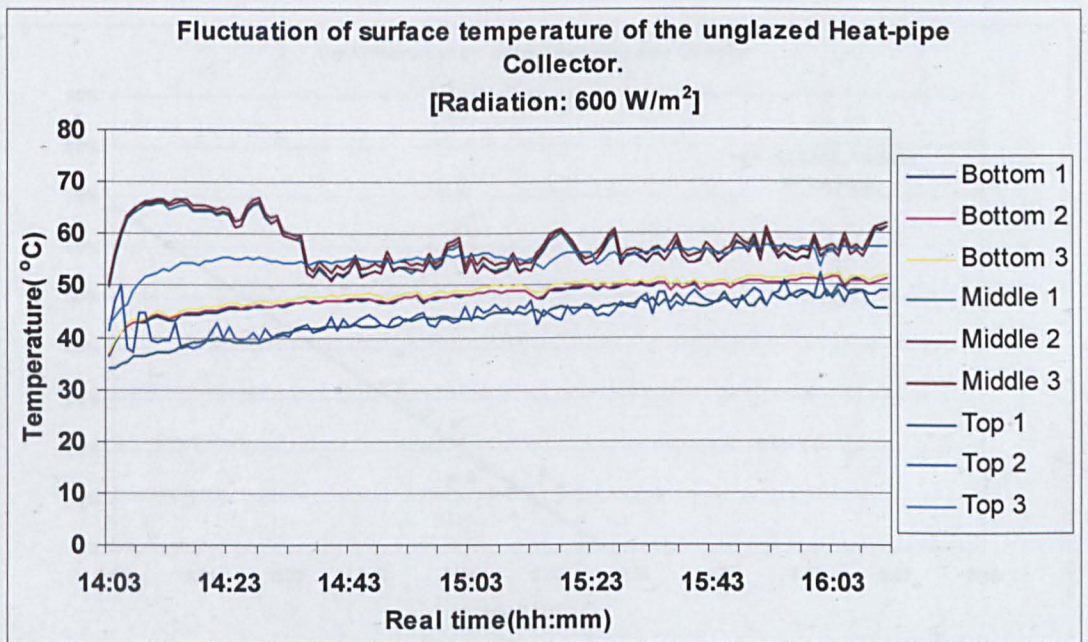


Figure 4.17 The Top, Bottom and Middle positions are as shown on page 43.

4.3 Summary

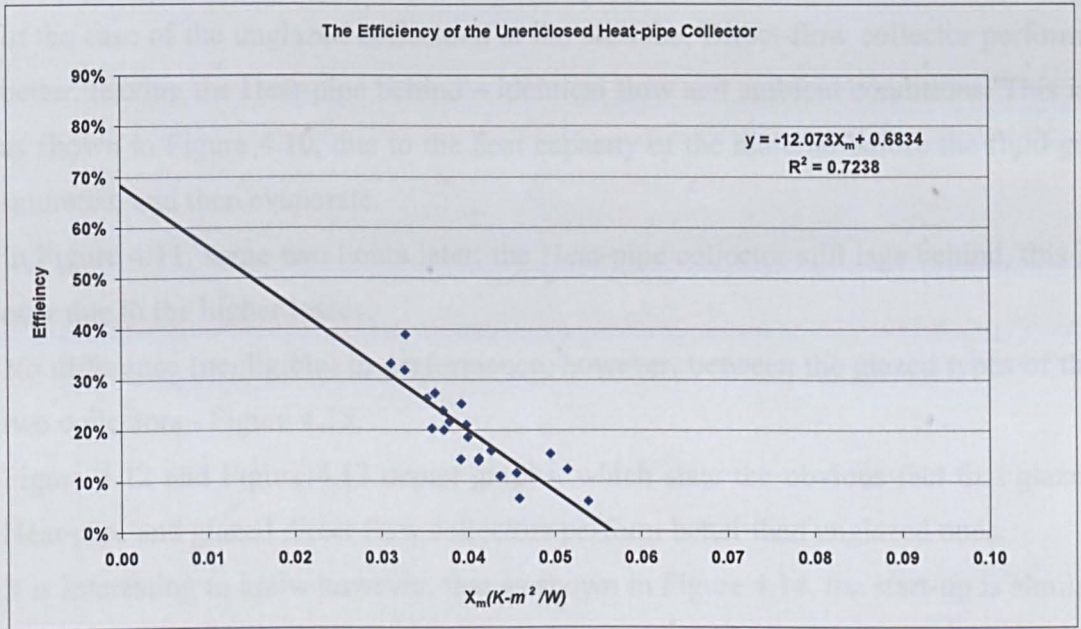


Figure 4.18 Efficiency of the solar collector as a function of $X_m = (T_{av} - T_a)/I$

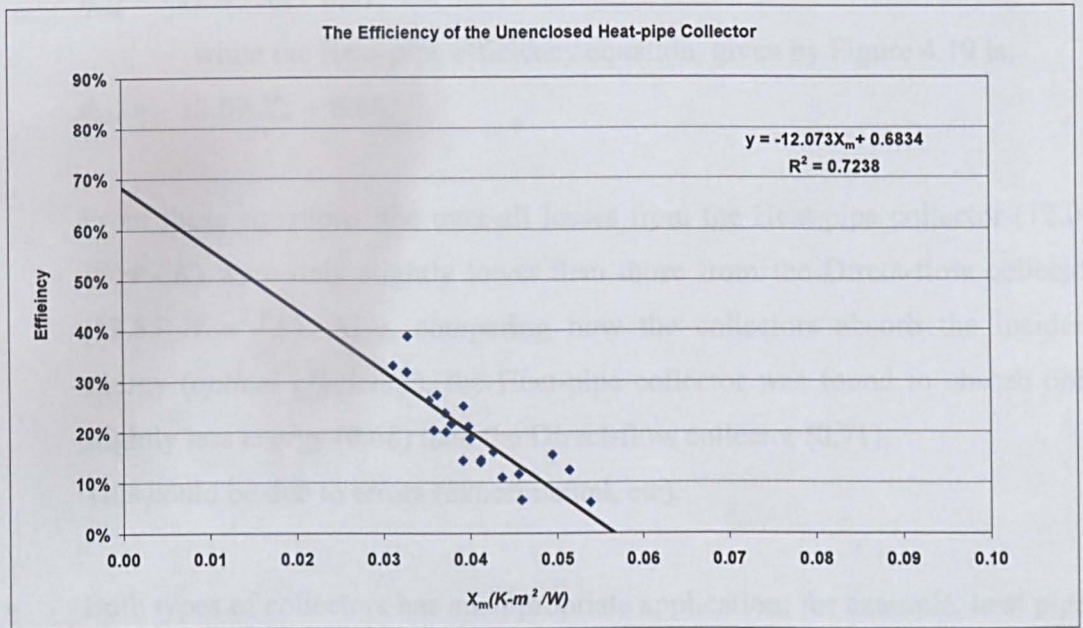


Figure 4.19 Efficiency of the solar collector as a function of $X_m = (T_{av} - T_a)/I$

4.5 Summary

In the case of the unglazed collectors, at the start the, Direct-flow collector performs better, leaving the Heat-pipe behind – identical flow and ambient conditions. This is, as shown in Figure 4.10, due to the heat capacity of the material before the fluid get saturated, and then evaporate.

In Figure 4.11, some two hours later, the Heat-pipe collector still lags behind, this is only due to the higher losses.

No difference (negligible) in performance, however, between the glazed types of the two collectors - Figure 4.15.

Figure 4.12 and Figure 4.13 depict graphs, which state the obvious fact that glazed Heat-pipe and glazed direct flow collectors perform better than unglazed ones.

It is interesting to know however, that as shown in Figure 4.14, the start-up is similar for both types of glazed collectors.

Figure 4.16, show the surface temperatures: the top-row is the lowest in temperature, as it is nearer to the circulating fluid. Figure 4.17 show the Middle-row exhibiting higher and fluctuating temperatures. Also there are fewer fluctuations at the top-row.

- The Direct flow efficiency equation, given by Figure 4.18 is:

$$\eta_{col} = - 12.85 X_m + 0.71,$$

while the Heat-pipe efficiency equation, given by Figure 4.19 is:

$$\eta_{col} = - 12.07 X_m + 0.68.$$

From these equations, the over-all losses from the Heat-pipe collector ($12.07 \text{ W/m}^2\text{-}^\circ\text{K}$) were only slightly lower than those from the Direct-flow collector ($12.85 \text{ W/m}^2\text{-}^\circ\text{K}$). Also, comparing how the collectors absorb the incident energy (*optical efficiency*), the Heat-pipe collector was found to absorb only slightly less energy (0.68) than the Direct-flow collector (0.71).

This could be due to errors (experimental, etc).

- Both types of collectors has an appropriate application; for example, heat pipes act as a thermal one-way valve, hence stopping heat from dissipating back to the environment.

For unglazed applications, as in heat recovery from used (warm) air in buildings, for example, Direct-flow collectors perform more efficiently than Heat-pipes collectors. This fact is supported by the fluctuation graphs –Figures 4.4.7 and 4.4.8, and by the collection graphs of the unglazed collectors – Figure 4.4.1 and Figure 4.4.2.

For glazed collectors, however, both types perform quite similarly under the circumstances.

- Finally, and most importantly, the overall results show consistency and general agreement, and the whole exercise has provided a reliable testing-facility that could be used for testing and help designing the actual prototype.

Chapter Five

The Design

5. The Design

Shading louvres have been categorised, in this research work, into two categories according to their geometrical shape. Those with flat laminar surfaces are termed *Laminar Louvres*, while those, having curved surfaces- looking like an ellipse - are termed *Voluminous Louvres* – Figure 5.1. Laminar louvres could not span as long as the voluminous louvres.



Figure 5.1 Laminar and Voluminous Shading Louvres

If one seeks to design the laminar louvres to accommodate a solar collector, then the possible outcome of the laminar louvres would, more or less, look like those depicted in Figure 5.2, below:

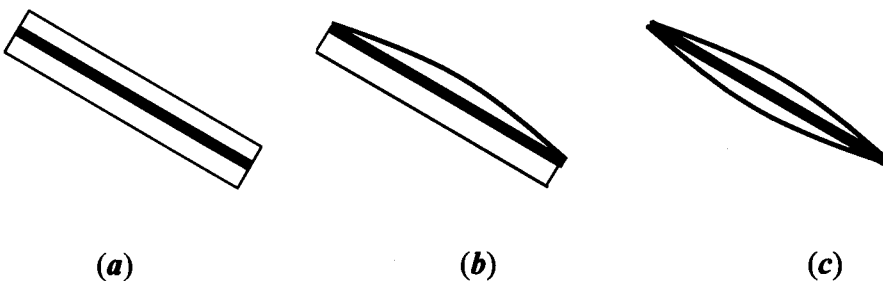


Figure 5.2 Sketches of laminar louvres, each incorporating a solar collector

The resulting configurations [(a), (b) and (c)] of the laminar louvre would benefit from the extra structural strengthening of the cross-section, which would allow for some extra spanning without sagging.

However, if these louvres, shown in Figure 5.2, were to be used externally, then configuration (a) would experience relatively substantial dynamic drag, while (b) would have some drag but dynamic lift, as well.

This consequently would lead to excessive fastening and securing measures - see Olson (1990, pp 421- 431).

On the other hand, the resulting shape, of configuration (c), is simply the voluminous louvre of Figure 5.1, only accommodating a collector. It would, therefore, still retain its slender aerofoil shape as well as its structural spanning characteristics. Figure 5.3, on the next page, depict the maximum spanning lengths of various louvre cross-sections.

As a building component, the shading louvres must have evolved through time.

These louvres have profiles with geometry that has been optimised such that:

- Structurally, strong enough to span out for long lengths without sagging,
- Aerodynamically, slender to withstand forces,
- Minimum cost,
- Aesthetically, pleasing.

The prevailing concept, within the process of the design of the solar louvre collector, has been that to adhere to the existing design of the louvre as shading device; hence acknowledging the above optimisation. Then building on these results of optimisation, to change the louvre to a solar collector.

This concept offers a ready foundation to build upon, but the slender aerodynamic shape offers limitation in terms of insulation thickness.

Therefore it seems reasonable to keep the same shape voluminous profile and endeavour to maximize its performance as a solar collector. This would at least act as a benchmark or reference point.

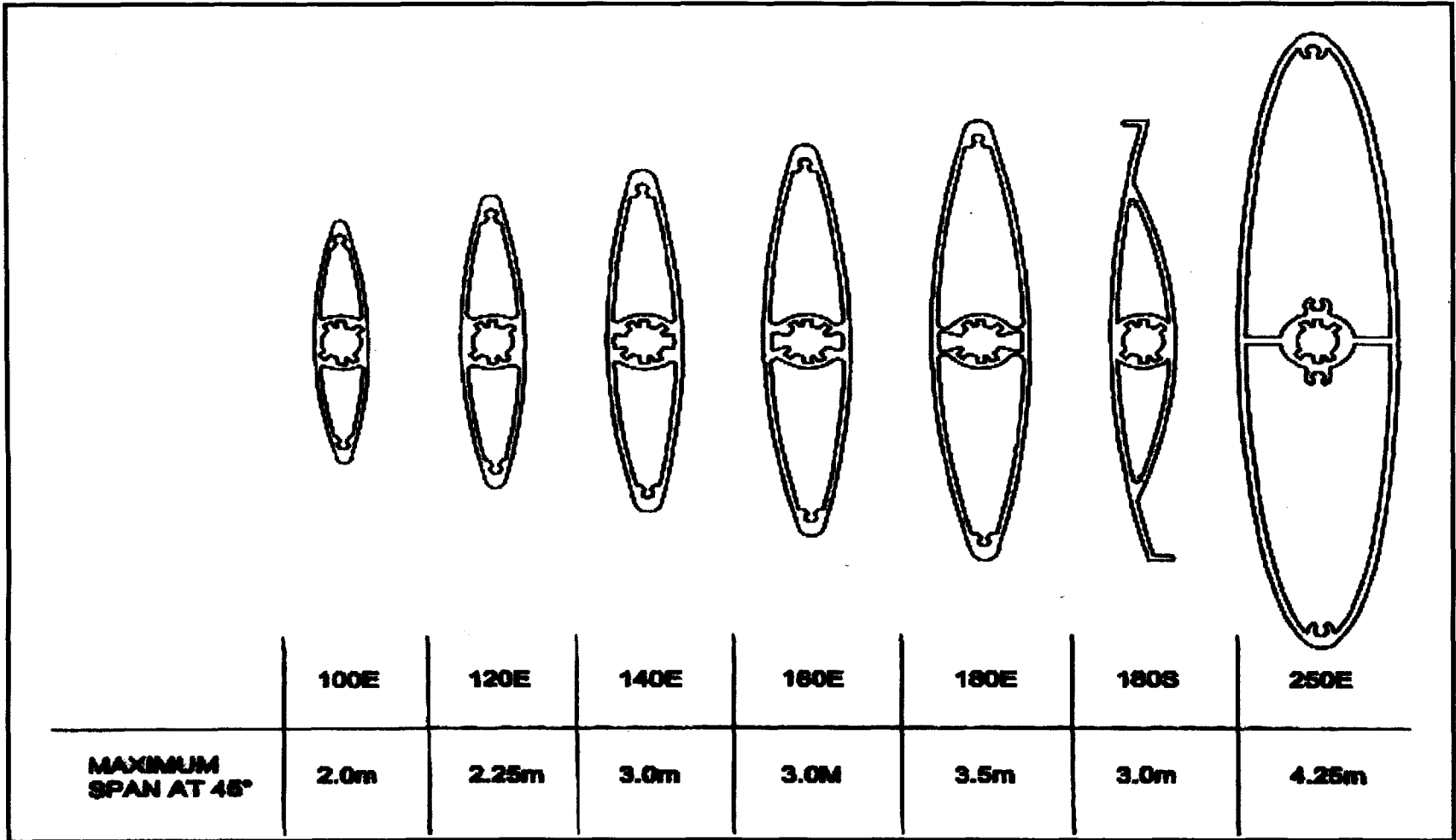


Figure 5.3 The span of various shading louvres' cross-sections – all having Aspect ratio of about 6.0.

5.1 Design considerations

It has been shown in the preceding section that voluminous louvres are the most suitable choice for the proposed design. In this section, various possible configurations for the proposed design have been examined as part of the design selection process. Sketches of these are shown in Figures 5.1.1 - 5.1.10.

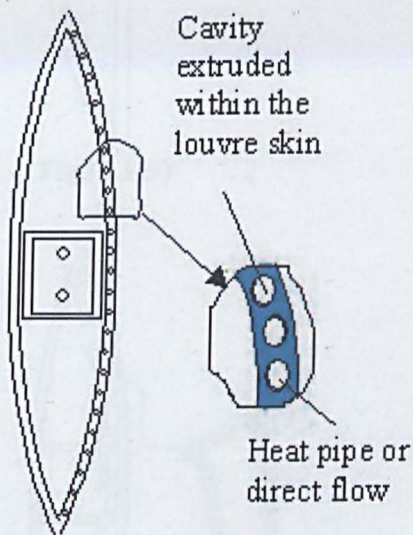


Fig (5.1.1)

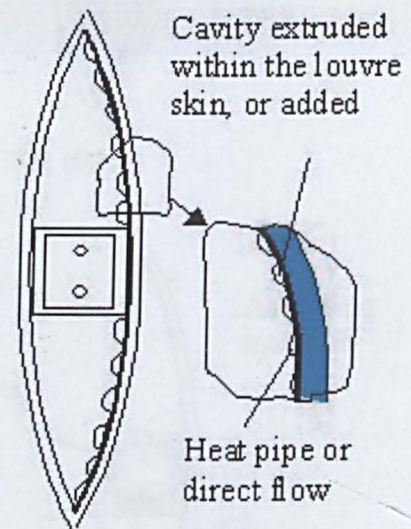


Fig (5.1.2)

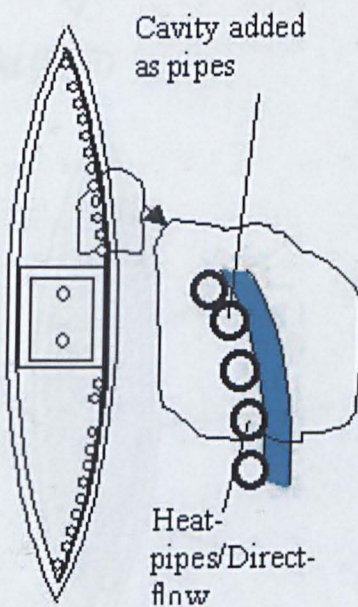


Fig (5.1.3)

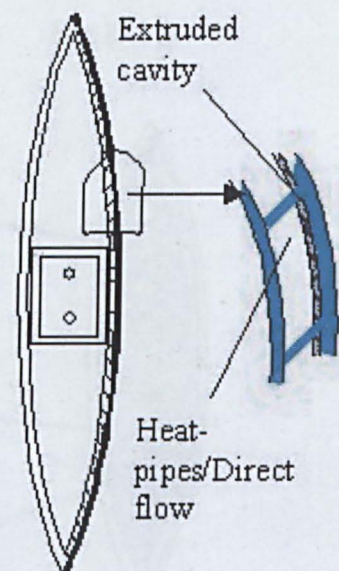


Fig (5.1.4)

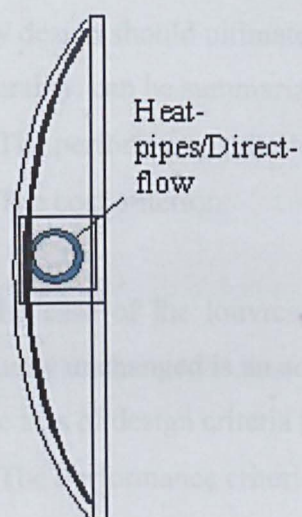


Fig (5.1.5)

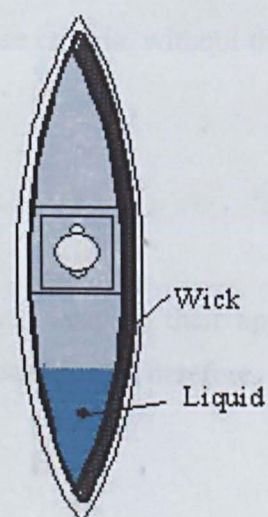


Fig (5.1.6)

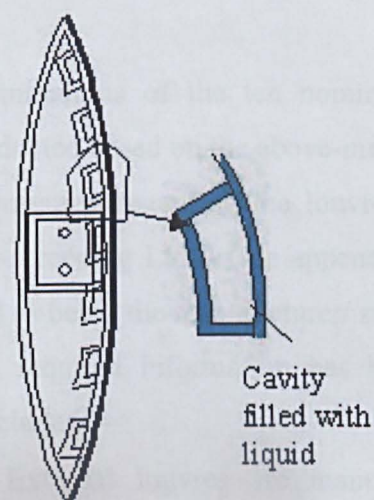


Fig (5.1.7)

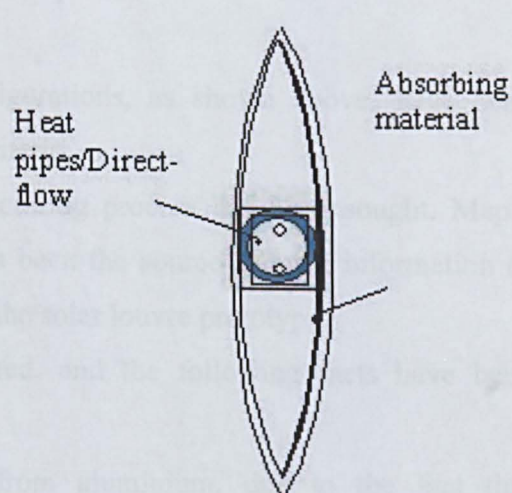


Fig (5.1.8)

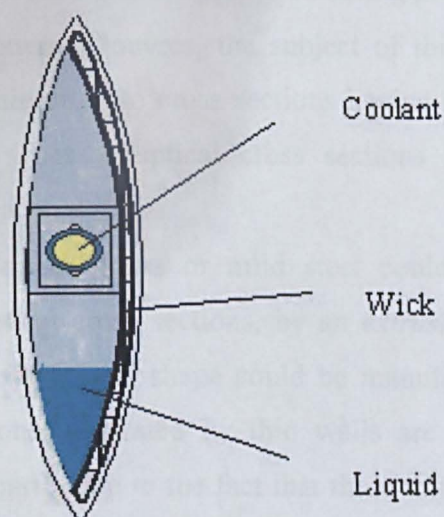


Fig (5.1.9)

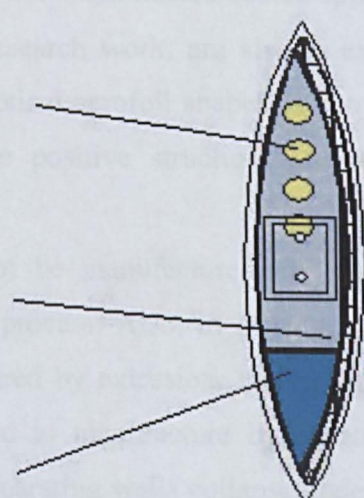


Fig (5.1.10)

Any design should ultimately fulfil certain criteria. These criteria, without the loss of generality, can be summarized as:

- The performance criterion, and
- The cost criterion.

In the case of the louvres, aesthetics is paramount, and keeping their appearance virtually unchanged is an additional, but salient design criterion. Therefore, there are three sets of design criteria to adhere to; namely:

- The Performance criterion / Scientific validity;
- The Cost criterion / Manufacturing-ease and material cost;
- The Aesthetics / Availability of choice and options.

Examinations of the ten nominated configurations, as shown above, have been conducted based on the above-mentioned criteria.

Information regarding the louvres manufacturing process has been sought. Maple Sun-screening Ltd – (see appendix A), has been the source of such information as well as being the manufacturer/ supplier of the solar louvre prototype.

The required information has been collated, and the following facts have been concluded:

- External louvres are manufactured from aluminium, due to the fact that aluminium is lightweight and cheaper when compared, for example, to copper or brass. Also it has a good weathering properties when treated/coated appropriately.
- External louvres, the subject of this research work, are always extruded from aluminium into cross sections having elliptical aerofoil shapes as shown in Figure 5.3. These elliptical cross sections have positive structural and aerodynamics characteristics.
- Copper, brass or mild steel could not be manufactured, in those particular elliptical cross sections, by an *extrusion* process. Also, in general, not any every cross-sectional shape could be manufactured by extrusion. In fact, small adjacent regions, separated by thin walls are hard to manufacture by extrusion. This is primarily due to the fact that these thin separating walls collapse under the thermal and pressure stresses of the extrusion process. A proposed design for extrusion must, therefore, undergo a finite element method (FEM) analysis, for identifying

and eliminating weak points/hotspots on the profile. That is to say, the profile must undergo a rapid prototyping, using FEM.

Now designing with aluminium brings with it some disadvantages. For the case at hand (collector metal/working fluid), it is the fact that:

- Aluminium is reactive with water (corrosion).
- Aluminium is a second-best thermal conductor, after copper.

The possibility of incorporating reflectors and/or concentrators on the louvre was ruled out, merely due to the fact that the focal points/lines require ample distances, which the minor chord of these elliptical louvres could not match (this is only 40.0 mm for the 250E). Also, aesthetically, the resulting product would be bulky and not pleasing on the front of buildings- please refer to Figure 2.2 and Figure 2.3 in *chapter (2) - Literature Survey*.

Based on the preceding discussion, the following decisions have been made about the above ten configurations:

- Case (1) to case (4), i.e. Fig (5.1.1) to Fig (5.1.4), would not be suitable for the proposed design due to the following facts:
 1. Extruding such small cavities within or just above the thickness of the louvre is not possible.
 2. Aluminium has a compatibility problem with water – corrosion, and gas generation.
- Case (5), i.e. Fig 5.1.5, would not be suitable for the proposed design due to the following fact:
 1. The half-ellipse shape would be subjected to a substantial dynamic-lift forces on windy days (Bernoulli's equation applied to potential flow) – see Olson, (1990, pp 217-218).
- Case (6), i.e. Fig (5.1.6), would not be suitable for the proposed design due to the following facts:

1. The whole louvre acting as a heat pipe would require vacuum pressure, within the louvre as well as in the associated components (piping and condenser), for operation. Large evacuated volumes are susceptible to leaks.
 2. The generated vapour within the louvre is removed to a central heat exchanger/condenser in the building, and the condensate returns to the louvre via pipe work. The resulting circuit involves two phases of the water and requires intricate balancing. Also the vapour would travel relatively long distances, which would make it susceptible to premature condensation (short-circuitry).
- Case (7), i.e. Fig (5.1.7) is a configuration that requires only minor modifications to become a solar louvre. Combining materials would optimise the design.
 - Case (8), i.e. Fig (5.1.8), apparently has the advantage of being simple to manufacture. It is, after all, the normal shading louvre with either a heat pipe or direct flow pipe inserted at its centre. It requires only few modifications to become a solar louvre.
 - Case (9) and case (10), i.e. Fig (5.1.9) and Fig (5.1.10) respectively, are quite similar, with the difference being that case (10) offers more surface-area for the vapour to condensate on (4 pipes rather than 1). Unlike case (6), these two cases have their evaporating/condensing liquid contained within the geometry of the louvre, and only the coolant travels into the building. This has been ruled out on the grounds that sustaining vacuum requires support between the two sheets, to withstand 11 ton/m^2 . Attempts have been made, as shown on Figure (C8) in appendix (C).

Out of these ten cases, case (7) and (8) have been chosen as suitable designs for modifications and further investigations.

It is good engineering practice, or rather common sense, to investigate designs by means of analytical and/or numerical methods prior to manufacturing.

Mathematical models for the two cases have been constructed as shown in the next section.

2. The Mathematical Models

Mathematical modelling is a powerful design tool. Although it could be somewhat difficult to construct a model at the start, and normally needing results for verification/validation at the end, modelling offers huge advantages.

Once a mathematical model has been constructed, it offers rapid prototyping for the design, and this advantage reflects favourably on the overall cost.

In order to characterize the direct flow or the heat pipe configuration, two-parameter models have been established. Both models were based on the energy-balance calculation method.

This method is well established, and there has been substantial experimental evidence that the method is a very satisfactory representation of the performance of most flat plate collectors-Duffie (1991, p.302).

In order to construct a mathematical model describing any physical phenomenon, assumptions and approximations must be made to simplify the analysis, without obscuring the physical situation at hand. Specific assumptions concerning each case (i.e. Direct-flow or Heat-pipe) have been included under their respective sections in this chapter.

However, assumptions common to both cases have been presented here as follows:

- Typical spans of these louvres are in the range of meters – see Figure 5.3; and therefore thermal entry length losses were neglected, flows were assumed fully developed.
- In the 2-D plane, edge effects are assumed relatively small so that can be neglected, and therefore heat flow through the cover to the plate, and the losses through the cover as well as through the back insulations were all taken as one-dimensional.
- The solar radiation that passes through the cover is mostly absorbed by the absorbing surface, but some may be reflected. The cover is assumed opaque to the reflected long-wave (infrared) radiation, and there is no absorption of solar energy by this cover insofar as it affects losses from the collector.

- The temperature drop through the cover, and through the wall of the channel, as well as through all the interfacing surfaces of the solar louvre can be neglected, due to the small thickness of these walls/interfaces.
- The smooth curvatures of the louvre surface allow the approximation of straight lines; hence taken as straight lines.
- Finally, the sky is considered as a black body at a temperature similar to that of the ambient environment, T_a .

5.2.1 The Direct-flow Model

It must be stated at this stage that the flow rate of water in this research work, was taken constant at 20 g/s/m^2 through out, for all the types of collectors, unless the effect of the flow rate itself is being examined.

In the case of the direct flow collectors there are two possible geometries for the working fluid duct.

The dimensions of the two types of fluid duct's cross-sections are as shown in Figure 5.4, below. Both have the same absorbing-plate surface area of 0.15 m^2 .

The other dimensions or are as follow:

- For the case of the channels:

Effective/hydraulic diameter = 0.0106 m , perimeter = 0.1620 m , cross-sectional area = 0.00043 m^2

- For the case of the fin-on-tube:

Diameter = 0.0080 m , perimeter = 0.0251 m , cross-sectional area = 0.00005 m^2

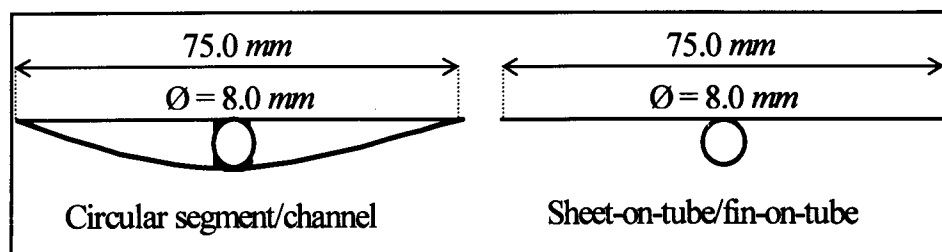


Figure 5.4 1mm -thick absorbing plates, coated with Black paint; 2.0 m length (along the paper), frontal surface area = 0.15 m^2 .

The Reynolds number (based on the diameter), is defined as $\frac{uD}{\nu}$, where u , D , and ν are the velocity/speed, the diameter (of the pipe)/effective diameter (of the channel) and the kinematics viscosity of the water, respectively.

For the same flow rate of 0.003 kg/s, through either of the cross sections, A_x , the velocity, u , is given by:

$$0.003 \text{ (kg)} = \rho \left(\frac{\text{kg}}{\text{m}^3} \right) A_x (\text{m}^2) d (\text{m})$$

The distance covered in a unit time (i.e. 1 second), d , is actually the velocity of the fluid mass (0.003 kg).

$$\text{Therefore: } 0.003 \text{ (kg/s)} = \rho A_x (\text{kg/s}) u (\text{m/s})$$

$$u (\text{m/s}) = 0.003 / \rho A_x$$

In the range of operation of this collector (about 20 – 80 °C), the density, ρ , the kinematics viscosity, ν , and the Reynolds number vary as shown in Table 5.1 below:

Table 5.1 The Reynolds number for the channel and fin-on tube at 20 and 80 °C

Temperature (°C)	Density, ρ (kg/m ³)	Kinematics viscosity, ν (m ² /s)	Velocity, u (m/s)		Reynolds number, Re	
			$[u]_{\text{channel}}$	$[u]_{\text{fin}}$	$[\text{Re}]_{\text{channel}}$	$[\text{Re}]_{\text{fin}}$
20	998.3	1.0×10^{-6}	0.007	0.060	7.4	48.0
80	971.6	0.37×10^{-6}	0.007	0.062	20.1	134.1

These values for the Reynolds number, $[\text{Re}]_{\text{channel}}$ and $[\text{Re}]_{\text{fin}}$ are very low ($\ll 2300$), for both cross-sections in the operating temperature range (20 – 80 °C).

Hence fluid flow thought out this analysis was taken as **laminar** flow.

A design that satisfies all of the aesthetic, structural and thermal criteria, as well as those concerned with manufacturability and cost has been designed as shown in Figures 5.5 and 5.6.

This has been based on the cross sectional dimensions of the E250 louvre.

The modelling of either of the two configurations would follow parallel steps similar to those of the analysis of flat plate collectors. This is especially so for the case of the sheet-on-tube/fin-on-tube. Attention, has therefore been turned to the channels.

The cross-sectional shape of these channels has no correlations currently available in the literature. However, analytical solutions for the circular-segment cross-sections, which are quite similar to these channels, are provided by Sparrow (1966).

To model the situation shown in Figure 5.5, further simplifying assumptions must be made in order to lay the mathematical foundation.

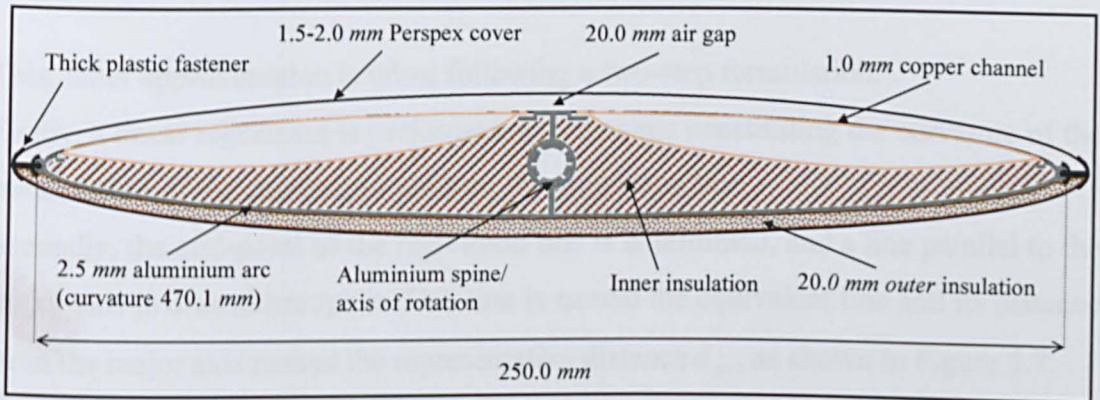


Figure 5.5 Schematic of the solar louvre cross-section accommodating, channels.

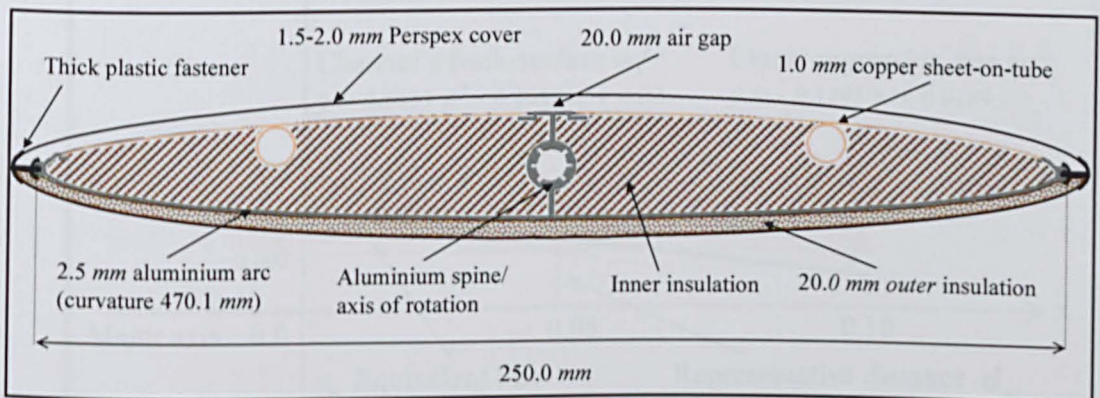


Figure 5.6 Schematic of the solar louvre cross-section, accommodating sheet-on-tubes.

5.2.1.1 Further Assumptions and Approximations

- The channels, as shown in Figure 5.5, are mounted on rubber; and hence the losses from these channels' edges are zero- (assumed adiabatic).
- To confine the work to one-dimensional analysis; the curvature of the back surface of the channel has been approximated by a straight line, parallel to the major axis of the louvre (as explained below).

This, latter approximation is taken following a two-step formulation.

Firstly, a linear regression is performed on the points constituting the curvature of the back surface of the channel, to produce the regression line.

Secondly, the mid-point of the regression line is determined, and a line parallel to the major axis is drawn through it. This line is named the equivalent line and its distance from the major axis named the representative distance d_{av} , as shown in Figure 5.7.

Now, with this approximation, the heat flow from the back surface of the channel to the major axis, for example, would be as if it was from the equivalent line to the major axis through the representative distance.

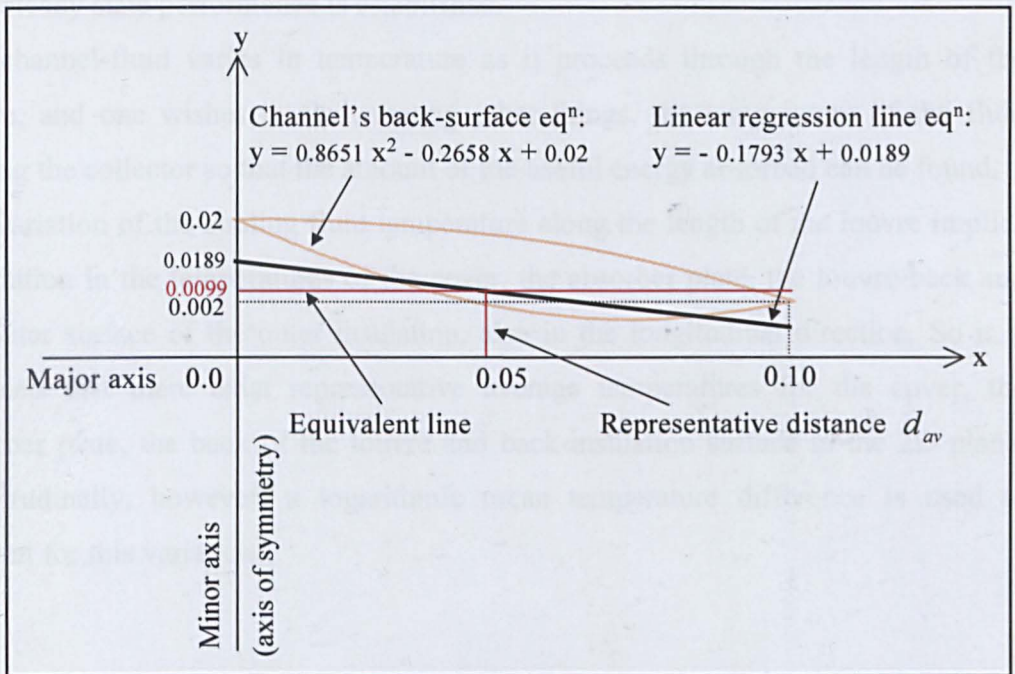


Figure 5.7 Approximation to heat flow from the back of the channel-
(Dimensions are in metres).

5.2.1.2 The Governing Equations

As shown in Figure 5.8, the absorber plate and the inner surface of the cover exchange radiation that results from their own emissions, and are also subjected to convective heat transfer. Let h_r, h_c denote the radiation and convection heat transfer coefficients respectively.

The outer surface of the cover and the outer surface of the outer insulation radiates to the environment at T_a . Let h_{ro}, h_{rs} denote these radiation coefficients respectively.

They are also subjected to convection to the same environment at T_a . Let h_{co} denote this, wind-induced, heat transfer coefficient for the outer perimeter of the louvre.

There is, also, convection between the working fluid in the channel and the channel's inner surface; let this coefficient be denoted by h_{ch} .

Conduction heat transfer is also present through the inner and outer insulations. Let k_i, k_o be the conductivities of the inner and outer insulation materials respectively (known values).

All of the energy-flows interact to establish equilibrium temperatures for the cover, the absorbing plate, the louvre-back and the outer surface of the outer insulation, once steady state performance is established.

The channel-fluid varies in temperature as it proceeds through the length of the louvre, and one wishes to find, among other things, the temperature of the fluid leaving the collector so that the amount of the useful energy absorbed can be found.

The variation of the cooling fluid temperature along the length of the louvre implies a variation in the temperatures of the cover, the absorber plate, the louvre-back and the outer surface of the outer insulation, also in the longitudinal direction. So it is assumed that there exist representative average temperatures for the cover, the absorber plate, the back of the louvre and back-insulation surface in the 2D plane. Longitudinally, however, a logarithmic mean temperature difference is used to account for this variation.

Assuming a steady-state performance, with the solar irradiation I and the ambient T_a known for the location and time in question, one proceed as follows:

Let τ_c, α_p be the transmissivity of the outer cover and the absorptivity of the channel's sun-facing surface, respectively (known values).

Let $(\tau_c \alpha_p)$ denote the apparent solar transmissivity-absorptivity of the cover-plate, so that in any event the $(\tau_c \alpha_p)I$ represents the solar energy absorbed at the absorbing surface.

Let T_c, T_p, T_s be the uniform average temperatures of the cover, the absorbing plate and the outer surface of the outer insulation respectively.

Let $\varepsilon_c, \varepsilon_p, \varepsilon_s$ be the emissivity of these surfaces at their respective temperatures (known values).

Let T_b denote the temperature of the back surface of the louvre.

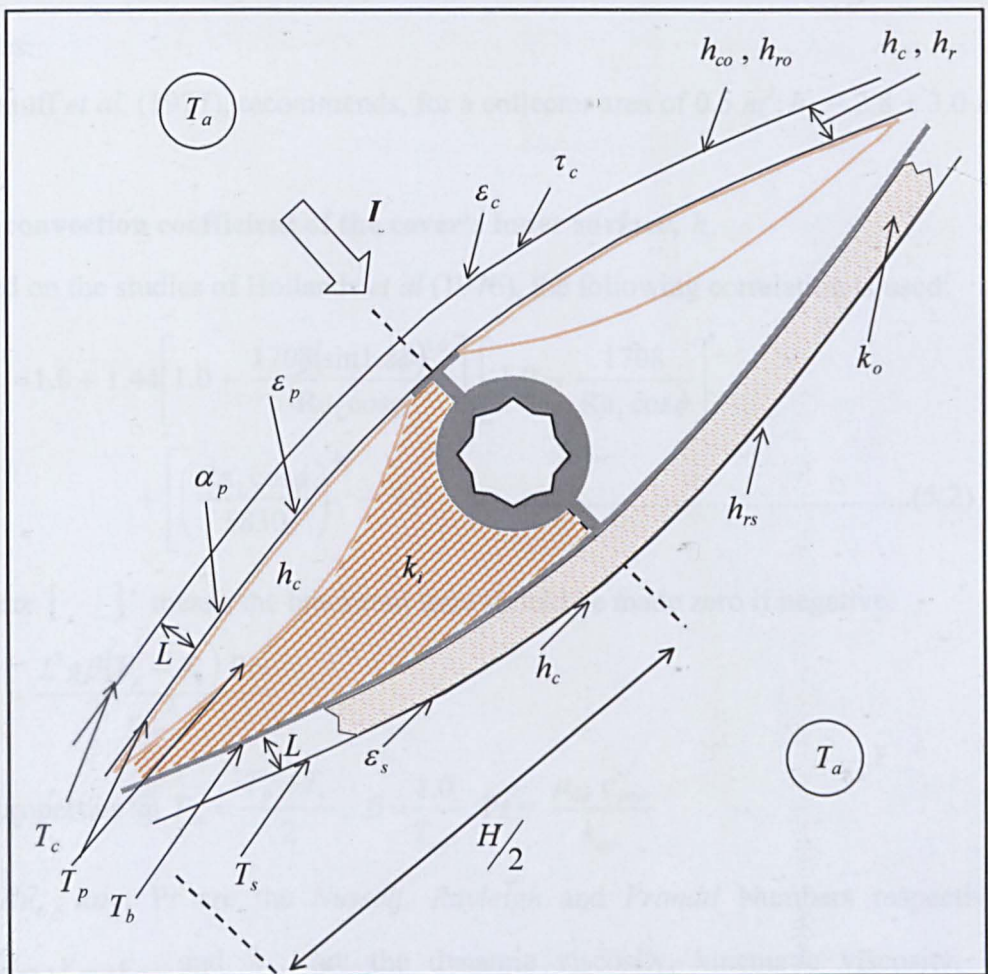


Figure 5.8 Schematic of the solar louvre cross-section. Unit length normal to the page.

The following sections describe the determination of the heat transfer coefficients for the model:

The convection coefficient of the louvre’s outer perimeter, h_{co} :

Calculations of wind-induced heat transfer coefficients, and correlations for mixed mode (free+forced) convection are not well established.

The coefficient of the outer surface of the cover and of the outer insulation outer surface h_{co} is determined following the guidelines recommended by McAdams (1954); see Duffie (1991, p.173):

$$h_{co} = \max. \left[5, \frac{8.6 u^{0.6}}{L_b^{0.4}} \right] \dots\dots\dots (5.1)$$

where u is the wind speed in m/s, and L_b is the cubic root of the building’s volume in metres.

Watmuff *et al*, (1977), recommends, for a collector area of 0.5 m^2 : $h_{co} = 2.8 + 3.0 u$.

The convection coefficient of the cover’s inner surface, h_c

Based on the studies of Hollands *et al* (1976), the following correlation is used:

$$\begin{aligned} Nu_L = 1.0 + 1.44 & \left[1.0 - \frac{1708(\sin 1.8\phi)^{1.6}}{Ra_L \cos\phi} \right] \left[1.0 - \frac{1708}{Ra_L \cos\phi} \right]^* \\ & + \left[\left(\frac{Ra_L \cos\phi}{5830} \right)^{1/3} - 1.0 \right]^* \dots\dots\dots(5.2) \end{aligned}$$

where []* means the bracketed term should be made zero if negative.

$$Ra_L = \frac{L^3 g \beta (T_p - T_c) Pr}{\nu_{air}^2}$$

Air properties @ $T_{av} = \frac{T_p + T_c}{2}$, $\beta = \frac{1.0}{T_{av}}$, $Pr = \frac{\mu_{air} c_{pair}}{k_{air}}$

Nu_L , Ra_L , Pr are the *Nusselt*, *Rayleigh* and *Prandtl* Numbers respectively. μ_{air} , ν_{air} , c_{pair} and k_{air} are the dynamic viscosity, kinematic viscosity, heat capacity and conductivity of air respectively. g is gravity, and ϕ is the louvre’s angle of inclination. β is the coefficient of thermal expansion.

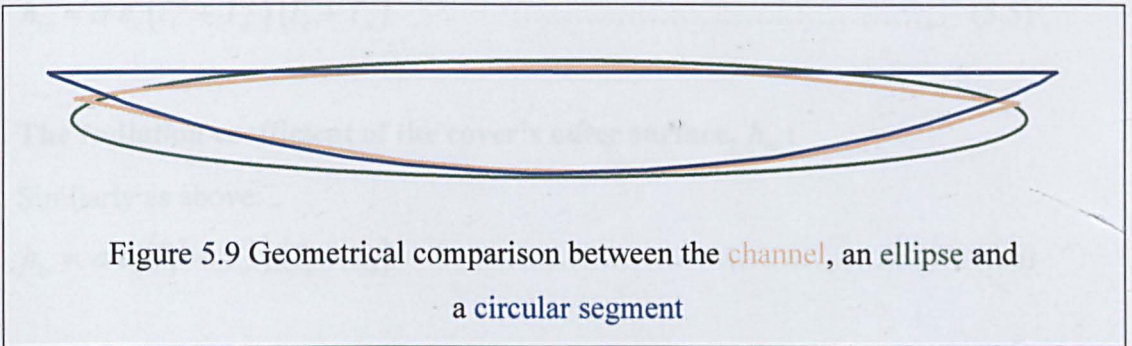
The correlation of equation (5.2) is valid for single glazed collectors; for double glazed, as in the model, Yiqin *et al.* (1991) have shown that the correlation of equation (5.1) is valid with the coefficient 1.44 replaced by 1.7.

With the Nusselt number determined, this coefficient is given by: $h_c = \frac{Nu_L k_{air}}{L}$.

The convection coefficient of the channel's inner surface, h_{ch} :

Correlations for these channels are not available. However, for the purpose of the analysis here, the channel is approximated as follows:

The shape of these channels is obviously not an ellipse, and not exactly a circular segment – Figure 5.9 below:



White (1991, p.309) provides for an ellipse (aspect ratio 8): $Nu = 3.72$.

Sparrow (1966, p.355) provides for a circular segment: $Nu = 4.09$.

Therefore, the Nusselt number for the channel is bound to be near these two values,

and one could approximate the Nusselt number as: $Nu = \frac{h_{ch} D_h}{k_w} \approx 4.0$

Hence $h_{ch} \approx 4.0 \times (k_w / D_h)$ (5.3)

Where D_h is the hydraulic (or effective) diameter, defined as four times the cross-sectional area divided by the wetted perimeter, P_{ch} , (i.e. $\frac{4A_{ch}}{P_{ch}}$);

k_w is the conductivity of the water. ($A_{ch} \approx 0.00043 m^2$, and $P_{ch} \approx 0.162 m$)

The radiation coefficient of the cover's inner surface, h_r :

Using the infrared radiation exchange between two grey parallel surfaces-
Duffie (1991, pp 156-157):

$$h_r = \frac{\sigma(T_p^2 + T_c^2)(T_p + T_c)}{\left(\frac{1}{\varepsilon_c}\right) + \left(\frac{1}{\varepsilon_p}\right) - 1} \dots\dots\dots (5.4)$$

where σ is Stefan-Boltzmann constant [$= 5.67 \times 10^{-8} \text{ W/m}^2 - \text{ }^\circ\text{K}^4$].

The radiation coefficient of the cover's outer surface, h_{ro} :

Here the sky is considered as a black body at an equivalent temperature T_a - see
Duffie (1991, pp 156-157):

$$h_{ro} = \sigma \varepsilon_c (T_c^2 + T_a^2) (T_c + T_a) \dots\dots\dots (5.5)$$

The radiation coefficient of the cover's outer surface, h_{rs} :

Similarly as above:

$$h_{rs} = \sigma \varepsilon_s (T_s^2 + T_a^2) (T_s + T_a) \dots\dots\dots (5.6)$$

In order to construct the model, a consistent set of equations (the governing equations) must be formulated from the physical situation at hand.

An overall energy balance on the louvre provides the governing equations. This states that:

$$\text{Useful energy} = \text{Absorbed energy} - \text{Losses.}$$

Heat loss from the top and bottom surfaces of the louvre, q_{loss} :

Let A_{col} be the surface area of the absorber plate; taken as equal to the area of the transparent cover; and also equal to the outer insulation area.

Let q_t and q_b represent the top and bottom losses respectively.

The top loss q_t is, in fact, the net heat flow between the cover at T_c and the ambient air at T_a , q_{c-a} ; it is expressed using Newton's law of cooling and the linearized radiation law as:

$$q_{c-a}/A_{col} = h_{co}(T_c - T_a) + h_{ro}(T_c - T_a) \dots\dots\dots (5.7)$$

rearranging gives: $q_t/A_{col} = (h_{co} + h_{ro})(T_c - T_a)$

The net heat transfer between the cover at T_c and the channel at T_p , q_{c-a} , is expressed using Newton’s law of cooling and the linearized radiation law as:

$$q_{p-c}/A_{col} = h_c(T_p - T_c) + h_r(T_p - T_c) = (h_c + h_r)(T_p - T_c) \dots\dots\dots(5.8)$$

But $q_{c-a} = q_{p-c}$;

Therefore equation (5.8) becomes:

$$q_t/A_{col} = (h_c + h_r)(T_p - T_c) \dots\dots\dots(5.9)$$

Now, equating (5.7) and (5.9) gives:

$$(h_{co} + h_{ro})(T_c - T_a) = (h_c + h_r)(T_p - T_c) \dots\dots\dots (5.10)$$

Also, adding (5.7) and (5.9) eliminates T_c , giving:

$$q_t = U_t A_{col} (T_p - T_a)$$

$$\text{where } U_t = 1 / \left[\frac{1}{(h_{co} + h_{ro})} + \frac{1}{(h_c + h_r)} \right] \dots\dots\dots(5.11)$$

The bottom loss, q_b , is the net heat flow between the outer surface of the outer insulation at T_s and the ambient air at T_a ; q_{s-a} , is expressed using Newton’s law of cooling and the linearized radiation law as:

$$q_b/A_{col} = q_{s-a}/A_{col} = (h_{co} + h_{rs})(T_s - T_a) \dots\dots\dots(5.12)$$

The heat-transfer between the back of the channel at T_p and the inner surface of the outer insulation at T_b ; is expressed using Fourier’s law as:

$$q_{p-b} / A_{col} = \frac{k_i}{d_{av}} (T_p - T_b) \dots\dots\dots(5.13)$$

where d_{av} is the average thickness of the inner insulation material. It is taken 0.03 m; (i.e. $0.02 + 0.0099 \approx 0.03$ m) – Figure 5.7.

Similarly, the heat transfer between the inner surface of the outer insulation at T_b and the outer surface of the outer insulation at T_s ; q_{b-s} , is expressed using Fourier’s law as:

$$q_{b-s} / A_{col} = \frac{k_o}{L} (T_b - T_s) \dots\dots\dots (5.14)$$

But $q_b = q_{s-a} = q_{b-s} = q_{p-b}$

Now, T_b is eliminated by adding (5.13) and (5.14), yielding:

$$\frac{q_b d_{av}}{A_{col} k_i} + \frac{q_b L}{A_{col} k_o} = (T_p - T_s) \dots\dots\dots (5.15)$$

Equating (5.12) and (5.15) gives:

$$(h_{co} + h_{rs})(T_s - T_a) = (T_p - T_s) / \left(\frac{d_{av}}{k_i} + \frac{L}{k_o} \right) \dots\dots\dots (5.16)$$

Also, T_s is eliminated by adding (5.12) and (5.15), yielding:

$$\frac{q_b}{A_{col}} \left[\frac{d_{av}}{k_i} + \frac{L}{k_o} + \frac{1}{(h_{co} + h_{rs})} \right] = (T_p - T_a),$$

which is expressed as:

$$q_b = U_b A_{col} (T_p - T_a)$$

$$\text{where } U_b = 1 / \left[\frac{d_{av}}{k_i} + \frac{L}{k_o} + \frac{1}{(h_{co} + h_{rs})} \right] \dots\dots\dots (5.17)$$

The total loss, q_{loss} , is therefore:

$q_{loss} = q_t + q_b$; and from equations (5.11) and (5.17), i.e.:

$$q_{loss} = A_{col} U_c (T_p - T_a) \dots\dots\dots (5.18)$$

where $U_c = U_i + U_b$

Energy Balance on the whole louvre:

If q_u is the net heat collected, and q_p is the heat absorbed by the absorber plate, then:

$$q_u = q_p - q_{loss}$$

$$q_u = A_{col} \left[(\tau_c \alpha_p) I - U_c (T_p - T_a) \right] \dots\dots\dots (5.19)$$

Equation (5.19) may be put into a more standard form by defining an equivalent environment temperature T'_a such that:

$$T'_a = T_a + (\tau_c \alpha_p) I / U_c \dots\dots\dots (5.20)$$

So (5.19) becomes:

$$q_u = A_{col} U_c (T'_a - T_p) \dots\dots\dots (5.21)$$

To account for the variation of temperatures in the longitudinal direction, the louvre can be characterised as a heat exchanger for which the hot fluid remains at a constant temperature equal to an equivalent environment temperature T'_a .

Therefore using the equation for the logarithmic mean temperature difference concept of a simple heat exchanger (flow past an isothermal surface):

$$\frac{T_{out} - T_{in}}{T'_a - T_{in}} = 1 - \exp\left(\frac{\bar{U} A_{col}}{m_w c_p}\right) \dots\dots\dots (5.22)$$

where T_{in} , T_{out} , m_w and c_p are the inlet temperature, outlet temperature, mass flow rate and specific heat capacity of the working fluid, respectively; all considered as known values, except T_{out} .

\bar{U} is an overall collector coefficient given by:

$$\bar{U} A_{col} = 1 / \left(\frac{1}{U_c A_{col}} + \frac{1}{h_{ch} A_{ch}} \right) \dots\dots\dots (5.23)$$

The useful heat gained by the working fluid (i.e. the net useful heat collected by the absorber) is determined by:

$$q_u = m_w c_p (T_{out} - T_{in}) \dots\dots\dots (5.24)$$

Substituting from (5.20) and (5.22) into (5.24) gives:

$$q_u = \frac{m_w c_p}{U_c} [(\tau_c \alpha_p) I - U_c (T_{in} - T_a)] \left[1 - \exp\left(-\frac{\bar{U} A_{ch}}{m_w c_p}\right) \right] \dots\dots\dots (5.25)$$

Equating (5.21) and (5.25) gives:

$$A_{col} U_c (T_a' - T_a) = \frac{m_w c_p}{U_c} [(\tau_c \alpha_p) I - U_c (T_{in} - T_a)] \left[1 - \exp\left(-\frac{\bar{U} A_{col}}{m_w c_p}\right) \right] \dots\dots\dots (5.26)$$

5.2.1.3 The Solution

In the previous paragraph, the necessary equations describing the model have been formulated. Some of these equations are non-linear, due to the involvement of radiation heat transfer. These have been reduced, by algebraic manipulations, into three non-linear equations in three variables, namely, T_c , T_p and T_s . These are equation (5.10), (5.16), and (5.26).

Mathematically, this is a consistent set of three, inhomogeneous, non-linear equations in three variables, and are much more difficult to solve than a linear set; (In fact some non-linear sets have no real solutions).

Non-linear sets are solved numerically, often using Newton's method. It has the advantage, from a computational point of view, to converge quadratically, provided that one starts the first guess near the solution. However, when a larger set (more than three non-linear equations) is to be solved, a modification of Newton's method must be used.

In the past, the solution of the above set would need a solution method, an iterating algorithm and a computer program (FORTRAN, for example) especially written for it. Today, however, there are various programs/packages especially designed for solving sets of linear, non-linear and even differential equations. Engineering Equation Solver (EES)- Klein (1997), is one such program, and has been used for the solution of the above set.

The basic function provided by EES is the numerical solution of non-linear and differential equations. In addition, EES provides built-in thermodynamics and transport property functions for many fluids, including water, dry and moist air. Additional property data can be added by the user. The combination of equation-solving capability, engineering property data and plotting facilities makes EES a suitable tool for this work.

Modelling for design dictates that various variables must be changed during the solution process, and constants are only those values that the user would not (perhaps could not) want to change (g, σ , for example).

For the purpose of solving the above set of equations, and evaluating the performance characteristics of the collector, the solution map has been divided into three regions:

- The first region contains a group made-up of known variables as follows:

$$L, H, d_{av}, D_h, A_{col}, L_b, V, \phi$$

$$I, T_a, \varepsilon_c, \varepsilon_p, \varepsilon_s, \tau_c, \alpha_p, T_{in}, m_w, k_i, k_o$$

The values for $\mu_{air}, \nu_{air}, c_{p,air}, k_{air}$ and k_w have been assigned automatically for air and water, respectively, from within the EES program.

- The second region contains a group made-up of the equations leading to the determination of the heat transfer coefficients h_{co}, h_c, h_r, h_{ro} and h_{rs} .

These are eqⁿ (1), (6). Also it contains sub-equations as follows:

$$T_{av} = \frac{T_p + T_c}{2}, \quad \beta = \frac{1.0}{T_{av}}, \quad Pr = \frac{\mu_{air} c_{p,air}}{k_{air}} \quad \text{and} \quad Ra_L = \frac{L^3 g \beta (T_p - T_c) Pr}{\nu_{air}^2},$$

which are needed for the determination of the Nusselt number, and hence the convection heat transfer coefficient h_c .

It, also contains minor equations as:

Equations (5.11) and (5.17) for the determination of $U_c (= U_t + U_b)$, and equations (5.20) and (5.23).

- The third region contains the major non-linear set of equations, namely:

$$\text{Equations (5.10), (5.16), and (5.26).}$$

In the EES environment, all of the three regions are placed in one window – the “*Equations Window*”.

Prior to solving the set, guessed values of T_c, T_p and T_s must be assigned in the “*Variable Information*” dialog window. These guessed values must be realistic and consistent with the rest of the data.

Once this is done, the program runs calculating repeatedly (iterate) for T_c , T_p and T_s until a satisfactory agreement between the assumed and calculated values of T_c , T_p and T_s is achieved (for example max. residual and max. variable-change in the order of 10^{-12} and 10^{-6} respectively).

The quantity of ultimate importance in solar collector analysis is the efficiency. That is so because the analysis leading to it provides other important information.

The efficiency of a solar collector is defined as:

$$\text{Efficiency} = \frac{\text{Useful output}}{\text{Input}}$$

Therefore the efficiency of the louvre is:

$$\eta_{col} = \frac{A_{col} [(\tau_c \alpha_p) I - U_c (T_p - T_a)]}{A_{col} I}$$

$$\eta_{col} = (\tau_c \alpha_p) - U_c \frac{(T_p - T_a)}{I} \dots \dots \dots (5.27)$$

It is useful to introduce a quantity that relates the actual gain of a collector to the useful gain if the whole collector surface were at the fluid inlet temperature. This quantity is called the heat removal factor F_R . In equation form it is:

$$F_R = \frac{m_w c_p (T_{out} - T_{in})}{A_{col} [(\tau_c \alpha_p) I - U_c (T_{in} - T_a)]}$$

As stated in Chapter (4), equation (5.27) becomes:

$$\eta_{col} = F_R (\tau_c \alpha_p) - F_R U_c \frac{(T_{in} - T_a)}{I} \dots \dots \dots (5.28)$$

Hence, the efficiency of the louvre is given by:

$$\eta_{col} = \frac{m_w c_p (T_{out} - T_{in})}{A_{col} I} \dots \dots \dots (5.29)$$

Equating (5.28) and (5.29) gives (as in eqⁿ 4.9):

$$\frac{m_w c_p (T_{out} - T_{in})}{A_{col} I} = F_R (\tau_c \alpha_p) - F_R U_c \frac{(T_{in} - T_a)}{I} \dots \dots \dots (5.30)$$

Equation (5.30) is the basis for providing the instantaneous efficiency values for plotting the efficiency curve of the collector, in accordance with the ASHRAE 93-77 standard procedure.

The European practice, however, is to base collector test results on the arithmetic average of the fluid inlet and outlet temperatures, T_{av} :

Therefore equation (5.30) becomes:

$$\frac{m_w c_p (T_{out} - T_{in})}{A_{col} I} = F_{av} (\tau_c \alpha_p) - F_{av} U_c \frac{(T_{av} - T_a)}{I} \quad \dots\dots\dots (5.31)$$

where $T_{av} = \frac{1}{2}(T_{in} + T_{out})$ and F_{av} is the heat removal factor based on T_{av} .

For a constant $(\tau_c \alpha_p)$, it is an acceptable approximation to assume that F_{av} and U_c do not change much, and the plot of equation (5.31) is a straight line with intercept $F_{av} (\tau_c \alpha_p)$ and slope $- F_{av} U_c$.

5.2.1.4 Results of the Direct-flow Model

The dimensions of the louvre were all taken as in Figure 5.5.

Thermal properties of air and water were assigned from with the built in tables provided by the EES program.

Radiation properties were taken for the cover, the copper channel, the aluminium louvre surface and the thin metallic outer surface of the outer insulation as follows:

The cover transmission, τ_c , was taken as 0.92, and its emissivity for long wave radiation, ε_c , as 0.84.

The upper surface of the channel was considered to be coated with a selective material (*Titanium Oxynitride*), having absorbtivity, α_p , as 0.96, and emissivity for long wave radiation, ε_p , as 0.10.

The conductivities of the inner and outer insulation materials, k_i , k_o , were both taken as 0.03 W/m-°K.

Climatic variables, (solar radiation, ambient temperature and wind speed), affect collector performance. However, the variation of the wind speed on a solar collector has the expected results of increasing the losses. Therefore, u was taken as 5 m/s (which is reasonable average wind speed), and L_b as 8 m, giving $h_{co} = 9.8 \text{ W/m}^2\text{-}^\circ\text{K}$ throughout the analysis.

Solar radiation was varied as: $I = 200$ to 800 W/m^2 . The ambient temperature was taken as, $T_a = 20 \text{ }^\circ\text{C}$.

Other operating variables are water flow rate and inlet water temperature. Water flow rates in the channels, m_w , were varied between 20 and 250 g/s/m^2 of collector area, and the inlet water temperature, T_{in} , between 20 to $60 \text{ }^\circ\text{C}$.

Based on the preceding modelling analysis, the program has been run on numerous situations to account for the effect of changing various parameters, and the results are as presented in the following graphs:

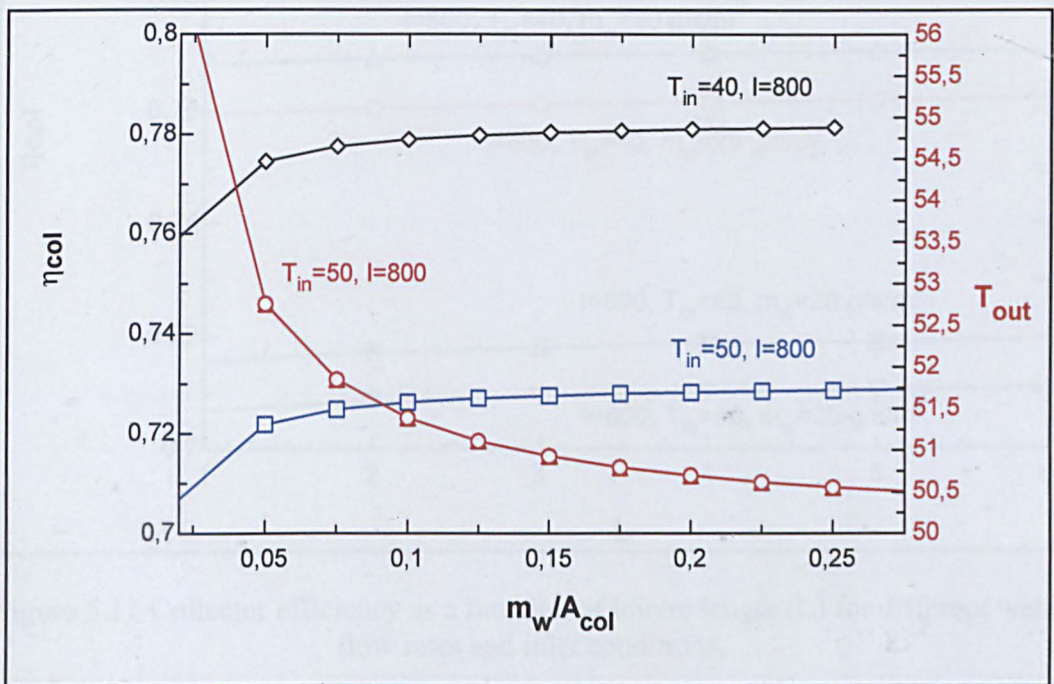


Figure 5.10 Collector efficiency and outlet temperature as a function of water flow rate (kg/s/m^2), for different inlet temperatures.

It can be seen from Figure 5.10 that there is an initial rapid increase in the efficiency. Beyond that the efficiency increases slowly, and becomes almost constant for larger

flow rates. The increase in water flow rate decreases outlet temperature and increases collector efficiency (collected energy).

This confirms that it is not practical to use high flow rates, as this would increase the pumping power without a significant increase in energy collection.

In practice, water flow rates around 20 g/s/m^2 are the best compromise between collector heat transfer coefficient, energy delivery and pumping power. Therefore, this is considered to be the reference value.

The effect of louvre length L (not L) on collector efficiency has been examined. This has been varied between 1m (reference length) and 6m , and the results are as shown in Figure 5.11.

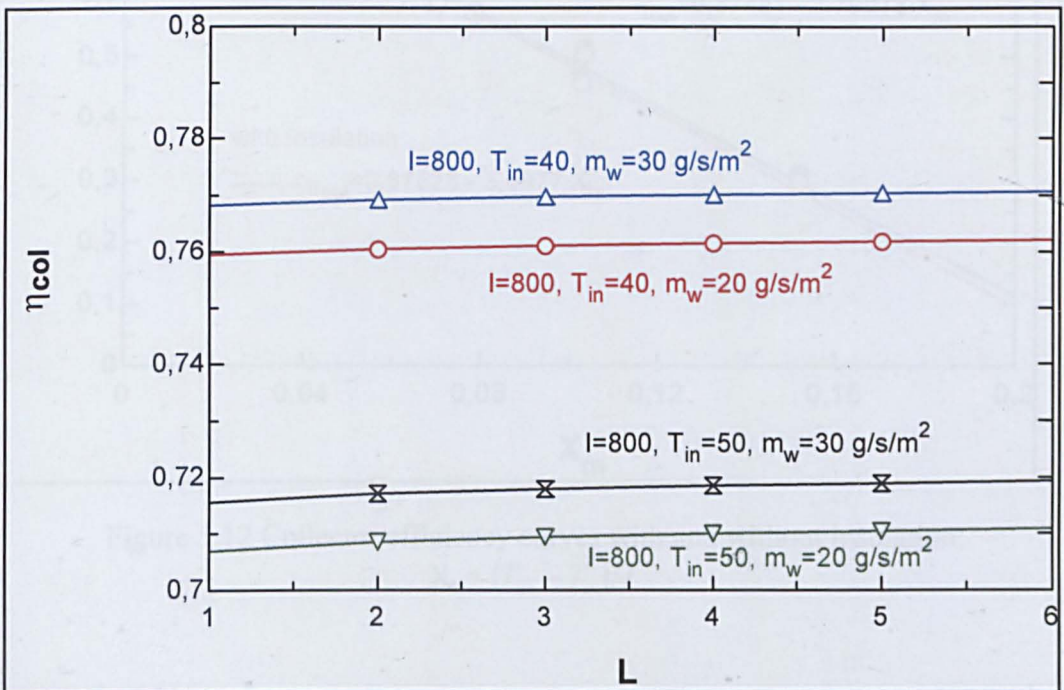


Figure 5.11 Collector efficiency as a function of louvre length (L) for different water flow rates and inlet conditions.

As depicted in Figure 5.11, maintaining the ratio of water flow rate/collector area (20 and 30 g/s/m^2), the collector efficiency remains approximately constant - (note that water rate increases as L increases but heat losses also increase with L).

Therefore, evidently, the increase of louvre length has a small influence on collector performance.

In order to simulate the thermal performance of the louvre, equation (5.31) must be plotted and the quantities $F_{av}(\tau_c \alpha_p)$ and $-F_{av}U_c$, be determined.

Therefore, for the ambient temperature T_a fixed at 20°C , and the water flow rate fixed at 20 g/s/m^2 , the water inlet temperature T_{in} was varied between 20 and 60°C for each solar radiation level (namely $I = 200, 400, 600$ and 800 W/m^2).

A linear regression was, then, performed on the set of these points, and the efficiency graph has been plotted as shown in Figure 5.12.

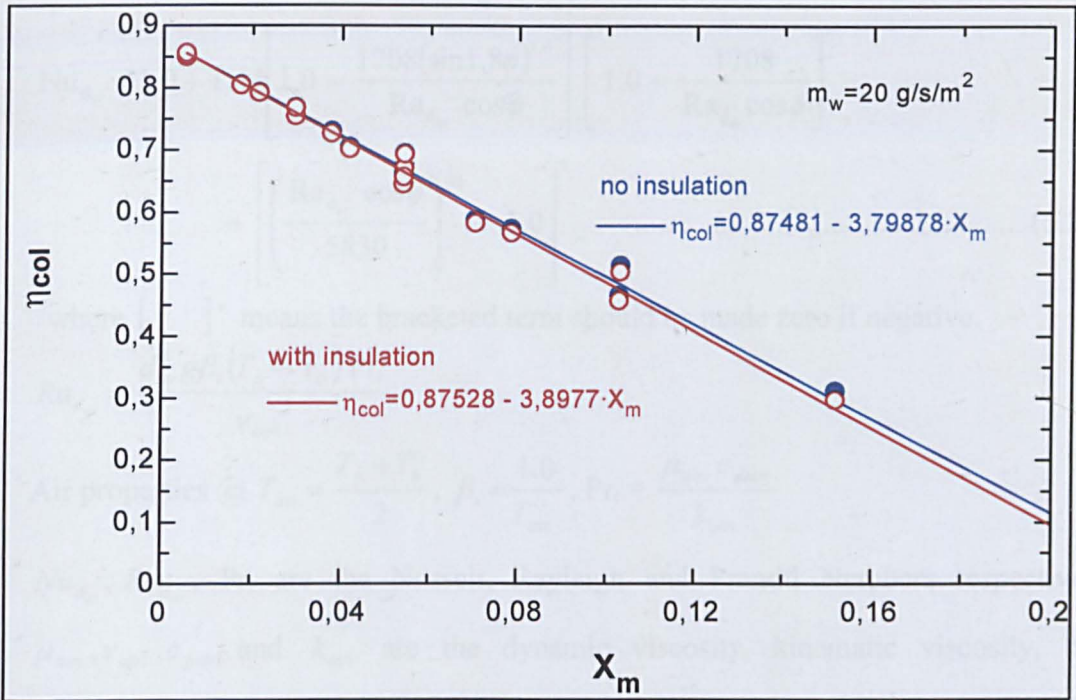


Figure 5.12 Collector efficiency curves with and without insulation;
 $X_m = (T_{av} - T_a)/I$

The removal of the inner thermal insulation, as a design decision, was considered, and its effect on collector performance was analysed. Air cavities act as an insulator; and for the operating temperature range of this collector, air has a thermal conductivity approximately equal to $0.03 \text{ W/m}^\circ\text{C}$.

Without the insulation, the heat-transfer between the back of the copper channel at T_p and the inner surface of the aluminium louvre at T_b is that of convection and radiation between these two surfaces. The convection coefficient is expressed using

the correlation of equation (5.2), while the radiation coefficient is expressed as in equation (5.4).

Let h_{ci} and h_{ri} be the convection and radiation coefficients at this cavity, respectively.

Let ε_{pi} and ε_{ai} be the emmissivities of the aluminium louvre surface, and the back surface of the channel respectively.

The convection coefficient, h_{ci} , is given by:

$$Nu_{d_{av}} = 1.0 + 1.44 \left[1.0 - \frac{1708(\sin 1.8\phi)^{1.6}}{Ra_{d_{av}} \cos \phi} \right] \left[1.0 - \frac{1708}{Ra_{d_{av}} \cos \phi} \right] + \left[\left(\frac{Ra_{d_{av}} \cos \phi}{5830} \right)^{1/3} - 1.0 \right]^* \dots\dots\dots(5.2a)$$

where []* means the bracketed term should be made zero if negative.

$$Ra_{d_{av}} = \frac{d_{av}^3 g \beta_i (T_p - T_b) Pr_i}{\nu_{airi}^2}$$

$$\text{Air properties @ } T_{avi} = \frac{T_p + T_b}{2}, \beta_i = \frac{1.0}{T_{avi}}, Pr_i = \frac{\mu_{airi} c_{pairi}}{k_{airi}}$$

$Nu_{d_{av}}$, $Ra_{d_{av}}$, Pr_i are the Nusselt, Rayleigh and Prandtl Numbers respectively.

μ_{airi} , ν_{airi} , c_{pairi} and k_{airi} are the dynamic viscosity, kinematic viscosity, heat capacity and conductivity of air respectively. With the Nusselt number determined:

$$h_{ci} = \frac{Nu_{d_{av}} k_{airi}}{d_{av}}$$

The radiation coefficient is therefore given by:

$$h_{ri} = \frac{\sigma (T_p^2 + T_b^2) (T_p + T_b)}{\left(\frac{1}{\varepsilon_b} \right) + \left(\frac{1}{\varepsilon_p} \right) - 1} \dots\dots\dots (5.4a)$$

Now with both heat transfer coefficient determined, the heat transfer between these two surfaces is given by:

$$q_{p-b} / A_{col} = (h_{ci} + h_{ri}) (T_p - T_b) \dots\dots\dots (5.13r)$$

Consequently, the bottom loss is given by:

$$q_b/A_{col} = (T_p - T_s) / \left[\frac{L}{k_o} + \frac{1}{(h_{ci} + h_{ri})} \right] \dots\dots\dots (5.15r)$$

Also, equation (5.16) becomes:

$$(h_{co} + h_{rs})(T_s - T_a) = (T_p - T_s) / \left[\frac{L}{k_o} + \frac{1}{(h_{ci} + h_{ri})} \right] \dots\dots\dots (5.16r)$$

And the bottom loss, $q_b = U_b A_{col} (T_p - T_a)$

$$\text{where } U_b = 1 / \left[\frac{1}{(h_{ci} + h_{ri})} + \frac{L}{k_o} + \frac{1}{(h_{co} + h_{rs})} \right] \dots\dots\dots (5.17r)$$

In the program, equations (5.2a) and (5.4a) has been added together with their sub-equations, while equation (5.16r) has replaced (5.16).

The emissivity of the back surface of the channel, ε_{pi} , was taken as 0.80, and the emmissivity of the aluminium louvre surface, ε_{al} , was taken as 0.04.

With these changes, the program was run with the ambient temperature T_a fixed at 20°C, and the water flow rate fixed at 20g/s/m².

The water inlet temperature T_{in} was varied between 20 and 60 °C for each solar radiation level (namely $I = 200, 400, 600$ and 800 W/m^2). A linear regression was performed on the set of these points, and the efficiency graph has been plotted as shown in Figure 5.12.

The effect of removing the thermal insulation on collector performance is depicted on Figure 5.12. As it can be seen, from the graphs, the use of the insulation material has no significant effect on the characteristics of the collector.

Therefore, theoretically the use of an air space instead of an insulating material is slightly better (collector loss coefficient of 3.8 instead of 3.9 $\text{W/m}^2\text{-}^\circ\text{K}$). It also leads to a cheaper solar louvre collector. However, under real operating conditions, if the air space is not well sealed, air infiltration and movement increases the loss coefficient. It is therefore advisable to use the insulation material in the design.

The basic design (i.e. with insulation) was examined further for performance enhancement with the use of fins in the water channel.

The use of 14 fins (seven in each channel) with the geometry and dimensions, as shown in Figure 5.13, was considered.

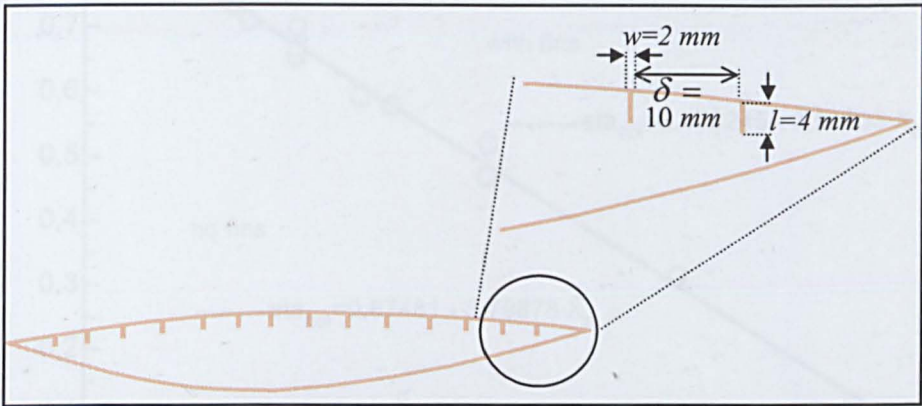


Figure 5.13 Fin geometry for configuration 1 – seven fins in each channel.

The model was adapted to this configuration by modifying equation (5.23).

To accommodate for the effect of the addition of the fins to the surface, the total surface temperature effectiveness, η_{ch} , must be incorporated into equation (5.23).

It is defined as:

$$\eta_{ch} = 1 - \frac{A_{fin}}{A_{tot}}(1 - \kappa)$$

where A_{fin} is the exposed surface area of the fins array only, A_{tot} is the total exposed surface area (including the fins and unfinned surface), and κ defined as:

$$\kappa = \frac{1}{ml} \tanh ml ; \text{ where } m = \sqrt{\frac{2h_{ch}}{k_{cop}w}}, k_{cop} \text{ is the conductivity of the channel material}$$

(i.e. copper). l and w are defined and given as in Figure 5.13., above .

The modified equation is, therefore:

$$\bar{U}A_{col} = 1 / \left(\frac{1}{U_c A_{col}} + \frac{1}{h_{ch} A_{tot} \eta_{ch}} \right) \dots\dots\dots (5.23r)$$

With equation (5.23r) replacing equation (5.23) in the basic configuration, the program was ran as previously described. The results have been used to plot the efficiency as shown in Figure 5.14.

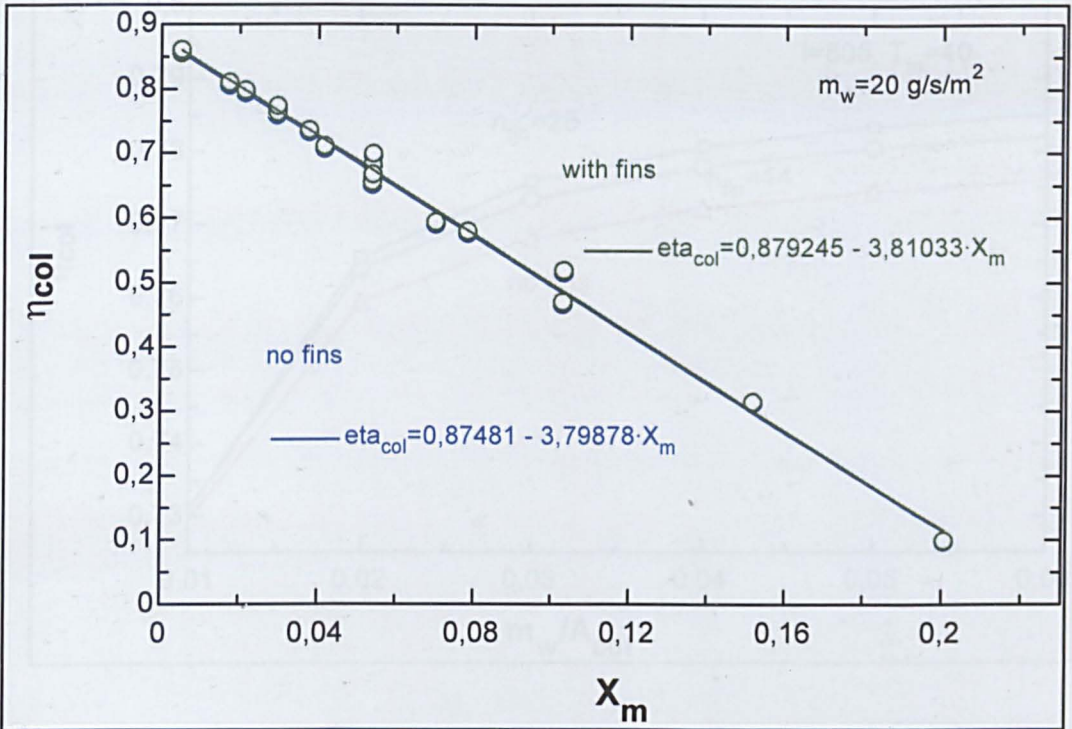


Figure 5.14 Collector efficiency curves with and without fins.

$$X_m = (T_{av} - T_a) / I$$

In Figure 5.14, the collector's efficiency-parameters are not significantly different from the previous ones.

The effect of increasing the number of fins and varying water flow rate was also analysed. As shown in Figure 5.15 below, the effect of increasing the number of fins is rather small.

For a flow rate of 20 g/s/m^2 , increasing the number of fins from 0 to 14 there is an increase of 0.005 in the collector efficiency, and from 14 to 28 there is an increase of 0.002.

For the higher flow of 60 g/s/m^2 , the increase is 0.006 (for the case of 0-14 fins) and 0.003 (for the case of 14-28 fins).

Therefore, it is not appropriate to use fins, as this would only increase the manufacturing costs without any significant efficiency improvement.

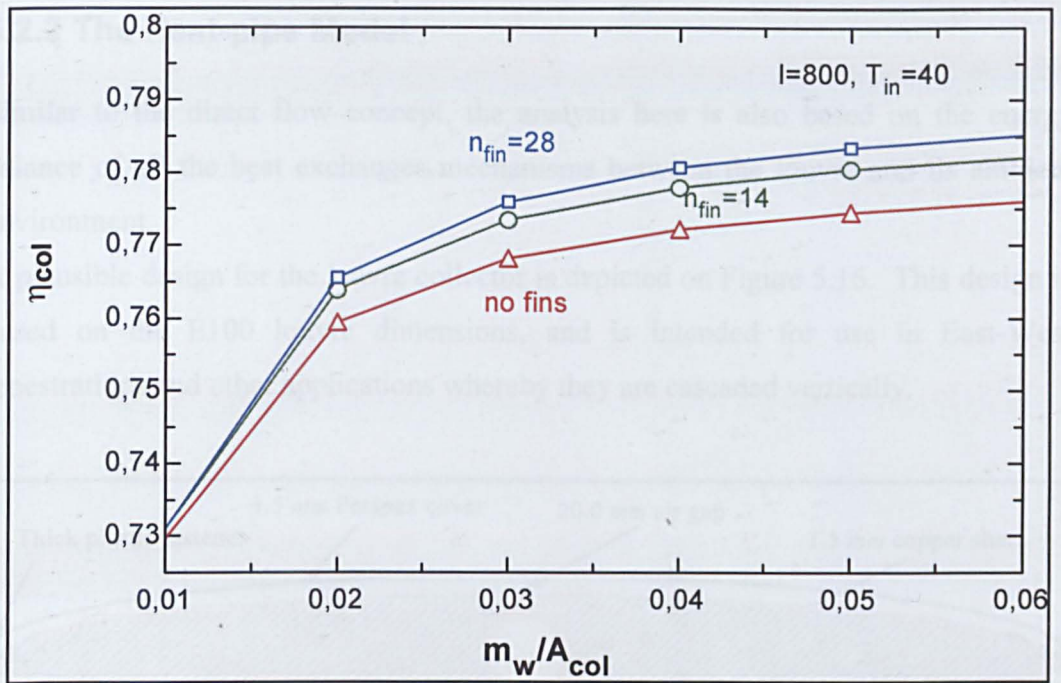


Figure 5.15 Collector efficiency as a function of water flow rate (m_w/A_{col}), for different number of fins (n_{fin})

Finally, it can be deduced from the foregoing discussion that the so-called basic design (i.e. with insulation and no fins) proved to be better than the other configurations.

Figures 5.12 and 5.14 show that for a water rate/collector area ratio of 20 g/s/m^2 , this basic configuration has:

$$F_{av}(\tau_c \alpha_p) = 0.87, \text{ and } F_{av}U_c = 3.9 \text{ W/m}^2\text{-}^\circ\text{K}.$$

These theoretical values indicate that the solar louvre collector could have a very good performance in practice.

A normal flat plate solar collector, with non-selective surface coating and non-evacuated cover, has $F_{av}(\tau_c \alpha_p) = 0.81$ and $F_{av}U_c = 7\text{-}8 \text{ W/m}^2\text{-}^\circ\text{K}$ as typical values, while with a selective coating the value of $F_{av}U_c$ drops down to about $4\text{-}5 \text{ W/m}^2\text{-}^\circ\text{K}$.

An evacuated tube heat pipe solar collector with a selective absorbing surface (Thermomax Ltd) has $F_{av}(\tau_c \alpha_p) = 0.72$ and $F_{av}U_c = 2.9 \text{ W/m}^2\text{-}^\circ\text{K}$.

5.2.2 The Heat-pipe Model

Similar to the direct flow concept, the analysis here is also based on the energy balance of all the heat exchanges mechanisms between the louvre and its ambient environment.

A plausible design for the louvre collector is depicted on Figure 5.16. This design is based on the E100 louvre dimensions, and is intended for use in East-West fenestrations and other applications whereby they are cascaded vertically.

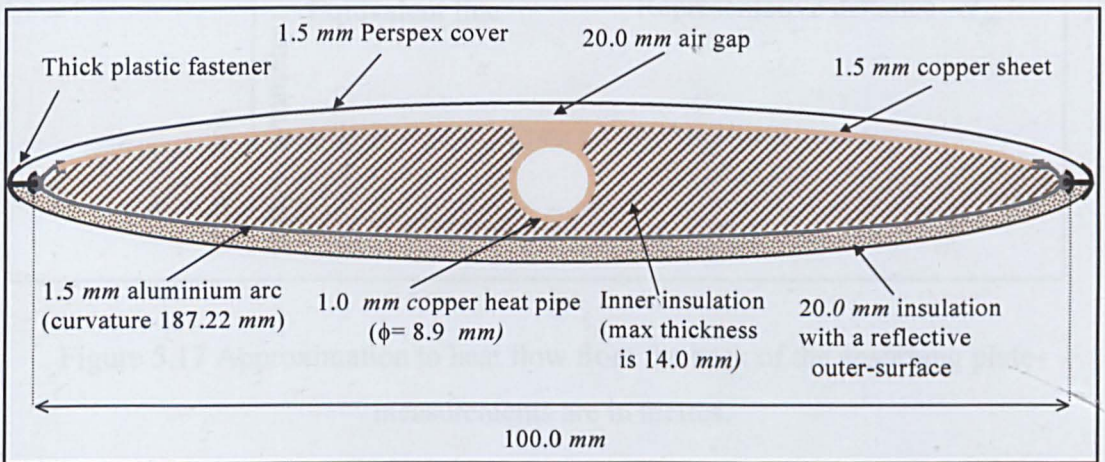


Figure 5.16 Schematic of the solar louvre cross-section incorporating a heat pipe.

(Aspect ratio = 5.9)

5.2.2.1 Further Assumptions and Approximations

- To confine this work to one-dimensional analysis, the curvature of the back surface of the channel is taken as a straight line parallel to the major axis of the louvre. This approximation is taken following a two-step formulation similar to that used for the direct flow design model of section (5.2.1.1). As shown in Figure 5.17, with this approximation, the heat flow from the back surface of the louvre to the major axis, for example, would be as if it was from the equivalent line to the major axis through the representative distance.
- The contact resistance between the absorbing plate and the heat pipe is assumed negligible such that the material is considered continuous.

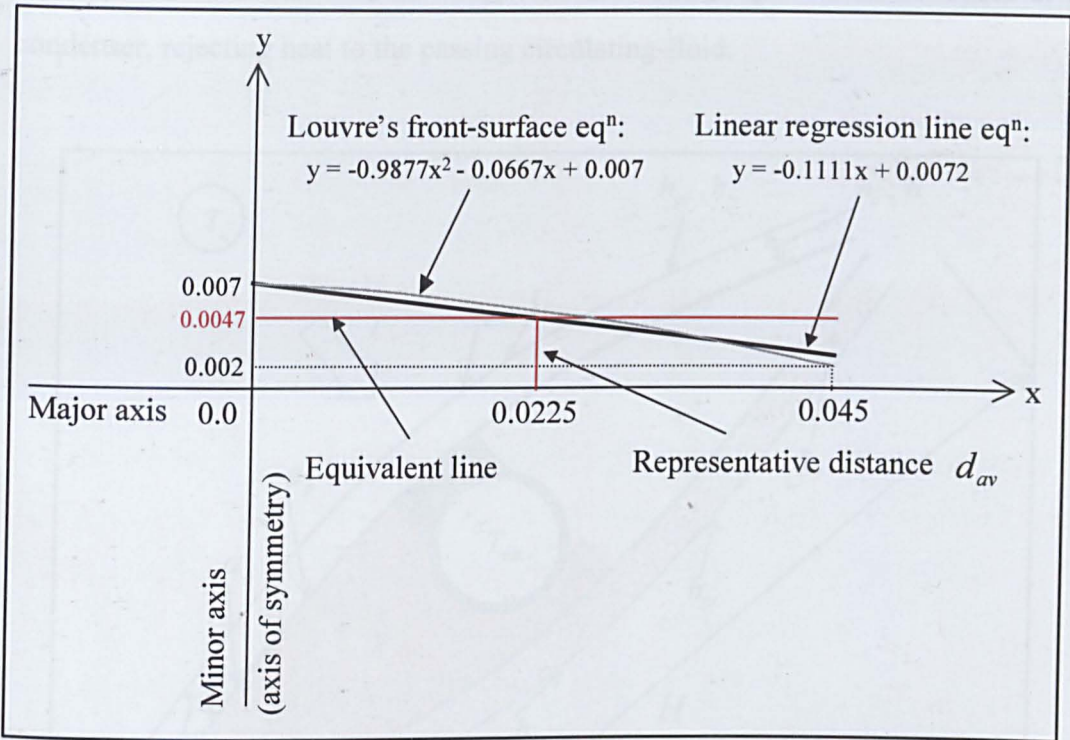


Figure 5.17 Approximation to heat flow from the back of the absorbing plate—measurements are in metres.

5.2.2.2 The Governing Equations

The absorber plate and the inner surface of the cover exchange radiation that results from their own emissions. They are also subjected to convective heat transfer. Let h_r, h_c denote these radiation and convection heat transfer coefficients respectively.

The outer surface of the cover and the back-insulation outer surface radiates to the ambient environment. Let h_{ro}, h_{rs} denote these radiation-coefficients respectively.

These surfaces are also subjected to convection to the same environment at T_a . Let h_{co} denote this, wind-induced, heat transfer coefficient.

Conduction heat transfer is also present through the inner and outer insulation materials.

Absorbed energy at the absorbing plate (fins) flow by conduction through the copper of the evaporator to saturate the working fluid (water) in the heat pipe, until the saturation temperature of the water is reached- [$P_{sat} = 0.018$ bar, therefore

$T_{sat} = 15^\circ\text{C}$]. Then, the vapour at T_{sat} travels vertically upwards to condense at the condenser, rejecting heat to the passing circulating-fluid.

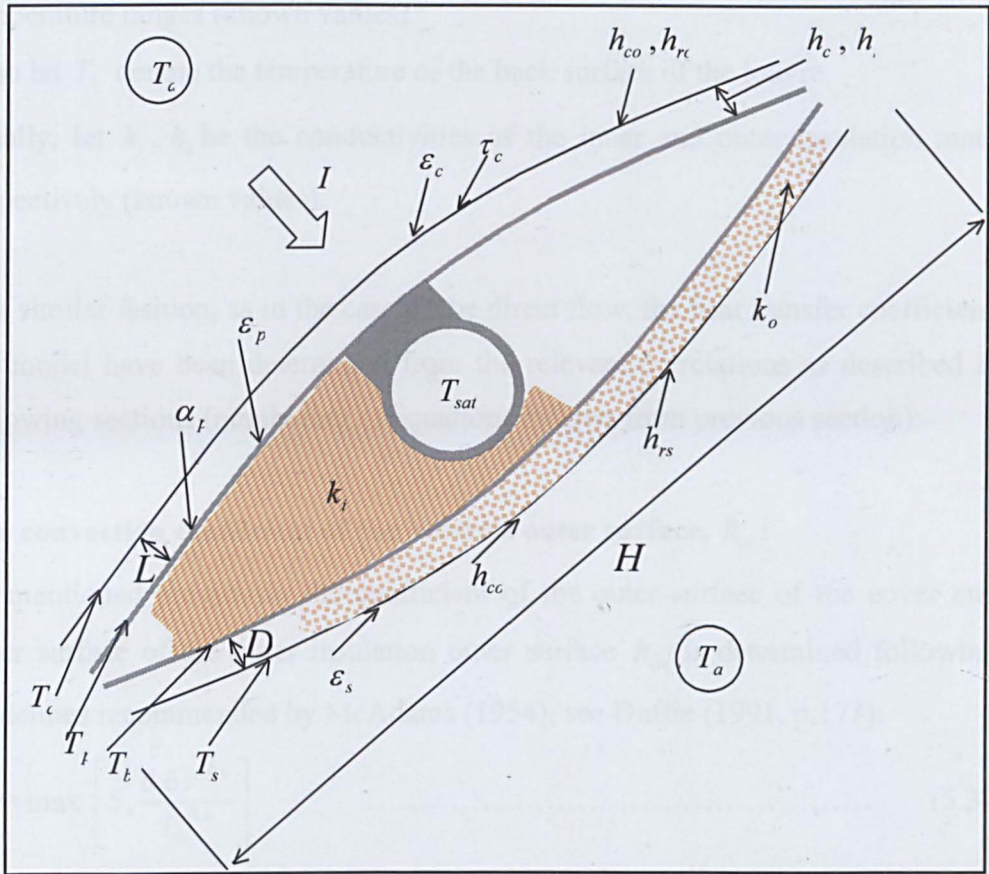


Figure 5.18 Schematic of the solar louvre cross-section - unit length, normal to the page.

Assuming steady-state performance, with the solar irradiation, I , known for the location and time in question:

Let τ_c , α_p be the transmissivity of the outer cover and the absorptivity of the absorbing surface, respectively (known values).

Let $(\tau_c \alpha_p)$ denote the apparent solar transmissivity-absorptivity of the cover-plate, so that in any event the $(\tau_c \alpha_p)I$ product represents the solar energy absorbed at the absorbing surface.

It is assumed that there exist representative average temperatures for the cover, the absorber plate, back of the louvre and back-insulation surface. So let T_c , T_p , T_s ,

represent the uniform temperatures of the cover, the absorbing plate and the back-insulation outer surface respectively. These temperatures are unknowns.

And let $\epsilon_c, \epsilon_p, \epsilon_s$ be the emissivities of these surfaces at their respective temperature ranges (known values).

Also let T_b denote the temperature of the back surface of the louvre.

Finally, let k_i, k_o be the conductivities of the inner and outer insulation materials respectively (known values).

In a similar fashion, as in the case of the direct flow, the heat transfer coefficients for the model have been determined from the relevant correlations as described in the following sections (numbering of equations follows from previous section):

The convection coefficient of the louvre’s outer surface, h_{co} :

As mentioned previously the coefficient of the outer surface of the cover and the outer surface of the outer insulation outer surface h_{co} is determined following the guidelines recommended by McAdams (1954); see Duffie (1991, p.173):

$$h_{co} = \max \left[5, \frac{8.6V^{0.6}}{L_b^{0.4}} \right] \dots\dots\dots (5.32)$$

where u is the wind speed in m/s, and L_b is the cubic root of the building’s volume in metres.

The convection coefficient of the cover’s inner surface, h_c

Based mainly on the studies of Hollands *et al* (1976), the following correlation is used:

$$Nu_L = 1.0 + 1.44[1.0 - B]^* \left[1.0 - B(\sin 1.8\phi)^{1/6} \right] + \left[0.664 B^{-1/3} - 1.0 \right]^* \dots\dots(5.33)$$

where $B = \frac{1708}{Ra_L \cos \phi}$; []* means the bracketed term should be made zero if

negative.

$$Ra_L = \frac{L^3 g \beta (T_p - T_c) Pr}{\nu_{air}^2}$$

Air properties @ $T_{av} = \frac{T_p + T_c}{2}$, $\beta = \frac{1.0}{T_{av}}$, $Pr = \frac{\mu_{air} c_{p,air}}{k_{air}}$

$\{\phi = 90^\circ, use \phi = 75^\circ, Ar = H/L > 12.0, 0.0 < Ra_L < 10^5\}$

Ar is the aspect ratio, H and L are the dimensions shown in Figure 5.18.

Nu_L, Ra_L, Pr are the Nusselt, Rayleigh and Prandtl Numbers respectively.

$\mu_{air}, \nu_{air}, c_{p,air}$ and k_{air} are the dynamic viscosity, kinematic viscosity, heat capacity and conductivity of air respectively. g is gravity, and ϕ is the louvre's angle of inclination (90°), taken as 75° .

With Nusselt number determined, $h_c = \frac{Nu_L k_{air}}{L}$.

The radiation coefficient of the cover's inner surface, h_r :

Using the infrared radiation exchange between two grey parallel surfaces Duffie (1991, pp. 156-157):

$$h_r = \frac{\sigma(T_p^2 + T_c^2)(T_p + T_c)}{\left(\frac{1}{\epsilon_c}\right) + \left(\frac{1}{\epsilon_p}\right) - 1} \dots\dots\dots (5.34)$$

where σ is Stefan-Boltzmann constant [$= 5.67 \times 10^{-8} W/m^2 - ^\circ K^4$].

The radiation coefficient of the cover's outer surface, h_{ro} :

Here the sky is considered as a black body at an equivalent temperature T_a .

$$h_{ro} = \sigma \epsilon_c (T_c^2 + T_a^2) (T_c + T_a) \dots\dots\dots (5.35)$$

The radiation coefficient of the cover's outer surface, h_{rs} :

As above:

$$h_{rs} = \sigma \epsilon_s (T_s^2 + T_a^2) (T_s + T_a) \dots\dots\dots (5.36)$$

Heat loss from the front and back surfaces of the louvre, q_{loss} :

The front loss, q_f , is the net heat flow between the cover at T_c and the ambient air at

T_a ; q_{c-a} , is expressed using Newton's law of cooling and the linearized radiation law as:

$$q_{c-a}/A_{col} = h_{co}(T_c - T_a) + h_{ro}(T_c - T_a) = (h_{co} + h_{ro})(T_c - T_a) \dots\dots\dots(5.37)$$

where A_{col} is the upper (unobstructed) surface area of the absorbing-plate that receives the radiation.

This same front loss is also the net heat transfer between the cover at T_c and the absorbing-plate at T_p , q_{p-c} , and is expressed using Newton's law of cooling and the linearized radiation law as:

$$q_{p-c}/A_{col} = h_c(T_p - T_c) + h_r(T_p - T_c) = (h_c + h_r)(T_p - T_c) \dots\dots\dots (5.38)$$

Now, since $q_{c-a} = q_{p-c} = q_f$; equating(5.37) and(5.38) gives:

$$(h_{co} + h_{ro})(T_c - T_a) = (h_c + h_r)(T_p - T_c) \dots\dots\dots (5.39)$$

Also, adding(5.37) and(5.38) eliminates T_c , giving:

$$q_f/A_{col} = (T_p - T_a) / \left[\frac{1}{(h_{co} + h_{ro})} + \frac{1}{(h_c + h_r)} \right]$$

Therefore:

$$q_f = U_f A_{col} (T_p - T_a)$$

$$\text{where } U_f = 1 / \left[\frac{1}{(h_{co} + h_{ro})} + \frac{1}{(h_c + h_r)} \right] \dots\dots\dots(5.40)$$

The back loss, q_b , is the net heat flow between the outer surface of the outer insulation at T_s and the ambient air at T_a ; q_{s-a} is expressed using Newton's law of cooling and the linearized radiation law as:

$$q_{s-a}/A_{col} = (h_{co} + h_{rs})(T_s - T_a) \dots\dots\dots (5.41)$$

This same back loss is also the heat transfer between the back of the absorbing-plate at T_p and the inner surface of the outer insulation at T_b ; q_{p-b} , is expressed using Fourier's law as:

$$q_{p-b} / A_{col} = \frac{k_i}{d_{av}} (T_p - T_b) \dots\dots\dots (5.42)$$

where d_{av} is the average thickness of the inner insulation material- (Taken as 0.01 m) – see Figure 5.17 above.

Also, this same bottom loss is the heat transfer between the inner surface of the outer insulation at T_b and the outer surface of the outer insulation at T_s ; q_{b-s} , is expressed using Fourier's law as:

$$q_{b-s} / A_{col} = \frac{k_o}{L} (T_b - T_s) \dots\dots\dots (5.43)$$

Now, T_b is eliminated by simply adding(5.42) and(5.43), yielding:

$$\frac{q_{p-b} d_{av}}{A_{col} k_i} + \frac{q_{b-s} L}{A_{col} k_o} = (T_p - T_s) \dots\dots\dots (5.44)$$

Also T_s is eliminated by adding(5.41) and(5.44), yielding

(since $q_b = q_{s-a} = q_{b-s} = q_{p-b}$):

$$\frac{q_b}{A_{col}} \left[\frac{d_{av}}{k_i} + \frac{L}{k_o} + \frac{1}{(h_{co} + h_{rs})} \right] = (T_p - T_a),$$

which can be rewritten as:

$$q_b = U_b A_{col} (T_p - T_a) \dots\dots\dots(5.45)$$

where $U_b = 1 / \left[\frac{d_{av}}{k_i} + \frac{L}{k_o} + \frac{1}{(h_{co} + h_{rs})} \right]$

Also equating equations(5.41) and(5.44), remembering that

($q_b = q_{s-a} = q_{b-s} = q_{p-b}$), gives:

$$(h_{co} + h_{rs})(T_s - T_a) = \frac{1}{\left(\frac{d_{av}}{k_i} + \frac{L}{k_o} \right)} (T_p - T_s) \dots\dots\dots(5.46)$$

Finally, the total loss, q_{loss} , is therefore:

$$q_{loss} = q_t + q_b$$

i.e.

$$q_{loss} = A_{col} U_c (T_p - T_a) \dots\dots\dots (5.47)$$

where $U_c = U_t + U_b$

Energy Balance on the whole louvre collector:

If q_u is the useful net heat flow to the working fluid, then:

$$q_u = A_{col} [(\tau_c \alpha_p) I - U_c (T_p - T_a)] \dots\dots\dots (5.48)$$

This useful heat is then absorbed by the water in the heat pipe, creating vapour which travels up the pipe, carrying the energy as a latent heat of vaporization. This heat, assuming no losses, is dissipated when condensation takes place; hence:

$$q_{con} = A_c \alpha (t_c - t_b) \dots\dots\dots (5.49)$$

where $A_c = \pi d h_c$, $t_c \approx (T_{sat} - vp) \text{ } ^\circ C$ (vp is a variable) and $t_b = \frac{t_1 + t_2}{2}$.

A_c and h_c are the area and height of the condenser respectively; d is the diameter of the heat pipe. t_c is the condenser temperature, taken optimally; while t_b is the bulk temperature of the cooling fluid in the vicinity/domain of the condenser, taken as the arithmetic mean (logarithmic mean would be better), and α is the convective heat transfer coefficient.

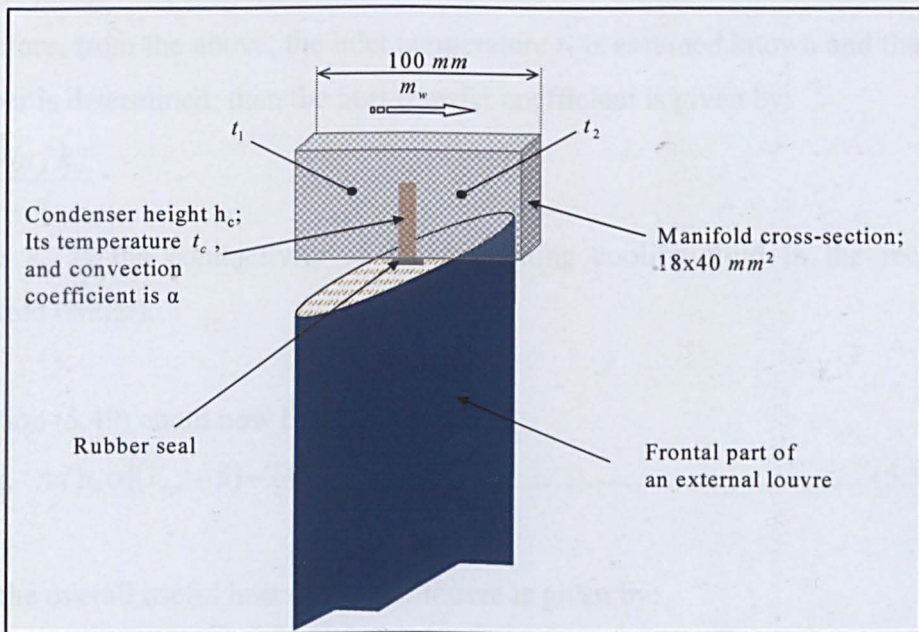


Figure 5.19 Schematic of a single solar louvre

The convective heat transfer coefficient, α , is given from the correlation provided by Zhukauskas (1972):

$$Nu_d = C Re_d^m Pr^n \left(\frac{Pr_1}{Pr_c} \right)^{1/4} \dots\dots\dots(5.50)$$

- 0.7 < Pr < 500
- 1 < Re_d < 10⁶
- C and m from the table below
- n = 0.37, Pr ≤ 10
- n = 0.36, Pr > 10
- properties at t_b, except Pr₁ and Pr_c at t₁ and t_c respectively

Here Nu_d and Re_d are the Nusselt and Reynolds numbers, based on the characteristic length d, which is the diameter of the heat pipe's condenser, in this case.

Range of Re _d	C	m
1 - 40	0.75	0.4
40 - 1000	0.51	0.5
10 ³ - 2×10 ⁵	0.26	0.6
2×10 ⁵ - 10 ⁶	0.076	0.7

Therefore, from the above, the inlet temperature t₁ is assumed known and the Nusselt number is determined; then the heat transfer coefficient is given by:

$$\alpha = \frac{Nu_d k_w}{d}$$

where k_w is the conductivity of the circulating cooling fluid in the rectangular manifold (water).

Equation (5.49) could now be rewritten as:

$$q_{con} = \pi d h_c \alpha \left[(T_{sat} - 5) - \frac{1}{2}(t_1 + t_2) \right] \dots\dots\dots(5.51)$$

Also the overall useful heat of the one louvre is given by:

$$q_w = m_w c_{pw} (t_2 - t_1) \dots\dots\dots(5.52)$$

Now, since $q_u = q_{con} = q_w$; equating (5.48), (5.51) with (5.52), in turn, gives:

$$m_w c_{pw} (t_2 - t_1) = A_{col} [(\tau_c \alpha_p) I - U_c (T_p - T_a)] \quad \dots\dots\dots (5.53)$$

$$m_w c_{pw} (t_2 - t_1) = \pi d h_c \alpha [(T_{sat} - 5) - \frac{1}{2}(t_1 + t_2)] \quad \dots\dots\dots (5.54)$$

5.2.2.3 The Solution

The final set of equations used for the solution are (5.39), (5.46), (5.53) and (5.54).

This is a non-linear set in the four unknowns: T_c , T_p , T_s and t_2 .

The dimensions of the louvre were all taken as shown in Figure 5.16. The manifold has a rectangular section with 18 mm x 40 mm. Condenser heat pipe length was equal to 30 mm. A reference length (height) of 1m was used for the louvre collector.

The same radiation properties as in the direct flow configuration (configuration 1) were used for the transparent cover, louvre material and selective coating.

Thermal properties of air and water, including Prandtl number were assigned from within the built-in tables provided by the EES program.

The conductivities of the inner and outer insulation materials, k_i , k_o , were both taken as 0.03 W/m-°K.

Climatic variables, (solar radiation, ambient temperature and wind speed), affect collector performance. However, the variation of the wind speed on a solar collector has the expected results of increasing the losses. Therefore, u was taken as 5 m/s (which is close to the world average wind speed), and L_b as 8 m, giving $h_{co} = 9.8$ W/m²-°K throughout the analysis, so that comparison between the different collector configurations/designs could be established.

Solar radiation was varied as: $I = 200$ to 800 W/m². The ambient temperature was taken as, $T_a = 20^\circ\text{C}$.

Other operating variables are water flow rate and inlet water temperature. Water flow rates in the channels, m_w , were varied between 20 and 500 g/s/m² of collector area, and the inlet water temperature, T_{in} , between 20 to 60°C.

Like the previous case, the efficiency curve is plotted using the following equation:

$$\frac{m_w c_p (T_{out} - T_m)}{A_{col} I} = F_{av} (\tau_c \alpha_p) - F_{av} U_c \frac{(T_{av} - T_a)}{I} \dots\dots\dots (5.55)$$

Based on the preceding analysis, the program has been run on numerous situations to account for the effect of changing various parameters, and the results are as presented in the graphs depicted on the following pages.

5.2.2.4 The Results of the Heat-pipe Model

Figure 5.20 shows collector efficiency for configuration 2. Here, the efficiency is significantly lower than for configuration 1 – very low $F_{av} (\tau_c \alpha_p)$ value. This is due to the low transfer surface – only one heat pipe is used.

Note that the increase in water flow rate has more influence than in configuration 1 – see Figure 5.20 and Figure 5.21.

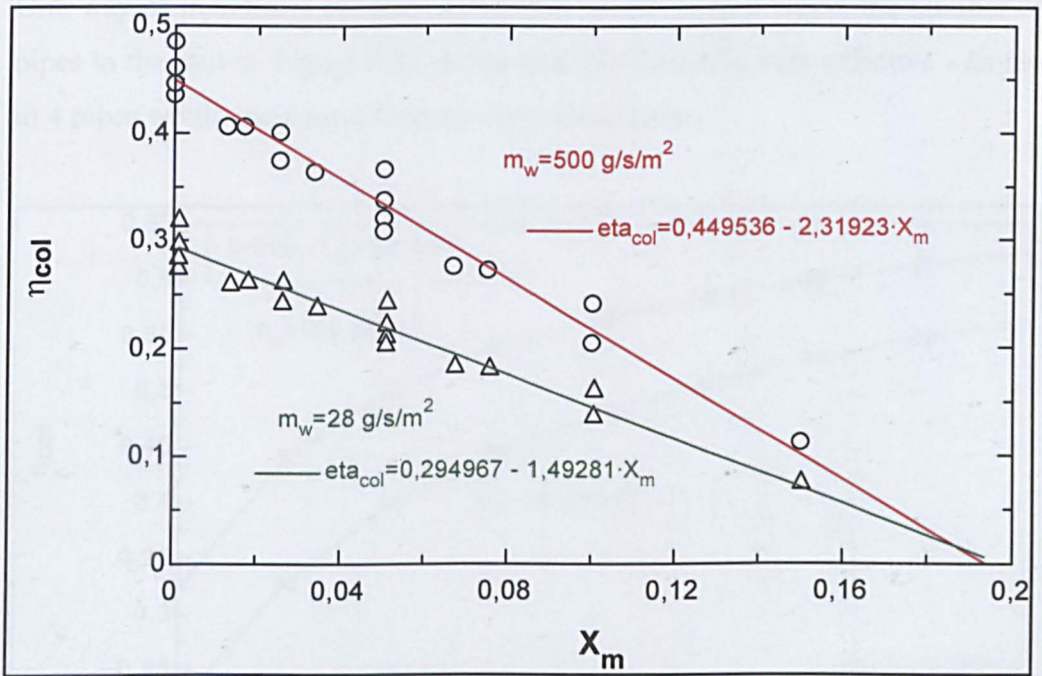


Figure 5.20 Collector efficiency curves for 2 water flow rates; $X_m = (T_{av} - T_a) / I$.

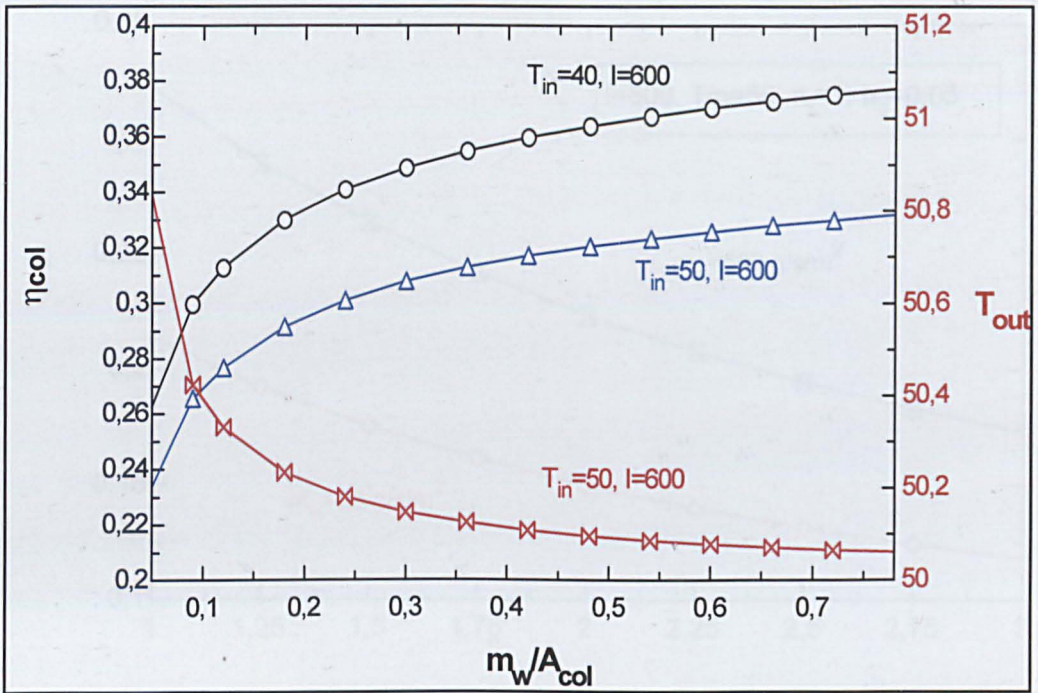


Figure 5.21 Collector efficiency and outlet temperature as a function of water flow rate (in $kg/s/m^2$), for different inlet

One way of increasing collector efficiency would be to increase the number of heat pipes in the louvre. Figure 5.22 shows that this would be very effective - an increase to 4 pipes would increase efficiency up to about twice.

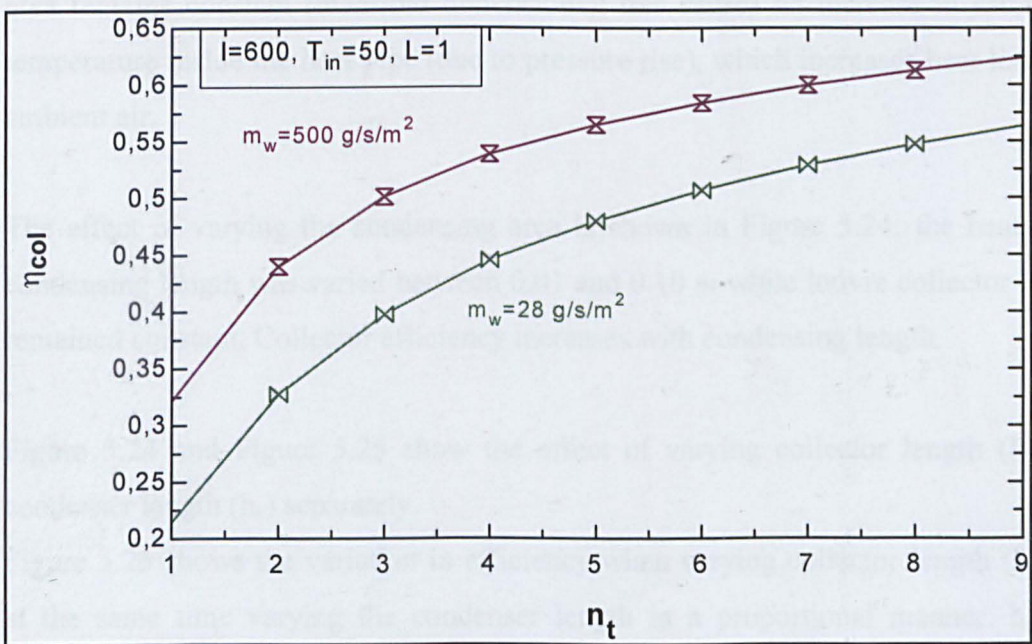


Figure 5.22 Effect of heat pipe number (n_t) on collector efficiency for two different water flow rates.

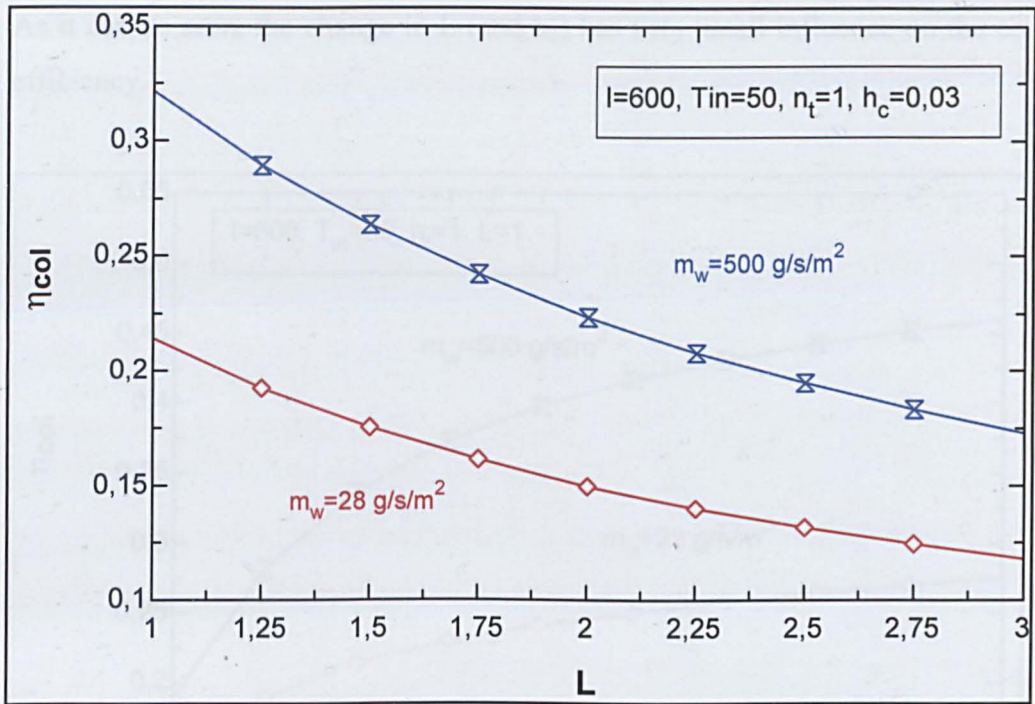


Figure 5.23 Effect of louvre collector length on collector efficiency for different water flow rates

The effect of changing louvre length (height) has also been analysed. Figure 5.23 shows results for lengths between 1 and 3 m. Collector efficiency decreases as length increases. This is due to the fact that evaporator area is increasing while condensing area remains constant (manifold dimensions): this causes an increase in saturation temperature inside the heat pipe (due to pressure rise), which increases heat losses to ambient air.

The effect of varying the condensing area is shown in Figure 5.24; the heat pipe-condensing length was varied between 0.01 and 0.10 m while louvre collector length remained constant. Collector efficiency increases with condensing length.

Figure 5.24 and Figure 5.25 show the effect of varying collector length (L) and condenser length (h_c) separately.

Figure 5.25 shows the variation in efficiency when varying collector length (L) and at the same time varying the condenser length in a proportional manner. h_c was varied between 0.025 and 0.065 m, while L was varied between 1 and 3 m.

As it can be seen, the change in L (and h_c) has very small influence on the collector efficiency.

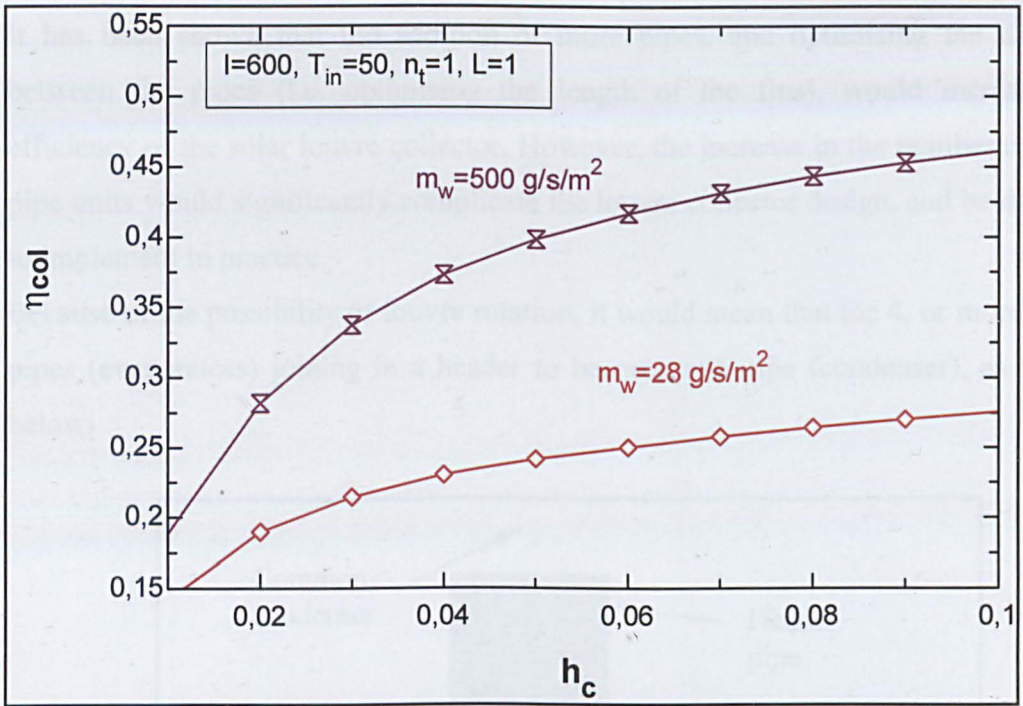


Figure 5.24 Effect of condenser length on collector efficiency, for two different water flow rates.

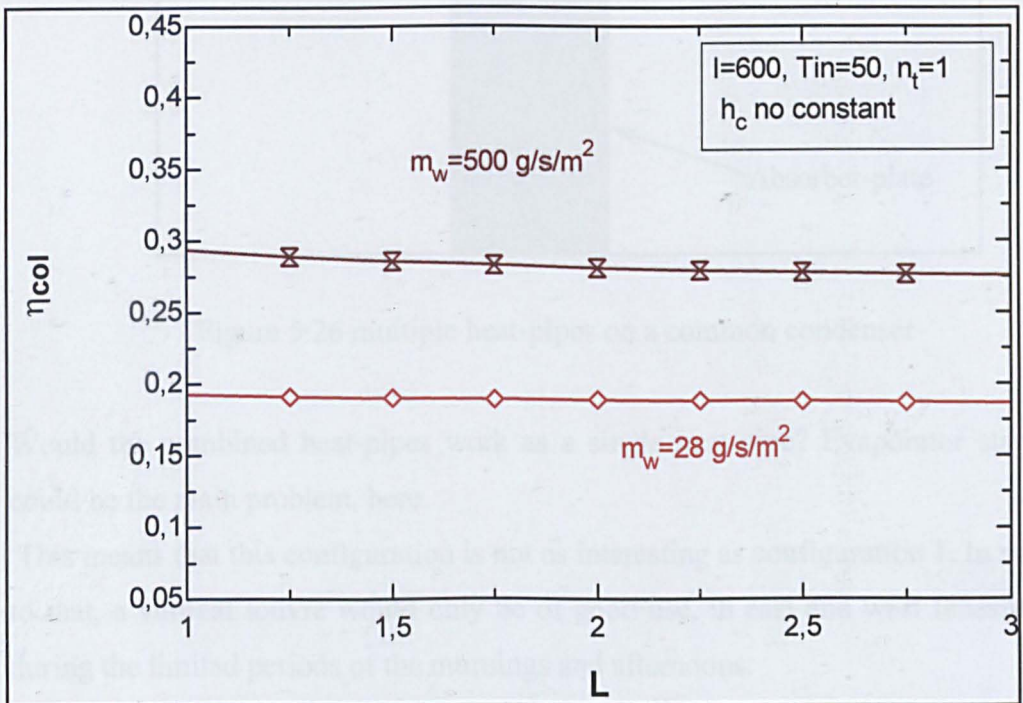


Figure 5.25 Effect of louvre collector length, with a proportional variation of condenser length, on collector

5.3 Summary

The results indicate that the Direct-flow configuration (configuration 1), would perform better than the Heat-pipe configuration (i.e. configuration 2).

It has been shown that the addition of more pipes, and optimising the distance between the pipes (i.e. optimising the length of the fins), would increase the efficiency of the solar louvre collector. However, the increase in the number of heat-pipe units would significantly complicate the louvre collector design, and be difficult to implement in practice.

Because of the possibility of louvre rotation, it would mean that the 4, or more, heat-pipes (evaporators) joining in a header to become one pipe (condenser), as shown below:

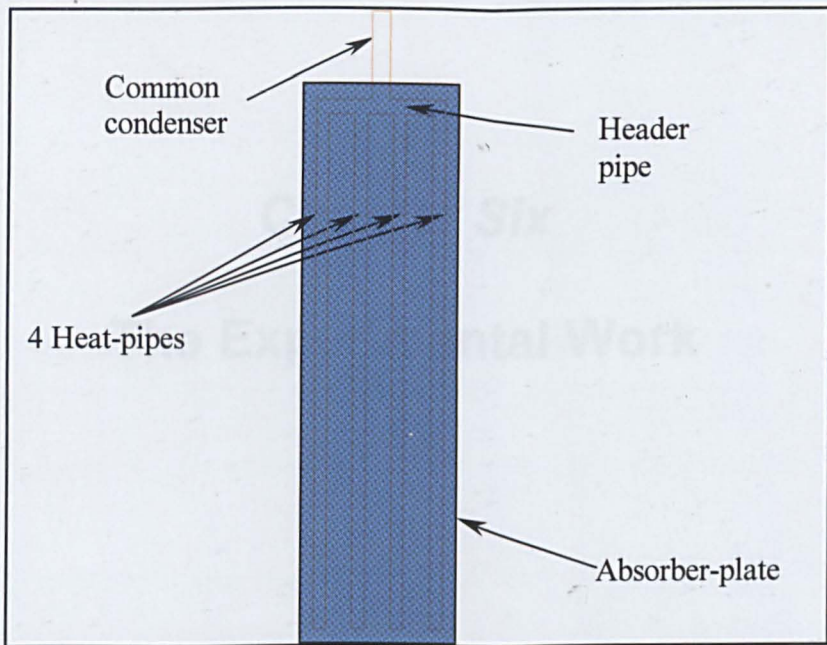


Figure 5.26 multiple heat-pipes on a common condenser

Would the combined heat-pipes work as a single heat-pipe? Evaporator starvation could be the main problem, here.

This means that this configuration is not as interesting as configuration 1. In addition to that, a vertical louvre would only be of good use, in east and west fenestrations, during the limited periods of the mornings and afternoons.

Attention has therefore been focused on the Direct-flow configuration.

Chapter Six

The Experimental Work

6. The Experimental Work

As mentioned in the previous chapter, the energy-balance calculation method is a satisfactory representation of most flat plate collectors. However, due to the fact that these louvres have geometry that is quite different (curvature, sharp edges and limited void) to normal flat plate collectors, validation of the modelling results would be necessary, and therefore must be performed.

The results from the pending experimental work is in fact expected to be somewhat different to those obtained from mathematical modelling. Nevertheless, they provide adequate information for the validation of the model.

As shown previously, the issue of the type of heat exchanger to be used has risen, and two plausible possibilities have been nominated; these are channel and the conventional fin-on-tube heat exchangers- Figure 6.1:

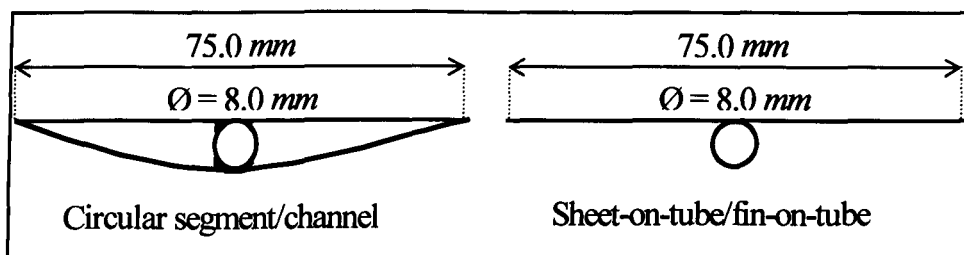


Figure 6.1 Same frontal surface-area (2000 mm length), coated with Black paint

The remaining part of this chapter is dedicated to establishing the energy performance (i.e. thermal characteristics) of the solar louvre collector.

In this, both circular segment/channel, and sheet-on-tube/fin-on-tube have been compared under identical operating and ambient conditions.

The schematic drawings used for the purpose of the mathematical modelling, in the previous chapter, were not and are not descriptive enough for the purpose of manufacturing. They do not realistically represent the exact measurements, nor they allow for thermal expansion or tightness against external elements.

Manufacturing a composite object, which is made out of three completely different materials, all carefully assembled by steel bolts and screws, could pose somewhat a challenge, if this object is to be placed outdoor; and for decades.

The different thermal expansion between the different materials cause, improperly fastened composite objects to break/shear.

Therefore, thermal-expansion gaps should be allowed for, and the various methods of fastening should, simultaneously, be thought through.

Allowing two different materials to slide freely against each other, rather than be bolted down, solves the problem of thermal expansion, but brings with it, hand-on-hand, the problem of external elements entering the solar collector. Rain and dust could ruin any solar collector.

The louvres manufactured for this experiments were only trial-run-samples for the extrusions process of the different materials.

The louvres, used for the experimental work (250E), have been made out of:

- Aluminium shell, extruded from Aluminium 6063T6. The outer surface of the shell has been coated, with an off-white colour (NCS-S 1002 B-collection 225/AKZO NOBEL).
- Copper fluid channels and absorber-plate, manufactured from Oxygen-free, high conductivity copper. Its upper surface coated with a matt-black selective paint, with optical properties approximately similar to those of Black-chrome coatings.
- Transparent cover, extruded in double pane, made out from a plastic/polycarbonate material.

Physical properties of the three above materials are included in appendix (B).

The method of fastening the transparent-cover to the aluminium shell has been by way of rubber.

The only other material used in the construction of these louvres is the glass-wool (Rock wool) insulation.

It had, therefore become necessary, at some stage of this work, to prepare exact AutoCAD drawings for manufacturing, to allow for exact measurements. These drawings are as depicted in Figures 6.3 to 6.7.

Figure 6.2 below, depicts the finished product of the different components of the louvre.

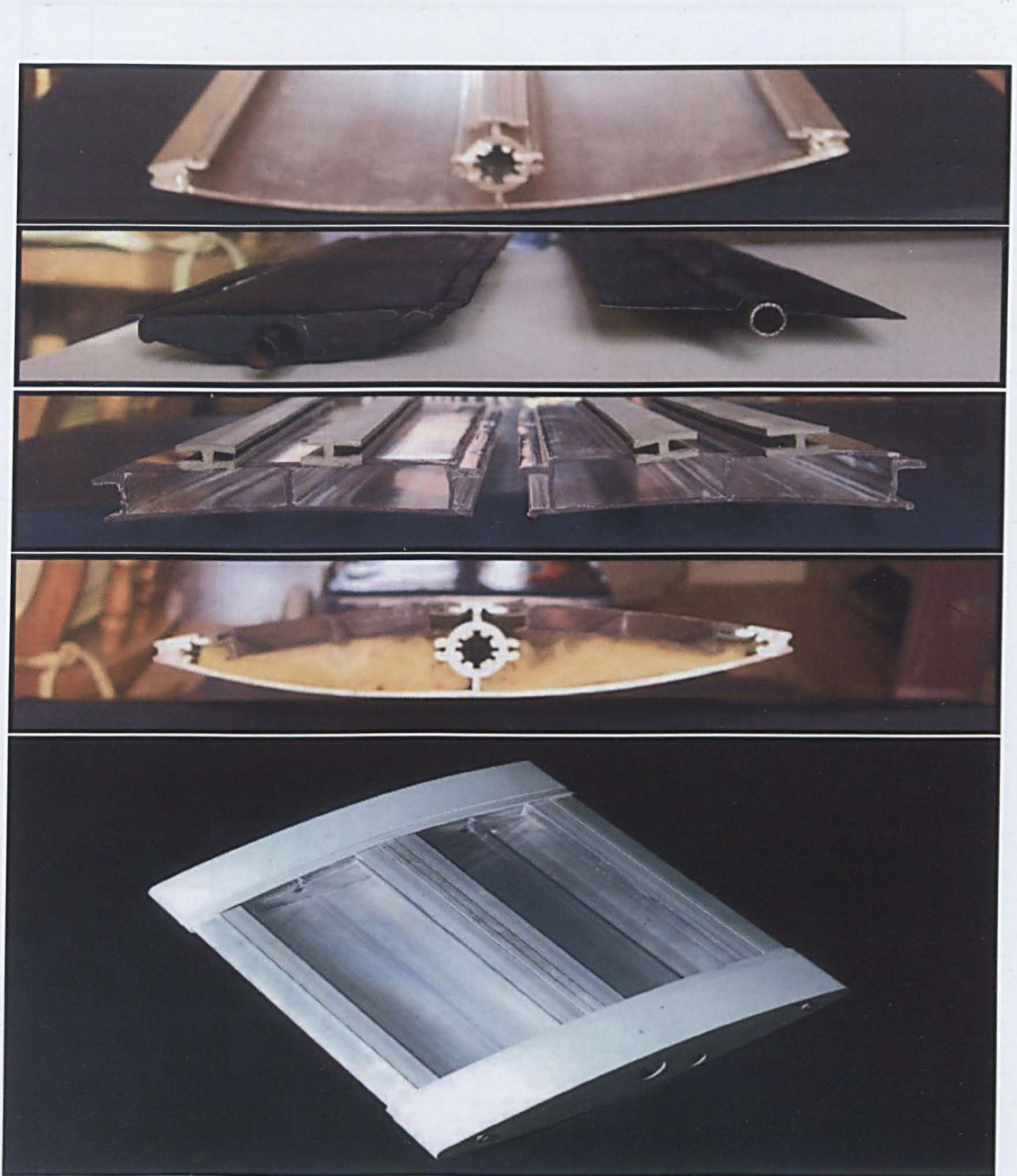
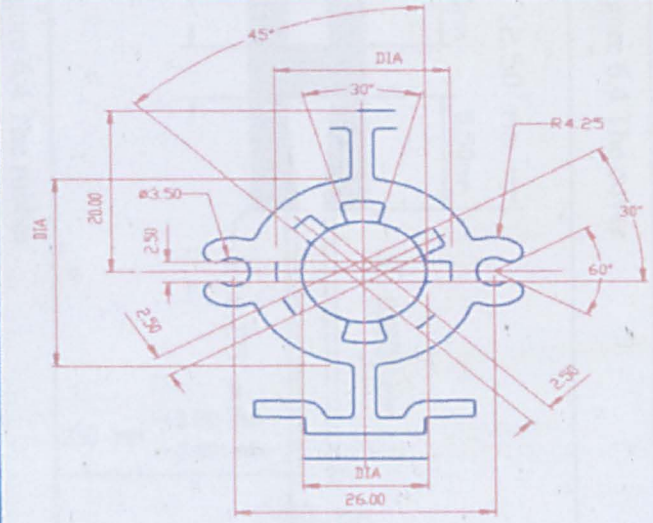
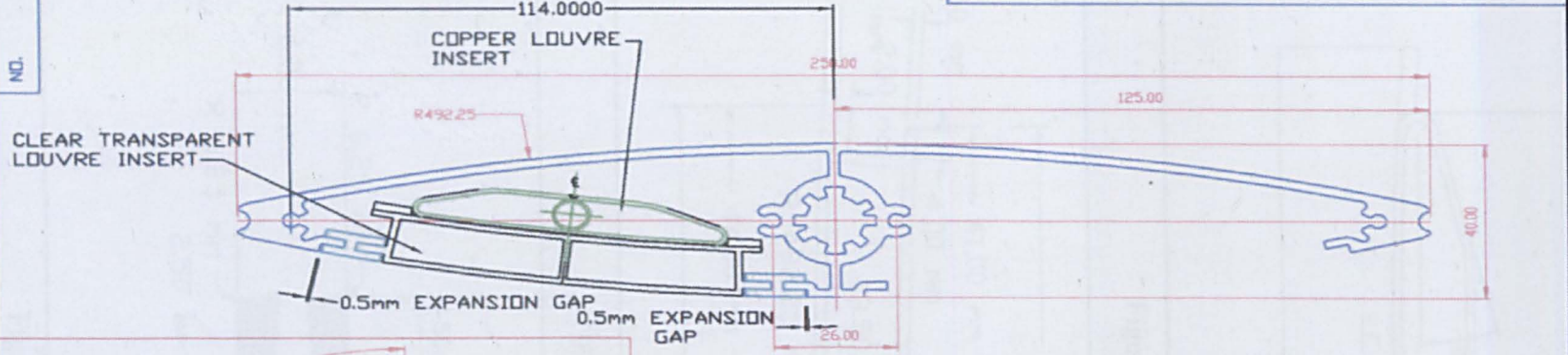


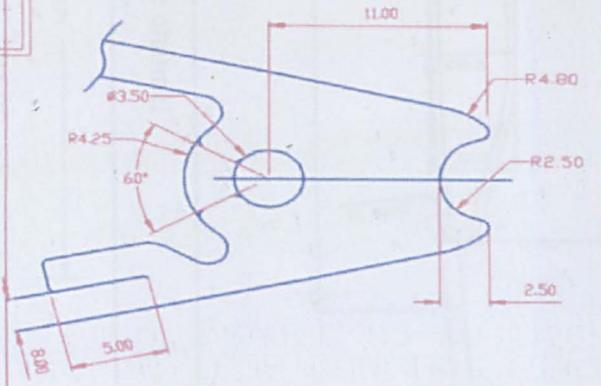
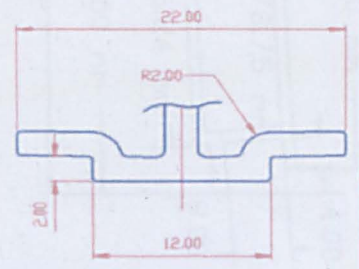
Figure 6.2 From top to bottom: Louvre shell (1st), channel and fin-on-tube (2nd), transparent covers (3rd) and the assembled louvre (4th) and a short sample (without the fluid duct), (5th).

ALCOA EUROPE
VAUNARLWYDD WORKS, SWANSEA, W GLAM.

NO.



DRAWING FOR CLIENTS
APPROVAL
APPROVED BY _____
DATE _____



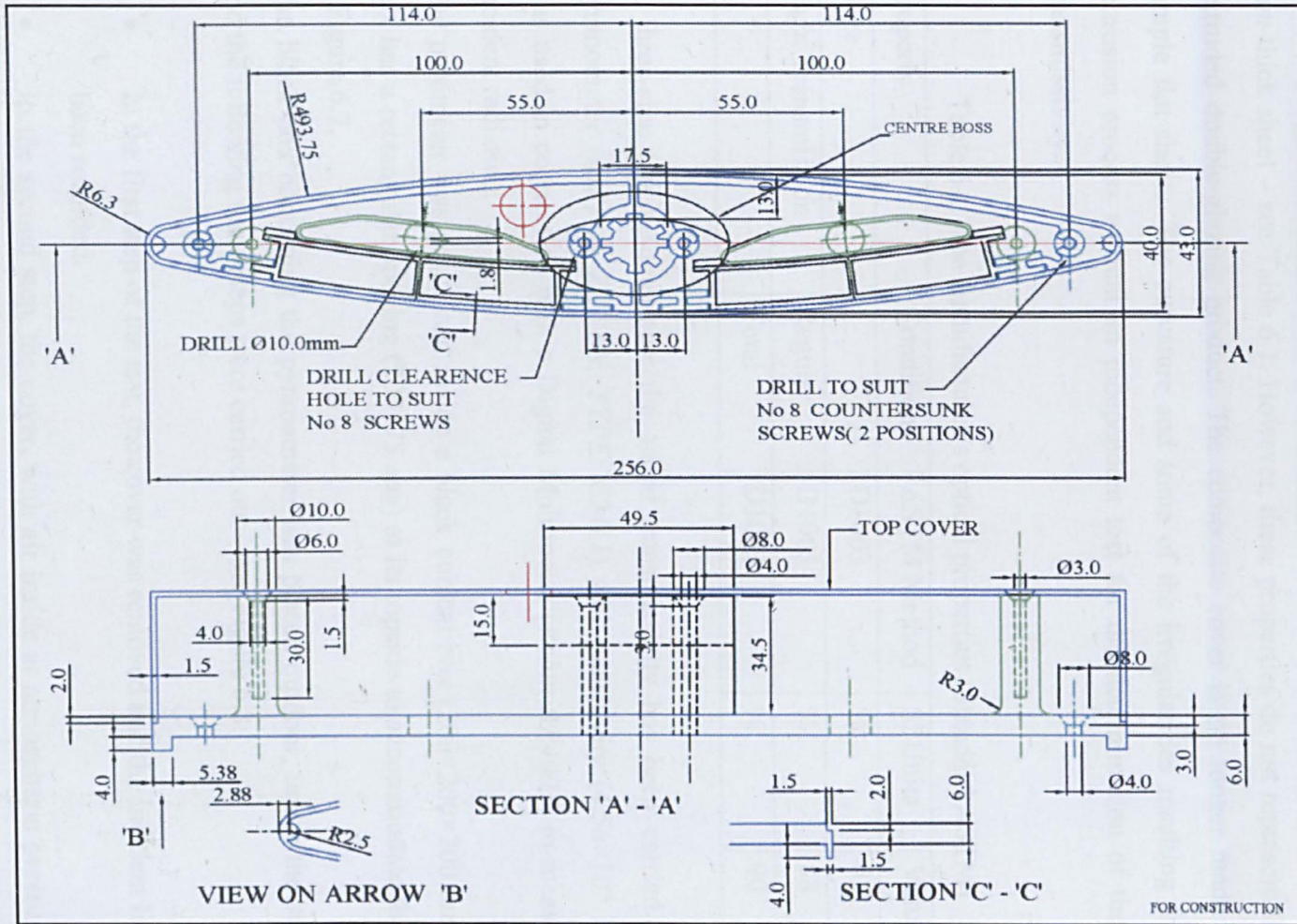


Figure 6.6 The shell, channel, cover and end-cap in position

6.1 Preparations

The cover material is known commercially as *Provisa*TM - see appendix (B). The manufacturer (EASTMAN) has supplied the optical properties of the cover for a 1.5 mm-thick sheet – see Table 6.1. However, these properties do not represent the final extruded double-glazing product. The composite cover is no longer made of two simple flat sheets. The curvature and some of the irregularities resulting from the extrusion process warrant an independent test for the determination of the actual transmissivity.

Table 6.1. The manufacturer's optical properties (Standard ASTM)

Property	Conditions	ASTM Method	SI Units	Value
Haze		D1003	%	0.6
Light Transmission	Regular	D1003	%	88
	Total	D1003	%	90

A three-step test to determine the actual transmissivity has been carried out. A pyranometer (*KIPP & ZONEN, TYPE: CM11*) with sensitivity ($4.56 \times 10^{-6} \text{ V/Wm}^{-2}$) was used in connection with a Digital Multimeter (*Robin AR4003*) to measure the incident radiation.

The pyrometer was positioned inside a black cubical box ($200 \times 200 \times 200 \text{ mm}$). The box has a rectangular opening ($200 \times 75 \text{ mm}$) at its topside to accommodate the cover – Figure 6.7.

The black box containing the pyranometer was placed outdoor, under the sunlight; and the following three steps were carried out – see Figure 6.8:

- In the first step of the test, the cover was removed and the incident light has been recorded.
- In the second step, the cover, with air inside at atmospheric pressure, was positioned in the opening and the transmitted light has been recorded.
- In the final step of the test, identical cover filled with Argon (90% minimum) up to atmospheric pressure, was positioned in the opening and the transmitted light has been recorded.

Data has been recorded, and the transmissivity calculated as shown in Table 6.2 below:

Table 6.2 determination of the actual transmissivity of the cover

(Location: Nottingham/England, Date: 30/05/2003)

Condition	Time	Multimetre reading (mV)	Light intensity (W/m^2)	Transmissivity
Without cover	12:30	3.2	702	1.00
Cover filled with Air	12:31	2.6	570	0.81
Cover filled with Argon	12:33	2.5	548	0.78

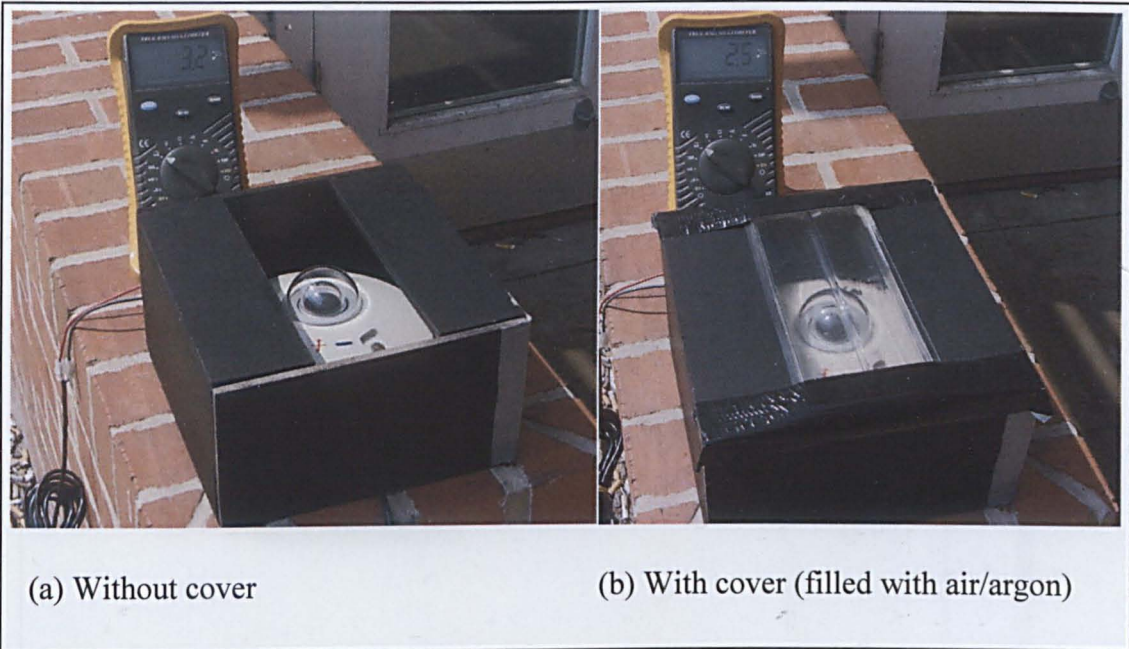
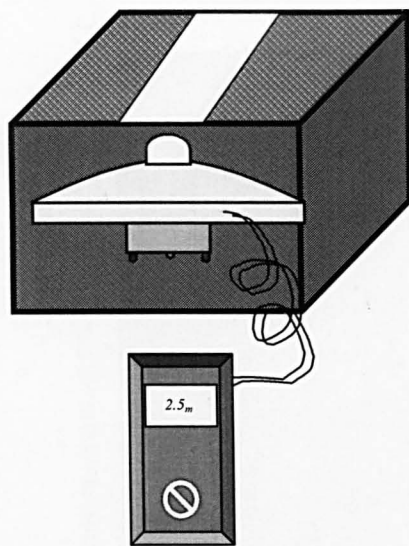
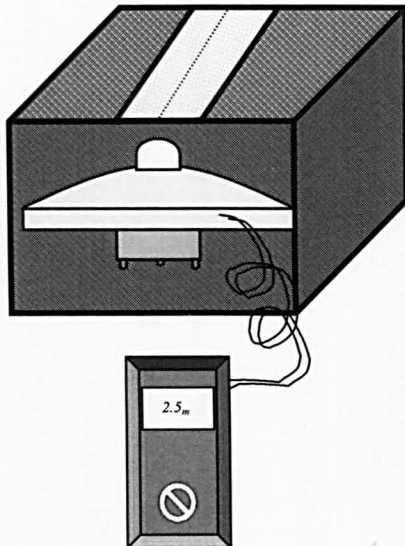


Figure 6.7 Determination of the actual transmittance of the cover

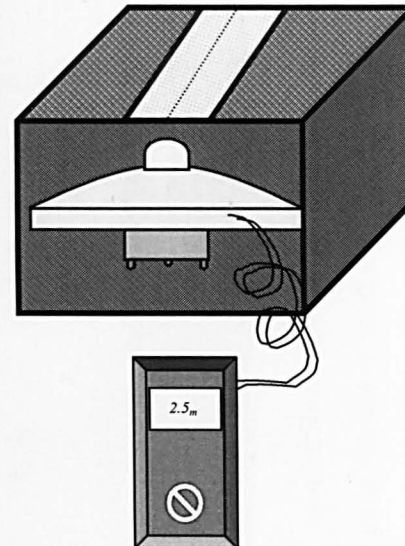
As it can be seen from Table 6.2 above, that the transmissivity of argon (0.78) is quite similar to that of air (0.81). This difference in transmissivity is rather small, and could well be neglected. However, the use of argon (mono-atomic gas) in glazing has the clear advantages in reducing convection losses, when compared to air, provided that the distance is optimised.



The first step;
Without cover.



The second step;
Cover charged with Air.



The final step;
Cover charged with Argon.

Figure 6.8 Determination of the actual transmissivity of the cover.

The cover, being a product of an extrusion process, comes with open ends; see Figure 6.1, 3rd photo from top. Therefore, it must be closed and sealed in order to reduce convection losses. For this purpose, cover-ends cut out from Perspex have been prepared, and one for each louvre has been drilled to accommodate an evacuation/charging port. This port, made out from a plastic material, which could be crimped, cut-down to size and sealed – Figure 6.9:

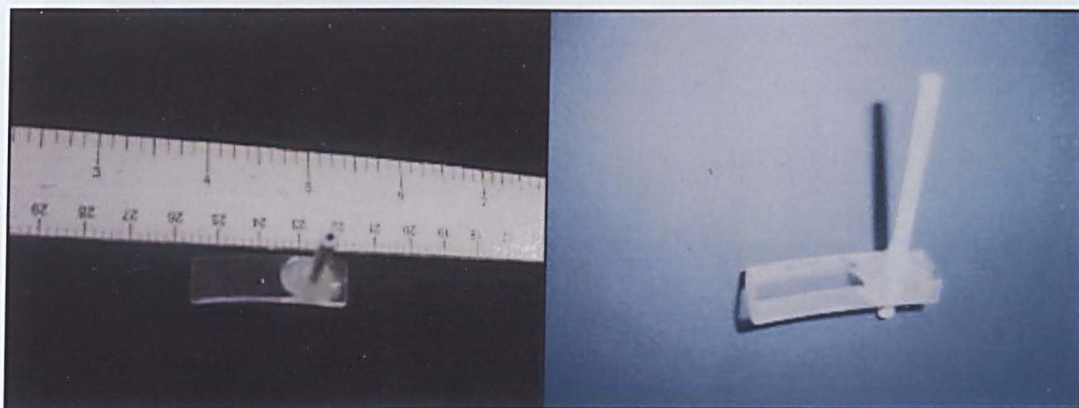


Figure 6.9 Cover-end with evacuation/charging port.

Ideally, vacuum would be the most suitable choice for insulation. However, as part of the preparations for the louvre experiment, the cover has been examined under vacuum, to test its structural integrity. A sample (200×75 mm) similar to that used for the transmissivity test, is depicted in Figure 6.10, below

The cover construction did not pass the vacuum test, and consequently argon has been used instead.

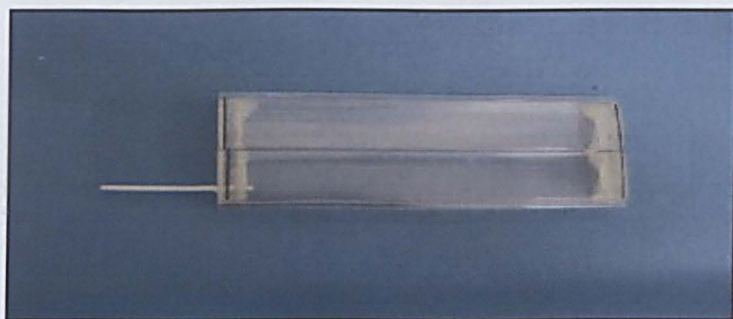


Figure 6.10 Cover with ends and evacuation/charging port fixed.

The following two pages contain some photographs of the preparation and assembly of the two louvres.

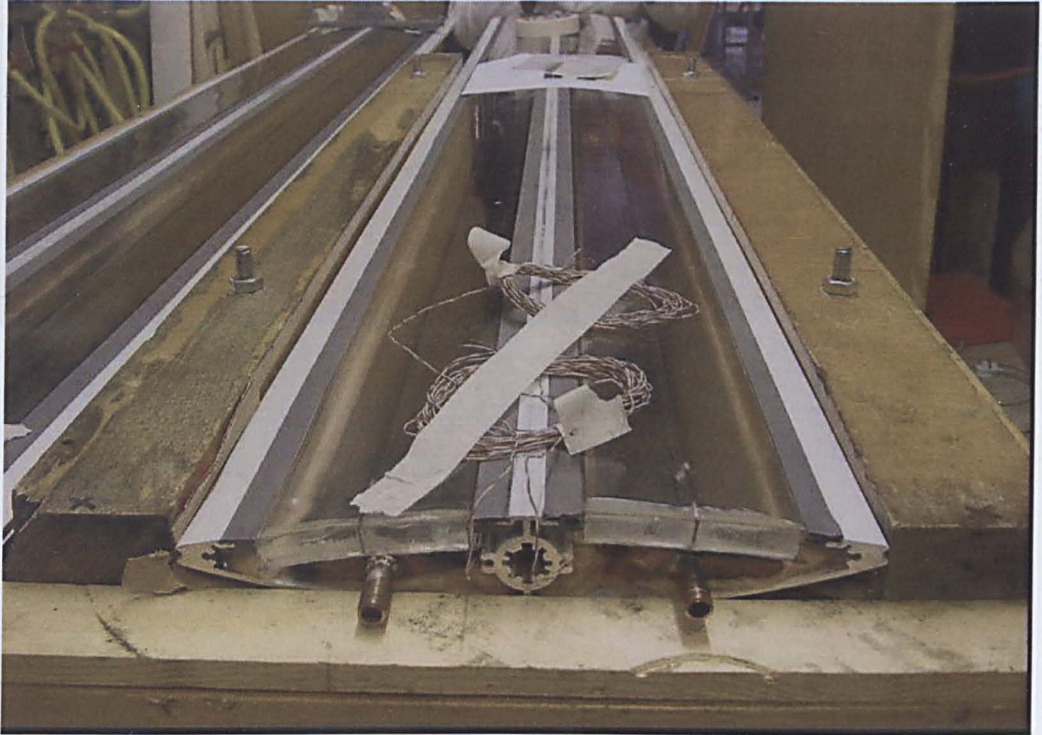


Figure 6.11 Circular segment/channel under preparation/assembly

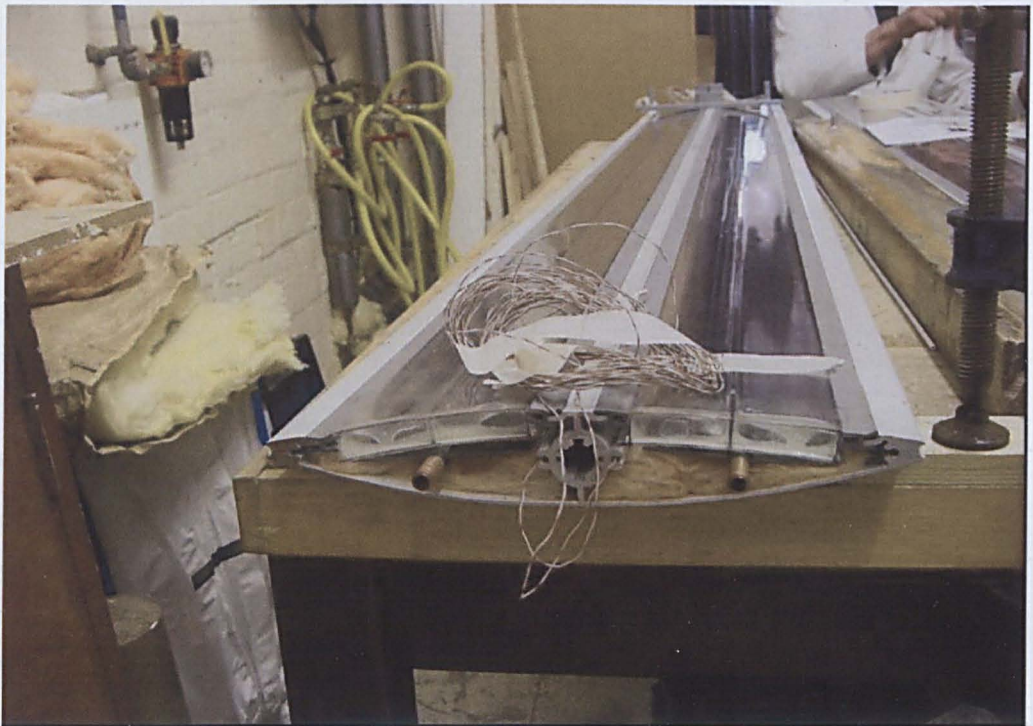


Figure 6.12 Sheet-on-tube/fin-on-tube under preparation/assembly

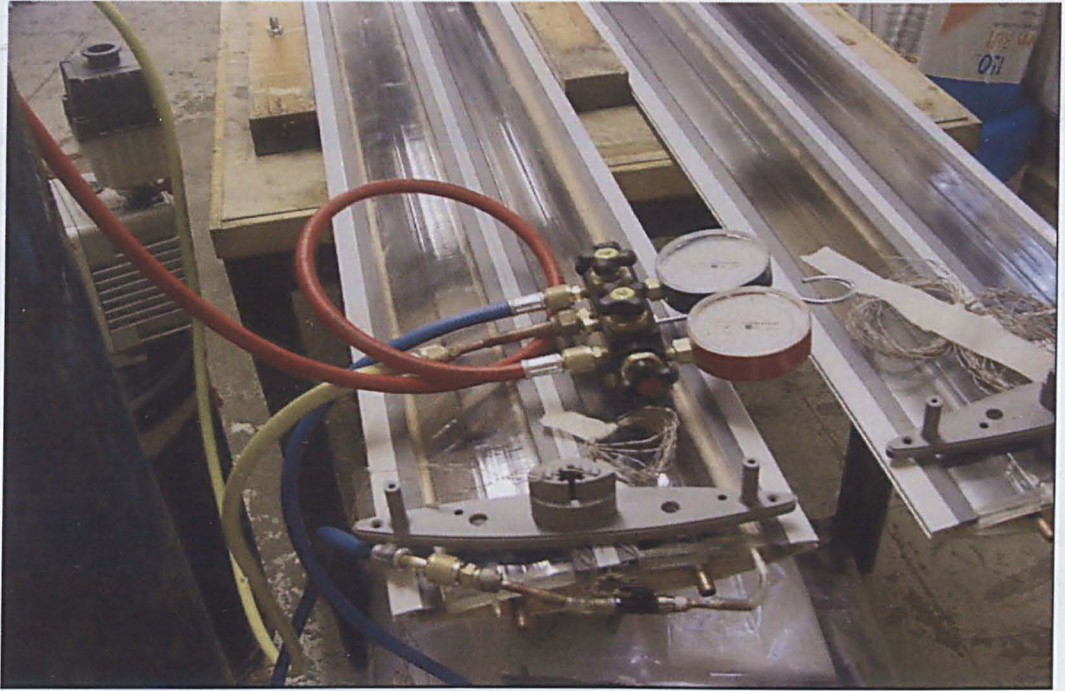


Figure 6.13 Vacuuming the double-glazing cover

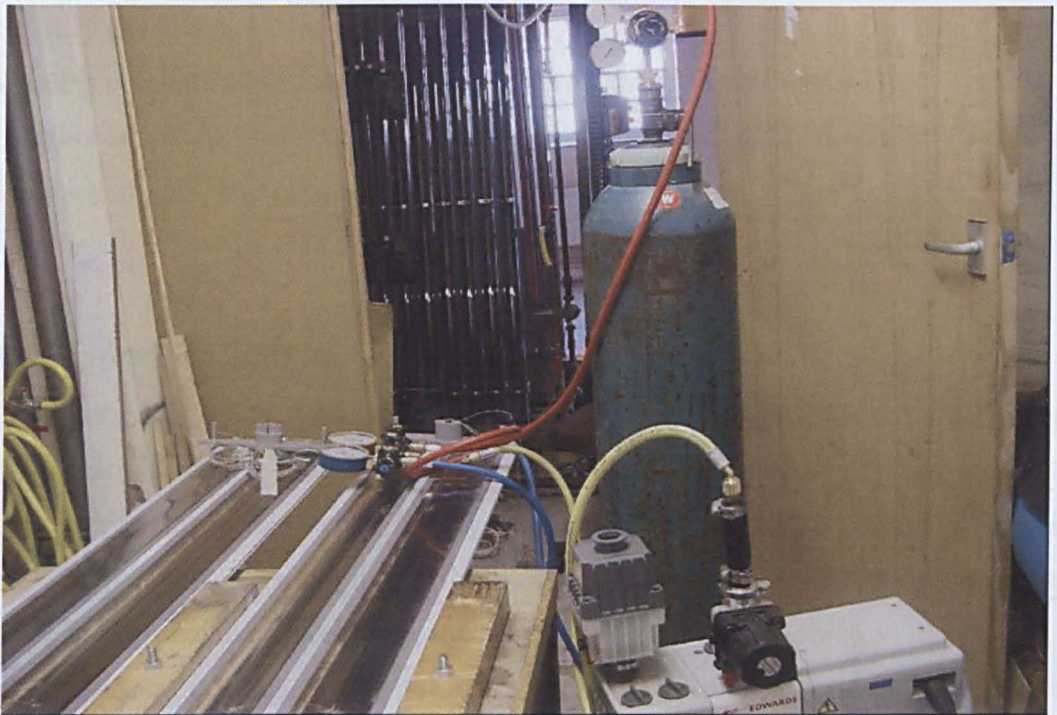


Figure 6.14 Argon filling the double-glazing cover.

Water has been the choice of this experiment. The selection of the system's working fluid was based on factors such as:

- Heat transport capability within a typical range of operating temperatures;
- Environmental impact;
- Toxicity;
- Flammability;
- Material reaction;
- Cost.

From a commercial point of view the overriding issue has to be the cost of the fluid so that the cost of the prototype system is kept to a minimum. It was clear that the modern refrigerants available on the market today are expectantly high in cost.

Water has a relatively high thermal conductivity over the range of working temperatures as well as high heat capacity.

For flat plate collectors, one assumes the operating temperatures to be (10 -100 °C). Within this range, the heat capacity of water is approximately 4.2 kJ/kg-°C, and its conductivity is 0.6-0.7 W/m-°K.

Water is compatible with copper (the chosen absorber-plate's material).

Last but not least, water is inflammable, non-toxic and most importantly it has no adverse environmental impact.

6.2 Apparatus and instrumentation

The testing-facility used here was the same testing facility used for the preprototype experiments of chapter (4).

The components of this testing facility were the same as those mentioned previously, and are all as labelled in Figure 6.16; the only difference being that of the orientation of the collector, and consequently, the positioning of the light-source.

As shown in the schematic on Figure 6.16, the solar louvre collectors were positioned horizontally, with the light source vertically above.

It must be reiterated here, that the purpose of this particular experiment has been two fold:

- First, the comparison of the two types of heat-exchanger geometries (i.e. channel and fin-on-tube).
- Second, the determination of the thermal characteristics of the louvre.

It can be seen from the schematic of Figure 6.15 that there are various points to be probed for measurements.

Six thermocouples have been connected to measure the surface temperature at various locations in each louvre.

Two identical pressure sensors and two thermocouples have been connected at the inlet and outlet of each louvre.

Also two identical visual flow meters have been installed at the inlet to each louvre.

The lengths of the piping in each circuit, as well as the positions of all sensors and flow meters were identically the same.

These sixteen thermocouples are on the top of the three couples that are at the tank (inlet, outlet and bulk water temperature), the two at the variable-load heat exchanger (inlet and outlet), and one thermocouple for sensing the ambient temperature – Figure 6.18.

The total sensing probes are: a total of 21 (*T-type*) thermocouples (accuracy: ± 1.0 or 75%), a conventional pressure gauge (accuracy class: 1.6 per DIN 16005), a digital flow meter (accuracy: Linearity at FSD frequency is $\pm 1.0\%$), 4 pressure sensors [Non-linearity & Hysteresis: ± 0.25 BSL max; Temperature errors $\pm 2\%$ max over ($-20\text{ }^{\circ}\text{C}$ to $80\text{ }^{\circ}\text{C}$)]. Two visual flow-meters (accuracy: ± 2.0 , repeatability: $\pm 1.0\%$)

Figure 6.15 depicts the two louvres side by side in a symmetrical position; one housing the two channels, and the other the two fins-on-tubes, all having identical length and frontal surface areas, as shown on Figure 6.1.

Such symmetry, in geometrical and flow conditions, coupled with the identical environmental/ambient conditions (radiation intensity and ambient temperature) creates the appropriate basis for the comparison.

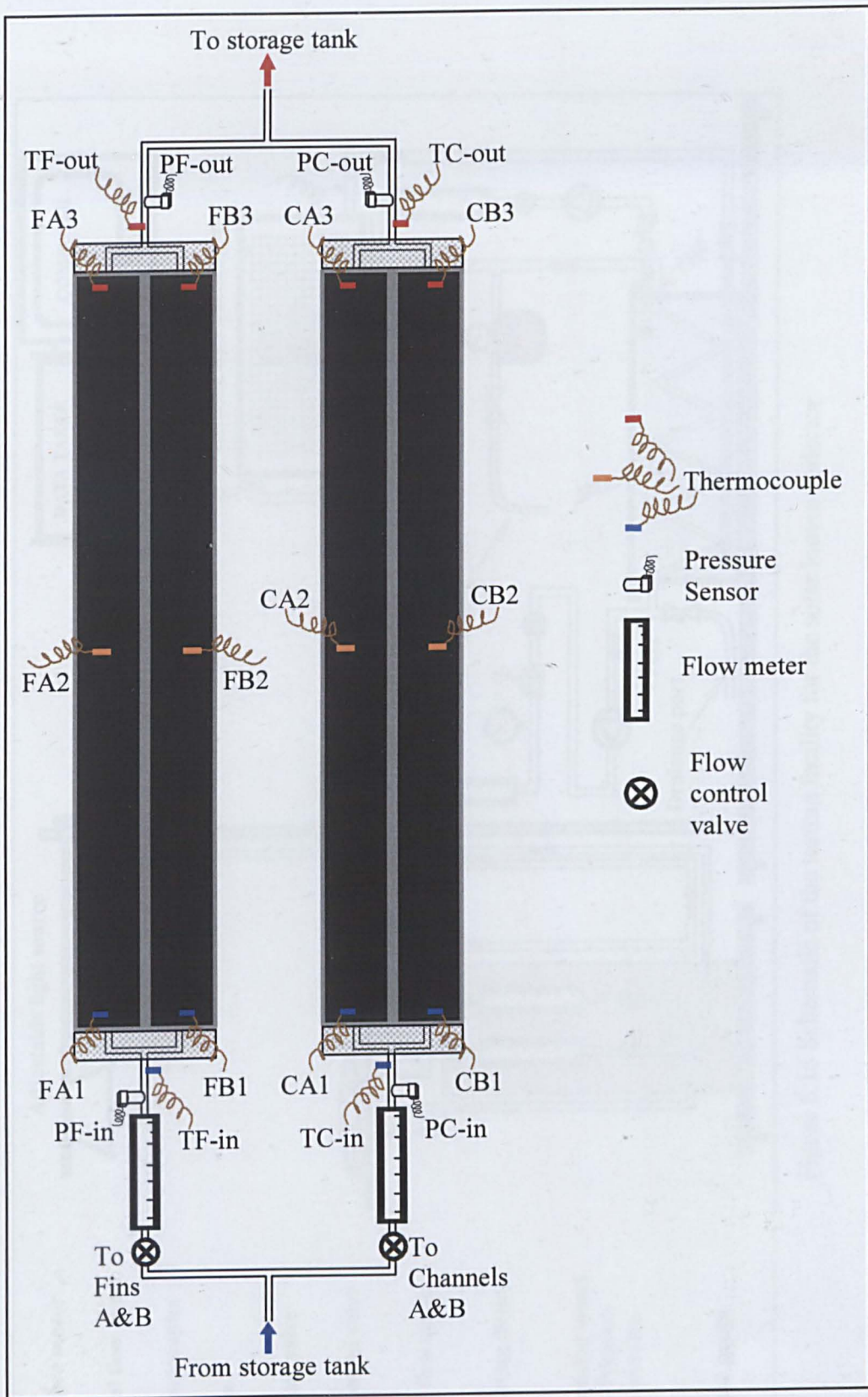


Figure 6.15 Schematic showing the layout of the two louvres and

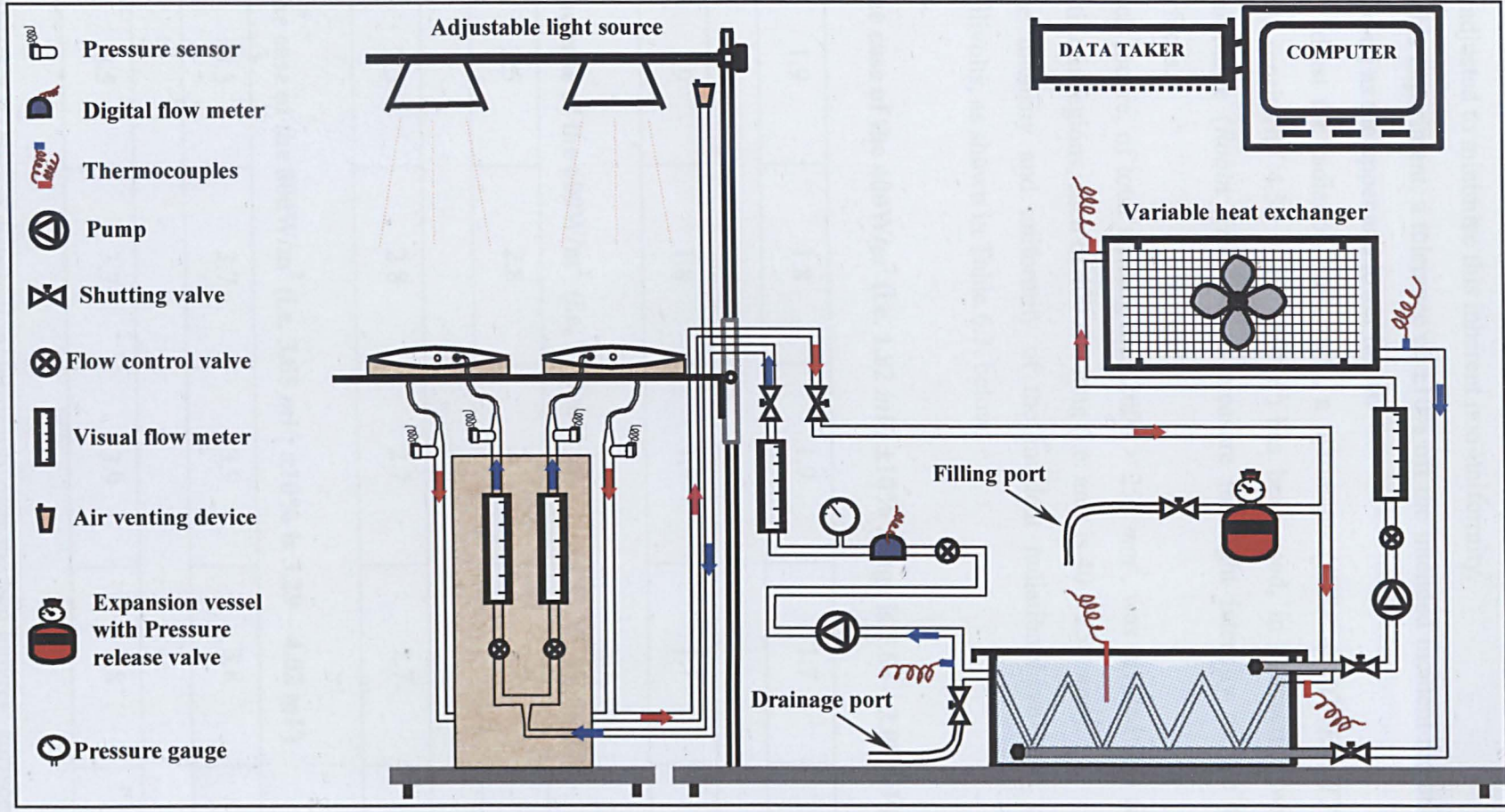


Figure 6.16 Schematic of the testing facility for the solar louvre collector

6.3 Experimental procedure

Unlike the Sun, point-light sources produce a nonuniform incident light, which must be adjusted to minimize this inherent non-uniformity.

In this experiment, a tolerance of $\pm 10\%$ off the intended incident radiation has been allowed as the upper and lower limits.

To adjust the radiation uniformity, a pyrometer (*KIPP & ZONEN, TYPE: CM11*; with sensitivity $4.56 \times 10^{-6} V/Wm^{-2}$) has been used, in connection with a digital multimeter (*Robin AR4003*), to measure the light intensity on the two louvres surfaces.

Each louvre, of total shading area $2000 \times 250 \text{ mm}^2$, was divided into five identical fictitious regions, each of 400 mm long (i.e. area is $40 \times 250 \text{ mm}^2$).

The intensity and uniformity of the incident radiation have been recorded, in millivolts, as shown in Table 6.3, below:

The case of the $400W/m^2$ (i.e. 1.82 mV ; $\pm 10\%$ range is $1.64 - 2.00 \text{ mV}$)

1.9	1.8	1.9	1.7	1.8
-----	-----	-----	-----	-----

1.9	1.8	1.9	1.7	1.8
-----	-----	-----	-----	-----

The case of the $600W/m^2$ (i.e. 2.74 mV ; $\pm 10\%$ is $2.46 - 3.00 \text{ mV}$)

2.5	2.8	2.7	2.7	2.6
-----	-----	-----	-----	-----

2.5	2.8	2.7	2.7	2.6
-----	-----	-----	-----	-----

The case of the $800W/m^2$ (i.e. 3.65 mV ; $\pm 10\%$ is $3.29 - 4.02 \text{ mV}$)

3.5	3.7	3.9	3.8	3.6
-----	-----	-----	-----	-----

3.5	3.7	3.9	3.8	3.6
-----	-----	-----	-----	-----

Table 6.3 Radiation distribution/uniformity over the two louvres' surfaces.

The analysis, and the experimental work, presented in this chapter, revolves around the “two-parameter model”, just as in chapter (4) - *Preprototype investigations*.

Following the European convention, the test results were based on T_{av} , the arithmetic average of the inlet and outlet temperatures, rather than inlet temperature (USA).

The procedure here has been based, principally, on the steady-state operation of the collector; and in order for this to be achieved the temperature of the storage tank, (where heat from the collector is being deposited), must be kept constant. This has been achieved during the tests via the variable load heat exchanger incorporated in the system as shown in the schematic of Figure 6.16 A photo of this variable load heat exchanger is shown below in Figure (6.3.2).



Figure 6.18 Variable-load, liquid-to-air heat exchanger.

The two louvres were positioned horizontally, side-by-side and subjected to the same ambient and operational conditions.

Water, as the working fluid, was circulated (total pressure of 1.0 *bar*) at 0.006 kg/s for each louvre, and flow meters (showing 0.36 *litre/min*) were observed for steadiness.

Choices of tank-temperatures (24,27,30,.....42 °C) were used for each radiation level, namely, (400,600, 800 and 1000 W/m^2). This variation in tank temperatures

automatically implies variation in inlet fluid temperatures, T_{in} , which is one of the ASHRAE 93-77 standard recommendations.

Random measurements, using a hand-held thermometer, were carried out to verify the thermocouples readings.

Once the steady-state conditions were observed, measurements were recorded for every minute, and averaged over 10-15 minutes, for each of the specified tank temperatures, at all of the radiation levels, in turn.

This consequently had produced a vast number of readings/data.

The outline of the analysis is as follows:

The equation needed for plotting the efficiency graphs is, as derived in *chapter (4) - Preprototype investigations*, given by:

$$\frac{m_w c_p (T_{out} - T_{in})}{A_{col} I} = F_{av} (\tau_c \alpha_p) - F_{av} U_c \frac{(T_{av} - T_a)}{I} \dots\dots\dots (6.1)$$

Where m_w , c_p , T_{in} and T_{out} are the mass flow rate, specific heat capacity, inlet and outlet temperatures of the working fluid, respectively.

A_{col} is the area of the unobstructed collector plate, and I is the normal incident radiation, most of which is assumed beam.

T_{av} is the arithmetic average of the fluid inlet and outlet temperatures. T_a is the ambient temperature.

F_{av} is the heat removal factor based on $T_{av} = (T_{in} + T_{out})/2$.

$(\tau_c \alpha_p)$ is transmittance-absorptance product of the cover-plate for normal incident radiation, and U_c is the overall loss coefficient.

Equation (6.1), under steady-state conditions, is the key to correlating the experimental data, and plotting the efficiency curves.

The following sections present the results and findings of the experiments.

6.4 The Experimental Results

The reliability of the results relies primarily on the appropriate application of the steady state energy balance concept (i.e. equations).

It is therefore paramount to keep the system as steady as practicably possible, so that readings are actually taken at steady state conditions. Quasi-steady-state is acceptable in most cases.

Having the light-source fixed at (400, 600, 800 or 1000 W/m^2), and the flow rate at (20 $g/s/m^2$), then the other sources, which derail the system from the state of steadiness, are:

- The rise in temperature of the water of the tank where the collected energy is deposited
- The variation in the ambient temperature, and wind speed.

The following two graphs (for the case of 600 W/m^2) indicate the level of steadiness under which the data has been collected.

Figure 6.19 depicts the constant nature of the tank temperatures, while Figure 6.20 shows little, or rather negligible variation in the ambient temperature during the tests.

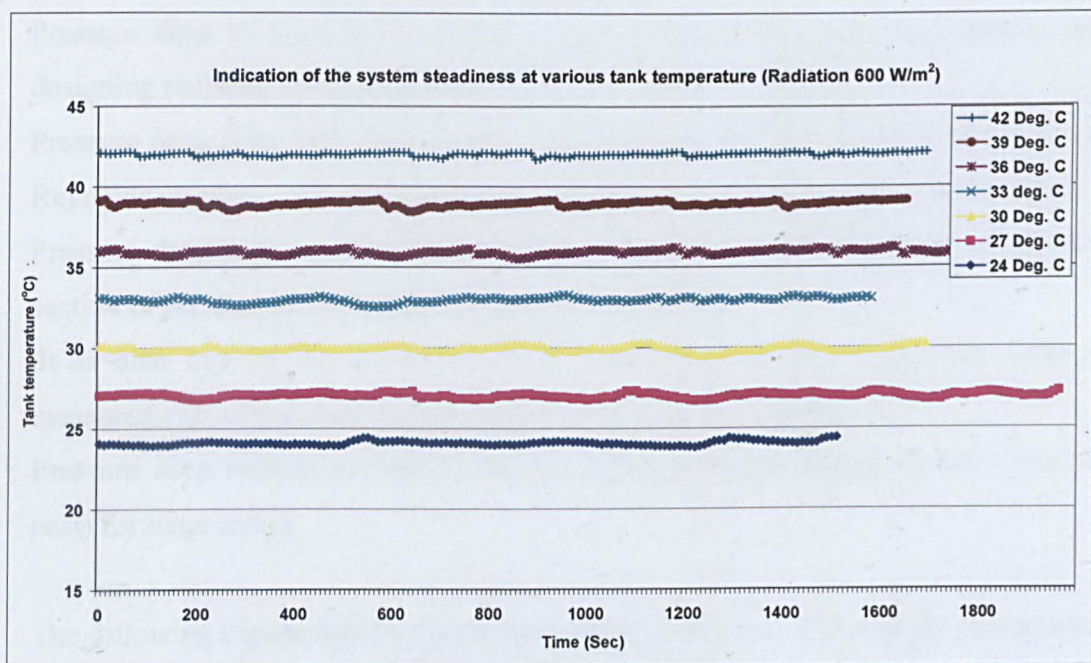


Figure 6.19 Tank temperature at each steady state level

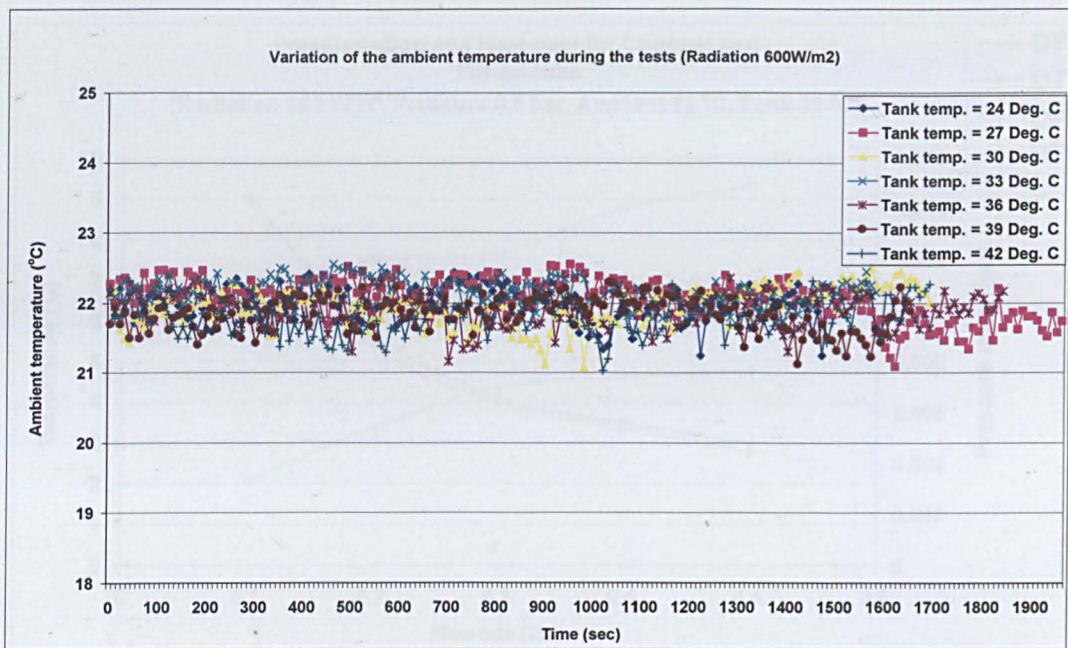


Figure 6.20 Ambient temperature at each steady state level (or tank temperature)

As part of the investigation for the choice of a suitable geometry for the fluid duct/plate, the issue of pressure drop has risen.

Pressure drop in fluid circuits, also known as head-loss, is a major parameter in designing building services systems (and solar collector circuits).

Pressure drop rises with duct length, and increases with the increase of the Re , the Reynolds number – it is in fact a strong function of velocity (see the Moony chart).

Pressure drop across a duct is also closely dependant on the geometry of the cross section of the duct as well as on its surface roughness.

It is also one of the ASHRAE 93-77 recommendations, to provide mean for measurements of pressure and pressure drop across the collector.

Pressure drop reflects vividly on the bill of the parasitic energy (mainly pumping cost) for large arrays.

The following Figure depicts the pressure-drops, DPC and DPF, and the temperature gain, DTC and DTF, across the channel and the fin respectively. Values of the pressure drop are per louvre length (i.e. per 2.0 m).

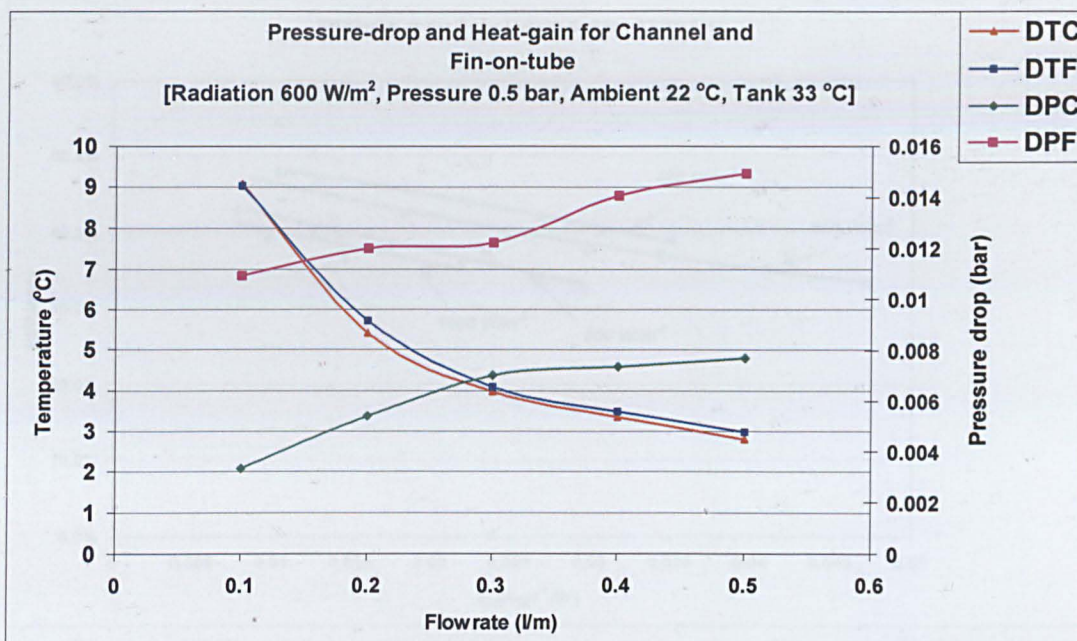


Figure 6.21 Comparison between the Channels and the Fin-on-tubes fluid ducts
DPC and DPF are the pressure-drops; DTC and DTF are the temperature gain,
across the channel and the fin respectively.

As it can be seen from Figure 6.21, that the temperature-rise ($T_{out} - T_{in}$) across the channel is similar to that across the fin-on-tube. This similarity in temperature-rise across either channel or fin-on-tube, does not, on its own, warrant identical performance. It indicates that the two collectors absorb energy, and transfers it to the working fluid, in similar rates; but, however, does not indicate their energy losses.

The pressure-drop ($P_{out} - P_{in}$), on the other hand, across the fin-on-tube is more than twice the pressure-drop that exits across the channel, and at all flow rates.

This saving in pressure drop for every unit-length of louvre would have positive effects on the pumping cost.

The following page contains two Figures - Figure 6.22 and Figure 6.23. They, respectively, depict the efficiency curves for the case of the fin-on-tube, and the case of the channel at the test's radiations range (200, 400, 800, 1000 W/m^2).

One could deduce from these graphs that both types behave almost linearly.

The interesting point to note from these is that both channel and fin-on-tube have better efficiency at radiation intensity of 600 W/m^2 than at 400 W/m^2 .

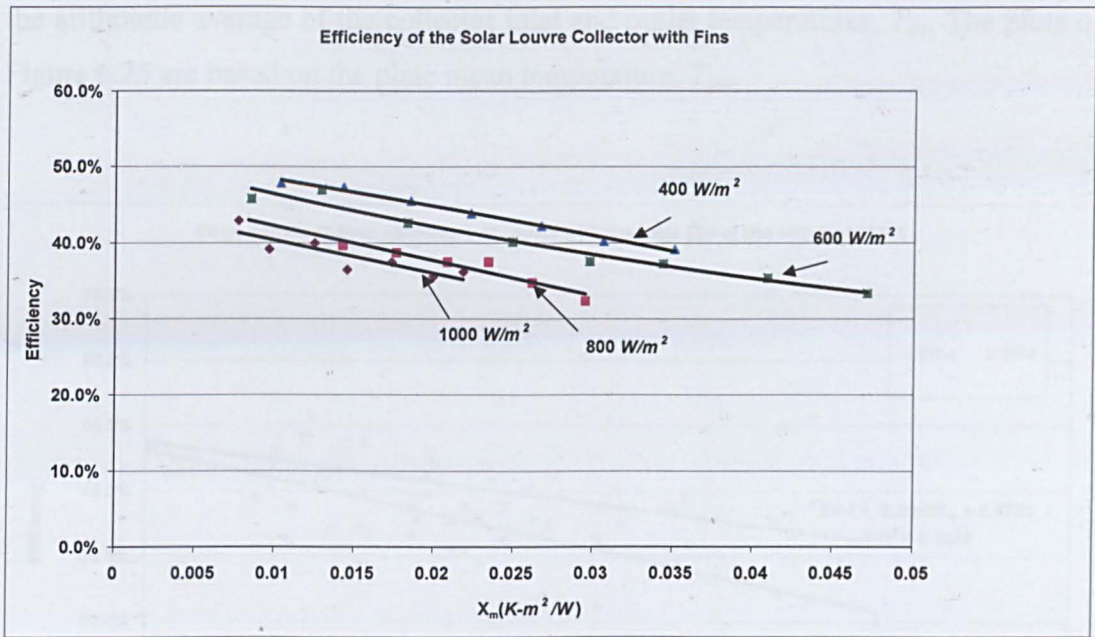


Figure 6.22 Efficiency curves for the solar louvre, incorporating channels.

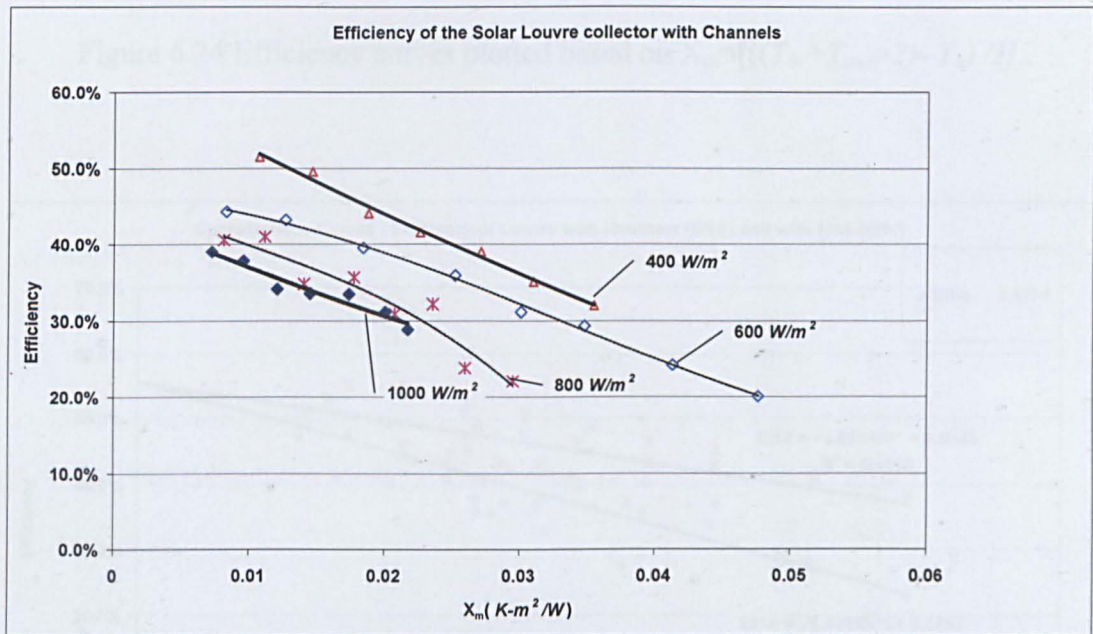


Figure 6.23 Efficiency curves for the solar louvre, incorporating fin-on-tubes.

The following two Figures present the linear efficiency-curves for the solar louvre with channels and with fin-on-tubes. On Figure 6.24, the calculations are based on

the arithmetic average of the collector inlet and outlet temperatures, T_{av} . The plots of Figure 6.25 are based on the plate mean temperature, T_{pm} .

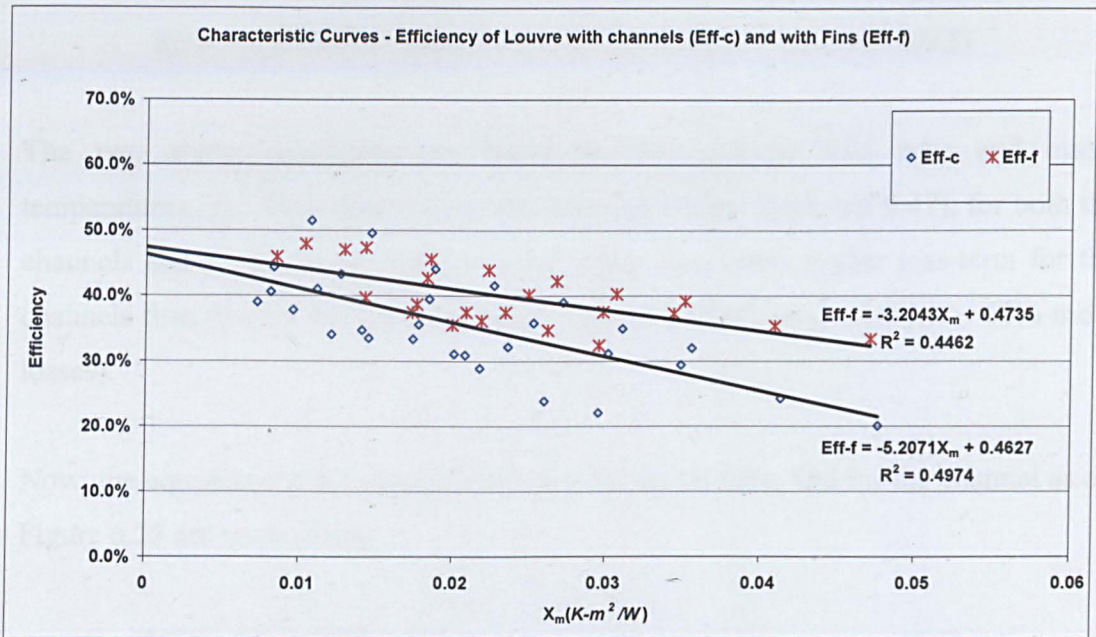


Figure 6.24 Efficiency curves plotted based on $X_m = [(T_{in} + T_{out})/2 - T_a] / I$.

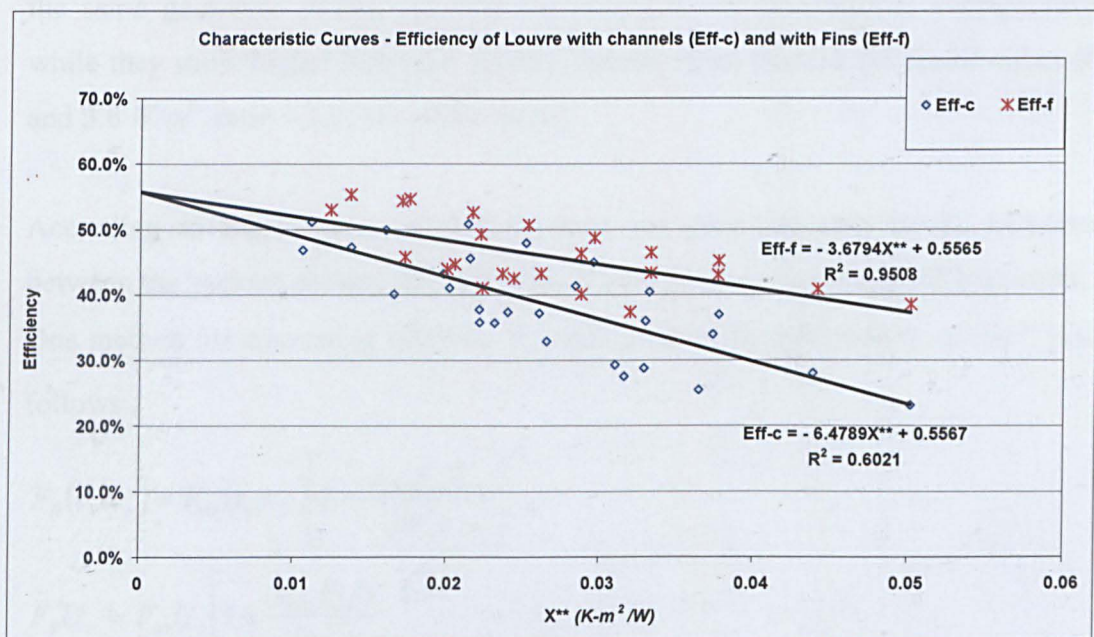


Figure 6.25 Efficiency curves plotted based on $X^{**} = [(T_{pm} - T_a) / I]$.

The equations of the straight lines, for the fin-on-tube, and for the channel as in Figure 6.24 are respectively:

$$Eff-f = - 3.23 X_m + 0.47 \quad \dots\dots\dots(6.2)$$

$$Eff-c = - 5.21 X_m + 0.46 \quad \dots\dots\dots(6.3)$$

The two above equations, are based on the average fluid inlet and outlet temperatures, T_{av} . They nearly show the same gain-term (0.46 and 0.47), for both the channels and fin-on-tubes configurations, while they show higher loss-term for the channels than that for the fin-on-tubes (5.2 and 3.2 W/m^2 , ratio ~ 1.6 i.e. $\sim 60\%$ more losses).

Now, the equations of the straight lines, for the fin-on-tube, and for the channel as on Figure 6.25 are respectively:

$$Eff-f = - 3.65 X^{**} + 0.56 \quad \dots\dots\dots (6.4)$$

$$Eff-c = - 6.48 X^{**} + 0.56 \quad \dots\dots\dots (6.5)$$

The two above equations, are based on the mean surface temperature T_{pm} . They show the same gain-term (0.56), for both the channels and fin-on-tubes configurations, while they show higher loss-term for the channels than that for the fin-on-tubes (6.5 and 3.6 W/m^2 , ratio ~ 1.7 , i.e. $\sim 70\%$ more).

According to Beckman *et al* (1977), there are generally only small differences between the various plotting methods (based on T_{pm} , T_i or T_{av}) for liquid collectors.

One method for converting between F_{av} and F_R given by Beckman *et al* (1977) is as follows:

$$F_R(\tau_c \alpha_p) = F_{av}(\tau_c \alpha_p) \left[1 + \frac{A_{col} F_{av} U_c}{2m_w c_p} \right]^{-1} \quad \dots\dots\dots (6.6)$$

$$F_R U_c = F_{av} U_c \left[1 + \frac{A_{col} F_{av} U_c}{2m_w c_p} \right]^{-1}$$

At the test conditions, (collector area, $A_{col} = 0.30 \text{ m}^2$, mass flow rate, m_w , fixed at 0.003 kg/s , average value for specific heat capacity taken as, $C_p = 4.18 \text{ kJ/kg-}^\circ\text{K}$), the quantities $F_{av}U_c$ and $F_{av}(\tau_c\alpha_p)$ are:

- For the case of fin-on-tube, from equation (6.2), $3.23 \text{ W/m}^2\text{-}^\circ\text{K}$ and 0.47 respectively.

Therefore, for the case of the fin-on-tube, using equation (6.6), $F_R(\tau_c\alpha_p)$ and F_RU_c are given by:

$$F_R(\tau_c\alpha_p) = 0.4735 \left[1 + \frac{0.3 \times 3.2043}{2 \times 0.0033 \times 4180} \right]^{-1} = 0.4735 \times [1.035]^{-1} = 0.46$$

$$F_RU_c = 3.2043 \left[1 + \frac{0.3 \times 3.2043}{2 \times 0.0033 \times 4180} \right]^{-1} = 3.2043 \times [1.035]^{-1} = 3.10 \text{ W/m}^2\text{-}^\circ\text{K}$$

These values are somewhat similar to those of equation (6.4).

- For the case of channel, from equation (6.3), $5.2071 \text{ W/m}^2\text{-}^\circ\text{K}$, and 0.4627 respectively.

Similarly, using equation (6.4), $F_R(\tau_c\alpha_p)$ and F_RU_c are given by:

$$F_R(\tau_c\alpha_p) = 0.4627 \left[1 + \frac{0.3 \times 5.2071}{2 \times 0.0033 \times 4180} \right]^{-1} = 0.4627 \times [1.057]^{-1} = 0.44$$

$$F_RU_c = 5.2071 \left[1 + \frac{0.3 \times 5.2071}{2 \times 0.0033 \times 4180} \right]^{-1} = 5.2071 \times [1.057]^{-1} = 4.93 \text{ W/m}^2\text{-}^\circ\text{K}$$

These values are somewhat similar to, or rather not too far from, those of equation (6.5).

The above calculation show that the channels and fin-on-tubes to have approximately the same gain-term (0.44 and 0.46), while they show higher loss-term for the channels than that for the fin-on-tubes (4.9 and 3.1 W/m^2 , ratio ~ 1.6 i.e. $\sim 63\%$ more losses).

Both methods of plotting, as well as the theoretical calculations, confirm that the solar louvres, incorporating fin-on-tubes has similar gain-term as when incorporating the channels, while they show higher loss-term ($\sim 60\%$ more) for the channels than that for the fin-on-tubes.

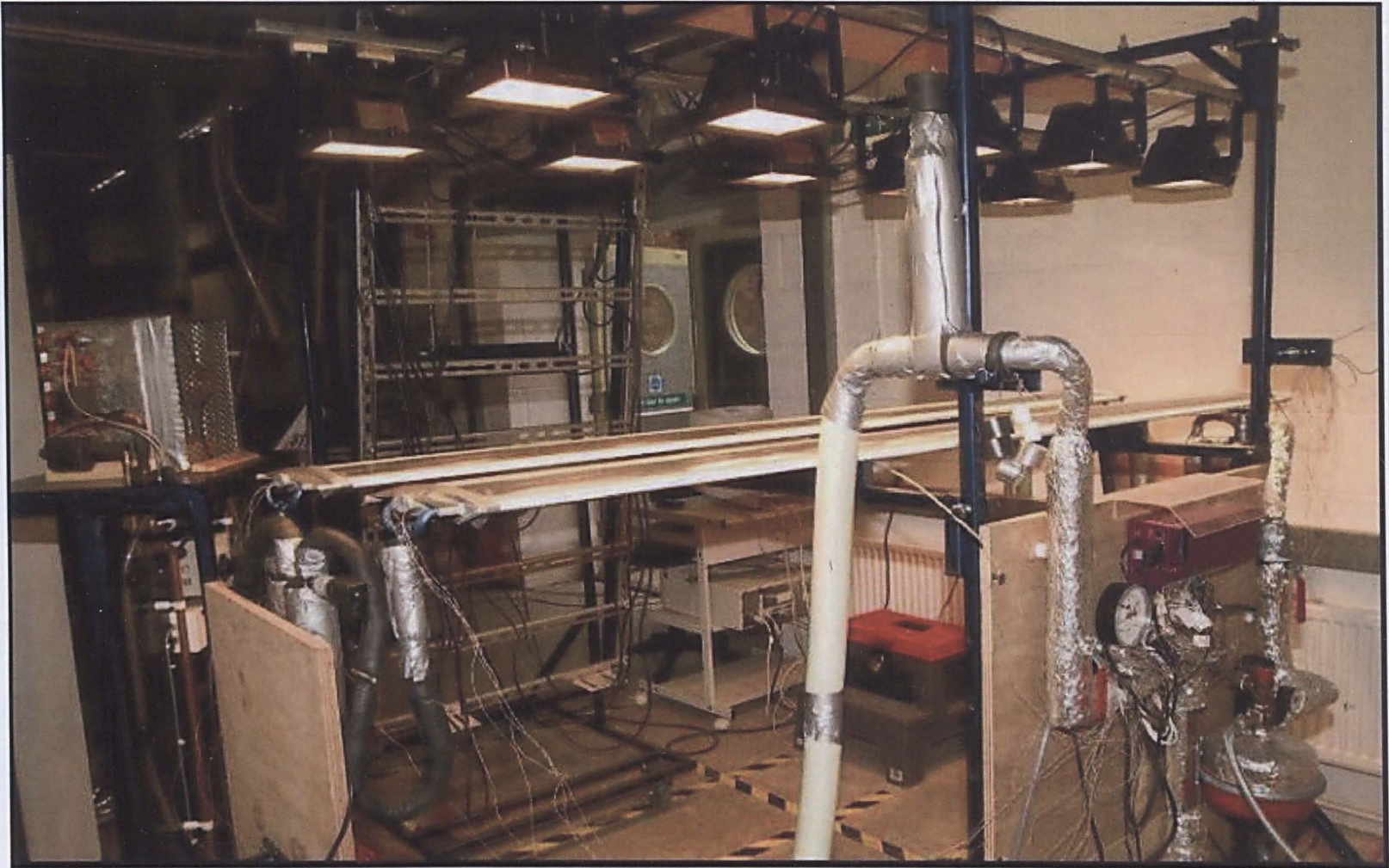


Figure 6.26 The two louvers, side by side, undergoing the indoor efficiency determination tests

6.5 Summary

It can be seen through out the tests results that the graphs show over all consistency and mutual confirmation.

Also, without a compromise to accuracy, one could conclude that these solar louvre collectors, thermally, are:

- Closely comparable (when incorporating fin-on-tubes) in performance to currently commercial hot water, flat plate collectors.
- Improvement to the efficiency (i.e. at all radiations) could be achieved if:
 - 1) The double cover is manufactured in glass, appropriately selected with favourable optical properties, and that it could be evacuated and sealed.
 - 2) The fin-on-tubes, with better selective absorbing-surface (with the appropriate plate-thickness and pipe-to-pipe distance), should be used, with the solar louvres, as they show lower loss-term than that for the channels.

It a fact that pipes and sheets of copper are readily available and it is only a matter of simple thermal bonding that would be needed to make a fin-on-tube exchanger.

Fin-on-tubes are manufactured from copper strips, of varying width (up to 1200 mm) and thickness (between 0.12 mm and 0.20 mm).

These strips come already coated with Titanium Oxynitride (known commercially as “TiNOX[®]”), and handled in rolls; refer to appendix (B).

The coating process of the Titanium Oxynitride is by way of “*vacuum deposition*”.

The rolls of coated copper is then cut to size and especially soldered on the pipe.

To manufacture a channel, however, has proved to be much more involved, and as a result the cost is much higher.

Further, the amount of material (and consequently its cost) is higher for channels than that of fin-on-tubes. This weight would, consequently, reflect on the price of handling, shipping and installations too.

Coating these channels with a selective coating after construction, via the method of vapour deposition was not possible as the coating equipment is designed for strip coating.

The verification of the modelling results has been carried out in chapter (7) – *Viability of the Design*.

However, comparing the results of the mathematical modelling with those of the experimental work:

- The model prediction of the efficiency equation as:

$$[Eff-c]_{model} = - 3.9 X_m + 0.87$$

- The experimental prediction of the efficiency equation as:

$$[Eff-c]_{lab} = - 5.2 X_m + 0.46$$

This is good agreement between the loss values. However, 0.46:0.87 is 53%, which is close to 60% - the ratio of transparent area to total area.

The experiment for the determination of the transmissivity showed that the transmittance of the cover to be only 0.78.

Also there are no reliable information available for the coating material of the absorber-plate, but these are expected to be of low absorbtivity, and high emissivity.

Having said that, it can be seen that there is good agreement between theoretical and experimental work results.

Chapter Seven
Viability of The Design

7. Viability of the Design

Designs, in general, must fulfil certain criteria in compliance with various performance and regulatory conditions. Cost, safety, reliability and efficiency are some aspects, but most importantly the environmental impact of the design/product. In recent years, the assessment of this environmental impact got stringier; and products are assessed holistically. Assessment of the environmental impact starts at the manufacturing process (even at mining stages), throughout its lifetime, until the end. At the end, it should be fully recyclable.

In order for the solar louvre design to be evaluated as a product, it must therefore be seen to fulfil these, above mentioned, criteria.

The following sections provide the environmental assessment, economic analysis and field trials of the design's first prototype.

7.1 Environmental Assessment

Externally mounted shading louvres are normally made from aluminium. The choice is due to the fact that aluminium is lightweight, relatively cheap and available. It is also readily recyclable.

It is therefore reasonable to consider it in designing the solar louvre. However, aluminium is not transparent, and a solar collector would incorporate a transparent material for its cover, such as glass, polycarbonate, etc. Also, aluminium is incompatible with water. It is, therefore, inevitable that various materials enter into the construction of most solar collectors. In the case of the solar louvre, these materials are: aluminium, copper, transparent plastic, rubber and hard plastic. The insulation material chosen was Glass wool/Rock wool.

All of these materials are currently used in manufacturing most solar collectors. It is therefore assumed, since these materials are recyclable and at-present widely used in solar collector construction, that the choice of these materials would pass the environmental assessment at the manufacturing stage, as well as those at the end of the product's life.

Another important objective of this assessment has been to analyse the environmental performance of the system during its lifetime.

For this purpose, Carbon Dioxide (CO₂) emissions, or rather emission savings have been calculated for a hot water system application. London and Lisbon have been chosen for contrast, and natural gas has been chosen as the fuel for heating water at both of these cities.

The scenario here is: a consumption of 200 *litres* of hot water per day (at 60 °C), and using the theoretical efficiency, a collector area of 4.5 m² and a gas burner efficiency of 80%. The efficiency equation used is given by the model (i.e. $Eff-f = - 3.9 X_m + 0.87$).

Taking a CO₂ emission of 230 *g/kWh* for natural gas, the savings in CO₂ emission to the atmosphere by using the solar louvre system, during the system life (N_p), is (in *g* of CO₂) given by:

$$CO_{2,savings} = Q_{load} \cdot f_{sol} \cdot N_p \cdot 230 \quad \dots\dots\dots (7.1)$$

Table 7.1 shows the solar fraction, heat load and CO₂ emission savings for a system life period of 15 and 20 years for Lisbon and London. This life expectancy is typical of flat plate collectors

Table 7.1 Savings in CO₂ emissions for a system life of 15, and 20 years, for cities of Lisbon and London.

City	f_{solar} (%) ($A_{col}=4.5m^2$)	Q_{load} (<i>kWh/year</i>)	$CO_{2, savings}(ton)$	
			15 years	20 years
Lisbon	60.2	3609.9	7.50	10.00
London	25.3	3609.9	3.15	4.20

The solar fraction for London is low; and consequently, the benefit of CO₂ savings is rather small.

7.2 Economic Analysis

Several economic criteria have been proposed and used for evaluating and optimising solar systems. There are various economic figures of merit, and each one has its own significance, and they must all be considered collectively.

To analyse the economic viability of the solar louvre design, three Figures of merit, namely, the *payback period*, the *averaged energy cost* and the *life cycle savings*, have been used.

In order to calculate for any of these, above-mentioned Figures of merit, the cost of the proposed solar louvre collector must be estimated.

A louvre manufacturer – Maple Sun-screening (UK) – see reference list at appendix (B), has provided the cost of the existing shading louvres, and the estimated cost for the new solar louvre collector. This is as presented in Table 7.2.

Table 7.2 Louvre cost and Solar Louvre Collector cost (250E-type).

Louvre area (m^2)	Solar Louvre without end support ($\text{€}/m^2$)	Solar Louvre Collector with end support ($\text{€}/m^2$)
1	416.79	639.08
≥ 2	416.79	583.51

In order to perform an economic analysis, energy costs and savings must be assessed. Both costs and savings depend on the energy source used.

It was assumed that natural gas was used for water heating, which is usually the cheapest solution available for Lisbon and London.

The system energy costs also depend on the solar fraction (f_{sol}) as well as on the gas burner efficiency (η_{burner}).

Heat from gas (Q_{gas}), known as auxiliary heat, can be related to the heat load for water heating (Q_{load}), from first principles, by:

$$Q_{gas} = \frac{Q_{load}(1 - f_{sol})}{\eta_{burner}} \dots\dots\dots (7.2)$$

Similarly, the annual energy savings (Q_{save}) for using the collector could be calculated by:

$$Q_{save} = \frac{Q_{load} \cdot f_{sol}}{\eta_{burner}} \dots\dots\dots (7.3)$$

Table 7.3, below, shows annual solar fraction f_{sol} , Q_{load} , Q_{gas} and Q_{save} for Lisbon and London, assuming a daily hot water consumption of 200 litre /day (at 60°C), a collector area of 4.5 m² and a gas burner efficiency of 80%.

Table 7.3 Annual solar fraction, heat load, auxiliary heat and energy savings for Lisbon and London ($A_{col}= 4.5m^2$).

City	f_{solar} (%) ($A_{col}=4.5m^2$)	Q_{load} (kWh/year)	Q_{gas} (kWh/year)	Q_{save} (kWh/year)
Lisbon	60.2	3609.9	1795.9	2716.4
London	25.3	3609.9	3370.7	1141.6

It can be seen from the table that the annual energy saving (Q_{save}) made in the case of Lisbon is more than twice. Such factors, together with other considerations dictate the viability of the collector.

7.2.1 Payback period

The *payback period* (N) is defined in many ways. The most common definition—according to Duffie (1991, p. 459), is: “The time needed for the cumulative fuel savings to equal the total initial investment, that is, how long it takes to get an investment back by savings in fuel.”

It can be calculated by considering the initial cost or investment ($C_{investment}$) for a given collector area, the annual energy savings (Q_{save}), the cost of auxiliary energy (natural gas) in the first year ($c_{gas, 1year}$), interest rate (d) and inflation rate (i).

The common way to calculate this pay back period is without discounting the fuel savings.

Table 7.4, below, presents the cost of natural gas (fuel cost and cost of one unit of useful energy), interest and inflation rates for Lisbon and London. These values have been taken from:

www.bportugal.pt, www.ine.pt and www.bankofengland.co.uk.

Table 7.4 Natural gas cost in the first year (fuel and useful energy, c , and c'), interest and inflation rates for Lisbon and London.

City	$c_{gas, 1year}$ (€/kWh) (fuel cost)	$c'_{gas, 1year}$ (€/kWh) (fuel with $\eta_{burner} = 80\%$)	d (Interest rate)*	i (Inflation rate)*
Lisbon	0.049	0.061	2%	3.8%
London	0.030	0.038	3.8%	2.5%

(*) Values for June 2003

The most complete approach to solar process economics is to use life cycle cost methods that take into account all future expenses. And if the obligation of paying recurs each year, and inflates at a rate (i) per period then the concept of *present worth factor* is appropriate. It is defined in other words as: What would have to be invested today at the best alternative rate to have the funds available in the future to meet all of the anticipated expenses.

The *payback period* (N) can be calculated, using Duffie (1991, p. 463), for both cities by:

$$C_{investment} = Q_{save} \cdot c_{gas, 1year} \frac{1}{(d - i)} \left[1 - \left(\frac{1+i}{1+d} \right)^N \right] \dots\dots\dots (7.2.1.1)$$

where:

$C_{investment}$ (cost) is calculated for a collector area of $4.5m^2$ (see Table 7.2.1),

$$C_{investment} = (C_{solar\ louvre\ collector} - C_{louvre}) \cdot A_{col} = 750.24 \text{ €}, \dots\dots\dots (7.2.1.2)$$

Q_{save} - see Table 7.2.2,

$c_{gas, 1year}$ (natural gas cost per kWh of energy in the first year) - see Table 7.2.2.

The payback period is obtained when these values are substituted in equation 7.2.1.1.

Table 7.2.1.2, below, shows the payback period (N) for Lisbon and London:

Table 7.2.1.2 *Payback period* (N) for Lisbon and London.

City	N (years)
Lisbon	5.5
London	26.6

Note that the payback period for UK is much greater than for Portugal (5 times). This is due to the lower solar fraction in England (~ 40% that in Portugal) and also to the lower cost of natural gas in England (~ 60% of the price in Portugal).

7.2.2 Average Energy Cost

The *Average Energy Cost* (\bar{C}_{total}) for a given system life period (N_p), is defined as the total cost of one unit of energy obtained with the system. It can be obtained through the expression:

$$\bar{C}_{total} = \frac{C_{investment} + C_{gas,Np}}{E_{total,Np}} \dots\dots\dots (7.2.2.1)$$

where, $E_{total,Np}$ is the total useful energy obtained through the system in the period N_p . This energy depends on the heating load and N_p as:

$$E_{total,Np} = Q_{load} N_p \dots\dots\dots(7.2.2.2)$$

$C_{gas,Np}$ is the cost of gas during N_p and it can be calculated using:

$$C_{gas,Np} = C_{gas,N1} \frac{1}{(d-i)} \left[1 - \left(\frac{1+i}{1+d} \right)^{Np} \right] \dots\dots\dots (7.2.2.3)$$

where $C_{gas,N1}$ is the natural gas cost in the first year, which can be calculated using :

$$C_{gas,N1} = Q_{gas} \cdot c_{gas,1year} \dots\dots\dots (7.2.2.4)$$

Table (7.2.2.1), below, shows the natural gas cost in the first year ($C_{gas,N1}$), the total gas cost ($C_{gas,Np}$), the total useful energy ($E_{total,Np}$) and the average energy cost (\bar{C}_{total}) for both Lisbon and London, for a system life period of 15-20 years.

The previous values of inflation rate and interest rate (see Table (7.2.1.1)), and an investment cost ($C_{investment}$ - see equation (7.2.1.2)) are considered.

Table 7.2.2.1 *Average energy cost* (\bar{C}_{total}) in a system life period of 15 and 20 years, for Lisbon and London.

City	$C_{gas,N1}$ (€/year)	$C_{gas,15}$ (€)	$E_{total,15}$ (kWh)	$\bar{C}_{total,15}$ (€/kWh)	$C_{gas,20}$ (€)	$E_{total,20}$ (kWh)	$\bar{C}_{total,20}$ (€/kWh)
Lisbon	88	1467	54149	0.041	2048	72198	0.039
London	101.1	1340	54149	0.039	1733	72198	0.34

The *average energy cost* values from Table 7.2.2.1 can be compared with the useful energy costs for natural gas from Table 7.2.1.1. Also, the *average energy cost* for Portugal is significantly lower than the cost of 1 kWh of useful energy obtained with natural gas (0.041 and $0.039 < 0.061$).

In UK, for a period of 20 years the louvre system *average energy cost* is higher than the cost for a conventional natural gas system ($0.34 > 0.038$).

7.2.3 Life Cycle Savings

The *life cycle savings* are defined as the difference between energy savings obtained with the solar louvre system and initial cost (investment), for the system life period. These savings depend on the collector area and, therefore, on the solar fraction. There is also an optimum solar collector area, which corresponds to the maximum life cycle savings.

The above equations and tables have been used to calculate for the *life cycle savings*, while the area has been varied between 2 – 9 m².

Figure 7.2.3.1 below, shows the relation between *life cycle savings* and louvre collector area.

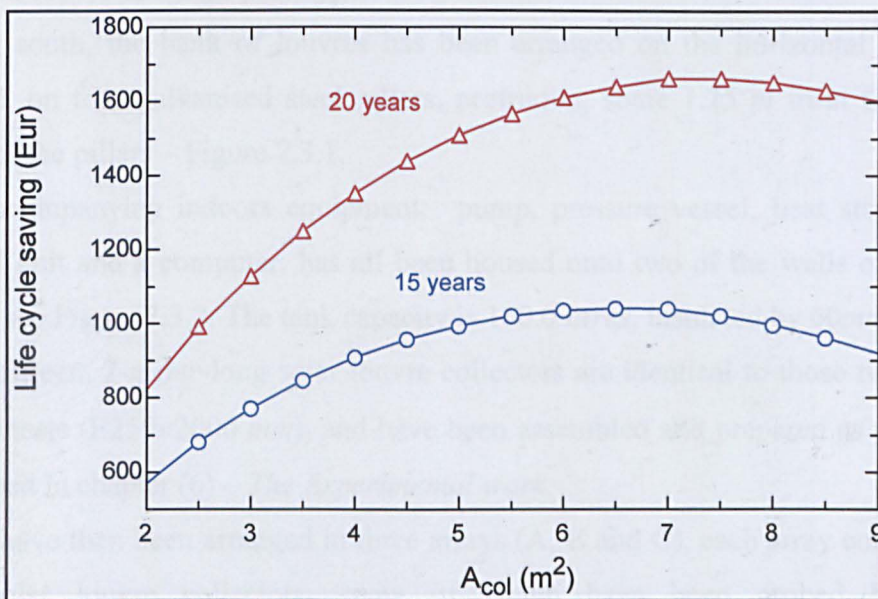


Figure 7.2.3.1 Life cycle savings as a function of louvre collector area, for a life period of 15 and 20 years. Lisbon.

(Hot water consumption: 200 litres/day at 60°C).

It can be seen from the Figure that the maximum savings are obtained for a collector area of about 6.5 m^2 , at the cost of 1041 €, with life expectancy of 15 years.

For 20 years this value is 1663 €, corresponding to a collector area of 7.5 m^2 . These values also depend strongly on the climate and energy prices.

7.3 Field Trials

To move a step closer towards having a successful design, various field tests must be conducted. And in the case of the solar louvre collector, the natures of these tests are structural, hydrodynamic and thermal; conducted under real life conditions. Aesthetics considerations also constitute part of these tests, and so as “*Weathering tests*”.

7.3.2 Trials in Nottingham

The size of the prototype has been decided up on, based on typical applications of these louvres in shading schemes. But also based on the value chosen in the theoretical calculations ($A_{col} = 4.5 \text{ m}^2$) at the modelling part of this work.

A site at the University of Nottingham, Nottingham NG7 2RD, was chosen to host the solar louvre collector prototype.

Facing south, the bank of louvres has been arranged on the horizontal plane and erected, on four galvanised steel pillars, protruding some 1.25 m from the vertical plane of the pillars – Figure 7.3.1.

The accompanying indoors equipment: pump, pressure vessel, heat storage tank, control unit and a computer, has all been housed onto two of the walls of a garden shed – see Figure 7.3.2. The tank capacity is 160.0 litres , insulated by 60mm blanket. These fifteen, 2-meter -long solar louvre collectors are identical to those two used in the lab tests ($E250 \times 2000 \text{ mm}$), and have been assembled and prepared as previously described in chapter (6) – *The Experimental work*.

These have then been arranged in three arrays (A, B and C), each array consisting of five solar louvre collectors, some of which have been probed by *T-type* thermocouples to measure the temperature of the surface of the louvre collectors as shown in Figure 7.3.3. The angle of inclination for the louvres was taken as 35° , suitable for the time of the year, at that location.

The outdoor plumbing has been arranged such that the three arrays, (A, B and C), could be run in series, parallel or a combination, by the turns of the appropriate valves.

Other devices installed for the outdoor monitoring tests, include ambient temperature sensor, anemometer, a pyranometer and data taker (*DT 800*)-see Figure 7.3.4.

The accompanying indoors equipment has all been arranged as shown in Figure 7.3.5. The piping used is a 22 mm copper pipe throughout, including the headers feeding the array. These headers have been positioned within the side support arms as depicted in Figure 7.3.6, and the support arms filled with the appropriate insulation foam as shown in Figure 7.3.7.



Figure 7.3.1 The Arrays of the Solar Louvre Collectors



Figure 7.3.2 Indoor Equipment – flow control, energy storage and data logging.

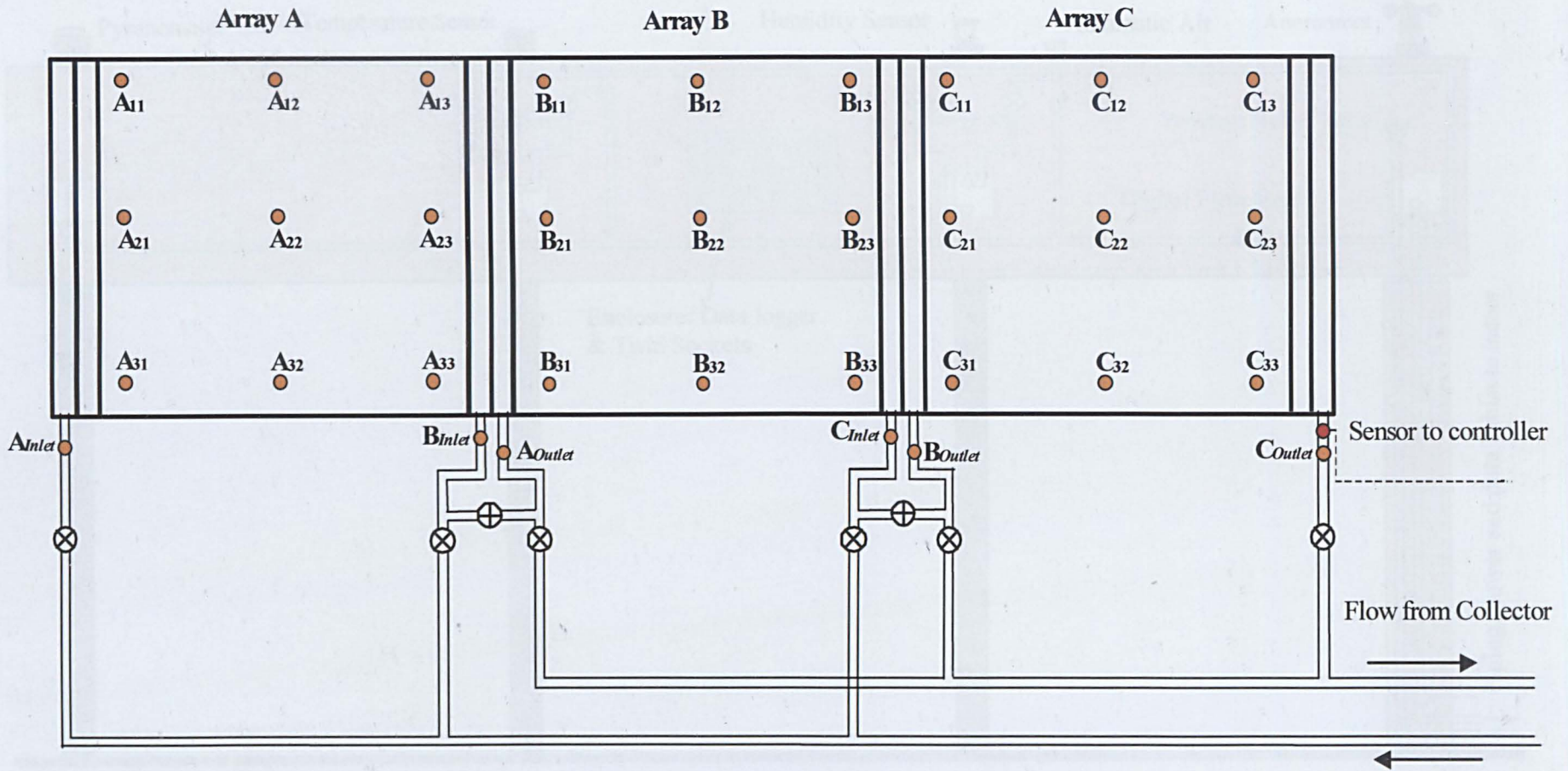


Figure 7.3.3 Thermocouples matrix - top and back views. (All connected to an outdoor Data logger)

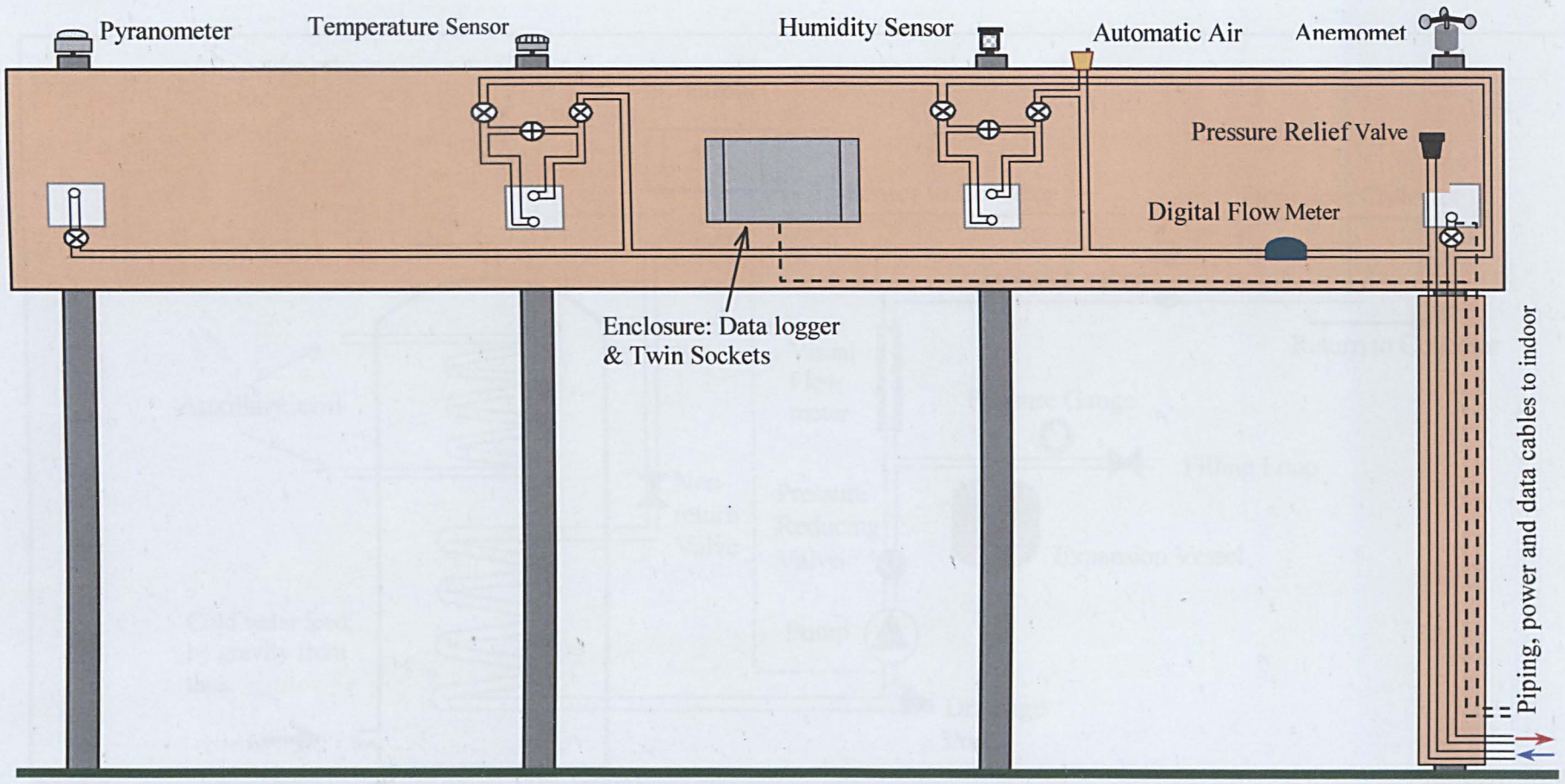


Figure 7.3.4 Schematic showing the fluid circuit for the solar louvre collectors – (The outdoor part)

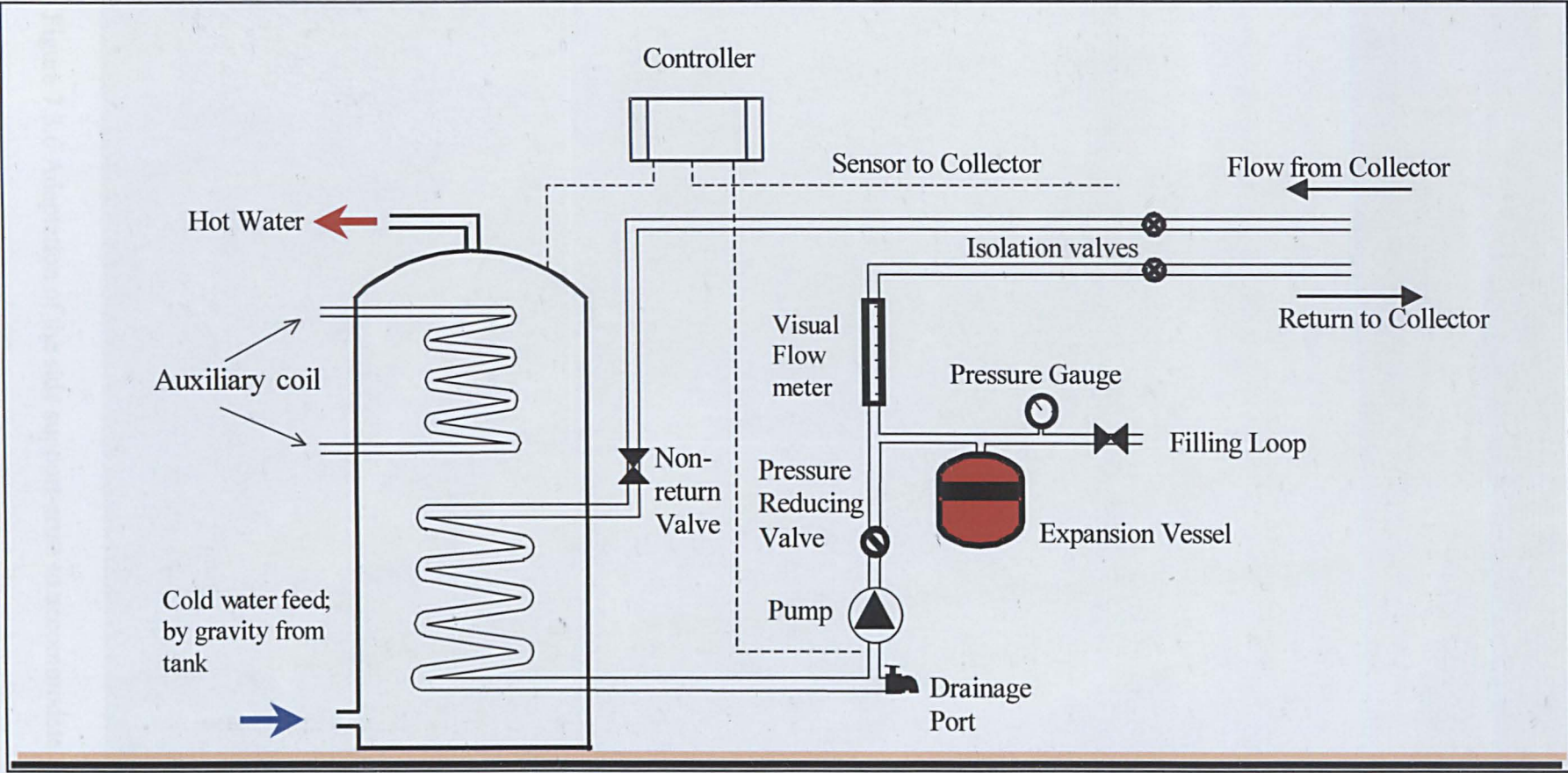


Figure 7.3.5 Schematic showing the fluid circuit for the solar louvre collectors – (the indoor part).



Figure 7.3.6 Adaptation of the side support-arms to accommodate the headers.

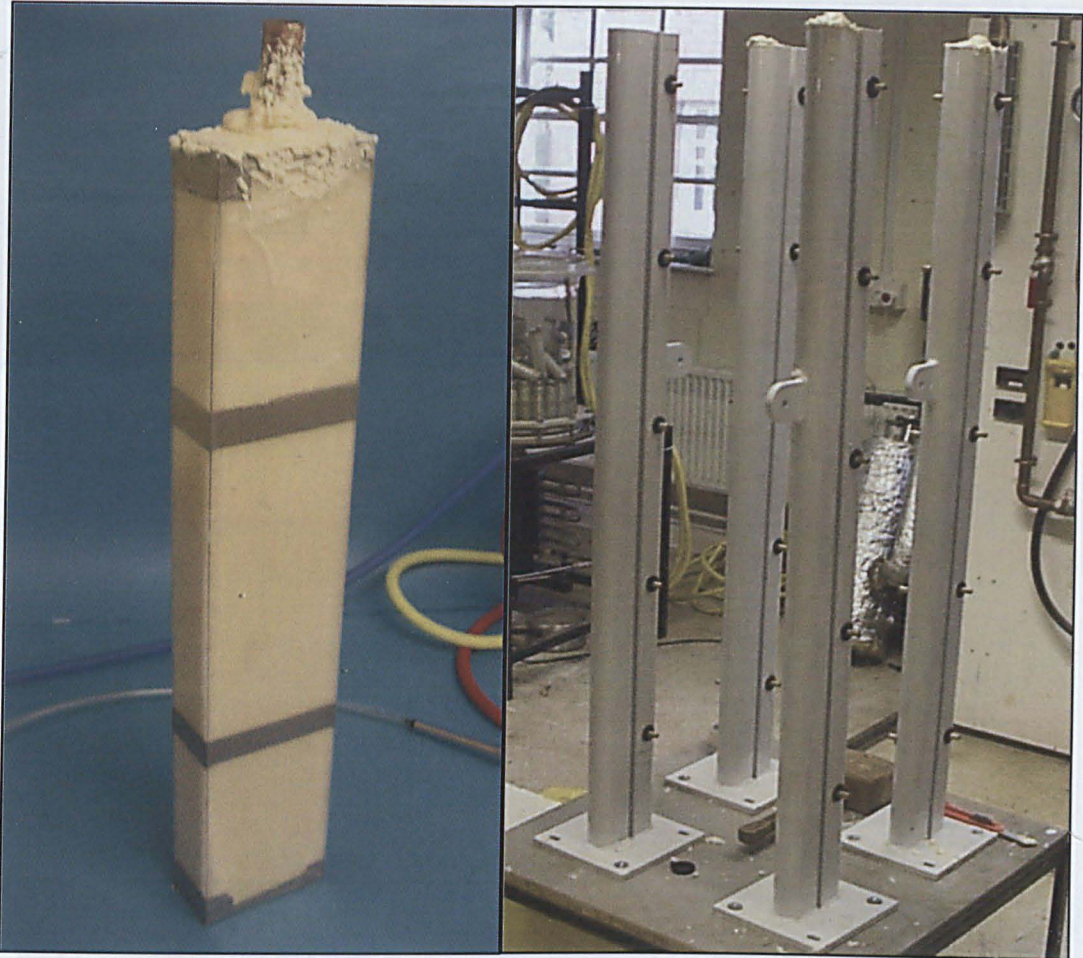


Figure 7.3.7 Testing the insulation-foam distribution (density) within a visible volume a (Perspex model), prior to filling the real arms.

The system has been filled with water, vented from air and circulated at approximately $20 \text{ g/m}^2/\text{s}$. This was recorded digitally via a digital flow meter at inlet, and verified by the visual flow meter.

The static pressure of the system was approximately 1.0 bar .

Temperatures were monitored every minute of the day at the following locations of the system: Inlet to the collector - T_{in} ; outlet from the collector - T_{out} ; mean-plate temperature - T_{pm} (matrix of Figure (7.3.3)); ambient temperature - T_a . Tank temperature has also been recorded.

T -type thermocouples were used through out this research work.

Solar radiation - I , with a pyranometer (Kipp & Zonen, model CM3; sensitivity: $19.58 \mu\text{V/W/m}^2$) on the plane of the collector, and wind speed u , with anemometer

(Switching type; accuracy: 1% of reading at 10-55 m/s, 2% of reading for >55 m/s), were also both recorded.

The logged data generated had been stored in a computer, which was unloaded periodically via a laptop – Figure 7.3.8.

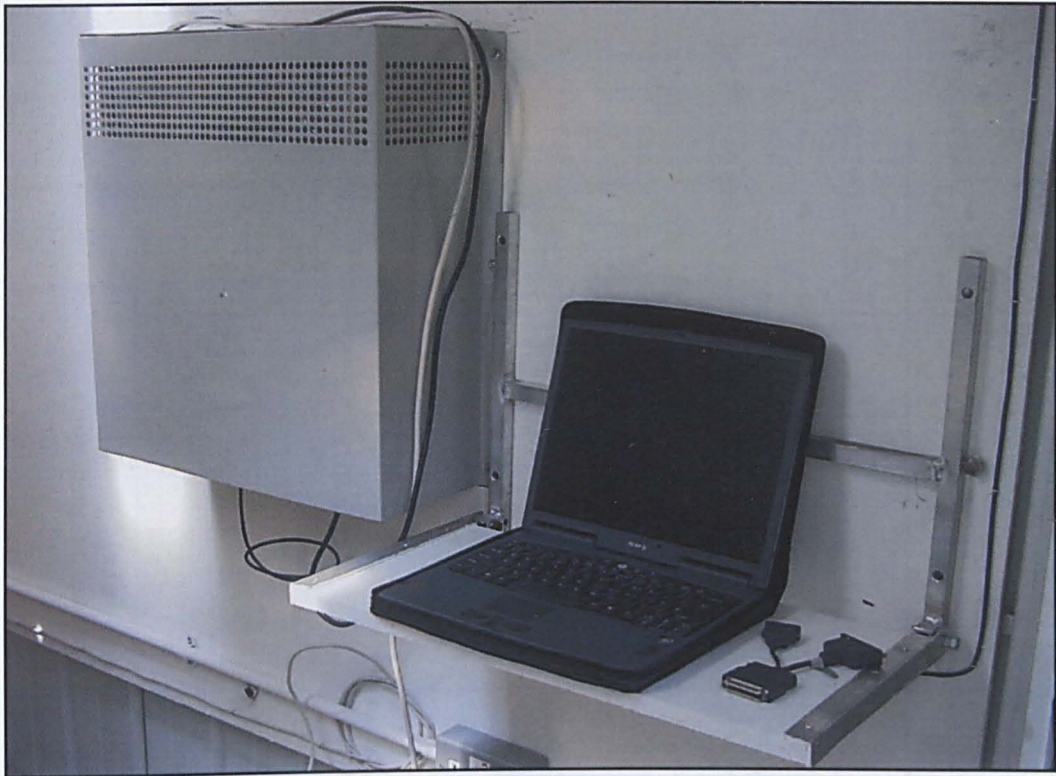


Figure 7.3.8 Computer permanently connected to the outdoor data logger, and periodically unloaded.

The generated data has been used for monitoring the prototype performance under Nottingham skies.

A sample plot of a three consecutive days (20th, 21st, 22nd of June 2003) is depicted on Figure 7.3.). In this it can be seen that the weather at the site was rather unstable or fluctuating, especially in terms of radiation levels.

That is why the determination of the experimental efficiency of the louvres has been carried out in a controlled environment, following the ASHRAE 93-77 guidelines for steady-state testing conditions-Chapter (6), *Experimental work*.

Leakage from the water channels, only the shown results were obtained.

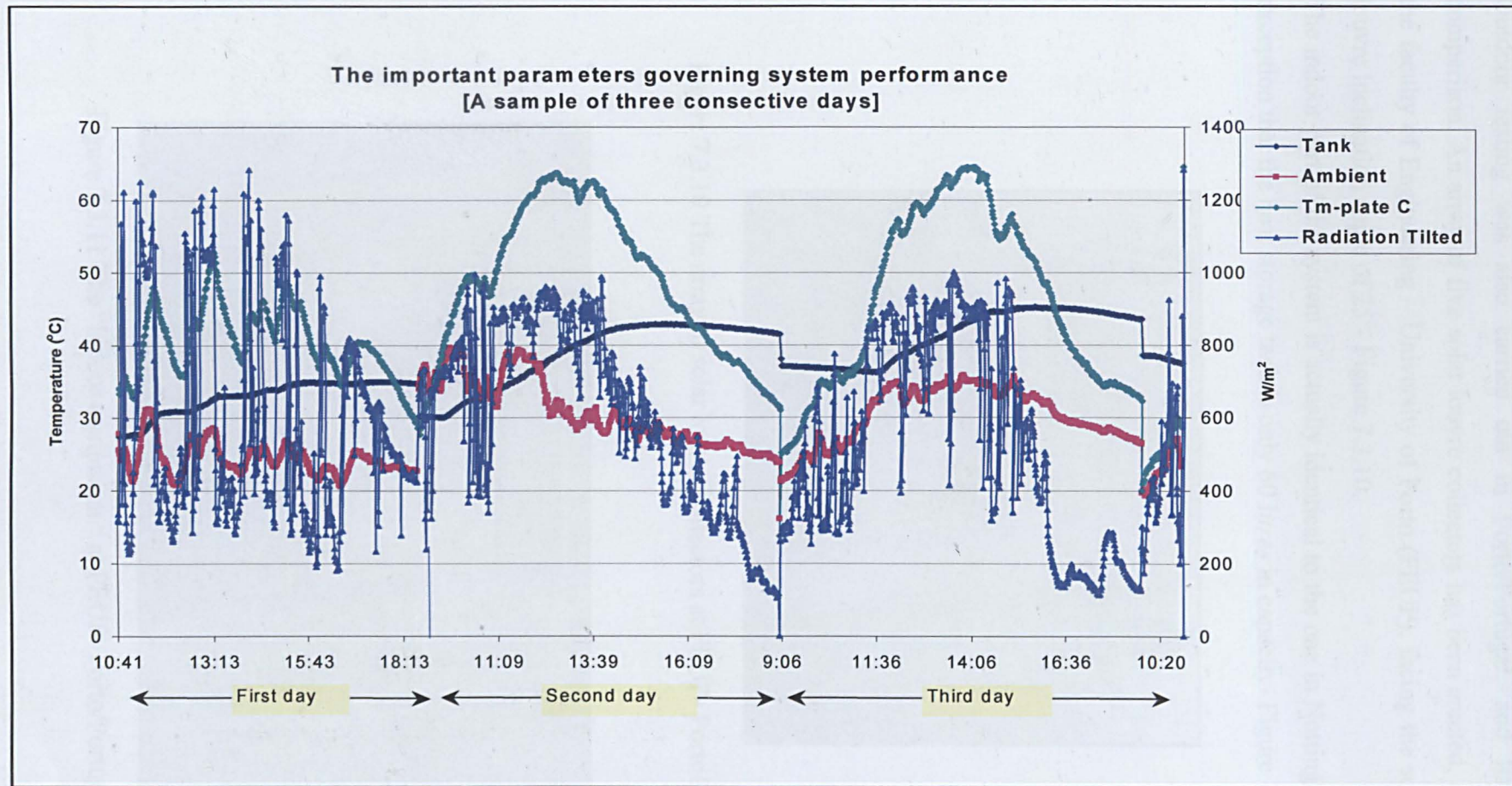


Figure 7.3.9 Solar louvre collectors prototype at Nottingham – (20th, 21st, 22nd August 2003)

7.3.2 Trials in Porto

Outdoor testing was also carried out in Porto/Portugal, and listed here for comparison. An array of five solar louvre collectors has been erected, on the roof of the faculty of Engineering – University of Porto (FEUP), facing the southern sky at louvre inclination angle of 25° - Figure 7.3.10.

The indoor part of the system is actually identical to the one in Nottingham, with the exception that the heat storage tank is only 60 litres in capacity- Figure 7.3.11.

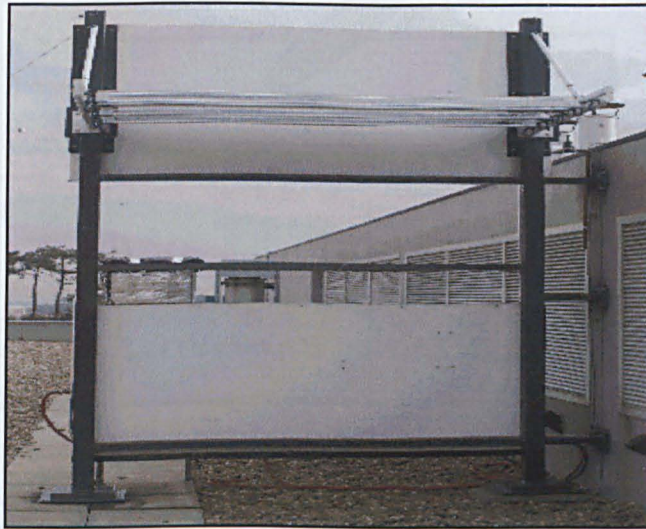


Figure 7.3.10 The array of solar louvre collectors at FEUP- Porto/Portugal.



Figure 7.3.11 The “Indoor equipment “ at FEUP- Porto/Portugal.

Instrumentation used for the outdoors test was as shown on Figure (7.3.12); solar radiation was measured with a pyranometer (Kipp & Zonen, model CM6B), and thermocouples (T -type) to measure water temperature at collector inlet, outlet and tank. Ambient temperature and wind speed were also recorded.

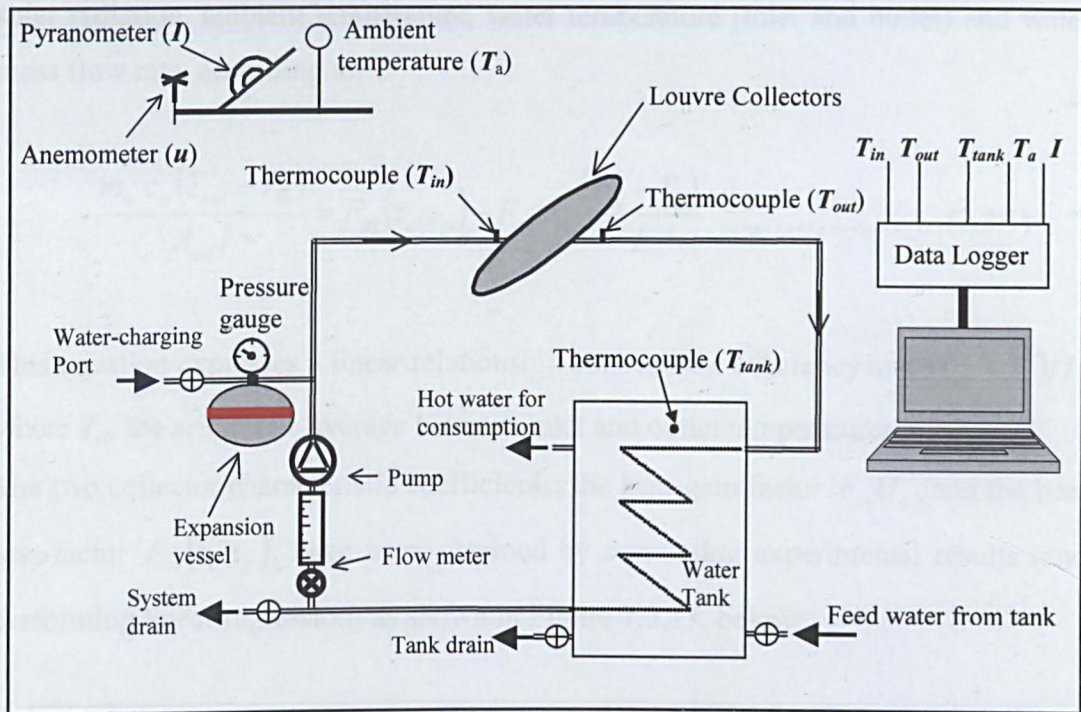


Figure 7.3.12 Schematic of the outdoor prototype testing facility and associated instrumentation at FEUP – Porto/Portugal.

Testing was carried out under summer, mid-season and winter outdoor conditions, between July and December 2003.

These were conducted, only during clear-sky days, between 10:00 *am* and 2:00 *pm*, so that the incidence angle on collector surface was always less than 30°. This allows quantification of the collector optical efficiency for semi-normal incident light. Water flow rate was fixed at 20 g/s/m².

All measured values T_{in} , T_{out} , T_m , T_a and I were recorded every minute. For each test point, a quasi steady-state condition was obtained, allowing a maximum variation of 2% in every measured variable during a period of 10 minutes. Average values for each 10 minute period were considered - a period which is longer than the collector thermal response time. More than 100 experimental points were obtained.

Points were obtained during both summer and winter operation conditions. Summer ambient temperature varied between 25 and 35 °C, and incident solar radiation varied between 650 and 850 W/m². Winter ambient temperature was in the range 10 -15 °C, and incident radiation varied in the range 200-500 W/m².

As shown in the previous chapters, the collector efficiency is a function of incident solar radiation, ambient temperature, water temperature (inlet and outlet) and water mass flow rate, according to:

$$\frac{m_w c_p (T_{out} - T_{in})}{A_{col} I} = F_{av} (\tau_c \alpha_p) - F_{av} U_c \frac{(T_{av} - T_a)}{I} \dots\dots\dots(7.3.1)$$

This equation expresses a linear relationship between the efficiency and $(T_{av} - T_a)/I$, where T_{av} the arithmetic average between inlet and outlet temperatures.

The two collector characteristic coefficients; the heat-gain factor $F_{av} U_c$, and the heat loss-factor $F_{av} (\tau_c \alpha_p)$, have been obtained by correlating experimental results (and performing linear regression) as shown in Figure 7.3.13, below:

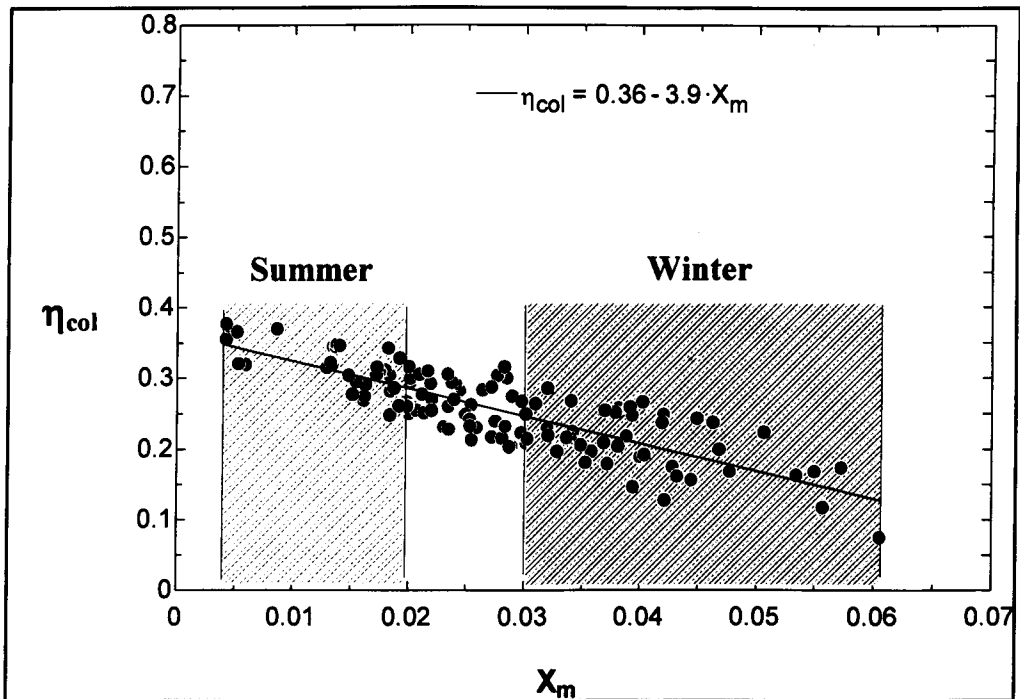


Figure 7.3.13 Out-door experimental collector efficiency curve;
 $X_m = [((T_{in} + T_{out})/2) - T_a] / I$.

From the graph of Figure 7.3.13, the equation of the efficiency is:

$$[Eff-c]_{outdoor} = -3.90 X_m + 0.36$$

Therefore the heat loss factor $F_{av}U_c$, is equal to $3.9 \text{ W/m}^2\text{-}^\circ\text{K}$, and the heat-gain factor $F_{av}(\tau_c \alpha_p)$, is equal to 0.36.

The mathematical model of chapter (5) – *The Design*, has been utilized to solve for the efficiency curve of the louvre; this time, however, incorporating more realistic values for the optical parameters (τ_c , α_p , ε_c , ε_p).

The cover transmission coefficient for solar radiation τ_c , was determined as 0.78, for both layers – see experiment of *chapter (6)*.

The cover's emissivity for long wave radiation, ε_c , was taken as 0.92.

It was considered that the receiving surface (the plate, coated with black paint) has an absorption coefficient for solar radiation, α_p , equal to 0.88, and an emissivity for long wave radiation, ε_p , equals to 0.95.

Results with these, new values, are shown in Figure 7.3.14, in comparison with the experimental results.

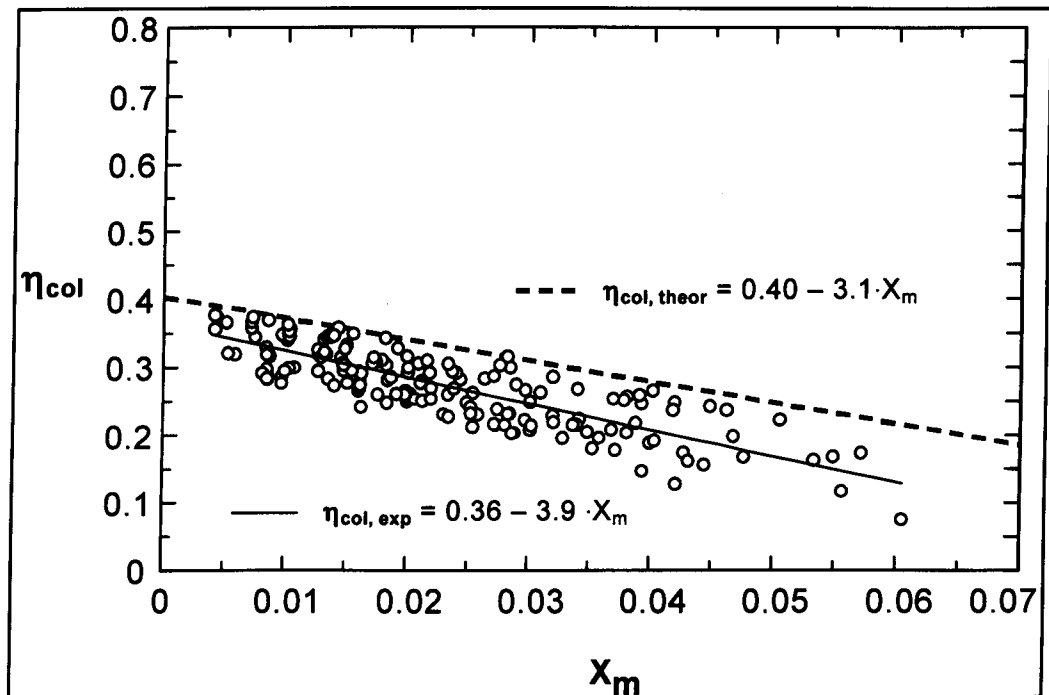


Figure 7.3.14 Comparison between out-door experimental (exp), and modelling (theor) results of the collector efficiency curve; $X_m = [(T_{in} + T_{out})/2 - T_a] / I$.

The model gives a slightly higher optical efficiency – (0.4 compared to 0.36), and a slightly lower loss coefficient – (3.1 instead of 3.9 $W/m^2\text{-}^\circ K$).

The experimental curve lies below the model's, which can be explained by the several ideal assumptions used in the construction of the model, that are not quite representing the real physical phenomenon: for instance, perfect contact between transparent cover and copper channels, one-dimensional heat transfer, curvature taken as straight line, neglecting edge losses, assuming fully developed flows (hydrodynamically and thermally) and many more.

Experiments are not spared from the issue of errors, either. In fact, outdoor solar collector experiments are more susceptible to errors than indoors'. So, in brief, there are many causes for discrepancies between experimental results and the modelling results.

These results show good agreements, and warrant the model its validation.

7.3.3 The Efficiency equation of the Solar Louvre Collector

The flow rate, through out this analysis, was kept at the recommended flow rate of 20 $g/s/m^2$. The efficiency values obtained thus far are as follows:

$$[Eff-c]_{lab} = - 5.21 X_m + 0.47$$

$$[Eff-c]_{model} = - 3.10 X_m + 0.40$$

$$[Eff-c]_{outdoor} = - 3.90 X_m + 0.36$$

The above results between laboratory, theoretical/numerical and outdoor experiments show reasonable agreements.

Average values to above efficiency equations yields, the “average” efficiency equation for the solar louvre collector, for the case of the channels as:

$$[Eff-c]_{actual} = - 4.1 X_m + 0.41$$

This efficiency equation has a reasonable (low enough) losses term, $F_{av}U_c = 4.1 W/m^2\text{-}^\circ K$. However, its gain term is too low by any standard: $F_{av}(\tau_c \alpha_p) = 0.41$.

One should keep in mind that this is due to the reduced transparent area (60% of the theoretical area)

A normal flat plate solar collector (single glazed with selective surface) has $F_{av}(\tau_c \alpha_p) = 0.78$ and $F_{av}U_c = 4.5 \text{ W/m}^2\text{-}^\circ\text{K}$ as typical values.

7.4 Summary

It has been shown from the preceding analysis that, the solar louvre collector design passes the environmental assessment, economic analysis (three Figures of merit, namely, the *payback period*, the *averaged energy cost* and the *life cycle savings*), as well as the field trials.

For the case of Lisbon, results (of the hot water system) favour the use of these collectors, in contrast with London, where the overall results score well below average or poor, due to the low solar fraction, and low fuel cost.

These results indicate low gain factor (optical efficiency), mainly due to the reduced collection/transparent area. The quality of material used for the cover and for the coating of the absorber surface has an effect on the heat gain.

Also not being able to use vacuumed cover clearly increases the rate of top heat loss through this cover.

Cover and absorber are particularly critical; their properties determine $(\tau_c \alpha_p)$, ε_p and ε_c ; thus affecting the thermal performance of the collector.

With the optical properties ($\tau_c = 0.92$, $\varepsilon_c = 0.84$, $\alpha_p = 0.96$, $\varepsilon_p = 0.1$), for the cover and absorber plate, at water flow rate of 20 g/s/m^2 , the results of the *direct-flow model*, for the channels, has given:

$$F_{av}(\tau_c \alpha_p) = 0.87, \text{ and } F_{av}U_c = 3.9 \text{ W/m}^2\text{-}^\circ\text{K}.$$

So, as the modelling results have been verified, these above values provide hope for improvement. This can be achieved primarily if a larger transparent area is used to increase the collection/gain term.

Improving the optical properties for the solar louvre collector is possible by employing Titanium Oxynitride as a coating material for the plate. This selective material has emissivity, ε_p , of 0.10 ± 0.02 , and absorbance, α_p , of 0.96 ± 0.02 .

Like the plate, ideally one would like the cover to have a high transmittance, τ_c , as well as low emissivity, ε_c .

In practice, however, low emissivity (low-e) glass, has low transmittance as well.

So, a pane with a good, low-e coating has $\varepsilon_c = 0.15$, and it transmits about 70 % (i.e. $\tau_c \approx 0.70$), and absorbs 20% (15% of which is re-emitted; $\varepsilon_c = 0.15$).

Improvement to the optical properties, to both cover and absorber plate, means more energy gain, which unavoidably implies more losses. These losses, however, are minimised by the use of evacuated double-pane cover, and back-insulation.

Chapter Eight
Simulation Case study

8. Simulation Case-study

In chapter (5) – *The Design*, a mathematical model has been developed and used to simulate the thermal performance of the solar louvre collector. This model is based on the steady state, energy balance concept, and does not account for the dynamic behaviour of the solar collector (i.e. varying ambient conditions and load). Rather, the model caters to characterize the solar louvre collector (its design), in terms of the two the parameters: $F_R(\tau_c \alpha_p)$ and $F_R U_c$, which are sufficient design parameters.

It is of paramount importance, in a solar collector design process, however, to determine the dynamic behaviour and integrated performance of the collector in the whole system, under real-life conditions (i.e. varying solar radiation, ambient, wind speed and thermal load).

In this chapter, however, the solar louvre collector has been simulated dynamically in an office building, using TRNSYS – Klein *et al*' (1997). The work here has been carried out partly by Axima-Switzerland.

TRNSYS is a transient process simulation program. It is a widely used, modular thermal process program, originally developed for solar energy applications; it is now used for simulation of a wider variety of thermal processes. It also has its own built-in library of components, combinations of components, property tables, etc.

The simulation, of the solar louvre collector, has been treated in two main parts; on the first instance, only shading by these louvres, and its impact on the annual total energy (heating and cooling) consumption, in a typical office building, has been analysed.

Secondly, the fraction of intercepted radiation that is absorbed by the louvre collector has been used to replace some of the annual total grid-energy used for the purpose of heating and cooling in this office building.

8.1 The typical office building floor

The building, located in Winterthur/ Switzerland, is oriented southwards, and the solar louvre collectors were simulated on the south-façade.

The prevailing identity of single floors, in multi-story buildings, is the substantiation for simulating only one floor.

The floor has a size of $55.40\text{ m} \times 7.10\text{ m} \times 2.76\text{ m}$; total floor area of 393.34 m^2 , and volume of 1085.62 m^3 . It is divided into offices of different sizes, separated by internal partition-walls.

As boundary conditions, it was assumed that the surrounding rooms have identical temperatures, hence a uniform temperature throughout the floor.

For each wall and for the floor, the individual assembly of different layers of different materials was considered, and only negligible losses were assumed there.

These losses are small compared to the losses from the single-pane windows used.

This adiabatic envelope has apertures made as 39 single-pane windows ($k = 2.8\text{ W/m}^2\text{-}^\circ\text{K}$, $g' = 0.75$), integrated in the south wall (only there), with a total glass-surface of 78.7 m^2 , which is approximately 40% of the outer wall surface. g' is the solar heat gain coefficient.

Heat loads for user attitude assumptions were made, as listed in Table 8.2.1, below:

Table 8.1.1 Internal heat loads in the office floor.

Loads	Amount	Specific and Max heat load [W]	Power-on or people in time, automatic controls
Staff	20	65 W/clerk, Max. 1300 W	Mon – Fri: No. of staff: 7.00 – 8.00: 5 8.00 – 17.00: 20 17.00 – 18.00: 10 18.00 – 19.00: 5
Computers	20	230 W/pc, Max. 4600 W	Mon – Fri: pc's online: 7.00 – 8.00: 8 8.00 – 17.00: 20 17.00 – 18.00: 8 18.00 – 7.00: 4
Lighting	91 shiners	13 W/m ² , Max. 5100 W	Mon – Fri: Percentage lit: 7.00 – 9.00: 50% 9.00 – 17.00: 20% 17.00 – 19.00: 100%
Heating	1 system ¹	Unlimited, depending on boundary and automatic control conditions.	Heating, if internal temperature $T_i < T_r$: Mon–Fri, 8.00–20.00: $T_r = 21.5^\circ\text{C}$ Else: $T_r = 18^\circ\text{C}$
Cooling	1 system ²	Unlimited, depending on boundary conditions	Every day: $T_i > 26^\circ\text{C}$: Activated

System¹: Underfloor heating, System²: Chilled Ceiling/cold slaps

According to the ASHRAE 62-1989, “Ventilation for acceptable Indoor Air Quality”, a 20 cubic foot per minute per person (i.e. $33.98 \text{ m}^3/\text{hour}/\text{person}$) was assumed.

8.2 Geometrical aspects of shading by Solar Louvre

The effect of shading depends on the latitude of the building’s location, as well as on the dimensions of the shading device. It is, therefore important to optimise the dimensions of the solar louvre collector to suit the building in the simulation scenario.

The solar louvres are assumed to be placed horizontal and sufficiently above the windows along the whole distance of the south wall, such that it guarantees total shading at noon of June, 21st ($h_{\max}-10^\circ$, h_{\max} is the maximum solar altitude at this time) and a complete window insolation at December, 21st ($h_{\min}+10^\circ$, h_{\min} is the minimal solar altitude at his time); - see Figure 8.2.1.

The window height H_w is given and the geometrical sizes H , L and E , as shown in Figure 8.2.1, were calculated to guarantee the intended boundary conditions.

Between the solar altitudes $h_{\min}+10^\circ$ and $h_{\max}-10^\circ$ the window is partially shaded. The upper direct sunbeam is given by the angle β .

The solar zenith angle, γ , defines the percentage of shading of the window below the solar louvre collectors, expressed by β :

$$\beta = 90^\circ - \gamma - (h_{\min} + 10^\circ).$$

Therefore, the bigger β or L , the longer the duration of total shading.

For a window height $H_w = 1.66 \text{ m}$, as used in the simulation, the resulting horizontal length L was calculated for different values of β , depending on the latitude φ . The locations of Nottingham, Porto and Winterthur are shown, as well as the duration of total shading for 5 or 7 rows of louvres; see Figure 8.2.2.

Figure 8.2.3 shows the necessary height H of the solar louvres above the windows.

Shading calculations have also been carried out for a window height of (2.6 m), a commonly used size in new office buildings- Figure 8.2.4.

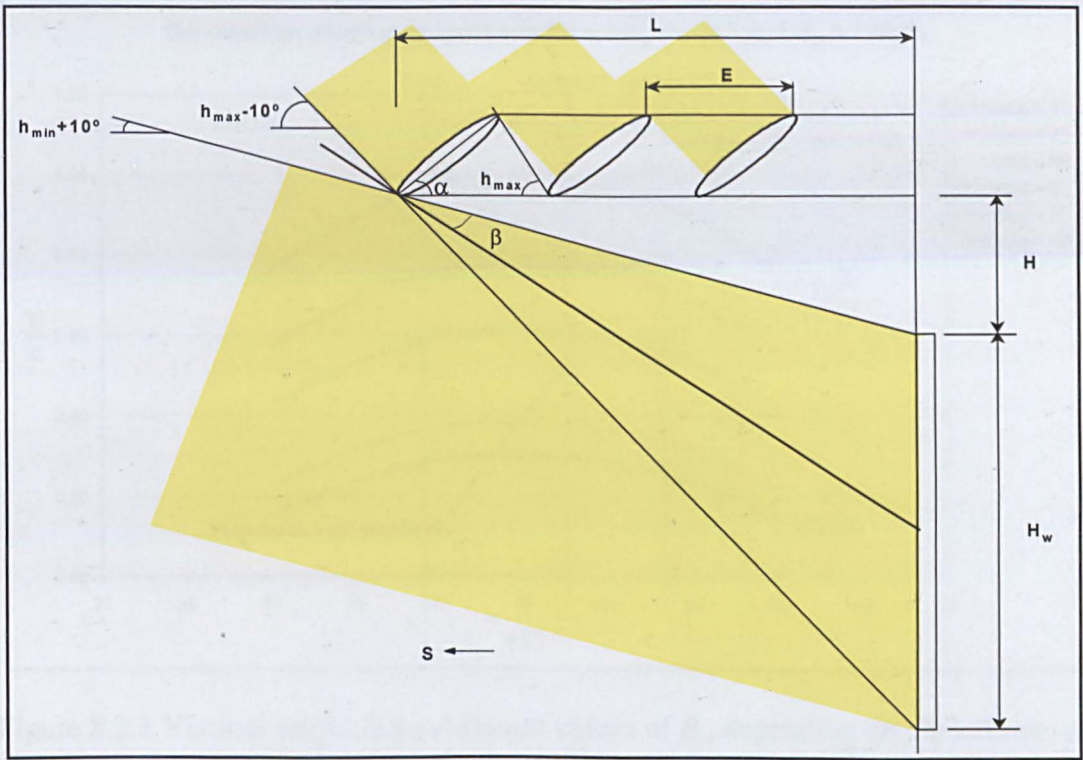


Figure 8.2.1 Optimum dimensioning of the solar louvre collectors to satisfy the conditions of total shading.

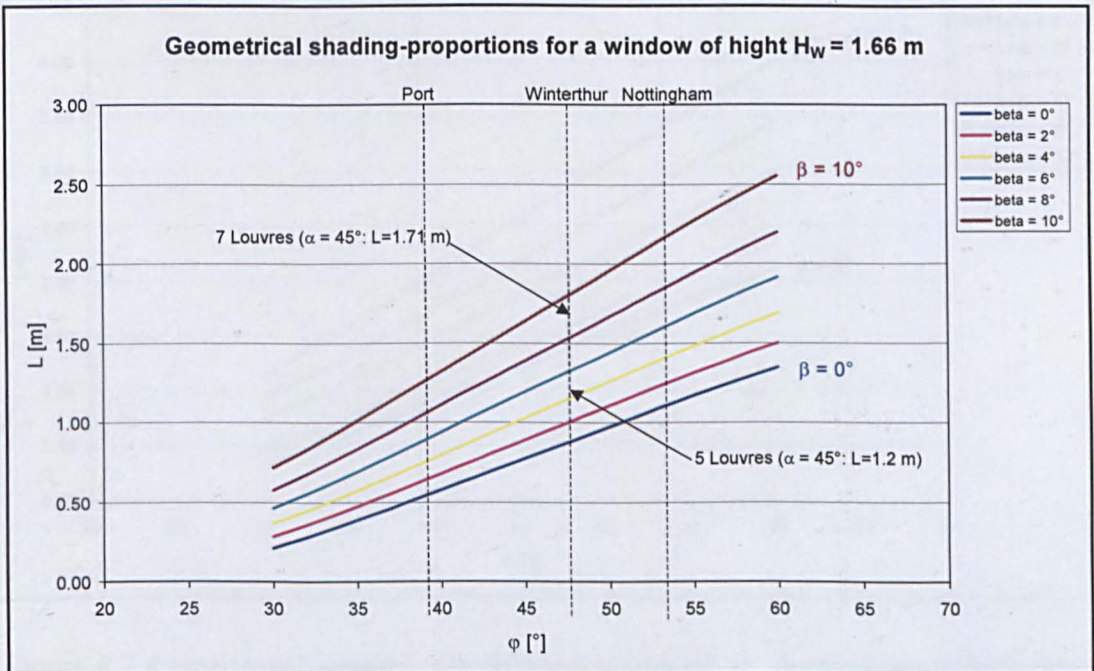


Figure 8.2.2 Horizontal length L for different values of β , depending on the latitude φ . The locations of Porto, Winterthur and Nottingham are shown, as well as the duration of total shading for 5 or 7 rows of Louvres mounted above the window.

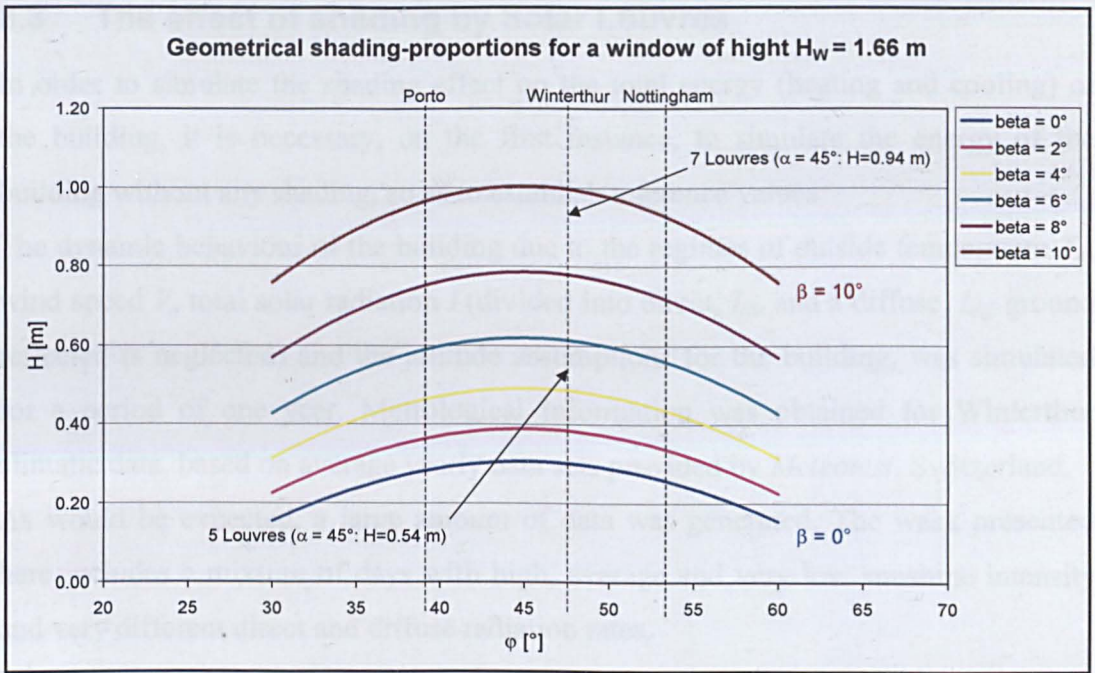


Figure 8.2.3 Vertical height H for different values of β , depending on the latitude ϕ . The locations of Porto, Winterthur and Nottingham are shown, as well as the duration of total shading for 5 or 7 rows of Louvres mounted above the window.

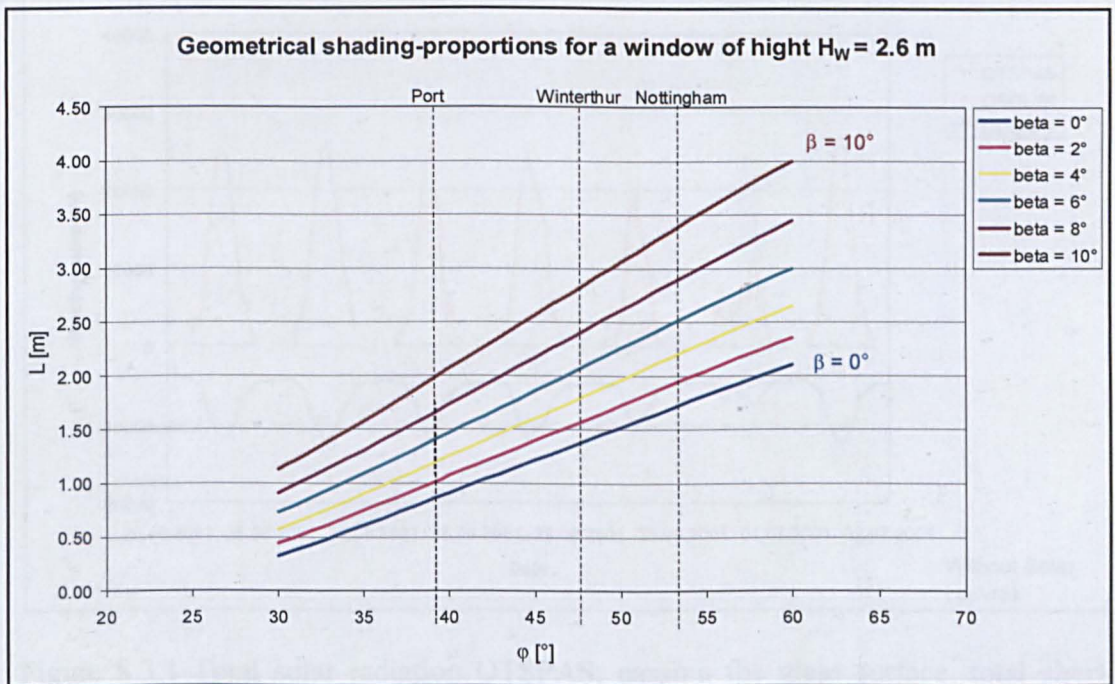


Figure 8.2.4 Horizontal length L for different values of β , depending on the latitude ϕ . The locations of Porto, Winterthur and Nottingham are shown, as well as the duration of total shading for 5 or 7 rows of Louvres mounted above the window.

8.3 The effect of shading by Solar Louvres

In order to simulate the shading effect on the total energy (heating and cooling) of the building, it is necessary, on the first instance, to simulate the energy of the building without any shading, so as to establish reference values.

The dynamic behaviour of the building due to the regimes of outside temperature T_a , wind speed V , total solar radiation I (divided into direct, I_{dir} and a diffuse, I_{dif} ; ground reflected is neglected) and the attitude assumptions for the building, was simulated for a period of one year. Metrological information was obtained for Winterthur climatic data, based on average yearly data sets provided by *Meteotest*, Switzerland.

As would be expected, a large amount of data was generated. The week presented here includes a mixture of days with high, average and very low sunshine intensity and very different direct and diffuse radiation rates.

The energy exchange (radiation and convection) of the building with its ambient surroundings, which is passing through the glass of the unshaded building (i.e. without solar louvres), can be seen in Figure 8.3.1:

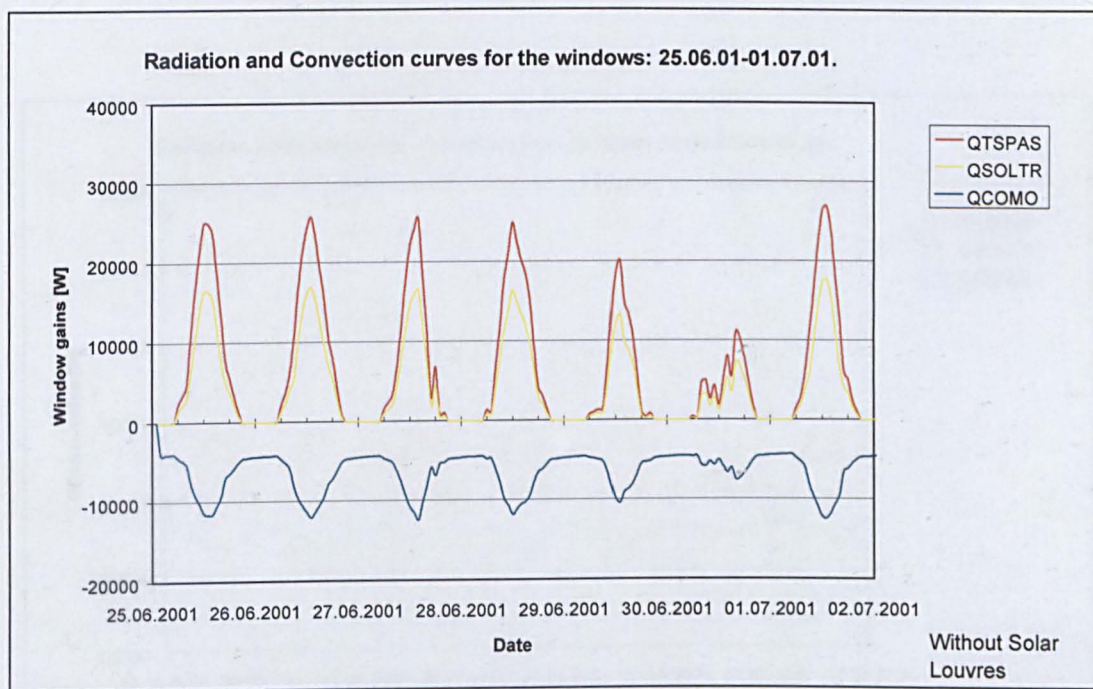


Figure 8.3.1 Total solar radiation QTSPAS, passing the glass surface, total short-wave radiation QSOLTR transmitted and the energy QCOMO, transmitted to the outside by radiation and convection (without shading).

Now with the solar louvres collector erected (30 louvres, 5 rows), simulations were performed, and results are as shown below:

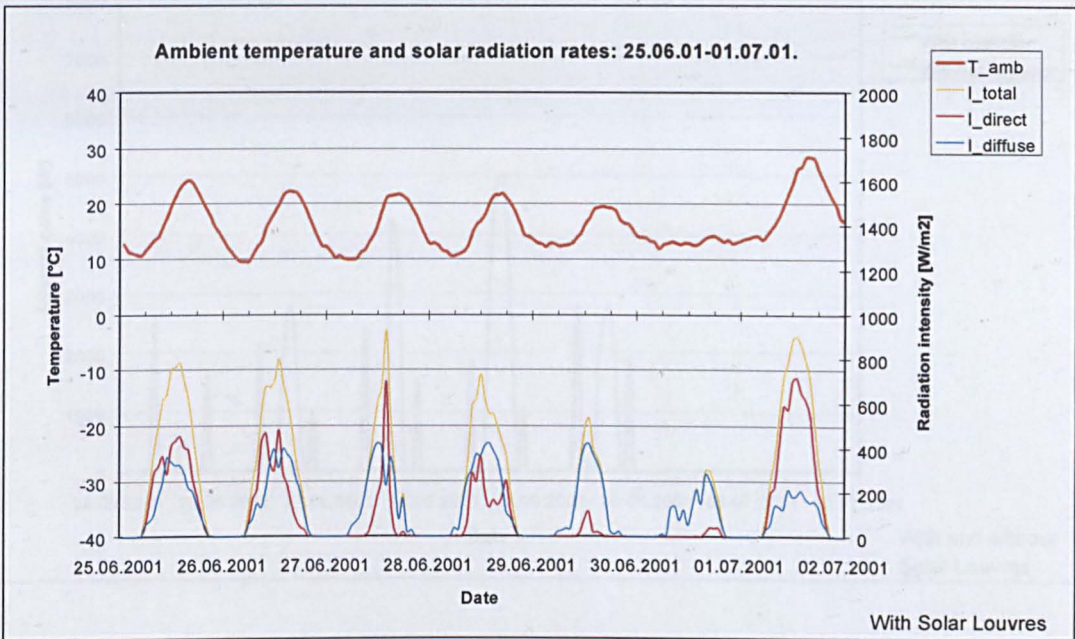


Figure 8.3.2 Metrological data for a week in early summer including the outside temperature, the total solar radiation and the rates of direct and diffuse radiation

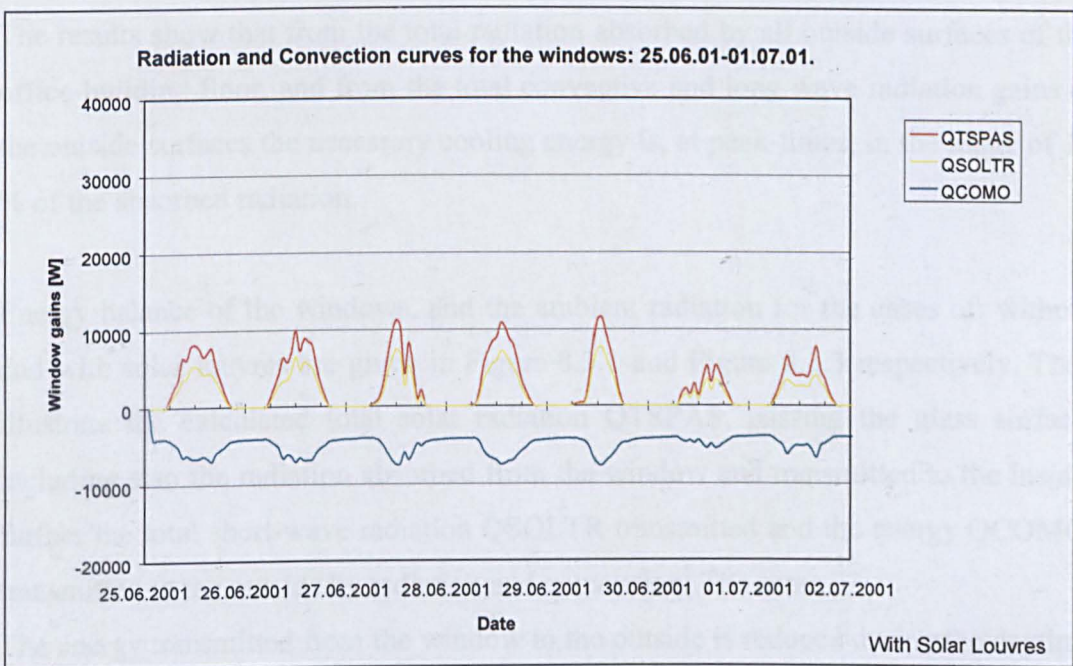


Figure 8.3.3 Total solar radiation QTSPAS, passing the glass surface, total short-wave radiation QSOLTR transmitted and the energy QCOMO, transmitted to the outside by radiation and convection (with shading by the solar louvres)

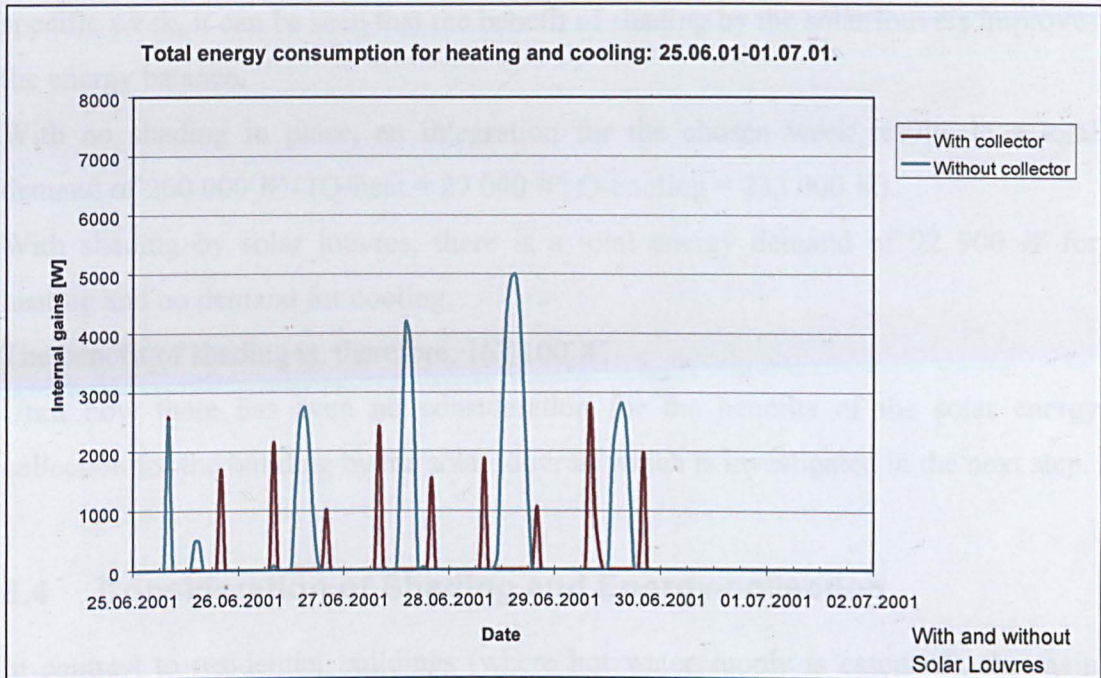


Figure 8.3.4 Comparison of heating and cooling demands for a week in early summer (with and without the solar louvre collectors)

The results show that from the total radiation absorbed by all outside surfaces of the office-building floor, and from the total convective and long wave radiation gains to the outside surfaces the necessary cooling energy is, at peak-times, in the range of 10 % of the absorbed radiation.

Energy balance of the windows, and the ambient radiation for the cases of: without and with solar louvres are given in Figure 8.3.1 and Figure 8.3.3 respectively. They illustrate the calculated total solar radiation $QTSPAS$, passing the glass surface, including also the radiation absorbed from the window and transmitted to the inside, further the total short-wave radiation $QSOLTR$ transmitted and the energy $QCOMO$, transmitted to the outside by radiation and convection. The same

The energy transmitted from the window to the outside is reduced during the daytime due to the minor insolation (less infrared radiation by the window itself).

Calculations show, for the considered week, that there is no necessity for cooling. Instead there is a little demand for heating during working day in the early morning and during the late afternoon.

Comparing the differences in energy consumption of heating and cooling for this specific week, it can be seen that the benefit of shading by the solar louvers improves the energy balance.

With no shading in place, an integration for the chosen week results in a total demand of 260 000 W - (Q-heat = 27 000 W , Q-cooling = 233 000 W).

With shading by solar louvres, there is a total energy demand of 92 900 W for heating and no demand for cooling.

The benefit of shading is, therefore, 167 100 W .

Until now there has been no consideration for the benefits of the solar energy collection for the building by the solar louvres, which is investigated in the next step.

8.4 Consideration of Shading and Energy-collection

In contrast to residential buildings (where hot water supply is essential), the main energy demands of office buildings are for heating and cooling.

The described office-floor was simulated for 30 louvres in line, with either 5 or 7, rows. It was assumed, that 100 % of the solar louvre surface acts as a collector.

Calculations were performed for five different situations, with 5 or 7 rows of solar louvres, two different window types: the present windows (old), and proposed (new) windows, and two different sizes of total window surface-areas (actual situation- 78 m^2 , and the proposed – 109 m^2). These are as shown in Table 8.4.1.

The efficiency of the collector, used in this calculation, is given as per the work presented in chapter (5) – *The Design*, and Chapter (6) – *The Experimental Work*; by:

$$\eta_{col} = F_{av}(\tau_c \alpha_p) - F_{av} U_c \frac{(T_{av} - T_a)}{I} \dots\dots\dots (8.4.1)$$

I is the normal incident radiation, most of which is assumed beam.

T_{av} is the arithmetic average of the fluid inlet and outlet temperatures:

$T_{av} = (T_{in} + T_{out})/2$, and F_{av} is the heat removal factor based on T_{av} .

T_a is the ambient temperature.

$(\tau_c \alpha_p)$ is transmittance-absorptance product of the cover-plate for normal incident radiation, and U_c is the overall loss coefficient.

Having known the values of $F_R(\tau_c \alpha_p)$ and $F_R U_c$, the efficiency η_{col} could be calculated at any instant.

Assuming the louvres incorporating **fin-on-tubes** with (favourable optical properties), a plausible efficiency equation of the proposed, improved design would be:

$$[Eff-f]_{proposed} = - 4.0 X_m + 0.87,$$

$$\text{i.e. } F_R(\tau_c \alpha_p) = 0.87, \text{ and } F_R U_c = 4.0 \text{ W/m}^2 \cdot \text{ } ^\circ\text{K}.$$

Table 8.4.1 Five combination of different numbers of solar louvre rows, different window quality and window sizes.

Louvres	Window Type	Window Size
7	$k = 2.8 \text{ W/m}^2 \cdot \text{ } ^\circ\text{K}$, $g' = 0.75$ (old)	78 m^2
7	$k = 1.1 \text{ W/m}^2 \cdot \text{ } ^\circ\text{K}$, $g' = 0.60$ (new)	78 m^2
7	$k = 2.8 \text{ W/m}^2 \cdot \text{ } ^\circ\text{K}$, $g' = 0.75$ (old)	109 m^2
7	$k = 1.1 \text{ W/m}^2 \cdot \text{ } ^\circ\text{K}$, $g' = 0.60$ (new)	109 m^2
5	$k = 2.8 \text{ W/m}^2 \cdot \text{ } ^\circ\text{K}$, $g' = 0.75$ (old)	78 m^2

A constant flow rate of 72 kg/hr/m^2 was assumed throughout this simulation. Also, no thermal energy storage is considered, at this stage. The net collected solar energy can only be used directly for solar heating (an efficiency factor of 0.85 is assumed) or solar cooling (an average efficiency factor (*COP*) of 0.5 is assumed).

Results are shown for one week in October, because there is an energy demand for heating as well as for cooling.

Figure 8.4.1 shows results, using the actual office-building situation; first line in Table 8.4.1.

For the considered week in October, for some days there is a demand for heating during the morning and a demand for cooling during the afternoon. The total energy, transmitted to the collector obviously exceeds the energy demand of the office during 3 days.

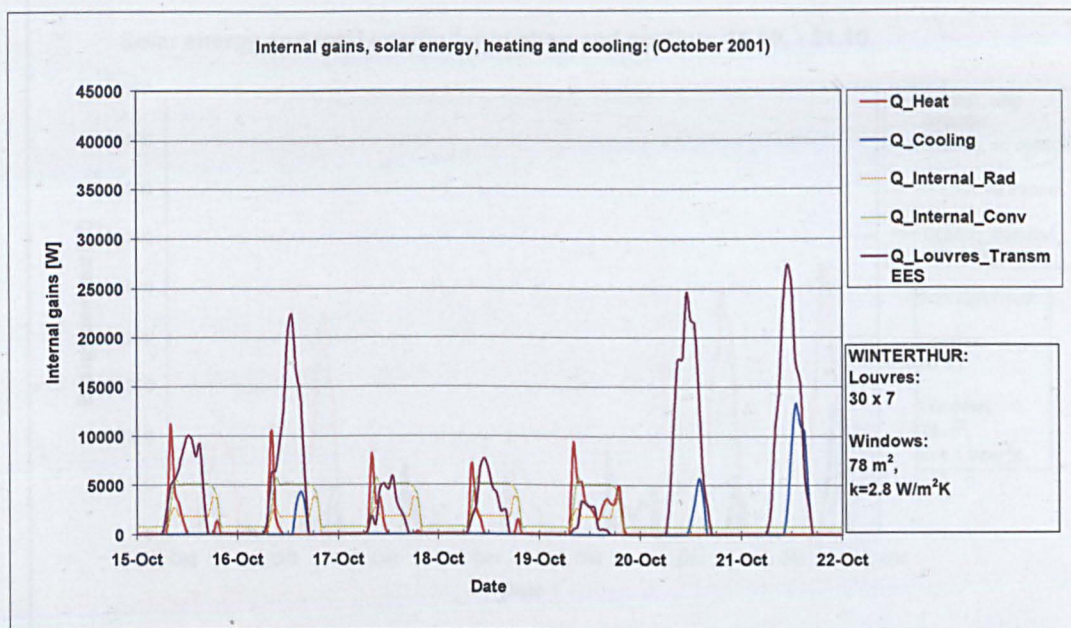


Figure 8.4.1 Energy demand for heating and cooling, internal gains (split into the contributions by radiation and convection) and energy transmitted to the solar louvres for a typical week in October.

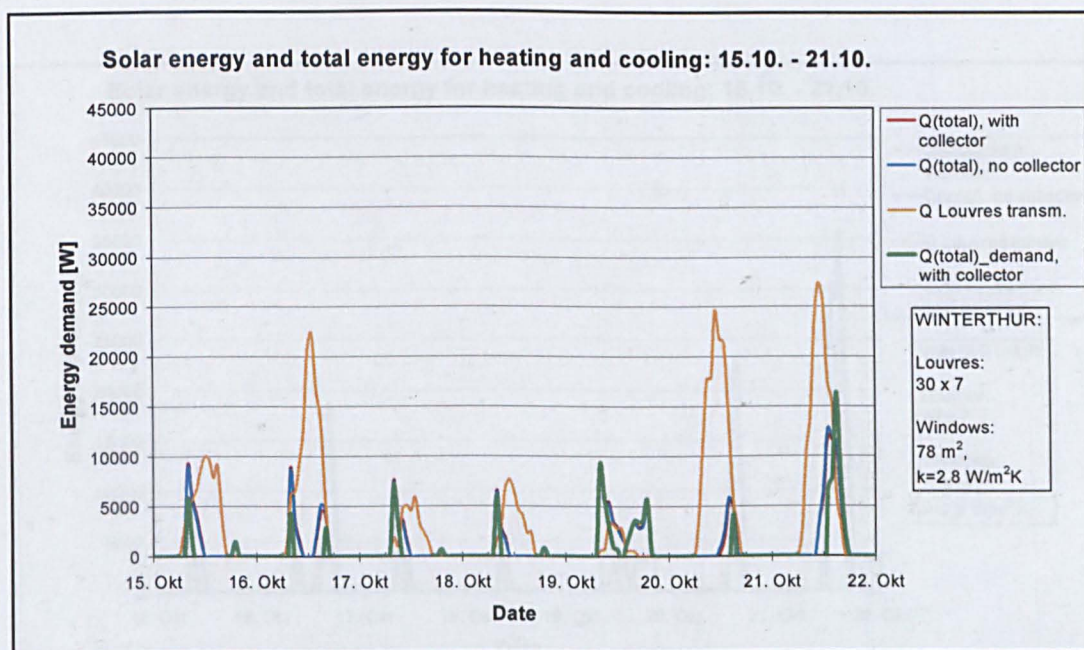


Figure 8.4.2 Actual office situation: Total energy demand (heating and cooling) for the calculated situation in October, energy demand for the existing building situation, (i.e. no solar louvre device is mounted above the window), total energy transmitted to the Solar louvres and the additional energy demand, if no, or not enough energy is provided by the collectors.

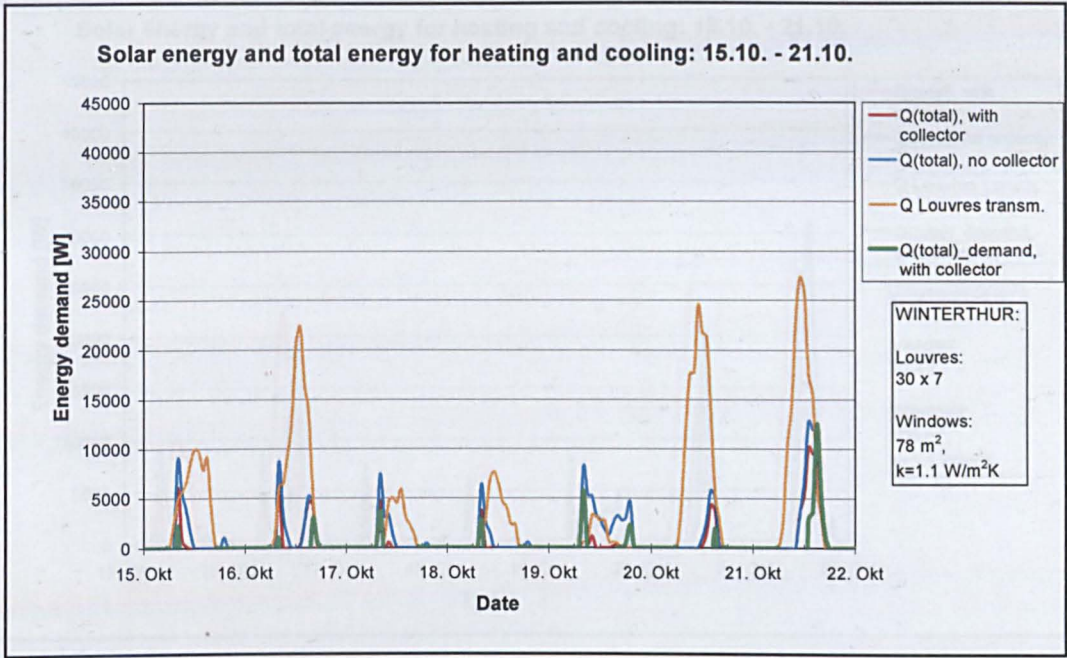


Figure 8.4.3 New windows: Total energy demand (heating and cooling) for the calculated situation in October, energy demand for the existing building situation (i.e. no solar louvre device is mounted above the window), total energy transmitted to the solar louvres and the additional energy demand, if no, or not enough energy is provided by the collectors.

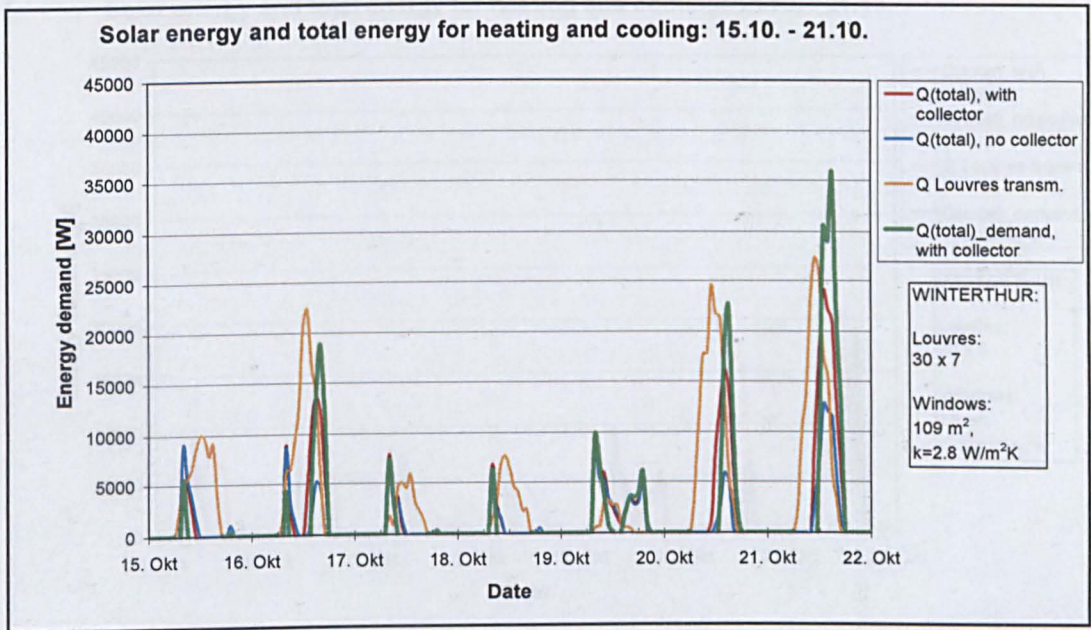


Figure 8.4.4 Window size 109 m²: Total energy demand (heating and cooling) for the calculated situation in October, energy demand for the existing building situation (i.e. no Solar louvre device is mounted above the window), total energy transmitted to the solar louvres and the additional energy demand, if no, or not enough energy is provided by the collectors.

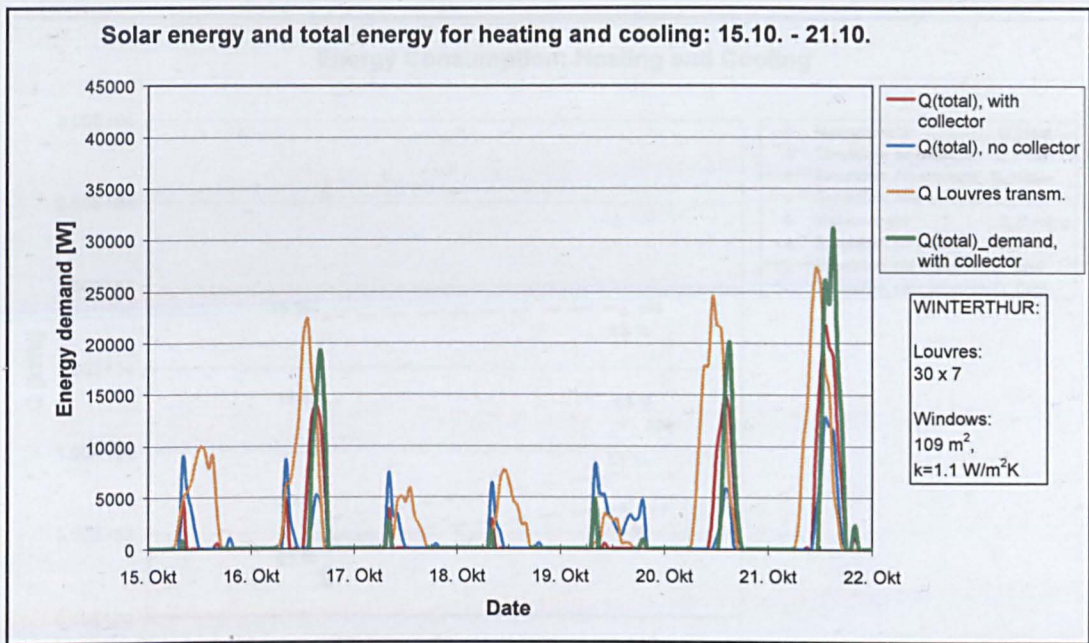


Figure 8.4.5 Window size 109 m^2 , new windows: Total energy demand (heating and cooling) for the calculated situation in October, energy demand for the existing building situation, (i.e. no solar louvre device is mounted above the window), total energy transmitted to the Solar louvres and the additional energy demand, if no, or not enough energy is provided by the collectors.

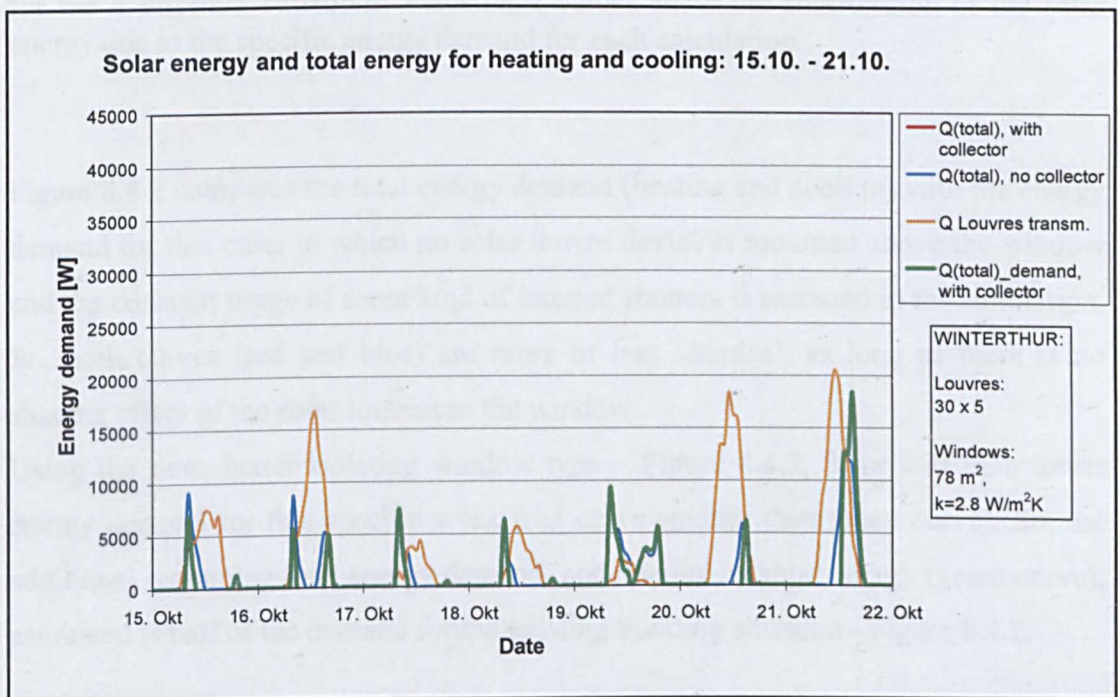


Figure 8.4.6 rows of solar louvres: Total energy demand (heating and cooling) for the calculated situation in October, energy demand for the existing building situation, (i.e. no solar louvre device is mounted above the window), total energy transmitted to the solar louvres and the additional energy demand, if no, or not enough energy is provided by the collectors.

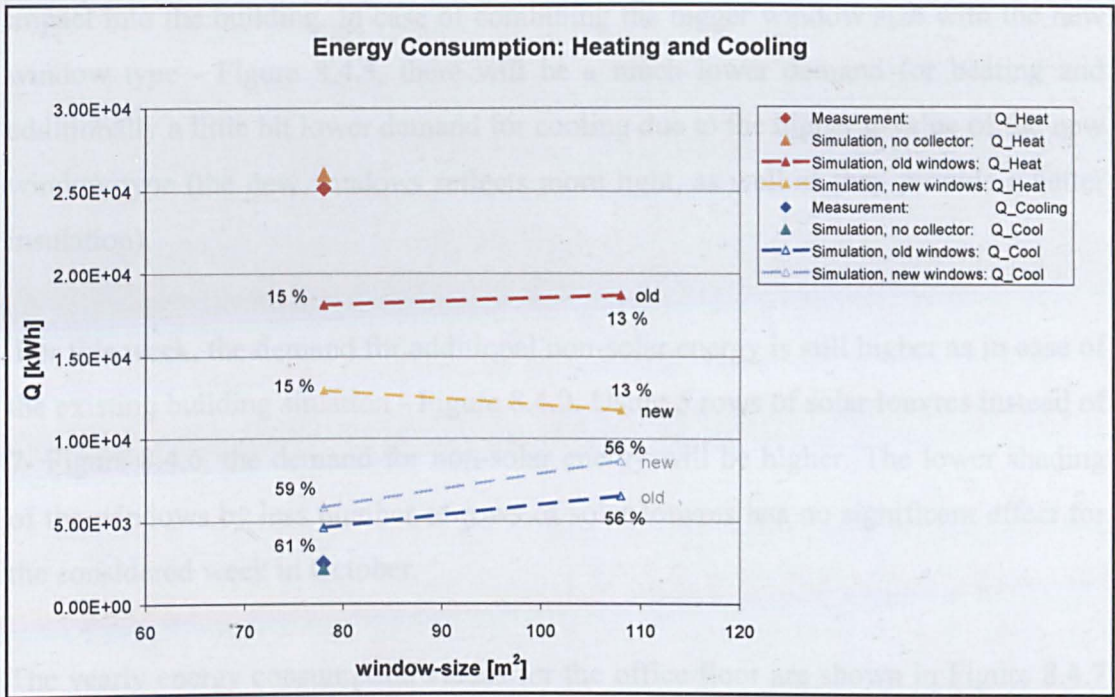


Figure 8.4.7 Yearly energy consumption values for the office floor for 4 different situations (table 1) with 7 rows of solar louvres, depending on window size. “old” represents the existing window type, “new” the new window type. Shown are the estimated results for the energy demands for heating and cooling, based on measurements, calculations for the existing building situation, and simulation results for the 4 different situations. Percentage values show the contribution of the solar energy due to the specific energy demand for each calculation.

Figure 8.4.2 compares the total energy demand (heating and cooling) with the energy demand for that case, in which no solar louvre device is mounted above the window and the constant usage of some kind of internal shutters is assumed in the simulation. So, both curves (red and blue) are more or less identical, as long as there is no shading effect of the solar louvres to the window.

Using the new, better isolating window type – Figure 8.4.3, there will be a lower energy demand for this specific week (red curve smaller than green curve). So, the additional remaining total energy demand, not covered by solar energy (green curve), estimated is half of the demand for the existing building situation - Figure 8.4.2.

Comparing the results of Figure 8.4.2, with the results in Figure 8.4.4 (window size 109 m²) shows that the bigger window size has no appreciable additional demand for heating (during the morning) but for some days an additional demand for cooling. The demand not covered by solar energy is obviously higher due to the higher solar

impact into the building. In case of combining the bigger window size with the new window type - Figure 8.4.5, there will be a much lower demand for heating and additionally a little bit lower demand for cooling due to the higher g-value of the new window type (the new windows reflects more light, as well as they provide a better insulation).

For this week, the demand for additional non-solar energy is still higher as in case of the existing building situation - Figure 8.4.2. Using 5 rows of solar louvres instead of 7- Figure 8.4.6, the demand for non-solar energy will be higher. The lower shading of the windows by less number of rows of solar louvres has no significant effect for the considered week in October.

The yearly energy consumption values for the office floor are shown in Figure 8.4.7 for the 4 different situations (Table 8.4.1) with 7 rows of solar louvres. The window size and the terms “old” for the existing window type and “new” for the new window type are shown. Further, the estimated results for the energy demand for heating and cooling, basing on measurements (rhombus plotting mark), simulation results (triangle plotting mark) for the existing building situation, and simulation results for the 4 different situations are pictured. Percentage values show for each calculation the contribution of the solar energy due to the specific energy demand. Results for the existing building situation without solar louvres match quite well the estimated values (conclusion from the known total building energy demand of the building). The simulations show the following conclusions for the specific building:

- For the considered building, located in Winterthur, the contribution for solar cooling is relatively high (~60%). To achieve this in reality, an elaborated technical concept for the solar cooling device will be necessary. Contribution for solar heating will be around 15% (this value could be significant higher, if the building would have been initially designed for passive solar heating).
- For the old windows, oriented to the south, the yearly energy demand for heating is only slightly increasing with the window size (bigger windows increase the heat flow out of the building, but the radiation impact into the

office will be increased as well). Therewith, the percentage of energy demand, which can be covered by solar heating, is also decreased.

- For the windows, oriented to the south, the yearly energy demand for cooling significantly increases with the window size (more solar radiation impact in summer increases the average inside temperature). The percentage of energy demand, which can be covered by solar heating, is decreasing (only slightly, because the provided solar energy is high during this periods).
- The new windows significantly reduce the total energy demand for heating, merely by its size, not properties (~30% for the small and ~ 40% for the bigger windows). Contribution of the solar heating (percentage) will be the same as in case of the old windows.
- For the new window type, the total energy demand for cooling will be higher (~25 %) compared with the old window type and for the bigger window size. This difference will be approximately 30%. The reason for the bigger demand for cooling is caused by a stronger effect of the lower k-value compared to the effect of the higher g'-value of the new window type.
- The total energy demand (heating and cooling) is lower for the new window type, provided that they are properly sized.

The analysis, thus far, does not consider any storage facilities for the solar energy. The benefit of storing energy for solar heating and solar cooling is obvious. For example, Figure 8.4.6 shows for the 21st October a high demand for solar cooling, while there is much solar energy provided during the whole day. Storage capacity will cover a higher demand in cooling by solar energy. The same situation appears for solar heating, especially during spring and autumn. The savings in energy and improvement to the efficiency, especially for solar cooling, depends strongly on the storage supply and the control technique used.

8.5 Shading, Energy Collection and Storage

It has been pointed out in the preceding sections, that the addition of a cold-water tank would improve the cooling performance, if cold water could be produced and stored ahead. This has an advantage in days without intensive sunshine, but high outside temperatures and internal loads.

Also, the kinds of temperatures produced from the solar louvre collector are on the low side, only accepted in practice by an adsorption chiller.

The chiller used in this simulation (NAK) is by GBU GmbH (1996). It has precise *COP*-values readily available.

For simplification the analysis, it was assumed that the cooling water for the chiller could be held constant, (at 25°C for Winterthur), by a non-simulated cooling tower.

The main system components and details are:

The solar louvre collector system is simulated with TRNSYS-*type 1b*, by using the collector efficiency curve as given by equation (8.4.1).

The energy collecting-surface of the 7 rows of 30 solar louvres has a total active surface of 56.7 m².

The solar collector is connected to a stratified fluid storage tank (TRNSYS-*type 4b*, water storage medium), located inside the building with (volume 10000 l, height 2.4 m and tank loss coefficient of 0.2 kJ/h m² °K. The energy losses over the tank surface are transferred to the outside of the building. For simplification, it is assumed to use this one storage tank for providing thermal energy for solar heating (direct) and solar cooling (powering the adsorption chiller).

The fluid flow rate (4082 kg/h) between collector and tank is constant, and controlled by a differential controller, with a dead-band temperature difference of 2°C. Heat losses by water pipes are neglected.

Solar heating was simulated by the assumption, that the thermal energy given by the temperature difference between the water temperature inside the tank (temperature to heat source) and the room temperature can be totally used for heating. The return flow temperature is set to be identical with the room temperature, which, for example, can be possible for a floor heating system. The heating is controlled by the

mass flow rate of the hot water into the heating units in the office floor, with an upper-limit to total flow rate of 1000 kg/h.

NAK closed cycle chillers have low operating temperatures, starting with approximately 55°C. The heat source temperature and the cooling water temperature give the driving temperature. The temperature of the chilled water was set at 8°C. Using the collector fluid water; the upper temperature is limited to 100°C.

Avoiding simulating the whole design system of a specific solar cooling device, which would be a project in its own, an efficiency curve for a closed cycle, depending on the operating temperature (tank temperature to the heat source) is used. A constant cooling temperature of 25°C was assumed (lower cooling temperatures will improve the performance of the system).

The coefficient of performance COP is calculated with the fluid temperature $T_{hot/top}$ to the heat source at top of the hot water tank, following the data catalogue from GBU GmbH (1996):

$$COP = 0.02 T_{hot/top} - 0.45 \quad \dots\dots\dots(8.5.1)$$

The resulting COP -value for $55^\circ \text{C} < T_{hot/top} < 85^\circ \text{C}$ ranges between 0.56 and 0.62.

A stratified fluid storage tank (TRNSYS-type 4b, water storage medium) was used for the cold water, located inside the building with (volume 2500 l, height of 1.8 m) and a tank loss coefficient ($0.2 \text{ kJ/hr m}^2 \cdot ^\circ\text{K}$). The fluid temperatures at the top and bottom of the tank are $T_{cold/top}$ and $T_{cold/bottom}$ respectively. The energy gains through the tank surface are transferred to the outside of the building.

The return flow temperature T_{back} to the tank is set to be 12°C below $T_{hot/top}$ due to manufacture with maximum temperature differences of 13°C. The fluid flow rate between chiller and hot water tank is $\dot{m}_{hot} = 1720 \text{ kg/h}$. This flow rate produces a refrigeration capacity of approximately 12 kW, depending on the actual COP -value. The refrigeration capacity is big enough to cover maximum demands for this floor in conjunction with the coldwater storage tank.

Regulation is controlled by the hot water tank temperature (activated only for temperature above 55 °C) and by the coldwater tank temperature (activated, if the tank temperature at the top is above 12°C).

The fluid flow rate \dot{m}_{cold} kg/h between the chiller and the cold-water tank is calculated, using the definition of COP (and neglecting heat capacity variations), by:

$$\dot{m}_{cold} = \dot{m}_{hot} COP \frac{T_{hot/top} - T_{back}}{T_{cold/top} - 8^{\circ}C} \dots\dots\dots (8.5.2)$$

This cold-water flow rate is limited to a maximum flow rate of 2500 kg/h.

The cooling inside the office floor is simulated by taking water from the bottom of the coldwater storage tank. The return flow temperature is set to be identical with the room temperature, which, for example, can be possible with cooled ceiling. The mass flow rate to the cooling units in the office is 1000 kg/hr and the flow is activated during the periods of cooling demands, and/or as long as the temperature inside the coldwater storage tank is below room temperature.

Representative simulation results are as shown below:

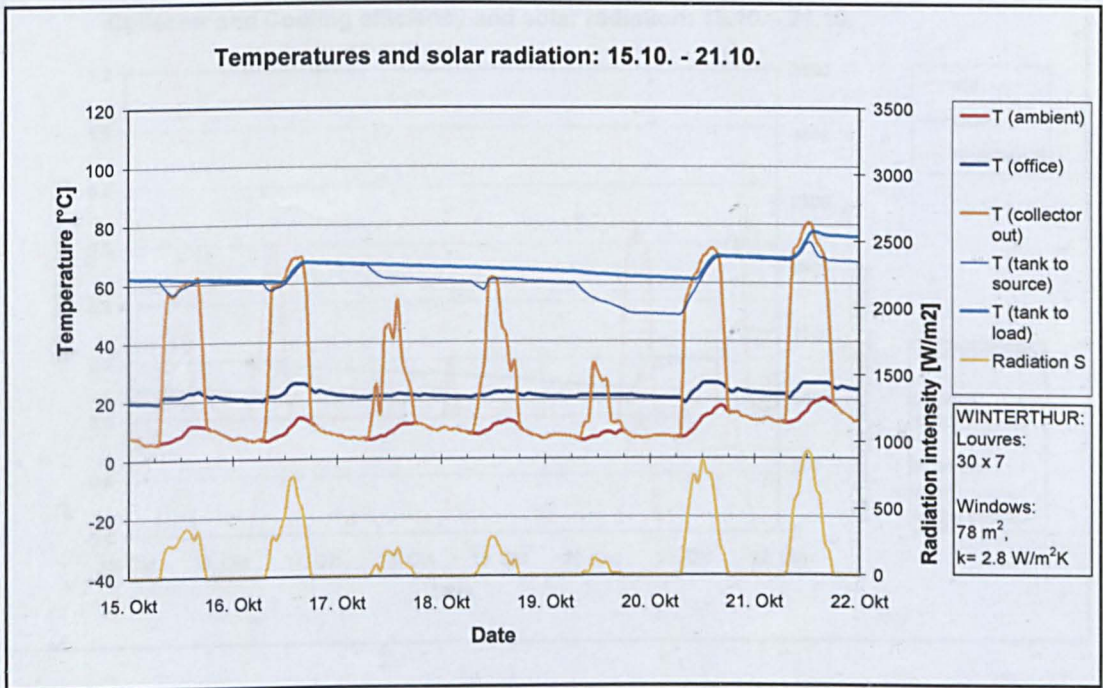


Figure 8.5.1 Ambient temperature, office temperature, collector inlet temperature, collector outlet temperature, temperature at the top of the hot water tank (temperature to load) and solar radiation intensity for the calculated situation in October.

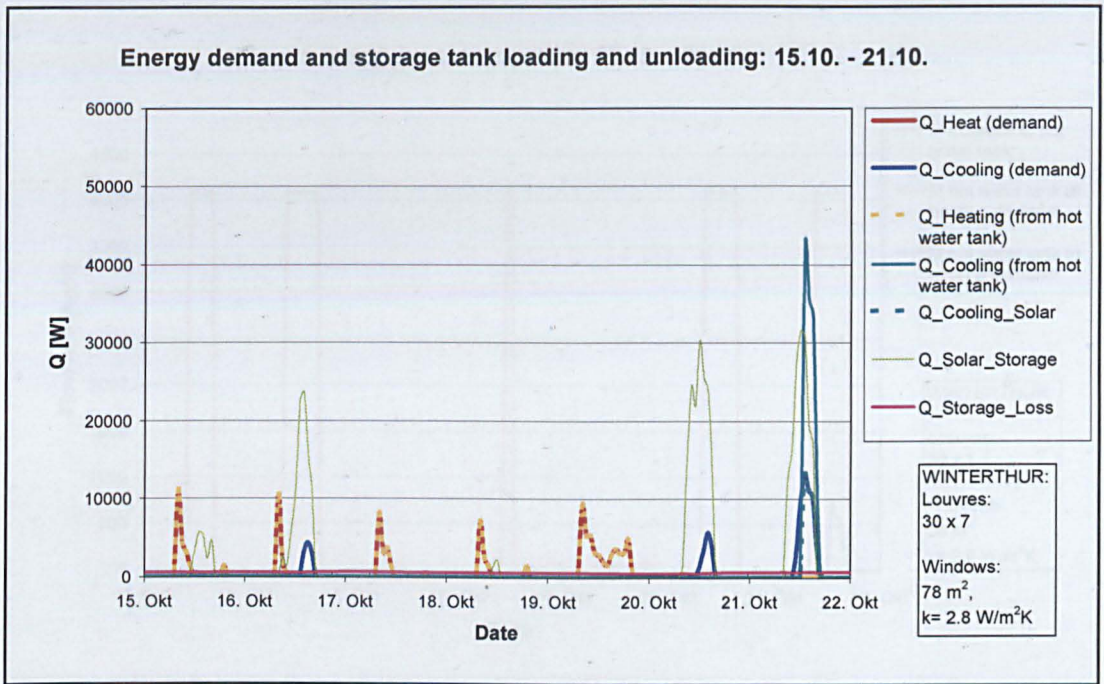


Figure 8.5.2 Energy demands for heating and cooling, energy, taken from the hot water storage tank for heating and cooling, solar energy input into the tank and storage lost (tank surface) for the calculated situation in October.

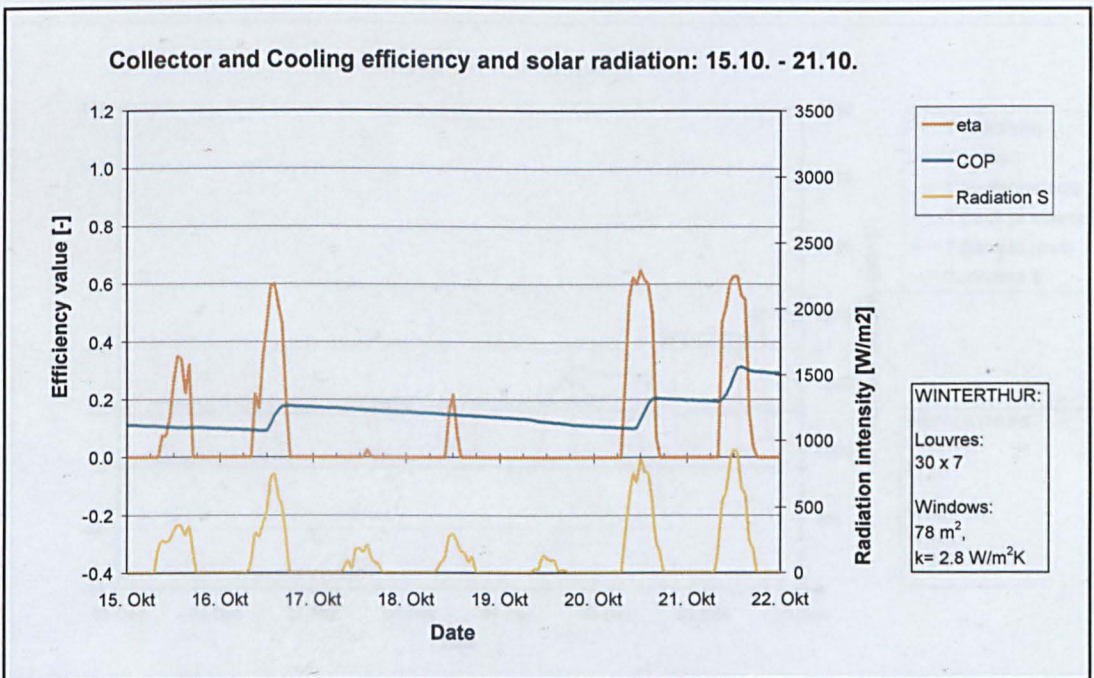


Figure 8.5.3 Collector efficiency value η_{col} , COP -value and the radiation intensity (south) for the calculated situation in October

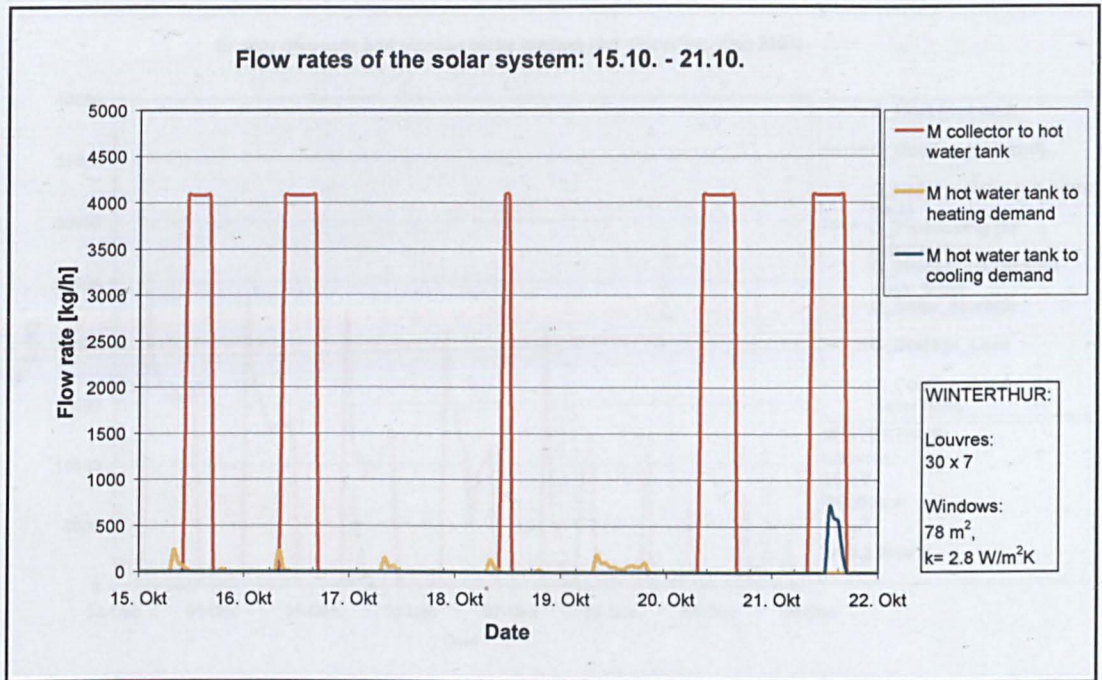


Figure 8.5.4 Mass flow rates from the solar louvres to the hot water tank and from the hot water tank to the heating and cooling demands for the calculated situation in October.

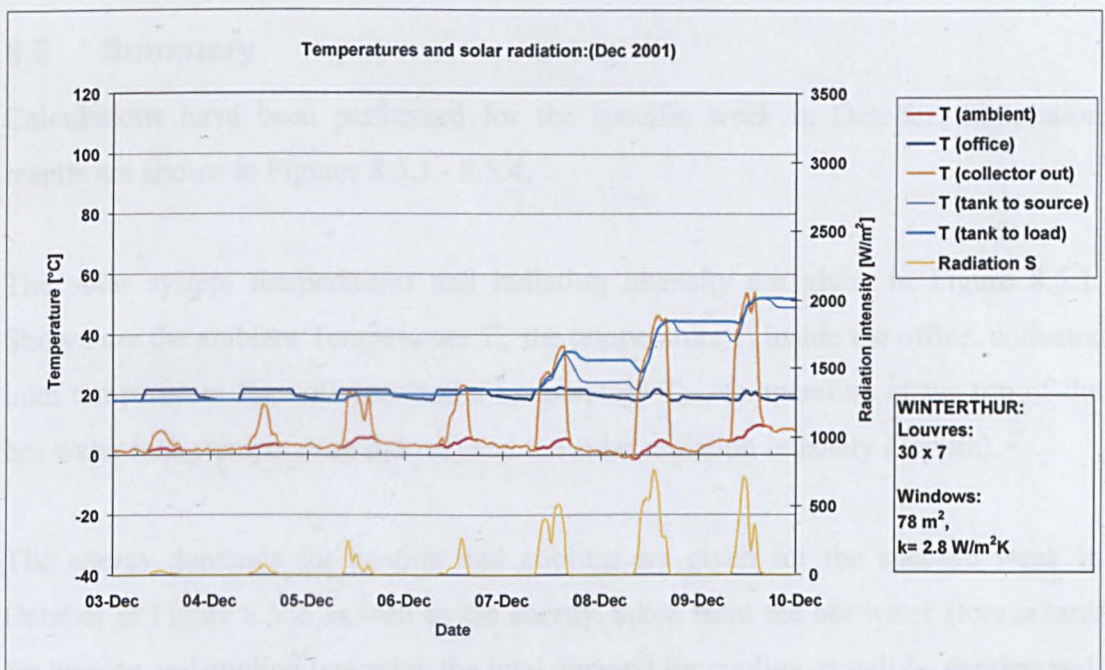


Figure 8.5.5 Ambient temperature, office temperature, collector inlet temperature, collector outlet temperature, temperature at the top of the hot water tank (temperature to load) and solar radiation intensity for the calculated situation in December.

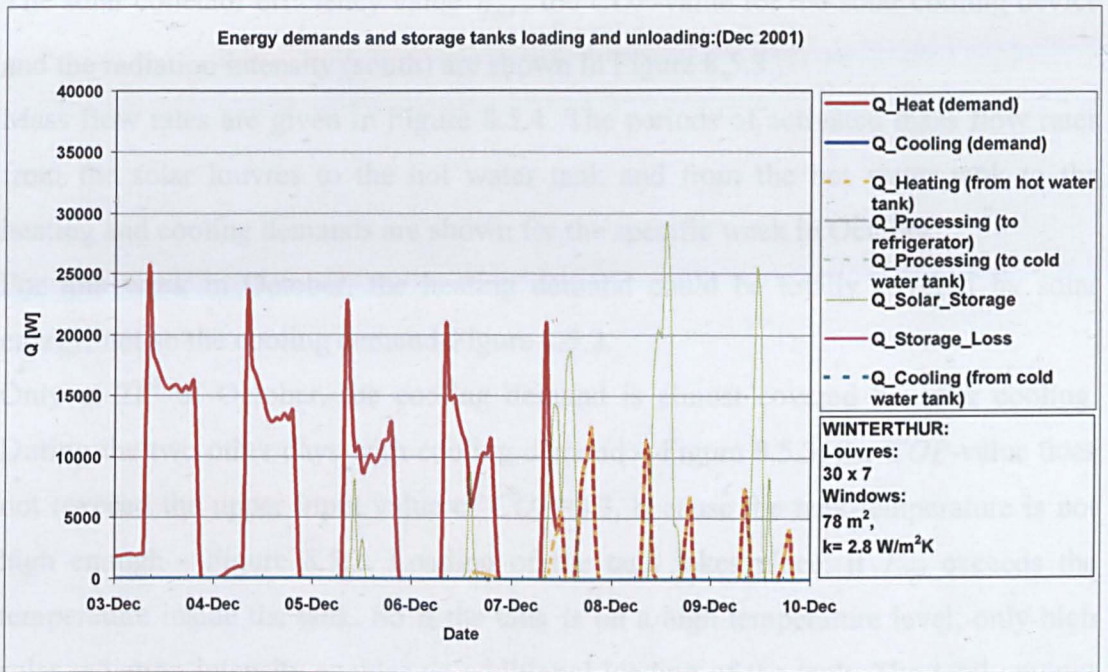


Figure 8.5.6 Energy demands for heating and cooling, energy, taken from the hot water storage tank for heating and cooling, solar energy input into the tank and storage lost (tank surface) for the calculated situation in December.

8.6 Summary

Calculations have been performed for the specific week in October. Simulation results are shown in Figures 8.5.1 - 8.5.4.

The solar system temperatures and radiation intensity are given in Figure 8.5.1. Shown are the ambient Temperature T_a , the temperature T_i inside the office, collector inlet temperature T_{in} , collector outlet temperature T_{out} , temperature at the top of the hot water tank (temperature to load) and the solar radiation intensity I (south).

The energy demands for heating and cooling are given for the specific week in October in Figure 8.5.2, as well as the energy, taken from the hot water storage tank for heating and cooling (covering the total demand for cooling, it will be the demand, multiplied with the reciprocal COP -value), the energy input into the tank by the solar louvres and the storage losses (tank surface).

The solar collector efficiency value η_{col} , the COP -value for the solar cooling device and the radiation intensity (south) are shown in Figure 8.5.3.

Mass flow rates are given in Figure 8.5.4. The periods of activated mass flow rates from the solar louvres to the hot water tank and from the hot water tank to the heating and cooling demands are shown for the specific week in October.

For this week in October, the heating demand could be totally covered by solar energy, not so the cooling demand-Figure 8.5.2.

Only at 21st of October, the cooling demand is almost covered by solar cooling. During the two other days with cooling demand – Figure 8.5.3, the COP -value does not (exceed the upper input value of $COP=0.3$, because the tank-temperature is not high enough - Figure 8.5.1. Loading of the tank takes place, if T_{out} exceeds the temperature inside the tank. So if the tank is on a high temperature level, only high solar radiation intensity enables an additional loading of the tank. The total amount of solar energy used can be seen in Figure 8.5.2- (green curve).

The collector efficiency η_{col} will be zero- Figure 8.5.3, if no loading of the tank takes place.

During winter, the temperature level inside the tank and solar radiation intensity are lower, but in contrast, no high storage temperatures are needed for contribution of solar heating.

Results are shown in Figures 8.5.5 (temperatures) and 8.5.6 (energy demands) for a specific week in December.

Analysing the energy demand over the whole year, simulation results show, that approximately 47 % of the solar cooling and 46% of the solar heating could be covered by solar energy. The rate of absorbed solar energy, used for covering the building demands for heating and cooling is approximately 59%.

During the first estimation - Figure 8.4.6, the rate for solar heating was just 16%, while solar cooling had been around 60%. The lower solar cooling rate in these calculations will be due to the design of the hot water tank, which results in a lower COP -value. It is not designed for the demands of solar cooling. The efficiency of the cooling device will be improved, if the temperature level inside the tank gets higher. This can be achieved with a smaller, better-insulated hot water storage tank.

Different considerations and simulations (using diverse tank sizes, tank isolations, flow rates and control input temperatures) could be done to improve/optimize the efficiency of the whole system.

Indications that for this specific building, collector size and efficiency, approximately up to:

- 50% of the heating demand
- 85% of the cooling demand

could be covered by solar energy, provided that a super-insulated storage tank is used for the solar cooling sub- process. High insulation-resistances are also expected through out the building.

In practise, the percentage of covering the energy demands by solar energy will be more a question of cost rather than a question of scientific or physical limitations.

9. Conclusions and Recommendations

In the previous chapters, the findings and conclusions have already been pointed out, as well as few recommendations.

In this chapter, the overall conclusion has been drawn, and an executive summary of remaining issues for future work has been presented.

9.1 Conclusion

With the aid of the various design tools (covered in the previous chapters), a design collector has been developed. Based on the distribution (current state) of the existing trading floors, and its performance degradation, the design of following similar design could provide some guidance. All the design recommendations are given in the design - and should be followed by the relevant parties and stakeholders.

The major challenge in this task, therefore, lies in the fact that the space available within the layout is limited, and the design must be able to accommodate the existing and the proposed new design within the same space.

Chapter Nine

Conclusions and Recommendations

As can be seen from Figure 9.1, the design is very close to the edge of the existing plot, which is about 25m, and on the other side of the existing plot it is only about 5m. This is a very tight design constraint.

As can be seen from Figure 9.1, the design is very close to the edge of the existing plot, which is about 25m, and on the other side of the existing plot it is only about 5m. This is a very tight design constraint.



Figure 9.1.1 Schematic showing the layout and the relative positions within the trading floor.

9. Conclusion and Recommendations

In the previous chapters some findings and conclusions have already been pointed out, as well as few recommendations.

In this chapter, an overall conclusion has been drawn, and an executive summary of recommendations for future work has been presented.

9.1 Conclusion

With the aid of the various design tools (mentioned in the previous chapters), a solar collector has been designed, based on the dimensions (aspect ratio) of the existing shading louvres, and its performance determined. The decision of following similar aspect ratios (major axis: minor axis = 6) has been discussed in chapter (5) – *The Design* – and shown to be merely for aerodynamic and structural reasons.

The major challenge in this task, therefore, lies in the fact that the space available, within the louvre void, is rather small.

In flat-plate solar collectors, the distance between the back of the absorbing plate and the collector's base is large enough for the back-insulation to be accommodated.

This is not the case with the louvres, where the maximum distance available is 40 mm (the minor axis).

As can be seen from Figure 9.1.1 that this distance, at best (i.e. at one edge of the absorbing-plate) is about 25mm, and on the other edge of the absorbing-plate is only about 5 mm. This is a major design constraint.

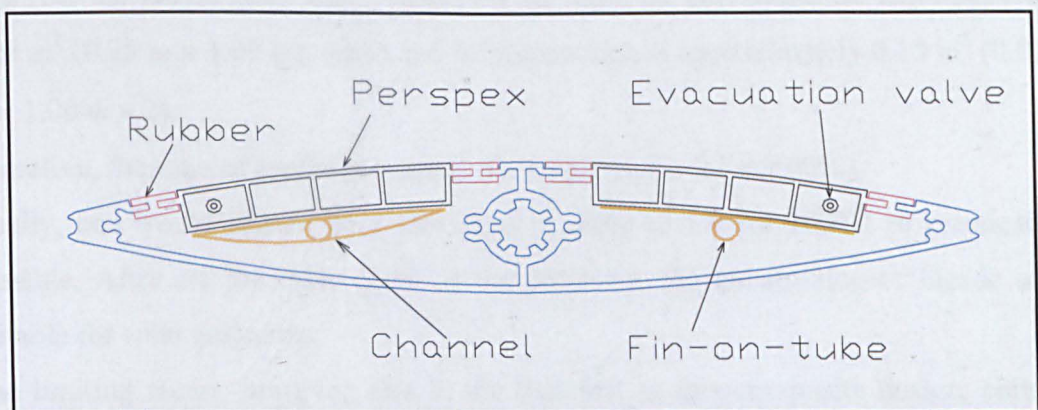


Figure 9.1.1 Schematic showing the channel and fin-on-tube positions within the solar louvre.

Despite this constraint, modelling results show (with favourable optical properties for both cover and absorbing-plate), that using channels in the solar louvre collector would provide energy comparable to that provided by flat-plate collectors.

Experimental results, comparing the two types of fluid ducts (channel and fin-on-tube), proved that the solar louvre collector perform better with fin-on-tubes than with channels.

Improvements to the thermal performance of the solar louvre, incorporating fin-on-tube, has been identified.

If the cover panes could have maintained vacuum, and if the fin-on-tube had a solar-selectively absorbing-plate (with optical properties comparable to those of Titanium Oxynitride, for example), then clearly the thermal performance of the louvre collector would have been considerably better. In fact it would be closely comparable to evacuated flat-plate collectors.

Adding more pillars between the cover panes (3 instead of 1), as shown in Figure (9.1.1) would help sustaining the atmospheric pressure ($\sim 11 \text{ ton/m}^2$).

A less significant design concern was the weight of the resulting collector.

The weight of the existing shading louvre is 41g/cm, while the weight of the solar louvre collector prototype (complete with channels) is 55g/cm.

Therefore, the prototype has $\sim 34\%$ more weight than the existing shading louvres - $[(55 - 41) \times 100/41] \times 100\% \approx 34\%$.

Another design concern was the ratio of collection area to shading area. The shading area (i.e. the louvre total area), based on the 250E of unit length, is approximately 0.25 m^2 ($0.25 \text{ m} \times 1.00 \text{ m}$), while the collection area is approximately 0.15 m^2 ($0.075 \text{ m} \times 1.00 \text{ m} \times 2$).

Therefore, the ratio of (*collection area: shading area*) is 0.6 (or 60%).

Ideally, one would like to have this ratio as close to 1.0 (or 100%) as practicably possible. After all, the main quest of the project is the maximizing of façade area suitable for solar collectors.

The limiting factor, however, lies in the fact that in this composite design, certain structural aspects (assembly) dictate to acquire parts of the collection area; see Figure 9.1.2.

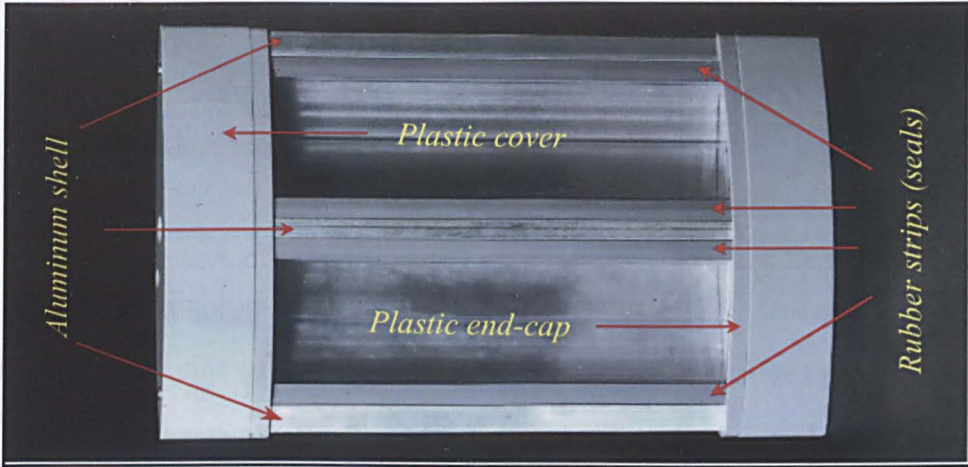


Figure 9.1.2 structural aspects dictate to acquire parts of the collection area.

The cost of the prototype, together with its performance, has been analysed for economic viability. Three Figures of merit, namely, the *payback period*, the *averaged energy cost* and the *life cycle savings* have been used in this analysis.

As *solar fraction* is an important parameter in this analysis, two different locations or latitudes (London and Lisbon) have been used for contrast.

Environmental assessment for the prototype has also been carried out, and the outcome of both, the economic analysis and environmental assessment have shown favourable results for Lisbon.

The second part of this research work, was the investigation of the possibility of using the solar energy, harnessed by these solar louvre collector, in the air-conditioning of office buildings.

Multi-storey office-buildings (even in moderate and cold climates) are often in need of air-conditioning. In view of the current and proposed legislations, low-temperature water chillers (adsorption), despite their low-efficiency, could be used in buildings today, if enough water, laden with solar energy, is provided at the right temperatures ($55^{\circ}\text{C} - 85^{\circ}\text{C}$). The problem repeatedly encountered, however, in providing hot water for the cooling of a building, is that there isn't enough roof area for collectors to be mounted on; hence lack of hot water (i.e. flow rate) for the absorption/adsorption chiller. This consequently focuses attention on the envelope, or specifically on the sun-facing façade, of building, as a possible collecting-surface.

One could see the need for increasing the mass flow rate (or energy), which, in turn, means an increase to the collecting surface area.

A one-storey building of a certain footing has better chances than a two-storey building of the same footing.

To illustrate this lack of proportionality between floor-area and façade-area, consider the building of Winterthur:

The floor has a size of $L = 55.40 \text{ m}$, $W = 7.10 \text{ m}$, $H = 2.76 \text{ m}$; total floor area of 393.34 m^2 .

As the east and west facades are not available for mounting solar collectors, consider the northern (albeit not suitable for energy collection) and southern façades:

$$1\text{-storey} \rightarrow \text{Floor area} = (LW) \rightarrow \text{Façade area} = [\text{Roof} + (LH)]$$

$$2\text{-storey} \rightarrow \text{Floor area} = 2(LW) \rightarrow \text{Façade area} = [\text{Roof} + 4(LH)]$$

$$3\text{-storey} \rightarrow \text{Floor area} = 3(LW) \rightarrow \text{Façade area} = [\text{Roof} + 6(LH)]$$

Therefore, for a building of N -storeys:

$$N\text{-storey} \rightarrow \text{Floor area} = N(LW) \rightarrow \text{Façade area} = [\text{Roof} + 2N(LH)]$$

For the case of the 40% window area (i.e. 60% façade):

$$\bullet \quad N\text{-storey} \rightarrow \text{Floor area} = N(LW) \rightarrow \text{Façade area} = [\text{Roof} + 2N(\frac{3}{5}LH)]$$

For the case of the 40% window area (i.e. 60% façade):

$$\bullet \quad N\text{-storey} \rightarrow \text{Floor area} = N(LW) \rightarrow \text{Façade area} = [\text{Roof} + 2N(\frac{2}{5}LH)]$$

The above two equations have been calculated, as in Table 9.1.1, and plotted as in Figure 9.1.3:

Table 9.1.1 Variation of floor-area, with façade-area

Number of Floors	Floor area (m^2)	Façade area available for collection (m^2) (40% windows)	Façade area available for collection (m^2) (60% windows)
1	393.34	773.49	515.66
2	786.68	956.99	637.99
3	1180.02	1140.46	760.31
4	1573.36	1323.94	882.63
5	1966.70	1507.44	1004.96
6	2360.04	1690.92	1127.28
7	2753.38	1874.4	1249.60
8	3146.72	2057.89	1371.93
9	3540.06	2241.37	1494.25
10	3933.40	2424.86	1616.57

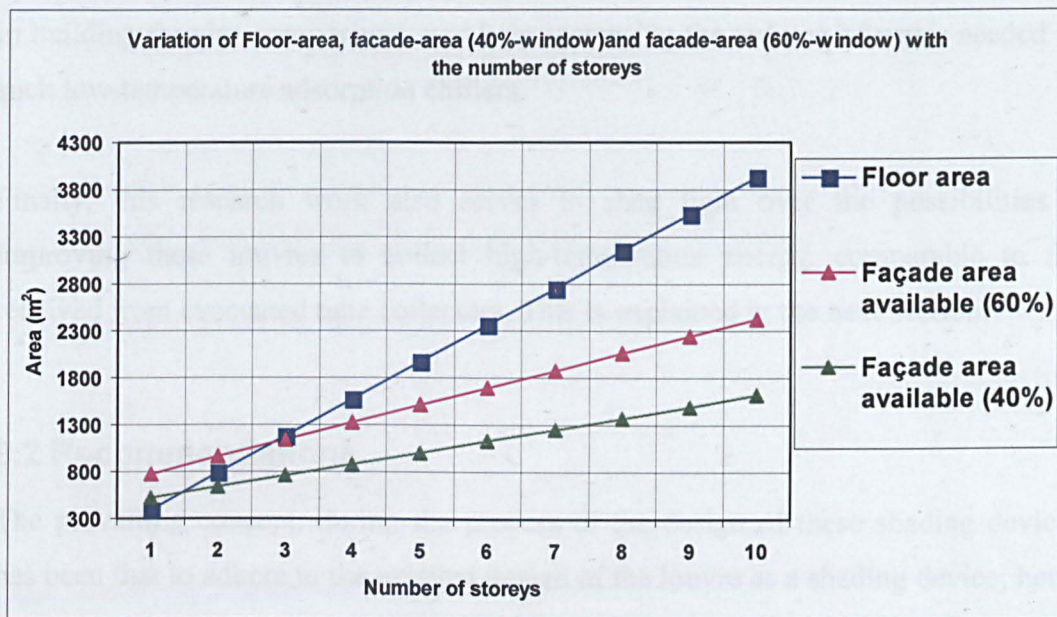


Figure 9.1.3 Variation of floor-area, with façade-area

As shown in Figure 9.1.3, the amount of floor-area increases more rapidly, with the increase of the number of storey, than the façade-area does.

This results holds for one façade (southern, say), or four as in the case of stand-alone buildings.

The result of the simulation study has indicated that shading and solar energy collection by these louvres could in fact provide a substantial amount of hot water (at around 60 °C) enough to cover:

- 50% of the heating demand
- 85% of the cooling demand could be covered by solar energy, provided that a well-insulated storage tank is used for the solar cooling sub- process.

The economical and energy efficiency of a solar-assisted air conditioning system does not depend on the maximum efficiency of the constituting parts only, but on their interaction and also their collective interaction with the load. Furthermore, different climates will favor different choices.

The success of this research work, here, adds support to the on-going research efforts in building facades components, and help increasing the volume of water needed for such low-temperature adsorption chillers.

Finally, this research work also serves to shed light over the possibilities of improving these louvres to collect high-temperature energy, comparable to that received from evacuated tube collectors. This is explained in the next section.

9.2 Recommendations

The prevailing concept, during the process of the design of these shading devices, has been that to adhere to the existing design of the louvre as a shading device; hence acknowledging the optimisation that these louvres must have gone through. Then building on these optimisations to change the louvre to a solar collector.

Here, in this section, the above-mentioned concept is reversed; one needs to look at it differently: collector first, then the shading device (with its structural/aerodynamic conditions).

Improvements to the performance of these solar louvre collectors could readily be achieved if the:

1. **Transparent to louvre ratio can be increased**
2. **Optical properties and efficiency factor of the absorbing-plate** are upgraded;
3. **Optical properties of the glazing material** are enhanced; and
4. **Losses (conduction and/or convection)** are minimized.

The **optical properties of the absorbing-plate** could be improved simply by using suitable selectively solar-absorbing coatings. Titanium Oxynitride, and Black Chrome are some examples.

Titanium Oxynitride has optical properties as:

Emissivity, ϵ_p , of 0.10 ± 0.02 , and absorbance, α_p , of 0.96 ± 0.02 .

Black Chrome has:

Emissivity, ϵ_p , of 0.10, and absorbance, α_p , of 0.87.

The **efficiency factor of the absorbing-plate**, F' could be improved by optimising the plate thickness (or material), tube spacing and bonding between plates and tubes. See Figure 9.2.1.

Optical properties of the glazing material, could be enhanced by reducing the absorbance and reflection of radiation by the material; hence increasing its transmittance, τ_c .

It is the impurities in glazing materials (for soda-lime glass it is the salts in the iron) that are responsible for absorbing the fraction of the incident radiation.

The use of pure glazing would reduce the absorbed fraction.

The reflected fraction could be reduced by etching the glass, but the resulting glass may not be stable when exposed to outdoor conditions.

Dielectric coating; such as porous SiO_2 layers, as well as certain novel high-rate-sputtered metal oxyfluoride coatings, seem to have a good potential for antireflection coatings on glass.

Having optimised the space between the panes (cavity), the radiant exchange constitutes the majority of the losses. To reduce these losses, one effective way is to coat the cavity-side-surface of the outer glazing with a low-e material. This results in reduction of emissivity down to about $\varepsilon_c = 0.1$. However, this desirable reduction, inevitably reduces the transmittance of the glazing down to about $\tau_c = 70\%$.

However, the overall conclusion is that the use of low-e coatings increases the thermal resistance much more than decreasing the solar gain received by the absorbing plate; Hollands *et al* (2001, p 54).

Once low-e has been incorporated, the dominant mode of heat transfer becomes convection in the cavity between the two panes of the cover. These **Losses (conduction and/or convection)** are minimized by the evacuation of the cavity. Vacuum produces atmospheric pressure of ($\sim 11 \text{ ton/m}^2$) on the cover panes. This pressure could be sustained by the use of supporting pillars in the evacuated glazing. These pillars, however, have the disadvantage of reducing the glazing and absorbing area.

Filling the cavity with air or argon (*Ar*) is one option, and the optimum pane spacing, from Figure (9.2.2), would be 12.5 *mm*. This could go down to 7.5 *mm* if a gas like krypton (*Kr*) or xenon (*Xe*) are used – see Figure 9.2.2.

This would spare some space within the void available in the louvre, hence reducing the back losses.

A second option is the use of aerogels (Silica aerogel) to fill the cavity between the cover panes.

In silica aerogel the labyrinth of cell walls surrounding the pores is made of silica (silica is another name for quartz or silicon dioxide). Typically, only 3% of the aerogel is silicon, the remaining 97% is either a gas or vacuum.

With the aerogel sandwiched, in the sealed cavity, between the two panes, the cover could be evacuated down to 500 *Pa* (0.005 *bar*). The aerogel is strong enough to support the panes against atmospheric pressure, replacing the action of the pillars in the evacuated glazing.

Favourable results, for the use of silica aerogel, have been reported by Duer and Svensen (1998).

To make these louvres collect higher temperature energy, suitable for absorption cooling, rather than adsorption, the above recommendations need be implemented. And since the future of solar energy application depends on the costs of solar energy systems, ways of reducing the cost is considered more important than improving the efficiency.

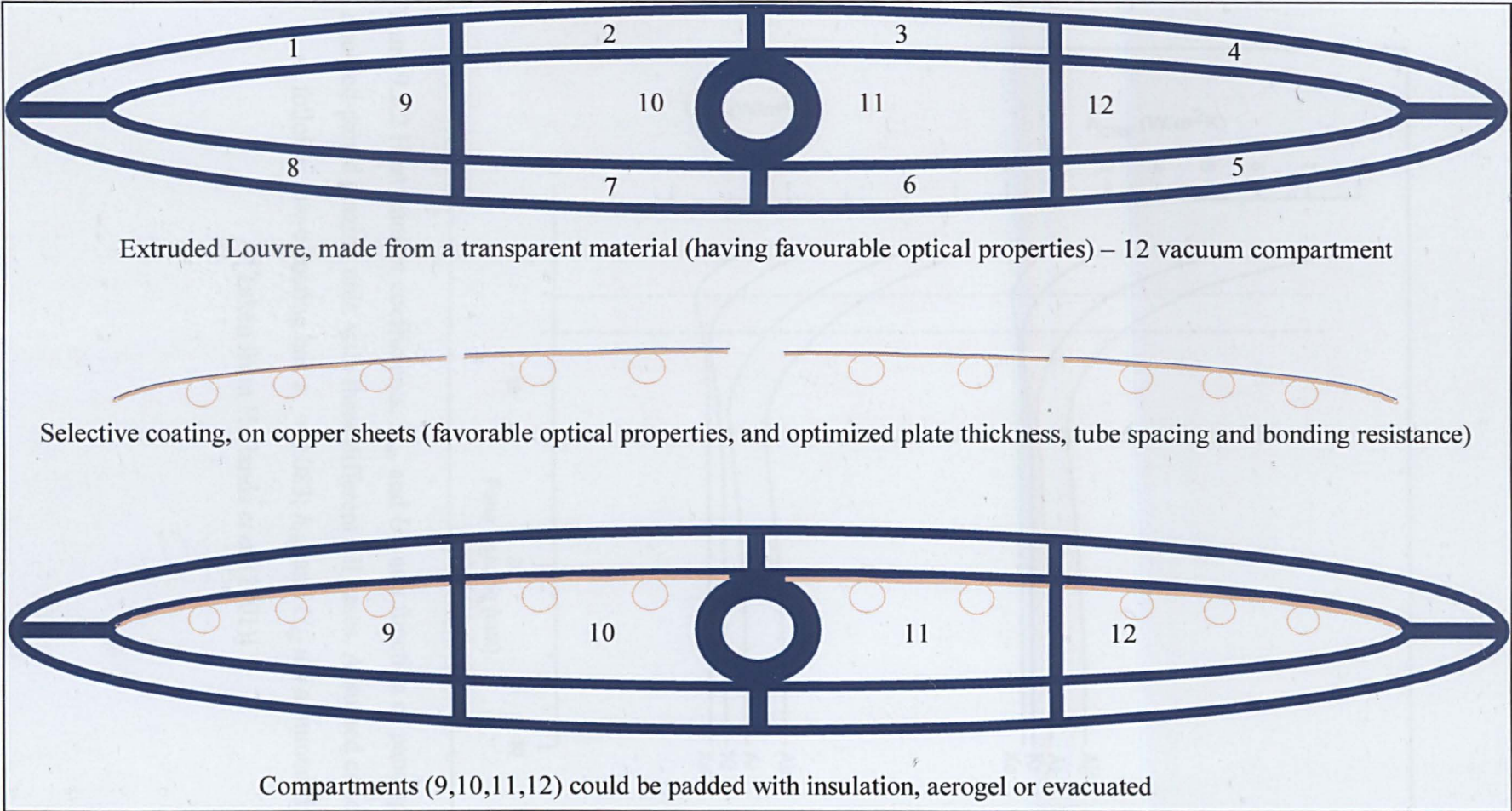


Figure 9.2.1 Outlines of the recommended design for the proposed solar louvre collector

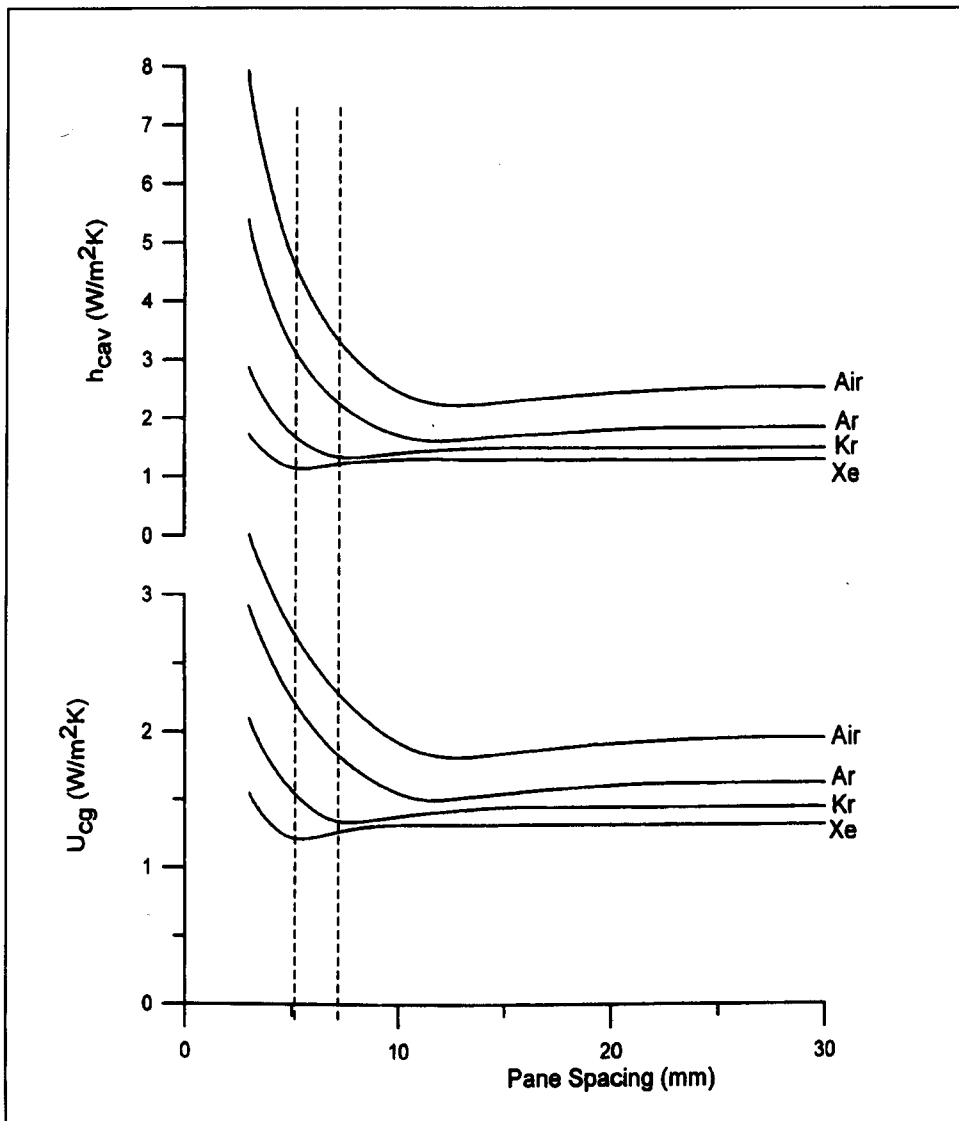


Figure 9.2.2 Heat transfer coefficients, h_{cav} and U_{cg} as a function of pane spacing for a doubled-paned glazing unit, with three different fill gases. Assumed conditions are as follows: low-e coating has $\epsilon_c = 0.083$; h_{cav} and U_{cg} are assumed fixed.

[Taken from Hollands *et al* (2001)]

Appendices

Appendix A

References

- Andresen**, I., Aschehoug, Ø., & Thyholt, M. (1995), Computer Simulations of Energy Consumption for Lighting, Heating and Cooling for an Office Using Different Light Control Strategies. *SINTEF* report. 20 pages. Trondheim: SINTEF.
- Applications manual** (1999): window design; *CIBSE*, London.
- ASHRAE** standard 93-77(1977), Methods of Testing to Determine the Thermal Performance of Solar Collectors, *American Society of Heating, Refrigeration, and Air Conditioning Engineers*, New York.
- ASME** (1977), Steam Tables, 3rd ed. New York, Am. Soc. Mech. Eng, 1977.
- Beckman** W. A., S.A Klein, and J. A. Duffie (1977), *Solar Heating Design by the f-chart Method*, Wiley, New York (1977).
- Bilgen**, E. (1994), Experimental Study of Thermal Performance of Automated Venetian Blind Window Systems. *Solar Energy*. Vol. 52. No.1. pp.3-7. Great Britain: Pergamon.
- Brambley**, M.R., Kennedy, E.M., & Penner, S.S. (1981), Fenestration Devices for Energy Conservation—IV. Field Study. *Energy*. Vol. 6. No. 9. pp. 883-894. Great Britain: Pergamon.
- British Standard Institute** (1992), BS 8206: Part 2 ‘Lighting for Buildings: Code of practice for day lighting’ BSI, London.
- Chapman** Alan J. (1984), *Heat Transfer*, Collier Macmillan, New York.
- Dubois**, M. (1997), Solar Shading and Building Energy Use, Report TABK-97/3049, ISSN 1103-4467
- Dubois**, M-C. (1998), *Solar-protective Glazing for Cold Climates. A Parametric Study of Energy Use in Offices*. Report TABK—98/3053, Dept. of Building Science, Lund Institute of Technology, Lund (Sweden).
- Duer**, K. and Svensen, S. 1998. Monolithic silica aerogel in super insulating glazings, *Solar energy* **63** (4), 259-268.
- Duffie**, John A, William A Beckman (1991), *Solar engineering of Thermal processes*, New York, John Wiley & Sons.
- Eames**, P. C. and Norton, B. (1993), Detailed parametric analysis of heat transfer in CPC solar energy collectors, *Solar Energy*, **50**, 321-338.

- Eames**, P. C. and Norton, B. (1995), Thermal and optical consequences of the introduction of baffles into compound parabolic concentrating solar energy collector cavities, *Solar Energy*, **55**, 129-150.
- ECOCOOL**(1997) - Ecological Cooling for Buildings by Combining Closed Wet Cooling Tower with Chilled Ceilings (Project No. JOR3-CT97-0195)
- Elsherbing**, S.M, G.D. Raithby, and K.G.T. Hollands (1982), "Heat Transfer by Natural Convection Across Vertical and Inclined Air Layers", *J. Heat Transfer, Trans, ASME*, Vol. 104, 1982, p96.
- Emery**, A. F., Johnson, B.R., Heerwagen, D.R., & Kippenhan, C.J. (1981). Assessing the Benefit-Costs of Employing Alternative Shading Devices to Reduce Cooling Loads for three Climates, *Proceedings of the International Passive and Hybrid Cooling Conference. American Section of the International Passive and Hybrid Cooling Conference. pp. 417-421.*
- Faghri** A. (1995), Heat Pipe Science and Technology, Washington DC, Taylor & Francis, 1995.
- GBU GmbH** (1996). Katalogwerk der Hinweise zur Planung und Einsatzvorbereitung der Adsorptionskältemaschine.
- Goetzberger**, A., Dengler, J., Rommel, M., Goettsche, J. and Wittwer, V. (1992) New transparently insulated, bifacially irradiated solar flat-plate collectors, *Solar energy* **49**, 403-401.
- Halmos**, G.B. (1974), Solar Protection - Costs and Benefits. *Heating and Air Conditioning Journal*. Vol. 44. No. 520. pp. 24-25.
- Harkness**, E.L. (1988). The Energy and Thermal Comfort Advantages of Shading Windows. *Australian Refrigeration, Air Conditioning and Heating*. Vol. 42. No. 10. October. pp. 33-41.
- Health and Safety Commission** (1992), 'Workplace (Health Safety and Welfare) Regulations 1992: *Approved Code of Practice and Guidance L24*' HMSO, London.
- Holland K.G.T.**, Solar Energy – State of the Art, ISES Position Papers 2001
- Holland, K.G.T., T. E. Unny, G.D. Raithby, and L. Konicek, *Trans. ASME, J. Heat Transfer*, **98**, 189 (1976). "Free Convection Heat Transfer Across Inclined Air Layers.
- Hottel**, H.C. and B. B.Woertz (1942), Performance of Flat-plate Solar Heat Collectors, *Tran. ASME*, **64**,91.

- Hunn, B.D., Grasso, M.M., Jones, J.W., & Hitzfelder, J.D. (1993),** Effectiveness of Shading Devices on Buildings in Heating-Dominated Climates. *ASHRAE Transactions*. Proceedings of the 1993 Winter Meeting of ASHRAE Transactions (Chicago). Vol. 99. Pt.1.pp. 207-222. Atlanta: ASHRAE.
- Hunn, B.D., Jones, J.W., Grasso, M.M., & Hitzfelder, J.D. (1990).** Effect of Shading Devices on Building Energy Use and Peak Demand in Minnesota. Conservation and Solar Research Report. No. 9. 100 pages. *Center for Energy Studies, Austin: The University of Texas at Austin.*
- Kienzlen, V., Gordon, J.M., and Kreider, J.F. (1988).** The reverse flat plate collector: a stationary, non-evacuated, low technology, medium temperature solar collector, *ASME J. Solar Energy Engineering*, **110**, 23-30.
- Klein, S.A., Alvarado, F.L. (1997);** Engineering Equation Solver. F-Chart Software, Middleton, USA.
- Maple Sun-screening,** Progress House, Newby Road Industrial Estate, Newby Road, Hazel Grove, Stockport SK7 5DA
- McAdams, W. H.,** *Heat Transmission* 3rd ed., McGraw Hill, New York (1954).
- McCluney, R. & Chandra, S. (1984),** Comparison of Window Shading Strategies for Heat Gain Prevention. *Ninth Passive Solar Conference (September 24-26, 1984, Columbus, OH). Vol. 9. pp. 414- 41, American Solar Energy Society.*
- Morrison, G.L.,** Solar Energy – State of the Art, ISES Position Papers 2001
- Olson, Reuben M., Wright, Steven J., 1990,** *Essentials of Engineering Fluid Mechanics*, 5th -Edition, Harper & Row.
- Pletzer, R.K., Jones, J.W., & Hunn, B.D. (1988).** Effect of Shading Devices on Residential Energy Use in Austin, Texas. Conservation and Solar Research Report. No. 5. 156 pages. *Center for Energy Studies. Austin: The University of Texas at Austin. June.*
- Rundquist, R.A. (1991a).** Calculation Procedure for Day lighting and Fenestration Effects on Energy and Peak Demand. *ASHRAE Transactions*. Vol. 97. No. 2. pp. 1138-1148. Atlanta: ASHRAE.
- Rundquist, R.A. (1991b)** Day lighting Controls: Orphan of HVAC Design. *ASHRAE Journal*. Vol. 33. No. 11. November. pp. 30-34. Atlanta: ASHRAE.
- Sparrow, E.M. and Haji-Sheikh, A. (1966),** “Flow and Heat Transfer in Ducts of Arbitrary Shape with Arbitrary Thermal Boundary conditions,” *J of Heat transfer, Trans.Am. Soc.Mech. Engrs*, Vol. 88, Ser. C, No. 4 (1966), pp. 351–358.

- Sullivan, R.A, Lee, E.S., & Selkowitz, S. (1992).** A Method of Optimising Solar Control and Day lighting Performance in Commercial Office Buildings. LBL-32931. 14 pages. *Lawrence Berkeley Laboratory*. Berkeley: University of California.
- Thermomax (GB) Ltd.,** Hawtin Park, Blackwood, UK NP12 2EU
- Treado, S., Barnett, J., & Remmert, W. (1984).** Effectiveness of Solar Shading for an Office Building. *NBS Building Science Series 161*. May. 102 pages. National Bureau of Standards. Washington: U.S.Department of Commerce.
- TRNSYS [Klein *et al.* (1997),** Solar Energy Laboratory, University of Wisconsin – Madison, 1500 Engineering Drive, Madison, WI 53706 USA.
- Watmuff, J. H., W.W.F. Charters, and D. Proctor, COMPLES, No. 2, 56 (1977).** “Solar and Wind Induced External Coefficients for Solar Collectors.”
- White, Frank M. (1991),** *Heat and Mass Transfer*, Addison-Wesley, USA, p 309.
- Yiqin Y., Hollands K. G. T. and Brunger, A. P. (1991).** Measured top heat loss coefficients for flat plate collectors with inner Teflon covers, *ISES Solar World Congress*, Denver, 1200-1205.
- Zhukauskas, A.,** “Heat Transfer from Tubes in Cross flow,” *Advances in Heat Transfer*,” Vol. 8, New York, Academic Press, 1972, p.93.

Appendix B

MatWeb.com, The Online Materials Database

Aluminium 6063-T6

Subcategory: 6000 Series Aluminium Alloy; Aluminium Alloy; Metal; Nonferrous Metal

Close Analogs:

Composition Notes:

Aluminium content reported is calculated as remainder.

Composition information provided by the Aluminium Association and is not for design.

Key Words: UNS A96063; ISO AlMg0.5Si; Aluminium 6063-T6; AA6063-T6

Component	Wt. %	Component	Wt. %	Component	Wt. %
Al	Max 97.5	Mg	0.45 - 0.9	Si	0.2 - 0.6
Cr	Max 0.1	Mn	Max 0.1	Ti	Max 0.1
Cu	Max 0.1	Other, each	Max 0.05	Zn	Max 0.1
Fe	Max 0.35	Other, total	Max 0.15		

Material Notes:

Data points with the AA note have been provided by the Aluminium Association, Inc. and are NOT FOR DESIGN.

Physical Properties	Metric	English	Comments
Density	2.7 g/cc	0.0975 lb/in ³	AA; Typical
Mechanical Properties			
Hardness, Brinell	73	73	AA; Typical; 500 g load; 10 mm ball
Hardness, Knoop	96	96	Converted from Brinell Hardness Value
Hardness, Vickers	83	83	Converted from Brinell Hardness Value
Ultimate Tensile Strength	241 MPa	35000 psi	AA; Typical
Tensile Yield Strength	214 MPa	31000 psi	AA; Typical
Elongation at Break	12 %	12 %	AA; Typical; 1/16 in. (1.6 mm) Thickness
Modulus of Elasticity	68.9 GPa	10000 ksi	AA; Typical; Average of tension and compression. Compression modulus is about 2% greater than tensile modulus.
Ultimate Bearing Strength	434 MPa	62900 psi	Edge distance/pin diameter = 2.0
Bearing Yield Strength	276 MPa	40000 psi	Edge distance/pin diameter = 2.0
Poisson's Ratio	0.33	0.33	
Fatigue Strength	68.9 MPa	10000 psi	AA; 500,000,000 cycles completely reversed stress; RR Moore machine/specimen
Machinability	50 %	50 %	0-100 Scale of Aluminium Alloys
Shear Modulus	25.8 GPa	3740 ksi	
Shear Strength	152 MPa	22000 psi	AA; Typical

Electrical Properties

Electrical Resistivity	3.32e-006 ohm-cm	3.32e-006 ohm-cm	AA; Typical at 68°F
------------------------	------------------	------------------	---------------------

Thermal Properties

CTE, linear 68°F	23.4 $\mu\text{m}/\text{m}\cdot^\circ\text{C}$	13 $\mu\text{in}/\text{in}\cdot^\circ\text{F}$	AA; Typical; Average over 68-212°F range.
CTE, linear 250°C	25.6 $\mu\text{m}/\text{m}\cdot^\circ\text{C}$	14.2 $\mu\text{in}/\text{in}\cdot^\circ\text{F}$	Average over the range 20-300°C
Heat Capacity	0.9 J/g·°C	0.215 BTU/lb·°F	
Thermal Conductivity	200 W/m·K	1390 BTU-in/hr-ft ² ·°F	AA; Typical at 77°F
Melting Point	616 - 654 °C	1140 - 1210 °F	AA; Typical range based on typical composition for wrought products 1/4 inch thickness or greater
Solidus	616 °C	1140 °F	AA; Typical
Liquidus	654 °C	1210 °F	AA; Typical

Processing Properties

Annealing Temperature	413 °C	775 °F	hold at temperature for 2 to 3 hr; cool at 50 °F per hour from 775 to 500 °F
Solution Temperature	521 °C	970 °F	
Aging Temperature	177 °C	350 °F	hold at temperature for 8 hr

References are available for this material.

MatWeb.com, The Online Materials Database

Oxygen-free Electronic Copper (OFE), UNS C10100, OS050 temper, flat products, rod, tubing, and shapes

Subcategory: Copper Alloy; Metal; Nonferrous Metal; Wrought Copper

Close Analogs: UNS C10100 - ASTM B48, B133, B152, B187, B272, B432, F68; 101A (Australia); C110 (UK); CDA 101 OFE; ISO Cu-OFE; JIS C1011 H3510 (Japan)

Key Words: BS C110, C103, ISO Cu-OFE, CEN CW009A, oxygen-free high conductivity copper (OFHC), CDA 101 OFE, ASTM B48, B133, B152, B187, B272, B432, F68, AS 101A 1567 (Australia), Cu/cl NF A53301, JIS C1011 H3510, flat products, plates, sheets, strips

Component **Wt. %**

Cu Min 99.99

Material Notes:

Test specimens: flat product, 1 mm thick.; rod, 25 mm (1 in) diam.; tubing, 25 mm (1 in) diam., 1.65 (0.065 in) mm wall thickness; shape, 13 mm (0.50 in) section.

Applications: bus bars, bus conductors, wave guides, hollow conductors, lead-in wires and anodes for vacuum tubes, vacuum seals, transistor components, glass-to-metal seals, coaxial cables, klystrons, microwave tubes, and rectifiers.

Processing: Excellent hot and cold workability; good forgeability. Fabricated by bending, coining, coppersmithing, drawing and upsetting, hot forging and pressing, shearing, spinning, swaging, and stamping.

Corrosion Resistance: Good to excellent. Susceptible to galvanic corrosion when coupled with iron, aluminium, magnesium, lead, tin, and zinc. Good resistance to atmospheric, brackish water, sea water, and non-oxidizing acid corrosion, but avoid heating in oxidizing atmospheres or exposing to oxidizing acids, moist halogens, sulphides, ammonia, or solutions with ammonium ions.

Physical Properties	Metric	English	Comments
Density	8.94 g/cc	0.323 lb/in ³	at 20°C (68°F)
Mechanical Properties			
Hardness, Rockwell F	40	40	
Tensile Strength, Ultimate	220 MPa	31900 psi	
Tensile Strength, Yield	69 MPa	10000 psi	0.5% extension
Elongation at Break	45 %	45 %	1mm thick flat specimen
Elongation at Break	45 %	45 %	6 mm specimen.
Elongation at Break	48 %	48 %	in 50 mm (2 in)
Reduction of Area	55 %	55 %	in 25 mm (1 in) rod specimen
Modulus of Elasticity	115 GPa	16700 ksi	
Poisson's Ratio	0.31	0.31	
Machinability	20 %	20 %	Based on 100% machinability for UNS C360000
Shear Modulus	44 GPa	6380 ksi	
Shear Strength	150 MPa	21800 psi	

Electrical Properties

Electrical Resistivity	1.71e-006 ohm-cm	1.71e-006 ohm-cm	at 20° C (68°F)
------------------------	------------------	------------------	-----------------

Thermal Properties

CTE, linear 20°C	17 $\mu\text{m}/\text{m}\cdot^\circ\text{C}$	9.44 $\mu\text{in}/\text{in}\cdot^\circ\text{F}$	from 20-100°C (68-212°F)
CTE, linear 100°C	17.3 $\mu\text{m}/\text{m}\cdot^\circ\text{C}$	9.61 $\mu\text{in}/\text{in}\cdot^\circ\text{F}$	from 20-200°C (68-390°F)
CTE, linear 250°C	17.7 $\mu\text{m}/\text{m}\cdot^\circ\text{C}$	9.83 $\mu\text{in}/\text{in}\cdot^\circ\text{F}$	from 20-300°C (68-570°F)
Heat Capacity	0.385 J/g·°C	0.092 BTU/lb·°F	at 20°C (68°F)
Thermal Conductivity	391 W/m-K	2710 BTU-in/hr-ft ² ·°F	at 20°C
Melting Point	1083 °C	1980 °F	

References are available for this material.

Data Sheet WL200
(Provided by Watson & Lewis; London)

WL200 Black Chrome is an alloy or composite consisting of 75% chromium metal and 25% of included chromium oxides.

Advantages

The inclusion of oxides in WL200 gives the finished coating a degree of porosity. This micro porosity helps to absorb oil or even paint and, of course, this property then improves the corrosion resistance, weather-durability and appearance of the coating.

Uses

WL200 Black Chrome provides black deposits, which are both decorative and functional. Decorative applications include: furniture, plumbing fittings, optical equipment, boat equipment, builders' hardware, communications and satellite equipment and automotive parts.

Important functional applications include: solar energy collectors for heat production, electricity production and anti-glare surfaces; machine tools and weaponry.

Absorption/Solar Emissivity

WL200 Black Chrome plating technology, along with its selectivity in solar absorption and heat emission has helped in establishing it as a leader in the field.

The following table shows the values of solar absorption and infrared emissivity that were reported.

Coating Sample	Absorptance	Emissivity
Black Chrome	0.868	0.088
Black Nickel	0.867	0.109
Nextel Black Paint	0.967	0.967

Appendix C

The data below are provided by GBU GmbH (1996), for the NAK adsorption chiller used in the simulation of chapter (8).

Table (C1)

Chilled water in °C	Cooling water in °C	Heat medium in °C								
		55	60	65	70	75	80	85	90	95
5	25		0,51	0,54	0,56	0,56	0,56	0,56	0,56	0,56
	28				0,5	0,53	0,54	0,55	0,55	0,54
	29				0,47	0,51	0,53	0,53	0,54	0,53
	30					0,49	0,51	0,52	0,52	0,52
	31					0,46	0,49	0,5	0,51	0,51
	32						0,47	0,49	0,49	0,5
	34							0,46	0,47	0,47
6	25							0,58	0,58	0,58
	28			0,51	0,54	0,56	0,57	0,57	0,57	0,57
	29				0,5	0,53	0,55	0,56	0,56	0,56
	30				0,47	0,51	0,53	0,54	0,55	0,55
	31					0,48	0,51	0,53	0,54	0,54
	32					0,45	0,49	0,51	0,52	0,52
	34							0,47	0,48	0,48
7	25		0,55	0,57	0,59	0,6	0,6	0,6	0,6	
	28			0,55	0,57	0,59	0,59	0,59	0,59	0,59
	29				0,54	0,56	0,58	0,58	0,59	0,58

	30				0,51	0,53	0,56	0,57	0,58	0,57
	31					0,51	0,53	0,55	0,56	0,56
	32					0,47	0,5	0,53	0,53	0,54
	34						0,44	0,47	0,48	0,49
8	25	0,56	0,58	0,6	0,61	0,62	0,62	0,62		
	28			0,57	0,59	0,61	0,61	0,61	0,61	0,62
	29			0,53	0,56	0,58	0,6	0,6	0,61	0,61
	30				0,52	0,56	0,58	0,59	0,59	0,59
	31				0,5	0,53	0,55	0,57	0,58	0,58
	32					0,5	0,53	0,55	0,55	0,56
	34						0,48	0,5	0,51	0,52
9	25	0,6	0,61	0,62	0,63	0,64				
	28		0,56	0,58	0,61	0,62	0,64	0,64		
	29			0,55	0,58	0,6	0,62	0,62	0,63	
	30			0,52	0,55	0,57	0,59	0,6	0,61	0,61
	31				0,52	0,55	0,57	0,6	0,61	0,62
	32				0,49	0,53	0,55	0,57	0,58	0,58
	34					0,48	0,5	0,53	0,54	0,55
10	25	0,62	0,63	0,64	0,65	0,65				
	28		0,59	0,61	0,63	0,64	0,65	0,65		
	29		0,54	0,58	0,6	0,62	0,63	0,64	0,64	
	30			0,54	0,57	0,6	0,61	0,62	0,63	
	31			0,51	0,55	0,57	0,59	0,6	0,6	0,61
	32				0,52	0,55	0,57	0,58	0,59	0,59

	34				0,49	0,5	0,53	0,54	0,56	0,56
15	29	0,64	0,65	0,68	0,69	0,7				
	30	0,59	0,62	0,65	0,67	0,68				
	31		0,59	0,62	0,65	0,66	0,67			
	32			0,6	0,62	0,64	0,65	0,66		
	34				0,58	0,61	0,62	0,63	0,63	0,63



Figure (C8) Case (10) of chapter (5) – *The design.*
Attempts of evacuating this sample failed, despite the internal support.

